A Conceptual Framework for IoT-based Healthcare System using Cloud Computing

Sapna Tyagi
Department of Computer Science
Institute of Management Studies,
Ghaziabad, India
sapna030280@gmail.com

Amit Agarwal
Center for Information Technology
University of Petroleum & Energy
Studies, Dehradun, India
coer.info@gmail.com

Piyush Maheshwari
Department of Engineering
Amity University Dubai
United Arab Emirates
pmaheshwari@amityuniversity.ae

Abstract

Internet of Things (IoT) envisions a future in which anything/anyone/anyservice can be linked by means of appropriate information and communication technologies which will bring technological revolution in the fields of domestics, smart homes, healthcare systems, goods monitoring and logistics. This paper presents the applications of IoT and addresses some essential parameters and characteristics of each of the applications of IoT. In this paper, we have deeply explored the role of IoT in healthcare delivery and its technological aspects that make it a reality and examine the opportunities. A cloud based conceptual framework has been proposed which will be beneficial to the healthcare industry implementing IoT healthcare solutions.

***Index Terms*—Internet of Things; Cloud Computing; Healthcare**

I. INTRODUCTION

Nowadays, the Internet is used by more than two billion customers around the world to browse contents, send and receive emails, access multimedia resources, play online games, and social networking. Moreover, the Internet is also expected to serve as a global platform to interconnect physical objects or *'Things'*, thus, enabling new ways of working, interacting, entertaining and living [12, 13]. Internet technology has become ubiquitous within our society which is infiltrating all aspects of our lives, and it is better to call it as necessity rather than a convenience. The term IoT, first used by Kevin Ashton, describes the emerging global, Internet-based information service architecture [15]. The IoT incorporates concepts from pervasive, ubiquitous, and ambient computing, which have been evolved in last two decades and have now reached at some level of maturity. The IoT is envisioned as a network of billion people, objects, machines interacting to one another, invisibly connected with sensors, actuators, making useful in everyday lives. The future will be dominated by the *'Internet of Things'* which will serve as a global platform to interconnect physical objects, things, humans, thus, enabling new ways of working, communicating, interacting, entertaining, and living. The IoT is a novel paradigm in which every physical object which you wear, what/where you drive, what you read/see, and anything including the people you meet, the places you go, will be connected, addressed and controlled remotely [1]. As the cost of IoT devices, mobiles and network connectivity continues to drop, and it is easy to see that everything and everyone are online over wireless network for 24 hours in a day. The Communication technology has become faster, ubiquitous and cheaper which will surely changes the way the people access information. The adoption of RFID based sensor technology and other similar technologies are spurring innovation and the development of the Internet of Things [7, 8]. This novel integrated RFID Sensor—Internet framework shall form the core technology around which a smart environment will be shaped. The information generated will be shared across diverse platforms and applications, to develop a common operating picture (COP) of an environment, where control of certain unrestricted *'Things'* is made possible [10]. The IoT uses the concept of object hyperlinking which promises humans to live in a smart, highly networked world, which allows for a wide range of interactions with this environment. Object hyperlinking aims to extend the Internet to the real world by attaching object tags with URLs as meta-objects to tangible objects or locations. Most of them rely on some kind of unique marker integrated in or attached to the object. Some of these markers can be analyzed using different kinds of wireless near field communication (for instance RFID tags [3] or Bluetooth beacons [4]), others are visual markers and can be analysed using cameras, for instance standard 1-D barcodes [5] or their modern counterparts, the 2-D barcodes [6]. These object tags can then be read by a wireless mobile device and information about objects and locations retrieved and displayed [2]. The computing for the IoT may be processed locally or embedded in microcontroller enabled devices or even implanted in the human body [11]. The huge data generated from various sources may even reside in the *'Cloud'*, which requires greater processing power to retrieve information in a secure and reliable manner.

The shift from the Internet used for interconnecting end-user devices to the Internet used for interconnecting physical objects that communicate with each other and/or

978-1-4673-8203-8/16/$31.00

with humans will open a multiple businesses and market opportunities in a seamless manner in the fields of smart city, e-health, real-time monitoring of industrial processes, and intelligent logistics and various others [14].

II The IoT-based Healthcare System

The healthcare represents one of the top challenges that every country is facing today. Although healthcare industry invests heavily in information technology, yet the promised improvement in patient safety and productivity have not been realized up to the standards. Even today organizations still rely on paper medical records and handwritten notes to inform and make decisions. Digital information is siloed between departments and applications. Sharing of patient data among clinicians, departments and even patients is rare and complex. Embracing cloud and IoT technology in healthcare may be the answer to enabling healthcare organizations to focus their efforts on clinically relevant services and improved patient outcomes which will make health monitoring, diagnostics and treatment in more timely and convenient manner with the reduced costs. The IoT can bring multiple benefits to healthcare through the use of RFID tags, sensors/ detectors, intelligent equipments, etc. It enables online interaction of patients, identification and tracking of patients, doctor‘s locations, tracking of patient medical reports and equipment‘s tracking and tracing medical supply chain, logistics, drug management and drug counterfeit detection, etc.

The Internet of Things has capabilities to connect D2M (Device-to-Machine), O2O (Object-to-Object), P2D (Patient-to-Doctor), P2M (Patient-to-Machine), D2M (Doctor-to-Machine), S2M (Sensor-to-Mobile), M2H (Mobile-to-Human), T2R (Tag-to-Reader). It intelligently connects humans, machines, smart devices, and dynamic systems which ensure the effective healthcare and monitoring system, medical asset monitoring and medical waste management system [27]. For instance, wearable bands on patient‘s wrist can track pulse, blood pressure, red blood cell counts, glucose and cholesterol level and constantly send the reports to medical actor‘s smart phones or tablets as well as reminders to take the medication, walking etc to patient‘s smart phones.

The Internet of Things is going to revolutionize healthcare in terms of investment, security, privacy, reliability and return-on-investment (ROI), if truly trusted by medical enterprises and community. The tracking and monitoring of patients and healthcare actors are one of the biggest challenging research directions for IoT Healthcare. In one of the findings by US Institute of Medicine argues that medical errors persist as the number 3 killer claiming the lives of some 400,000 people each year. Some of these errors involve:

- Missed and delayed diagnoses.
- Failing to order appropriate tests or initiate follow up.
- Inability to access patient‘s medical history.
- Prescribing the wrong pharmaceutical drug.
- Not knowing whether a patient is allergic to a certain drug.

Due to possibility of such human-entered error, healthcare needs automation where the devices have the ability to gather data on their own which reduces the risk of errors. Fewer errors can mean increased efficiency, lower costs and improvements in healthcare services where an error can literally be the difference between life and death.

III Related Work

Recent technological advances in sensors facilitate are highly suitable for Healthcare Application. Wireless Body Area Sensor Networks (WBASNs) are emerging as promising enabling technologies to implement e-health [19]. A WBASN for health monitoring consists of multiple sensor nodes worn by patient that can measure and report the patient‘s physiological state.

Microsoft has launched a web page [16] where consumers using PHR from Google Health can have their personal health information transferred to a Microsoft Health Vault account. As the demise of Google Health brings into sharper focus the challenges of establishing an online PHR business model, PHRs will see a 33% gain in revenue through 2015 as doctors push patients to use health IT systems [17]. The Microsoft Connected Health Framework (CHF) architecture [18] consists of process models, service models and information models.

Henry Mayo Newhall Hospital in Valencia, California (USA) has implemented the concepts of IoT. They wanted to enable doctors to spend less time at computers and more time with the patients. Realizing the potential of the Internet of Things, the hospital has created an Intelligent System using Microsoft technology that vastly speeds up the access of patient data. The system connects 175 new thin clients‘ devices that draw centralized computing power and its physicians‘ own tablets and other devices from existing data centres and systems, creating anywhere, anytime access to data from patient records to test results, prescriptions and more. By focusing on this one aspect of its business, the hospital is able to provide better care while vastly improving doctor efficiency. Henry Mayo implemented an intelligent single sign-on solution from Health Cast and Microsoft to vastly simplify the data-access process.

The major advantages seen by hospital after implementing this new system were:

1. Advances in sensor and connectivity technology are allowing devices to collect records and analyze data that was not accessible before. The new system allows doctors the secure access to review lab tests, enter prescriptions, or look at patient records, cut-in

medication delivery time by two-thirds from either installed terminals or their own laptops, tablets or smart phones, so they can provide care from anywhere in a fraction of the time.

2. Hospital's previous system was cumbersome and time-consuming, running a variety of separate software applications, including those for patient medical records, timekeeping systems, medical imaging repositories, speech recognition software and emails. The doctors and staff needed to access information throughout the day from different locations across the hospital and logging in each time could take up to two minutes and doctors had to memorize a large number of usernames and passwords. Now with new emergence of this solution, the proximity badge automatically enters the username, and only one password needed to be entered at the beginning of the day. Because of this staff members are less likely to forget their login information or locking themselves out of the system. The new solution was so easy to use that Henry Mayo's IT staffs has seen a 70 percent drop in password-related help-desk calls.

The AT&T Medical imaging and information Management Solution (MiiM)[20], enables health professionals, to expedite patient care by means of web-enabled virtual collaboration and mutual interpretation of patient images, such as X-rays, computed tomography (CT) or Magnetic Resonance Imaging (MRI) scans[20]. The system allows users access to review patient images almost instantly, from anywhere, giving attending physicians critical point-of-care updates and time to see more patients. This significantly reduces long-term technology costs and speeds patient care management.The solution can also enable national hospital networks to manage referral patient image when transferring to and from other institutions, anywhere in the world. Accenture cloud migration services help these advances in clinical workflow gain faster adoption in the healthcare.

It is clearly visible from all above implementations of e-healthcare by Microsoft, Henry Mayo or AT&T have contributed significantly in building the environment for e-Health Cloud. But these efforts are still limited to Cloud-based storage solutions and Healthcare applications or systems or platform solutions automating single entity in the health care industry. These are the cloud-based system to automate the process of collecting patients' vital data via a network of sensors connected to legacy medical devices, and to deliver the data to a medical center's ~~–e~~loud" for storage, processing, and distribution. The main benefits of the system are that it provides users with 7-days-a-week, real-time data collecting, eliminates manual collection work and the possibility of typing errors, and eases the deployment process.

Through Our proposed system we would like to build a network among all the entities (hospitals, doctors, patients, Labs, Pharmacist, Nurses) participating in healthcare. This proposed model will not only limited to the entities under one umbrella but will cover nationwide entities. We tried to implement the concepts of IoT where these entities would be directly communicating to cloud. For example, the patient would be wearing some sensors/RFID tags continuously fetching his current health conditions and simultaneously uploading on the cloud which can be accessed by other health actors almost instantly. It replaces the process of having a health professional come by at regular intervals to check the patient's health condition (BP, sugar level, heart beat, pulse rate), instead providing a continuous automated flow of information. In this way, it simultaneously improves the quality of care through constant attention and lowers the cost of care by eliminating the need for a caregiver to actively engage in data collection and analysis. There are people all over the world whose health may suffer because they don't have ready access to effective health monitoring. But our proposed model where we are creating the network among all healthcare actors are now making it possible for reaching the doctors to the patients to make health recommendations instead of vice-versa by securely capture patient health data(medical history, reports) from a cloud.

IV. **Proposed Framework for IoT-based Healthcare System on Cloud**

Patients today are more educated to their diseases and better advocates for their own healthcare which increasingly demands access to the latest technologies. They want to seek the best care at the best cost and are willing to investigate their options. As a result, demands for access to personal patient records are increasing and organizations need to keep up. When citizens can access bank accounts from anywhere in the world, withdraw money, get balances and make payments, why they cannot have universal access to their secure health information. With advancement of technologies like IoT and Cloud, and rising adoption of bring-your-own-device (BYOD) working practices , the sharing of data and collaboration among services will have transformative impact on personal healthcare. Based on the same concept, we proposed a comprehensive *Cloud-IoT* healthcare system to empower depressed patients over their treatment process. In this proposed framework we created a Network consisting of all the health Actors for sharing and collaboration of data and service on single platform.

The stakeholder involved in the healthcare scenario include: patients and family members, healthcare professionals (doctors, nurses, attendants), pharmacists, medical labs, hospitals and public authorities such as auditing or legal authorities that need to access healthcare data under specific conditions and which are also responsible for validating and authorizing of these health actors. The proposed *Cloud-IoT* based integrated solution will consists of various applications like e-prescribing system, EHR (electronic health records), personal health records, clinical decision systems, pharmacy system etc. Figure 1 presents a proposed *Cloud-IoT* based healthcare framework. This framework will offer broad range of healthcare applications to different stakeholders at

different levels. The physicians can use *Cloud-IoT* for their improved clinical results and improved diagnosis of patients. The patients can do their self assessment for monitoring their health. They can find hospitals and other related organizations for providing improved healthcare services. The personal monitoring devices are used to monitor and collect patient‘s physical activity data or sleep information. Besides it, the cloud service provider offers *Platform as a Service (PaaS)* and *Infrastructure as a Service (IaaS)* to host Cloud-IoT healthcare applications.

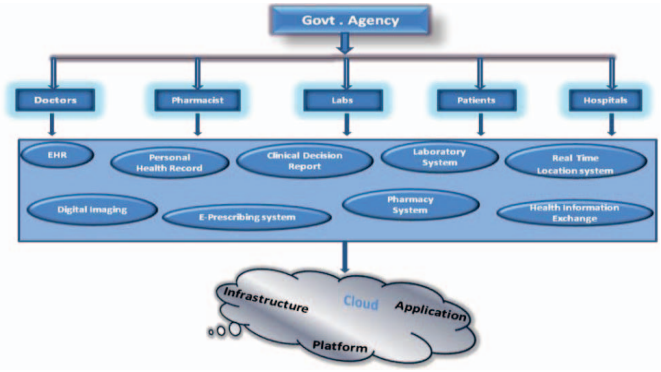

Figure 1. Cloud-IoT based healthcare framework

A) Use Case Scenario

The above proposed framework is presented below in more detailed manner. In order to refine the application framework presented in Figure 1, we have analyzed the processes of the proposed system. The actors and data flows involved in above framework are highlighted in Figure 2.

Consider an example use case as shown in Figure 2. The patient wears a monitoring device to collect own physical and sleep activities information. These monitoring devices can be sensors/RFID tags which are strategically placed on the human body. Sensors/RFID tags can be worn as stand-alone devices or can be built into jewellery, applied as tiny patches on the skin, hidden in the user‘s clothes or shoes, or even implanted in the user‘s body thus creating WBASN. Each node in the WBASN is typically capable of sensing, sampling, processing, and wirelessly communicating one or more physiological signals. It can also help to determine the user‘s location, discriminate among the user‘s states (e.g., lying, sitting, walking, running), or estimate the type and level of the user‘s physical activity. The activity data are uploaded from the device, via the EHR system, to user front end for manual uploading. The data then hosted in the cloud‘s EHR application back-end and saved in the patient‘s medical profile. The stored data may be shared with the doctors and hospitals on demand by the patients. The health professionals, such as cardiologists and radiologists expedite patient care by accessing the stored patient data. The patients and labs by mutual consent can also upload X-rays, Computed Tomography (CT) Scans or Magnetic Resonance Imaging (MRI) scans in patient‘s medical e-profile and that would be shared via cloud platforms in real time with top specialists anywhere in the world, enabling diagnosis and recommendations overnight. Courses of treatment and outcomes could also be monitored anywhere in the same way. If someone travelling overseas fell ill, they could provide local doctors on the ground with direct and immediate access to their health records, and get more appropriate treatment as a result.The medicines precribed by Doctors is available to Pharmacist also. A pharmacist would be able to check a person‘s allergies when issuing a prescription through patient‘s medical profile. A hospital attending a traffic accident could check an individual‘s blood type and pre-existing conditions mentioned in his profile.

By means of above IoT-Cloud collaboration patients‘ digitized health information—medical histories, scan images, blood types, allergies, medical labs reports can flow freely across the world, accessible via secure authentication and will be easily interpreted by health actors. The system allows health actors access to review patient images almost instantly, from anywhere, giving physicians critical point-of-care updates and time to see more patients. This system will significantly reduce long-term technology costs and enhance speedy patient care management. The solution can also enable private and government hospital networks across the nation to manage referral patient image when transferring to and from other institutions, anywhere in the country.

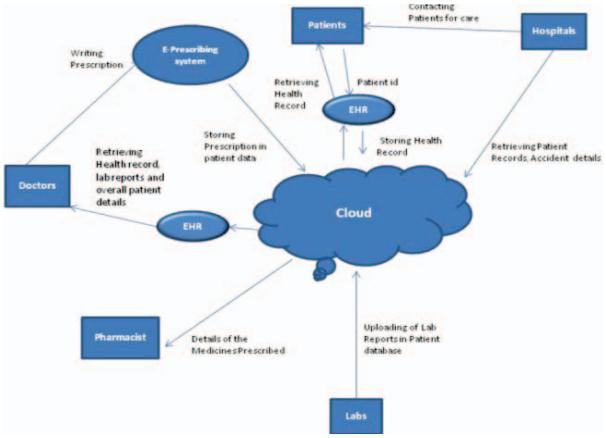

Figure 2. Actors and data flows in Cloud-IoT based healthcare framework

V. Conclusions and Future Scope

This paper tries to emphasize on an IoT-Cloud enabled healthcare system not only to realize the illustration and traceability of healthcare actors but guarantee the improved healthcare services. We have proposed a cloud-IoT framework in which medical information can be safely transferred, with the consent of the patients and other health actors. Through our proposed system we would like to build a network among all the entities (hospitals, doctors, patients,

Labs, Pharmacist, Nurses) participating in healthcare which certainly leads to the improvement in communication and collaboration among these entities providing better care and services to the patients. The proposed IoT-Health Cloud represents an enabling technology for many healthcare providers to face many challenges such as rising healthcare delivery costs, information sharing, and shortage of healthcare professionals better care and enhanced services for the patients. However, the benefits gained are offset by issues of trust, privacy, and security in addition to several technical issues that must be addressed before healthcare providers can fully adopt and trust the IoT-Health Cloud. A complete model for implementing the security is still required.

REFERENCES

[1] Atzori, Luigi, Antonio Iera, and Giacomo Morabito. ―The Internet of Things: A Survey", Computer Networks 54, no. 15 (2010): 2787-2805.

[2] G. Broll, E. Rukzio, M. Paolucci, M. Wagner, A. Schmidt, H. Hussmann. ―PERCI: Pervasive Service Interaction with the Internet of Things", IEEE Internet Computing, 13(6), 2009, 74–81.

[3] Want, Roy. ―RFID: A key to automating everything". Scientific American 290, no. 1 (2004): 56-65.

[4] Quack, Till, Herbert Bay, and Luc Van Gool. ―Object recognition for the internet of things". In The Internet of Things, pp. 230-246. Springer Berlin Heidelberg, 2008.

[5] Rouillard, José. ―Contextual QR codes". In Computing in the Global Information Technology, 2008. ICCGI'08. The Third International Multi-Conference on, pp. 50-55. IEEE, 2008.

[6] Rohs, M., Gfeller: Using camera-equipped mobile phones for interacting real- world objects . In : ferscha , A., Hoertner, H., Kotsis, G.(eds.) Advances in Pervasive Computing, Austrian computer Society (OCG)(2004)

[7] Li, S., Xu, L., Wang, X. (2013). ―Compressed Sensing Signal and Data Acquisition in Wireless Sensor Networks and Internet of Things." IEEE Transactions on Industrial Informatics, in press DOI: 10.1109/TII.2012.2189222.

[8] E. Welbourne, L. Battle, G. Cole, K. Gould, K. Rector, S. Raymer, et al.," Building the Internet of Things Using RFID The RFID Ecosystem Experience." IEEE Internet Computing13 (2009) 48-55

[9] A. Juels, ―RFID security and privacy: A research survey.", IEEE Journal of Selected Areas in Communication 24 (2006) 381–394

[10] Jayavardhana Gubbia, Rajkumar Buyya, Slaven Marusic, Marimuthu Palaniswami. ―Internet of Things (IoT): A vision, architectural elements, and future directions", 0167-739X/$ © 2013 Elsevier B.V. http://dx.doi.org/10.1016/j.future.2013.01.010

[11] I.F. Akyildiz, W. Su, Y. Sankarasubramaniam, E. Cayirci, ―Wireless sensor networks: a survey", Computer Networks 38 (2002) 393–422.

[12] D. Miorandi, S. Sicari, F. Pellegrini, I. Chlamtac, ―Internet of Things: Vision, Applications & Research Challenges." Ad Hoc Networks (Elsevier) Journal (2012).

[13] M. Weiser, ―The computer for the 21st century." Scientific American 265 (3) (1991) 94–104.

[14] Daniele Miorandi , Sabrina Sicari , Francesco De Pellegrini , Imrich Chlamtac, ―Internet of things: Vision, applications and research challenges." Ad Hoc Networks journal homepage: 1570-8705/$ - 2012 Elsevier B.V.

[15] K. Ashton, "That ‗Internet of Things' Thing," RFiD Journal, vol. 22, pp. 97-114, 2009.

[16] Microsoft Health Vault, ―Welcome, Google Health Users." http://www.microsoft.com/en-us/healthvault/google-health.aspx?WT.mc_id=M11071406&WT.ad=text::GHConvertPR::MSPress::HvGH::1406

[17] N. Lewis, ―Google Health Dies, but PHR Market Still Growing," Information Week 201 http://www.informationweek.com/news/healthcare/EMR/231000876

[18] E. Jovanov et al. A wireless body area network of intelligent motion sensors for computer assisted physical rehabilitation. J. Neuroengineering Rehabil. 2, 2005

[19] Microsoft, ―Connected Health Framework Architecture and Design Blueprint," 2009 http://www.microsoft.com/health/ww/ict/Pages/Connected-Health-Framework.aspx

[20] AT&T press release: http://www.att.com/gen/press-room?pid=22076&cdvn=news&newsarticleid=33395, Accenture and AT&T Launch Medical Imaging Solution, 28 November 2011.

A Software approach for the prediction of Efficiency of three phase Induction motor at optimize iron losses

Raj Kumar Saini[1*], Devender Kumar Saini[1], Rajeev Gupta[1], Piush Verma[2]
[1] Department of Electrical Engineering, university of petroleum and Energy study, Dehradun (U.K), India
[2] Rayat –Bahra group of institutes, Patiala campus (Pb)

Email:rajsaini.acet@gmail.com

***Abstract*—This research article describe the prediction of best performance of three phase induction motor at optimized iron losses by using two different rotor cages of copper and aluminum at room temperature to maximum working temperature of the motor up to 70^0 C. The target is to compare the efficiency of the motor by using different combination of stator and rotor design (Discussed in Table-1), and to calculate the variables dimensions of this combination in terms of sensitivity analysis under the condition of above said temperature. With the help of mathematical equations of three phase induction motor a program is prepared on the MAT LAB by using GUI tool. The output of this program is put in the targeted input value of JMAG express for performance calculations of three phase, 11Kw squirrel cage induction motor. Genetic Algorithm (GA) is used as an inbuilt tool for optimization techniques and calculations of sensitivity analysis are completed by using correlation matrix.**

Keywords—Efficiency; optimized iron losses; temperature rise; JMAG Express.

I. INTRODUCTION

In the recent past years there has been an increasing interest for the optimum design of induction motors to reduce the energy crises and increasing cost of material used. Based on the discussion it was found that the motors which are not used at the full load and if they are oversized, then it increases the wastage of energy. One of the best solution to overcome this problem is to use computer tools such as motor master+ and Euro Deem and many more [1]. However, the circuit parameters of high speed induction motor feed by the investors are calculated including straw load and harmonic torque [2].The loss of life of motor was estimated for continuous motor operation at constant temperature and temperature variation with time. The electrical model, thermal model and the thermal aging equations are used to estimate the insulation life of the motor[3], but in another research article the author presented a general approach to modeling temperature rise phenomena in induction motor and compared the results with the results of experimental measurements [4].It is not possible to calculate the exact value of iron losses in induction motors, because it depends upon the material used, however on the bases of theoretical and empirical formulas some limits have been received with in which these losses are excepted to lie [5]. While methods for evaluating life time expectations of the motor are discussed under the variables conditions like temperature rise under variable load conditions [6].While in the meantime the authors presented a research article based on a new approach for the prediction of iron losses in soft magnetic materials having a direct mathematical relationship between iron losses and supply voltage. For this purpose eight magnetic materials of different thickness and alloys composition are used [7]. An improved time domain iron loss estimation method is presented in [8]. The core losses will increase on increasing the load due to that of harmonic content generated by the slot geometry and also proved that closed rotor geometry have less harmonic content as compared to open slots [9]. The methods proposed by different authors for the predictions of iron losses with PWM supply in a magnetic materials have been used for the same purpose in three phase induction motor. In fact a percentage error of 5% between the predicted and measured results have been obtained [10]. Recently a new testing device called “Tester” have been developed to measure the magnetic losses in yoke and teeth of the machine. The new designed three phase tester have an ability to generate the magnetic flux that would be created by the motor under regular functioning [11]. A domain finite element method is used for the design of three phase 5 H.P squirrel cage induction motor [12]. Simulation and experimental results on prototype has been compared and observe that copper cage rotor have more efficiency with better torque, which is best suitable for both industrial and agriculture sectors [13]. While JMAG designer software is used in [14] to perform the electromagnetic analysis and optimized model.

II. LOSSES AND TEMPERATURE RISE

In electrical rotating motors there are mainly two types of losses: fixed losses and variable losses. Fixed losses consists of magnetic core losses, friction and windage losses. Magnetic core losses also consists of eddy and hysteresis losses in the body of the motor. These losses depends upon the material used and power quality. The variable losses depends upon the load and these are the losses present in the stator and rotor of the motor. The variable losses are proportional to the square of the current and resistance of the material, while the stray loss which is a part of the variable losses are difficult to measure and calculate. Steinmetz

978-1-5090-4530-3/16/$31.00 ©2016 IEEE

develop an empirical formula to calculate the hysteresis losses [15].

$$p_h = k\,h\,f\,B_m^{\,k}$$

where

$p_h = Hyteresis\ losses$

$B_m = flux\ density\ in\ wb/m^2$

$k = steinmetz\ coefficient$

$f = frequency\ in\ Hz$

The total eddy current in a sheet of one meter length and one meter width is given by the relation

$$P_e = \int_{x=0}^{x=t/2} \frac{4\pi^2 f^2 B_m^{\,2}}{\rho} l\,b\,x^2 dx$$

And eddy current loss /unit volume is given by the relation

$$p_e = k_e\ f^2 B_m^{\,2}\ w/m^2$$

Total iron losses is given by the relation

$$p_t = k_h\, f B_m^{\,k} + k_e f^2 B_m^{\,2}\ \ w/kg$$

The calculation of temperature rise is not so simple due to complex heat flow process [6]. The main reason of temperature rise in motors are due to bearing friction, windage losses, copper losses and stray losses. Only stray and copper losses vary with load variations. Copper losses occurs in the winding of the motor, however these losses can be calculated with the help of resistance method. This method is applicable only for winding temperature measurement .For practical purpose the following relation can be used for the calculation of temperature rise [15].

$$\psi = \psi_2 - \psi_a = \frac{\alpha_2 - \alpha_1}{\alpha_1}(235 + \psi_1) + \psi_1 - \psi_a$$

Where,

$\psi = Temperature\ rise$

$\psi_2 = Temperature\ rise\ at\ the\ end\ of\ the\ test$

$\psi_a = Temperature\ of\ the\ cooling\ media$

$\alpha_1 = Initial\ resis\tan ce\ of\ the\ winding$

$\alpha_2 = Temperature\ of\ the\ winding\ at\ the\ end\ of\ the\ test$

$\psi_1 = Temperature\ of\ the\ cold\ winding$

III. JMAG EXPRESS AND ITS OPTIMIZATION TOOL

It is a set of integrated software tools which have an aim to support electric motor designers throughout the complete design process .This software allows calculations for the basic motor properties in very short time, just by entering the input parameters. This can be used not only for the design of three phase induction motor, but it can be used for all rotating type electric machines like brushless motor (IPM),brushless motor(SPM),brushless motor(outer rotor/SPM).,single phase induction motor reluctance motor and brush motor etc. This software embedded the response surface method and genetic algorithm (GA) as the optimization engine. It generates the parameters in terms of sensitivity analysis by using correlation matrix and generates Pareto curves by using response surface method.

IV. INPUT DATA

To optimize the iron losses of the motor operating in terms of rated voltage, a three phase squirrel cage induction motor have been proposed with the following input specifications as shown in Table 1

TABLE 1. Input Specifications for the Design

Particulars	**Values**
Rating of the induction machine	11kw
Rated speed of the motor	1425 R.P.M
Maximum Speed	1500 R.P.M
Number of poles	4
Number of slots	36
Supply voltage in RMS	284 V
Maximum current	20Amp
Stator design	so_016 straight teeth, round bottom, teeth width, slot depth
Rotor design	rim_006 parallel sided tooth

V. SIMULATION RESULTS AND DISCUSSION

The proposed techniques is used on 11 kw three phase squirrel induction motor by applying the rated voltage under the variation of base temperature of **20º**C to the maximum working temperature of **70ºC**.The JMAG express is used to optimized the iron losses as an objective function with calculations in terms of sensitivity analysis of stator and rotor design. This software can be used as a basic tool to check the performance of newly design electric motors. Normal and optimized parameters are calculated by selecting copper and aluminum cage rotor, discussed in Tables 2-5.

TABLE 2.
Normal parameters Calculation of 11 kw, 50Hz, 4 pole induction motor by selecting copper Cage at base temperature of 20^0 C.

Speed (R.P.M)	Iron Losses (w)	Copper Losses (w)	Primary current (R.M.S)	Power (W)	Torque (Nm)	Second current loss(w)	Power factor	Magnetizing Current (Amp)	Efficiency (%)
75	4.77	2239.39	5.12	85.01	10.82	1615.27	0.535	0.438	3.65
300	5.11	1917.77	4.77	343.79	10.84	1375.16	0.558	0.453	15.17
450	5.42	1702.22	4.52	520.92	11.05	1215.5	0.580	0.467	23.37
525	5.61	1592.09	4.38	610.80	11.11	1134.36	0.592	0.474	27.66
675	6.08	1363.1	4.08	790.86	11.18	966.61	0.622	0.494	36.61
825	6.71	1124.61	3.74	966.88	11.19	791.08	0.659	0.519	46.08
975	7.56	866.51	3.33	1118.02	10.95	602.011	0.701	0.551	56.12
1125	8.73	577.13	2.77	1182.91	10.94	394.302	0.751	0.592	66.87
1275	10.25	276.87	1.98	1036.59	7.76	182.93	0.78	0.642	78.31
1425	11.84	48.83	0.99	478.73	3.21	25.19	0.64	0.689	88.75

TABLE 3.
Normal parameters Calculation of 11 kw, 50Hz, 4 pole induction motor by selecting aluminum Cage at base temperature of. 20^oC

Speed (R.P.M)	Iron Losses (w)	Copper Losses (w)	Primary current (R.M.S)	Power (W)	Torque (Nm)	Second current loss(w)	Power factor	Magnetizing Current (Amp)	Efficiency (%)
75	5.87	2069.52	4.18	86.98	11.07	1652.77	0.608	0.489	4.022
300	6.19	1661.79	3.79	329.81	10.49	1319.26	0.619	0.502	16.508
450	6.50	1410.97	3.52	477.97	10.14	1115.27	0.632	0.514	25.22
525	6.69	1289.71	3.38	547.62	9.96	1017.02	0.641	0.521	29.69
675	7.14	1052.16	3.08	675.30	9.55	825.37	0.661	0.539	38.93
825	7.68	830.81	2.79	787.64	9.11	644.43	0.684	0.559	48.43
975	8.32	618.82	2.49	874.35	8.56	470.80	0.708	0.582	58.23
1125	9.19	401.83	2.09	892.96	7.57	297.65	0.733	0.612	68.47
1275	10.32	192.07	1.54	765.66	5.73	135.11	0.736	0.648	79.09
1425	11.52	37.11	0.88	354.81	2.37	18.67	0.539	0.685	87.95

A three phase, 50Hz, 4pole induction motor rated at 11 kw is used to investigate the normal parameters by using copper and aluminum cage rotors as discussed in Table 2 and Table 3 .The iron losses which occur only due to the main and leakage fluxes will depends upon the quality of the power supply. In this research article it is observed that the core losses are more in aluminum cage rotor as compared to copper cage rotor. The second major loss is the copper loss, which occur due to current losses in the material of stator and rotor winding. This loss is less in aluminum cage rotor as compared to copper cage rotor. Similarly primary current is more and power,torque develop is less in case of copper cage rotor. Moreover efficiency of copper cage rotor is more as compared to aluminum cage rotor at its rated speed and base temperature .

TABLE 4.
Optimized parameters Calculation of 11 kw, 50Hz, 4 pole induction motor by selecting copper Cage at base temperature of 20^oC to the working temperature of 70^oC at optimization iron losses.

Speed (R.P.M)	Iron Losses (w)	Copper Losses (w)	Primary current (R.M.S)	Power (W)	Torque (Nm)	Second current loss(w)	Power factor	Magnetizing Current (Amp)	Efficiency (%)
75	4.47	2339.01	4.96	79.52	10.12	1510.81	0.575	0.424	3.28
300	4.79	2008.65	4.62	321.98	10.25	1287.9	0.594	0.439	13.78
450	5.08	1786.34	4.38	488.31	10.36	1139.39	0.612	0.452	21.42
525	5.27	1675.56	4.24	572.86	10.41	1063.89	0.623	0.460	25.45
675	5.72	1435.62	3.95	742.73	10.51	907.79	0.649	0.479	34.06
825	6.33	1189.21	3.63	909.78	10.53	744.37	0.682	0.504	43.21
975	7.15	922.39	3.24	1055.54	10.33	568.36	0.721	0.536	53.17
1125	8.30	621.22	2.70	1124.42	9.54	374.81	0.764	0.577	64.11
1275	9.86	304.47	1.95	998.27	7.47	176.17	0.792	0.629	76.05
1425	11.65	57.81	0.98	471.43	3.16	24.81	0.81	0.706	87.16

TABLE 5.
Optimized parameters Calculation of 11 kw, 50Hz, 4 pole induction motor by selecting aluminum Cage at base temperature of 20ºC to the working temperature of 70ºC at optimization iron losses.

Speed (R.P.M)	Iron Losses (w)	Copper Losses (w)	Primary current (R.M.S)	Power (W)	Torque (Nm)	Second current loss(w)	Power factor	Magnetizing Current (Amp)	Efficiency (%)
75	5.53	2112.71	4.18	81.92	10.43	1556.44	0.637	0.475	3.72
300	5.86	1706.47	3.79	311.85	9.92	1247.39	0.645	0.488	15.40
450	6.16	1454.61	3.52	453.10	9.61	1057.25	0.656	0.501	23.67
525	6.35	1332.32	3.38	519.83	9.45	965.40	0.663	0.508	27.97
675	6.80	1091.84	3.08	642.90	9.09	785.77	0.68	0.526	36.91
825	7.33	876.66	2.79	752.11	8.70	615.37	0.700	0.546	46.72
975	7.98	652.28	2.49	837.89	8.20	451.17	0.722	0.570	55.92
1125	8.86	29.21	2.09	860.67	7.30	286.86	0.74	0.601	66.27
1275	10.04	210.04	1.54	744.98	5.57	131.47	0.75	0.639	77.19
1425	11.39	44.29	0.880	350.72	2.35	18.46	0.79	0.681	86.29

Table 4 and 5 depicts the performance characteristic of multiple optimized parameters in terms of speed. Iron losses in case of copper cage rotor are less as compared to aluminum cage rotor under the variation of temperature, but copper losses are less in case of aluminum cage rotor as compared to copper cage rotor. Similarly the primary current in aluminum cage rotor is less as compared to copper cage rotor. Also the power and torque develop in copper cage rotor are more as compared to aluminum cage rotor. Therefore, it Will give better performance for large loads. Similarly the power factor of copper cage rotor is better as compared to aluminum cage rotor. The magnetizing currents and efficiencies in case of aluminum cage rotor are slightly less as compared to copper cage rotor. The overall performance of copper cage motor seen to be better as compared to aluminum cage rotor. The performances characteristic of both type of motor have been discussed in fig.1.to fig.5.

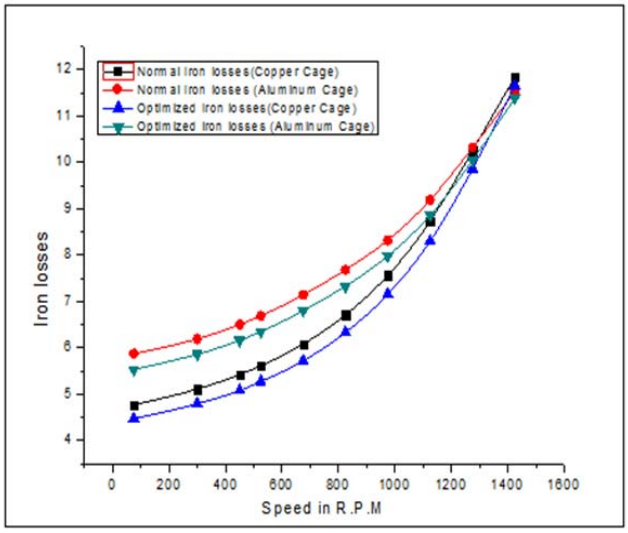

Fig.1.Speed Vs losses

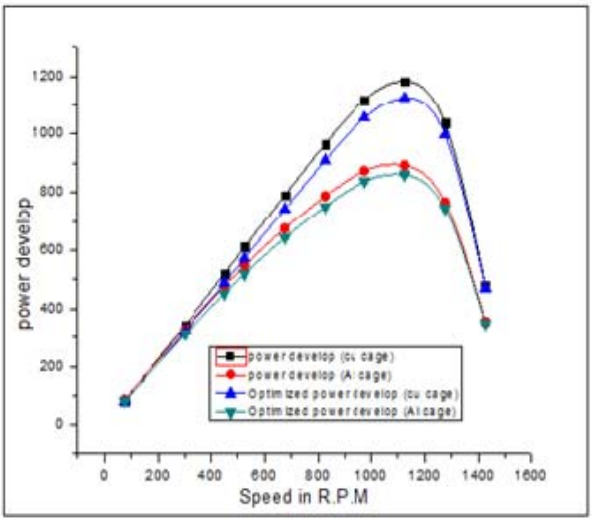

Fig.2.Speed Vs magnetizing losses

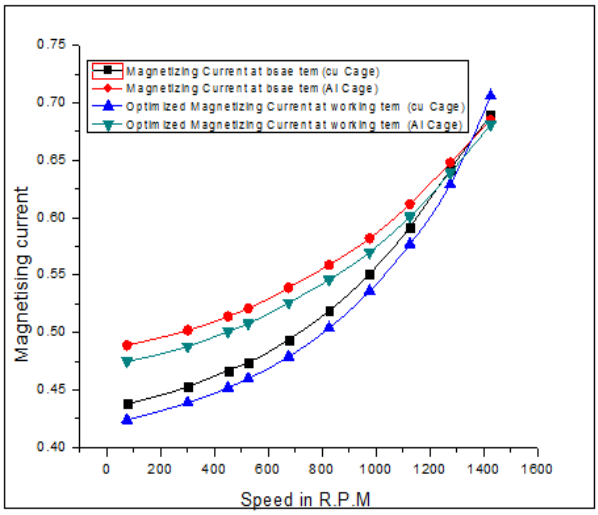

Fig.3. Speed Vs power develop

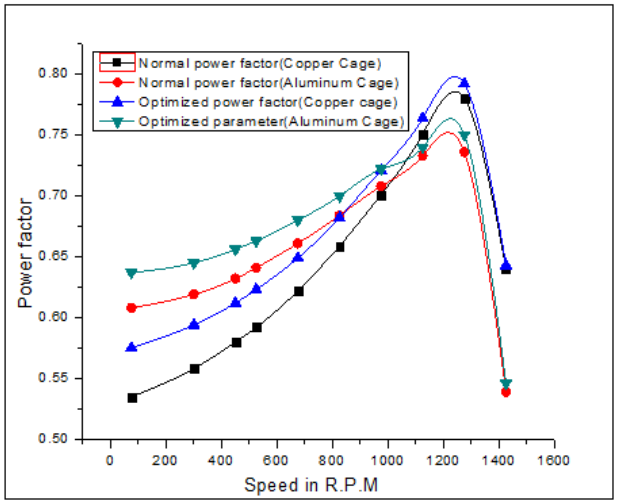

Fig.4.Speed Vs Power factor

Fig. 1.shows the results between speed Vs iron losses. In case of normal parameter calculations at base temperature of 20^0C, the iron losses are less in case of copper cage rotor as compared to aluminum cage rotor. Also at optimization stage under the variation of temperature from base temperature to maximum working temperature, the losses occur in copper cage rotor is less as compared to aluminum

Overall results shows that copper cage rotor is suitable to reduce the losses under the variation of temperature. Similarly the results presented in fig.2, shows that the power developed in case of copper cage rotor is more as compared to aluminum cage rotor.

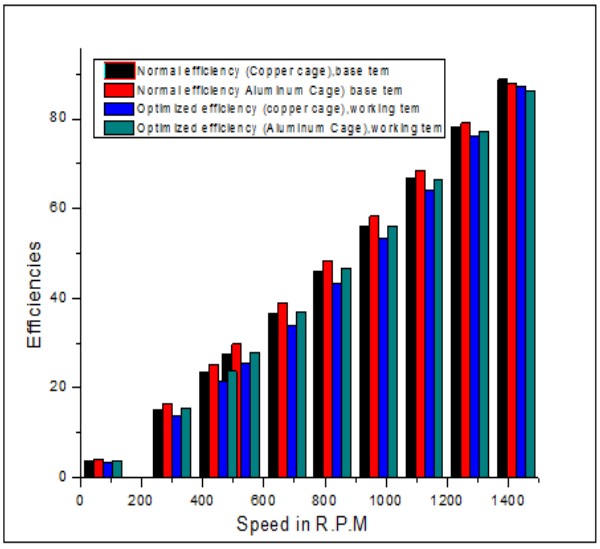

Fig.5.Speed Vs efficiencies

However the results presented in fig.5 shows that the overall efficiency of copper cage rotor is more as compared to aluminum cage rotor at its rated speed under both the conduction of temperature variation.

The dimensions of stator and rotor in terms of sensitivity analysis are calculated and are presented in Table 6.

Table 6. Calculation of optimized stator and rotor dimensions of 11kw, 50Hz, 4 pole three phase induction motor in terms of sensitivity analysis, using copper and aluminum cage rotor under the variation of temperature.

Variables (copper cage)	Values	Variables (Aluminum Cage)	Values
Width of stator tooth	2.6 mm	Width of stator Tooth	2.6 mm
Rotor slot opening width	0.66 mm	Rotor outside diameter	60.8 mm
Depth of stator slot	19.8 mm	Rotor slot opening width	0.66 mm
Rotor tooth tang thickness	0.912 mm	Depth of stator slot	19.8 mm
Rotor outside diameter	60.8 mm	Stator bore diameter	61.99 mm
Rotor tooth width	3.3 mm	Rotor tooth tang thickness	0.912 mm
Stator bore diameter	61.99 mm	Rotor tooth width	3.3 mm
Stator outside diameter	212.5 mm	Stator outside diameter	212.5 mm
Phase voltage (amp)	400V	Phase voltage (amp)	400V
Rotor bar thickness	8.2 mm	Height of stator tooth -tang	1.64 mm
Height of stator tooth -tang	1.64 mm	Rotor bar thickness	8.2 mm
Rotor shaft diameter	18.22 mm	Rotor shaft diameter	18.22 mm

In table 6. Sensitivity parameters are calculated at optimized iron losses by using copper and aluminum cage rotors. The variables values of stator and rotor are same in both the cases of rotor, but the order of sensitivity of variables have been changed. In case of copper cage rotor the width of stator tooth, rotor slot opening and depth of stator slot are highly sensitive variables, while in case of aluminum cage rotor width of stator tooth, rotor outside diameter and rotor slot opening are highly sensitive variables. Calculations of sensitive variables plays a very important role to get the desired efficiency at optimized iron losses under the variation of temperature i.e. form base to maximum working temperature.

VI Conclusion

Since the iron losses occurs in the induction motor depends upon the material used and machine construction. In this research article JMAG express is used for the prediction of efficiency under a wide range of temperature rises at optimized iron losses by using copper and aluminum cage rotors under a design combination of rim_006 parallel sided rotor tooth with so_016 straight teeth, round bottom ,teeth width, slot depth as a stator. This is observed that under normal temperature by using copper cage rotor, the efficiency of the machine at its rated speed is 88.75 %, while by using aluminum cage rotor it was 87.95 %. However under a wide range of temperature at optimized iron losses the efficiency of the motor decreases slightly, it is 87.16 % in case of copper cage rotor and it was 86.29 % in case of aluminum cage rotor. The proposed method of optimization is very simple and the reported results can be used by the designers without consuming much more time with an advantage of getting sensitivity parameters of stator and rotor parts as discussed in table 6. The overall performances made by the copper cage motor is better as compared to aluminum cage motor.

Acknowledgment: - The corresponding author is grateful to the Engineering Technology Division JSOL Corporation Tokyo, 1040053- Japan for providing the license key of the software.

REFERENCES

[1] R. Saidur, “A review on electrical motors energy use and energy savings,” Renewable and sustainable energy reviews 14 (2010), pp. 877–898.

[2] Katsumi Yamazaki, Member, IEEE, Akihiro Suzuki, Motomichi Ohto, and Teruyuki Takakura, “Circuit Parameters Determination Involving Stray Load Loss and Harmonic Torques for High-Speed Induction Motors Fed by Inverters,” IEEE Transactions on energy conversion. October 17 (2012), PP. 1-10.

[3] Pragasen Pillay and Marubini Manyage, “Loss of Life in Induction Machines Operating with Unbalanced Supplies,” IEEE Transactions on energy conversion, vol. 21, no. 4, December (2006), pp. 813-822.

[4] Ing Huaia, Roderick V.N. Melnik and Paul B,“Thogersen. Computational analysis of temperature rise phenomena in electric induction motors,” Applied Thermal Engineering 23 (2003), pp. 779–795.

[5] S. Wahsh and M. El-Bakry, “Additional Core Losses in Induction machines with PWM Inverter,” ETEP vol. 1, no. 4, July/August (1991), pp.189-193.

[6] Emanuel L. Brancato, “Estimation of Lifetime Expectancies of Motors,” IEEE Electrical Insulation Magazine. May/June, 1992-vo1.8, no.3, pp. 5-13.

[7] ldo Boglietti, Andrea Cavagnino, Mario Lazzari, and Michele Pastorelli, “Predicting Iron Losses in Soft Magnetic Materials with Arbitrary Voltage Supply an Engineering Approach,” IEEE Transactions on magnetics, vol. 39, no. 2, March (2003),pp. 981-989.

[8] Zbigniew Gmyrek, Aldo Boglietti and Andrea Cavagnino, “Estimation of Iron Losses in Induction Motors, Calculation Method, Results, and Analysis,” IEEE Transactions on industrial electronics, vol. 57, no. 1, January 2010, pp.161-171.

[9] E. Dlala, “Numerical Investigation of the Effects of Loading and Slot Harmonics on the Core Losses of Induction Machines,” IEEE Transactions on magnetics, vol. 48, no. 2, February (2012), pp. 1063-1066.

[10] Aldo Boglietti, Andrea Cavagnino and Mario Lazzari, “Fast Method for the Iron Loss Prediction in Inverter-Fed Induction Motors,” IEEE Transactions on industry applications, vol. 46, no. 2, March/April (2010),pp. 806-811.

[11] D. Schmitz, “Three-Phase Electromagnetic Device for the Evaluation of the Magnetic Losses in Electric Motors’ Stators,” IEEE Transactions on energy conversion, vol. 30, no. 2, June (2015), pp. 515-521.

[12] Govindasamy. K. Sathishkumar, N. Vimalraj, T. S. Sivakumaran and A. Paramasivam, “Design and fabrication of high efficiency squirrel cage induction motor using finite element method,” ARPN Journal of Engineering and pplied Sciences. vol. 10, no. 4, March (2015), pp. 1852-1858.

[13] Govindasamy. K. Sathishkumar, “Design and fabrication of high efficiency squirrel cage induction motor using finite element method. ARPN Journal of Engineering and Applied Sciences, vol. 10, no. 4, March 2015.

[14] Motor models furthering based Design–Introducing JMAG RT, Ed: JSOLCorp.,https://www.jmag-international.com/products/pdf/jmag-rt_en.pdf,Date accessed: 30/08/2010.

[15] A.K.Sawhney and A.Chakrabarti, “A course in electrical machine design,” .Dhanpat Rai and Co. (p) Ltd.

An Approach to IoT based Car Parking and Reservation system on Cloud

Vaibhav Hans[1]
Centre of information Technology
University of Petroleum & Energy Studies
Dehradun, India
vaibhav.hans01@gmail.com

Parminder Singh Sethi[2]
Centre of information Technology
University of Petroleum & Energy Studies
Dehradun, India
parmindersinghsethi94@gmail.com

Jatin Kinra[3]
Centre of information Technology
University of Petroleum & Energy Studies
Dehradun, India
jatin.kinra95@gmail.com

***Abstract*— This paper introduces the concept of using IoT and Cloud based technology in car parking services in cities. A high-level view of the proposed system is outlined. Our solution makes the ancient parking system smarter by leveraging the power of IoT and embedding it with the latest innovation of electronic sensors & computers. An IoT-based intelligent car parking system is described. A number of software solutions, including Python, PHP web gateway with MySQL database, Cloud based storage and mobile applications, are proposed to provide pleasant parking experience to mobile users. Also, Data generated by the sensors, Image detection cameras and mobile application will be used to gain insights by storing it in cloud foundry and applying Big Data analytics using Hadoop.**

Keywords—Internet of Things(IoT); Cloud Computing; smart cities; Car Parking; Hadoop; Big Data; Cloud Foundry

I. INTRODUCTION

Since the inception of global computer networks, there has been a vision of smart and communication objects. The essence of connecting everything-to-everything gave birth to terms like Machine-to-Machine (M2M), Radio Frequency Identification (RFID), Wearables and Web of Things. The Internet of Things allows objects to be sensed and controlled remotely across existing network infrastructure [1].

A major problem that people face today is to park their vehicles in multi-level parking lots. Whether its a shopping mall, Airport or a multi national company, facilitating parking is a major part of any infrastructure. The survey of drivers found that 81 per cent say it often takes them 20 minutes or more to find a parking slot, with 45 per cent describing parking as their biggest motoring headache [2]. We plan to create a system which makes this facility hassle free, time saving and convenient for the customers. Today in the era of technology when everything is turning smart, public parking lots are still far away from being smart. Creating an efficient and proficient parking system in real time is still a big challenge for any multi level pubic parking facilities.

II. PROBLEM STATEMENT

The following statement has been divided into two modules for simplicity. The first module focuses on the current demands of the customers and the second module describes the Organizational level challenge.

A. Customer Level

In order to make the entire system easily adaptable and generic for all types of people, There are a lot of parking facilities which people visit on daily basis (e.g.- Offices). Keeping that in mind we have created an addition express entry and express exit for such valuable customers. Standing in queues for entry, searching for a parking slot and then standing in queues again for payment are a big challenge. Also, often people forget the pillar number where they parked their vehicle and end up searching for their vehicle on the entire floor.

B. Organizational Level

With the current progress in the field of analytics and cloud computing, it's a challenge for any organization to gain business insights and enhance customer experience. In order to attain such business advantage it's necessary for any organization to possess humungous amounts of data that can be used by analytical tools to gain insights.

III. OVERVIEW

Before we begin to explain the technical and business components of our solution, lets define our objectives clearly. These objectives are as follows:

A. Objectives

- Allocating the nearest parking slot at the entry point.
- Payment can be done through payment wallet. No need to wait in queues to pay.
- Locate your vehicle through your mobile app.
- Special reservation system for senior citizen/physically handicapped visitors near the lift.
- Image Processing will be used to recognize the number plate.

978-1-4673-7910-6/15/$31.00 ©2015 IEEE

B. Components

- Cloud Foundry is used for storage. Cloud Foundry is an open source cloud-computing platform as a service. (PaaS) [3]
- The express entry check point has a passive infrared sensor (PIR) and a processing board (Arduino UNO, Intel Edison etc.) connected to it.
- Each parking slot has a proximity sensor and LED lights to indicate if a parking slot is available or not.
- Server Side scripts run to allocate the nearest parking slot, calculate the duration for which the vehicle was parked and the total billing amount.
- Mobile application for android and iOS are developed which require the customers to register one time. Also, payment wallets are linked for faster payment.

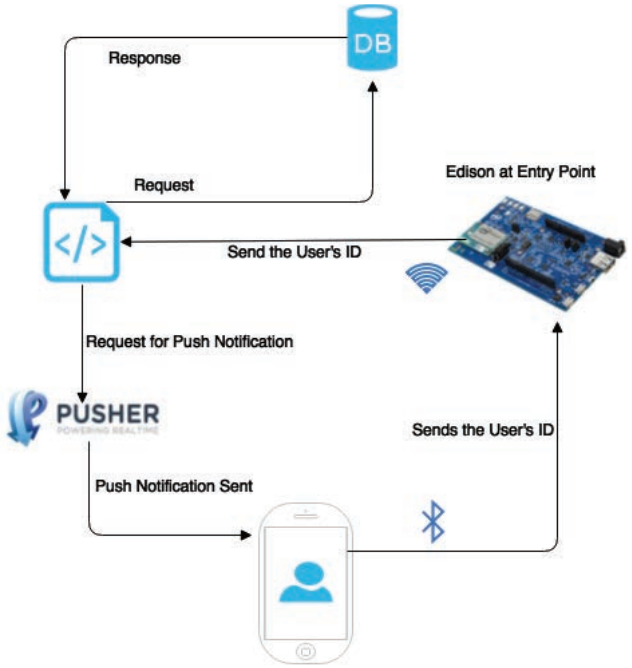

Figure-1. The main components of the IoT-based car parking system

IV. Ease of Use

A. Mobile Application for customers

A mobile application is developed for the customers. By downloading and registering on this mobile application, users can benefit from a wide range of facilities provided to them. They can reserve parking slots (e.g.: near the elevators) before arriving to the facility itself by easily paying through payment wallets. This can be beneficial for a large group of people including senior citizens and physically handicapped citizen. Also, they will get electronically generated parking slip on their app which will have all the details of their vehicle including the slot number where they placed their vehicle.

B. Express Entry and Exit

Customer loyalty and satisfaction is a major priority for any organization. In order to give our registered customers ease of entry and exit, an express entry and exit is available. These entry and exit points will recognize your car by the power of Digital Image processing and allocate you the nearest parking slot available. You don't have to wait in queues anymore to get a parking slip. Your parking details along with the allotted slot will be pushed to your Mobile Application.

Upon express exit, you don't have to stand in queues for payment anymore. As soon as you leave your parking slot, total bill amount will be deducted from your payment wallet and you will get your receipt on your mobile application.

V. Proposed Work

The solution will describe the design and explain the implementation along with a flow chart showing different the interaction of different components.

A. Mobile Application Development

Mobile Application developed for android and iOS will have a one time sign up during which the user is asked to enter his name, phone number, email id, card details and car number. The user can add multiple cars to his account. After successfully signing up he'll be assigned a user id. All his details will be updated in the database and stored in cloud foundry.

B. Sensors

PIR sensor will be used to detect the vehicle at the entry checkpoint. As soon as the vehicle arrives at the entry, the PIR sensor will trigger an event which in our case is the camera at the entry point. This camera will capture the image of the number plate and using digital image processing at the server side identifies the user id of the car owner. Parking slip with the nearest parking slot or the pre-reserved slot will be displayed on the owner's mobile application upon verification. Also, the LED on the allotted slot will turn red indicating that the slot has been booked/allotted.

Once the vehicle is parked on the allotted slot, the proximity sensor installed will trigger and update the database that the car has been parked. Upon completion of this event, the parking time of the customer will start.

C. Payment and exit

As soon as the vehicle leaves the parking slot, proximity sensor will trigger and the timer will stop. The total billing amount will be calculated according to the parking time and will be withdrawn from the linked payment wallet of the

customer. The acknowledgment receipt will be sent on the mobile app and the user's linked email id.

Upon the express exit, as he approaches the barricade, the PIR sensor will trigger thereby capturing the image of the number plate and verifying whether the payment has been done or not. After verification the barricade will open and the customer can drive away.

D. Cloud Tier

The cloud provides data storage and computing resources for the car parking service. It stores the 'big data' of available car parking lots, car parking area, car's location, user's location and profiles, etc. The most recent data is usually stored in the Hadoop's HBase [4] database to support real-time queries, whereas the historical data is serialized to Hive [5] (a warehousing in Hadoop). For computing, a number of Map/Reduce algorithms [6] are used, such as a recommendation algorithm for suggesting the 'best' car parking lots to users, a profile-updating algorithm based on user's parking history, etc. To build an efficient and scalable system, a rule engine Drools [7] is used to make decisions, based on facts, quickly and reliably.

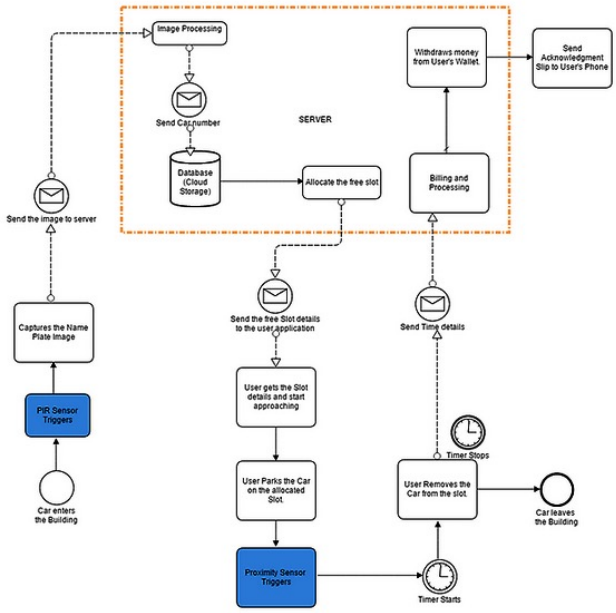

Figure-2. Flow chart of the system.

E. Business Value

- Eco Friendly Solution. Looking for a parking space leads to carbon emission that has major impact on environment.
- Saves Paper. In 2011, Chicago alone recorded 33.1 million meter receipts and about 54.5 tons of waste. [8]
- Since the parking tickets will be digital, Need for human supervisor will be eliminated
- Valuable data generated by the sensors, camera and customer interaction can be used to gain business advantage and insights.
- Providing offers with promotions through mail or mobile app can attract customers.

VII. Conclusion

We have proposed an approach to IoT based car parking and reservation system on cloud. The future scope of the work is to design the algorithm, test the solution and implement it in simulated environment.

Acknowledgment

We are indeed grateful to many groups of people who have helped us with various aspects of this study. We want to thank Mr. Hitesh Kumar, for guiding us. His knowledge and experience about various analytical techniques and ongoing trends influenced us in overcoming many hurdles.

References

[1] "Internet of Things Global Standards Initiative". ITU. Retrieved 26 June 2015.

[2] http://www.telegraph.co.uk/motoring/news/10082461/Motorists-spend-106-days-looking-for-parking-spots.html .

[3] "Cloud Foundry Foundation a Key Driver in PaaS Adoption".

[4] Thusoo, A.; Sarma, J.S.; Jain, N.; Shao, Z.; Chakka, P.; Zhang, N.; Antony, S.; Liu, H.; Murthy, R. HIVE-A petabyte scale data warehouse using hadoop. Available online: http://infolab.stanford.edu/~ragho/hive-icde2010.pdf (accessed on 24 November 2014).

[5] Dean, J.; Ghemawat, S. Mapreduce: A flexible data processing tool. Commun. ACM 2010, 53, 72–77.

[6] Michal, B. Drools JBoss Rules 5.0 Developer's Guide; Packt Publishing Ltd.: Birmingham, UK, 2009.

[7] http://gapersblock.com/mechanics/2013/02/19/parkings-a-mess-45-tons-of-non-recyclable-stickers/

An efficient Cryptographic Algorithm for Securing Biometric Template using AES and Scrambling the Pixels of Row and Column

Manmohan Lakhera
Research Scholar
Uttarakhand Technical University
Dehradun, Uttarakhand
Lakhman07@gmail.com

Dr MMS Rauthan
Dean, Computer Science
HNB Garhwal University
Srinagar Garhwal, Uttarakhand
mms_rauthan@rediffmail.com

Dr Amit Agarwal
Associate Professor
University of Petroleum and Energy Studies
Dehradun, Uttarakhand
coer.info@gmail.com

Abstract **- Ciphering is a main technique to secure the confidentiality of Biometric data at that time when biometric template is send to source to destination via non secure channel. Nowadays biometric is used for providing the better verification system in different field so it is essential to secure the biometric data from illegal access. Proposed paper, we using an AES as a cryptographic algorithm with scrambling the pixels of biometric template using basic principle of Rubki's Cube Algorithm**

Key Word **– Biometric Template, Encryption, Decryption, AES.**

I. INTRODUCTION

Cryptography is an art and science of creating a secrete data. It provides technique for securing, authenticating the transmission of information through non-secure channel. We are protecting data from illegal access or attacker. Cryptographic algorithm is depends upon two type of tool first one is symmetric key and another is asymmetric key. In symmetric key mechanism both source and destination shared the one key for cryptographic operations i.e. encryption and decryption. But in the case of asymmetric key, algorithm require separate keys for encryption and decryption. After analyzing the performance of both cryptographic keys, we find that symmetric key is faster than asymmetric key cryptography. The current study is around the AES. ASE is a robust encryption algorithm. It is a symmetric key block cipher algorithm that process data block of 128 bits using three different cipher keys 128, 192, 256 bits. For performing the basic operation of AES, the complete part of data is distributed into 4x4 array of small block. These 4x4 block of array is called state. The AES is ineffective to provide the better security of biometric template. So to improve the security of biometric template using AES, we are scrambling the pixels of biometric template.

II. LITERATURE REVIEW

Kamal et al.[1] proposed method modify the shift row process of AES. In this modification two row will be shifted with respect to three initial ASE depending based on the parity of 1'st element of status. In this study Liu et. al[2] use gyrator domain method for image encryption. Author use the 2D chaotic mapping for generation the random data for random phase encoding scheme. Zhang and Liu [3] use the permutation diffusion architecture and skew tent map system for image encryption process. For the purpose of shuffling, we are choosing P-box. The size of P box is similar to the size of biometric image. P box is used to shuffles the pixels position to achieve a better security. The key stream in the diffusion step based on the original biometric image and key. M. Zeghid [4] have been introduce a new key stream generation method A5/1, W7 for AES algorithm to improve the performance of AES for image encryption. N.G Baurbakis [5] have been projected that, how to increase the security of secret image. Author show that the centralized storage system is a common defects of these security policies where an entire protected image is usually maintained in single information carrier. If a cracker defects an abnormally in the information carrier in which the protected image is reside, he or she may intercept it and try to decipher the secrete image inside and receive the secrete data. AES is developed by Joan Daemon and Vincent Rijman [6] and has been selected by NIST as standard ciphering algorithm. Four sequential process are executed by the AES algorithm where the process are made on state with 10, 12, 14 rounds based on the key length of 128, 192,256. The first transformation is sub bytes second transformation is shift rows and final transformation is mix column. Mitra, Y et al. [7] use the grouping of three permutation technique in which one is bit level another one is pixels level and finally block level are applied in same order. Zhu et al. [8] use chaos technique for bit level permutation. In this technique not only the pixels position are changed but the value of pixels is also altered. Author [9] proposed that the image is different from the text in lots of aspect like high correlation among pixels and high redundancy. It means that the cryptographic algorithm is used for text is not sufficient for securing an image. So a diversity of new encryption algorithm is developed for securing a biometric image. Samlim M wade [10] proposed the solution of AES algorithm's drawback like high computation pattern remain in ciphered image. Author explain that the above problem is more complicated when we are using a high definition images for encryption. Two solution is introduce by author to resolve the above problem first one is to decrease the number of round and another one is replace the existing S-box with new developed S-box. Author [11] introduce the permutation diffusion and total shuffling technique for securing the image. In this technique P-box is used in permutation where the shuffling of pixels position of a biometric image is based on its own P-Box. Amnesh Goel et al. [12] proposed that before encryption of an

978-1-5090-3411-6/16 $31.00 © 2016 IEEE
DOI 10.1109/ICMETE.2016.112

image rearrange the pixels of an image on the basis of RGB values then send it for encryption. P. K. Naskar et al. [13] use linear geometry for developing a new encryption algorithm. In this algorithm pixels of ciphered image again shuffled. In the proposed paper author used two technique as substitution and transposition.

III NOTATIONS

Symbol	Meaning
b1, b2	Two Prime number
Rmax	Maximum row in the biometric template
Cmax	Maximum column in the biometric template
m	Size of row of column
PMAT	Plaint biometric template matrix
CMAT	Cipher matrix of biometric image
p	Number of place shifting
AES	Advance Encryption Standard

IV. PROPOSED ALGORITHM

Protecting the biometric template is an essential issue now-a-days. In the proposed research, the algorithm start with taking a prime numbers b1 and b2. PMAT store the extracted feature of the biometric template and Rmax, Cmax store the maximum row and column of PMAT. Scrambling the column and row is depend upon the output of S. If the output of S is 0 then shift the row left and column up, if output is 1 then shift row right and column down. Finally the scrambled matrix is send to the AES algorithm.

A. Encryption Algorithm

Begin:

Input b1, b2=prime numbers
PMAT =Biometric Template
(R_{max}, C_{max})=size (PMAT)
Loop 1 to R_{max}
Loop i=1: m

$$sum_{row\_i} = \sum_{i=1}^{m} PMAT(i,j)$$

$$M_{row\_i} = sum_{row\_i} (mod\ b_1)$$
$$S_{row\_i} = M_{row\_i} (mod\ 2)$$
If $S_{row\_i} = 0$ then
PMAT=right_shift (PMAT, p)
If $S_{row_i} = 1$then
PMAT=left_shift (PMAT, p).
End
End

Loop 1 to C_{max}
Loop j=1 to m

$$sum_{col\_j} = \sum_{j=1}^{m} PMAT(i,j)$$

$$M_{col\_j} = sum_{col_j} (mod\ b_2)$$
$$S_{col\_j} = M_{col\_j} (mod\ 2)$$
If $S_{col\_j} = 0$ then
PMAT =shift_up (PMAT, p)
If $S_{col\_j} = 1$ then
PMAT =shift_down (PMAT, p)
End
End
CMAT=AES (PMAT)

END

B. Decryption algorithm

BEGIN:
(R_{max}, C_{max})=size (CMAT)

Loop 1 to C_{max}
Loop j=1 to m

$$sum_{col\_j} = \sum_{j=1}^{m} CMAT(i,j)$$

$$M_{col\_j} = sum_{col\_j} (mod\ b_2)$$
$$S_{col\_j} = M_{col\_i} (mod\ 2)$$
If $S_{col\_j} = 0$ then
CMAT =shift_up (CMAT, -p)
If $S_{col\_j} = 1$ then
CMAT =shift_down (CMAT, -p)

Loop 1 to R_{max}
Loop i =1: m

$$sum_{row\_i} = \sum_{i=1}^{m} CMAT(i,j)$$

$$M_{row\_i} = sum_{row\_i} (mod\ b_1)$$
$$S_{row\_i} = M_{row\_i} (mod\ 2)$$
If $S_{row\_i} = 0$ then
CMAT=shift_up (CMAT, -p)
If $S_{row_i} = 1$then
CMAT=shift_down (CMAT, -p).

PMAT=AES (CMAT)

END

V. BLOCK DIAGRAM OF PROPOSED ALGORITHM

A. *Encryption Diagram*

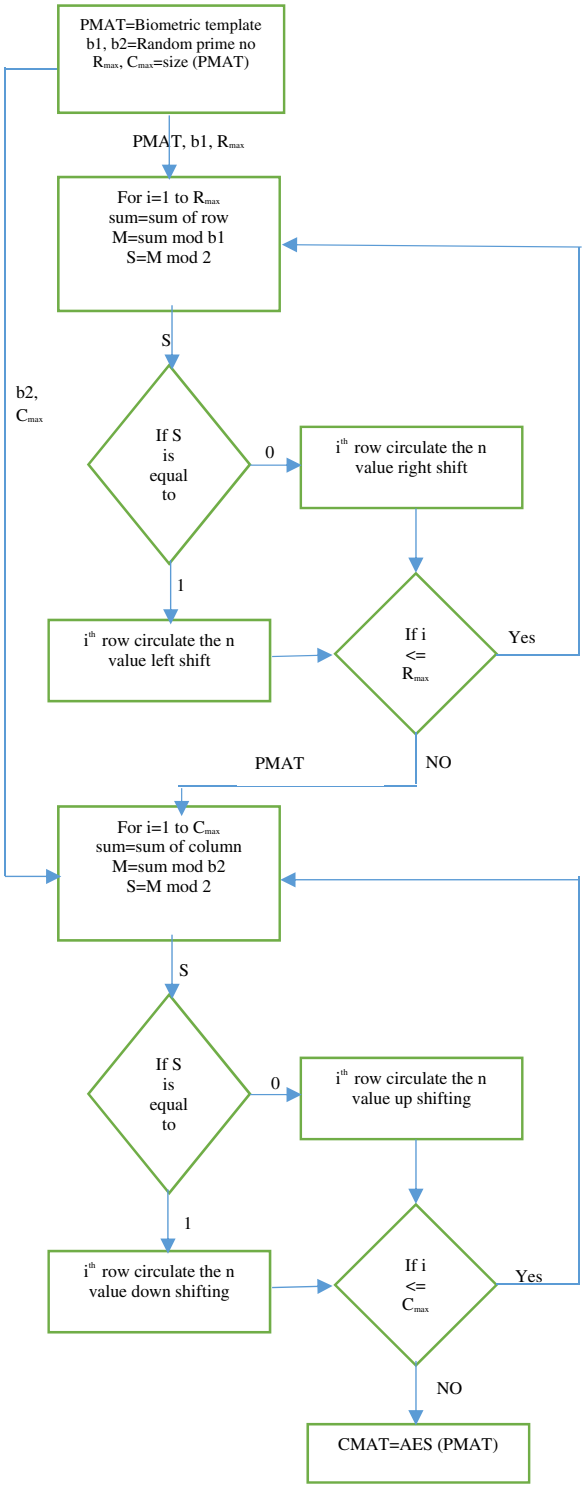

Figure 1 Encryption Algorithm of proposed method

B. *Decryption Diagram*

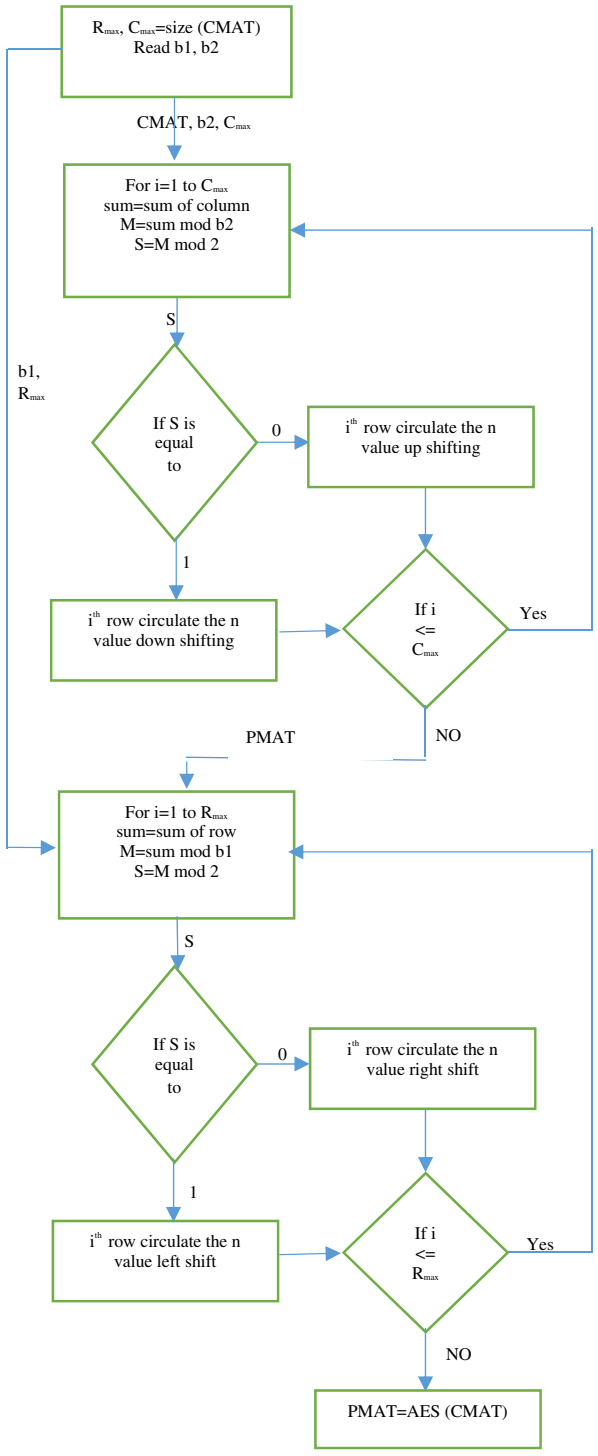

Figure 2 Decryption Algorithm of proposed method

VI. CONCLUSION

In the suggested algorithm, the biometric template is secure using AES Algorithm with Scrambling in the pixels of row and column. The proposed algorithm is compared with the AES algorithm and produces a better result as compared to the traditional AES algorithm. In the future, we will present a result comparison among the existing and proposed method.

REFERENCES

[1] Kamali, S., H., Shakerian, R., Hedayati,., Rahmani, "A New Modified Version of Advanced Encryption Standard Based Algorithm for Image Encryption". International Conference on Electronics and Information Engineering, IEEE, 2010.

[2] Z. Liu, L. Xu, C. Lin, J. Dai, and S. Liu, "Image encryption scheme by using iterative random phase encoding in gyrator transform domains," Optics and Lasers in Engineering, vol. 49, no. 4, pp. 542–546, 2011

[3] G. Zhang and Q. Liu, "A novel image encryption method based on total shuffling scheme," Optics Communications, vol. 284, no. 12, pp. 2775–2780, 2011

[4] M. Zeghid, M. Machhout, L. Khriji, A. Baganne, and R. Tourki, "A Modified AES Based Algorithm for Image Encryption," World Academy of Science, Engineering and Technology, 2007

[5] S.S. Maniccama, N.G. Bourbakis, "Image and video encryption using SCAN patterns", in Pattern Recognition 37, pp 725 – 737,2004.

[6] NIST, Advanced Encryption Standard (AES), Federal Information Processing Standards Publication 197, 2002

[7] A.Mitra, Y. V. Subba Rao and S. R. M. Prasanna, "A New Image Encryption Approach using Combinational Permutation Techniques", International Journal of Electrical and Computer Engineering 1:2, communications on ACM, 2006

[8] Zhi-liang Zhu, Wei Zhang, Kwok-wo Wong, Hai Yu, "A chaos-based symmetric image encryption scheme using a bit-level permutation", Information Sciences 181 1171–1186 Elsevier, 2010.

[9] G. Zhang and Q. Liu, "A novel image encryption method based on total shuffling scheme," Optics Communications, vol. 284, no. 12, pp. 2775–2780, 2011.

[10] Salim M. Wadi, Nasharuddin Zainal, "Rapid Encryption Method based on AES algorithm for Gray Scale HD Image Encryption", ICEEI 2013, Procedia Technology, vol.11, pp.51-56, 2013.

[11] Yan Shen, Guoji Zhang, XCuan Li, Qing Liu, "An Improved Image Encryption Method Based on Total Shuffling Scheme", Advances in CSIE, SpringerVerlag, vol.2, AISC-169, pp.643-650, 2012.

[12] Amnesh Goel, Nidhi Chandra, "A Technique for Image Encryption with Combination of Pixel Rearrangement Scheme Based on Sorting Group-Wise of RGB Values and Explosive Inter-Pixel Displacement", International Journal of Image, Graphics and Signal Processing, vol.2, pp.16-22, 2012

[13] P. K. Naskar, A. Chaudhuri, A. Chaudhuri, "A secure symmetric image encryption based on linear geometry", Applications and Innovations in Mobile Computing (AIMoC), IEEE, pp.67-74, 2014.

SAE INTERNATIONAL®

An Experimental Study of Mechanism of Body Panel Vibration in Booming Noise Reduction of Passenger Vehicles

2016-28-0198

Published 02/01/2016

Joydeep Chatterjee and Harveen Talwar
Maruti Suzuki India Ltd

Srishti Garg
University of Petroleum Energy Studies

CITATION: Chatterjee, J., Talwar, H., and Garg, S., "An Experimental Study of Mechanism of Body Panel Vibration in Booming Noise Reduction of Passenger Vehicles," SAE Technical Paper 2016-28-0198, 2016, doi:10.4271/2016-28-0198.

Abstract

In a typical passenger vehicle, there can be different types of noises generated which are broadly categorized as Interior Noise and Exterior Noise. The interior noise sources can be further classified into noises which can be Structure Borne or Air Borne. One of the major sources of both structure borne and airborne noise generation is the powertrain of the vehicle. The structure-borne noise and vibrations generated from the powertrain is usually transferred to the vehicle body through its attachment points to the body and the powertrain driveline. These induced body vibrations can sometimes cause the acoustic cavity of the passenger cabin to go into resonance which results in an annoying and disturbing noise for the passengers, called Booming Noise. Very often, one or more than one vehicle body panels show a dominant contribution in inducing this acoustic cavity resonance. In this research, the backdoor of the selected passenger cars were identified to be one of the primary contributors in causing the booming noise phenomena. The objective of this research was to study the mechanism of the contribution of backdoor towards booming noise in these hatchback style passenger vehicles. The study was carried out on three differently styled hatchbacks namely Model A, Model B, and Model C. The study of the mechanism behind this contribution was carried out in three phases. The first phase included the response measurements of the individual grid points created on the backdoor which were excited using a low frequency sound source. In the second phase, a computer model of the grid structure of the backdoor was created and the response measurements obtained were superimposed on the geometry model to identify the modal parameters of the backdoor. The identification of the modal parameters helped in understanding the modal behavior of the backdoor which is causing the acoustic resonance of the cabin cavity thus creating the booming noise phenomena. In the third phase, in cabin acoustic measurements were carried out during vehicle acceleration tests and the results were correlated with the modal parameter data. This helped in identification of the dominant modal frequencies to be targeted for further design improvements during concept & vehicle design stage.

Introduction

In the automotive community, the term NVH has been widely used to describe unwanted sound and vibration. In the current market scenario, vehicle sound and vibration are major qualities that customers consider when they purchase a vehicle [1]. They are a measure of ride comfort and perceived quality and reliability. The combination of vibration and noise is one of most significant performance indexes of a vehicle. Interior noise control and vibration reduction as well as sound quality design of a vehicle are critical for attracting customers. The vehicle noise can be broadly classified into Exterior and Interior Noise. The interior noise and vibration problems in a vehicle can be typically caused by the vehicle powertrain, tire-road interaction or the vehicle body interaction with the wind [2]. The typical requirement is to reduce noise and/or vibration levels; to eliminate the characteristics that are annoying to the customer; and that are delightful to the customer to give the customer the needed impression about the vehicle such as its sportiness, responsiveness. When one or more of these noise generating sources excite the acoustic modes of the vehicle cabin, a phenomena called booming noise is produced.

Booming Noise

Booming noise is an important part of vehicle interior noise. Interior ‘boom’ noise in the passenger compartment of an automotive vehicle results from the vibration excitation of the vehicle body panels that couple with the lower-order interior acoustic modes of the passenger compartment cavity [3]. Road and powertrain loads are the typical sources of causing such structure-borne excitations in a passenger vehicle. The interaction between these structural and acoustic modes in the low to mid-frequency range (approximately 20 ~ 200 Hz) creates a resonance behavior inside the cabin [2]. For the customer, this low frequency acoustic cavity resonance might be perceived as a low tone rumbling noise which will create some hearing discomfort [4].

One of the conventional ways to reduce this booming noise phenomena is to reduce the excitation force generation at the source itself (powertrain, tire-road interaction etc) resulting in reduction of excitation energy to create the resonance effects. However, very often automotive OEMs face a common challenge that reduction of the force excitation at the source level is not possible due to various constraints. Hence, studying the effect at the vehicle body side becomes important for an NVH engineer so that he/she can take the necessary counter-measure.

Experimental Modal Analysis of the vehicle body structure is one of the most important technical methods to identify the structural excitation phenomena.

Experimental Modal Analysis

Experimental Modal Analysis is a process whereby we determine a structure in terms of its natural characteristics which are Frequency, Damping and Mode Shapes [5]. This step is normally carried out to obtain the mode shape (also called spatial description of amplitudes of each structural resonance of interest). A series of frequency response measurements is typically made between a single excitation point and several response points. The modal parameters namely the modal frequencies, damping, and mode shapes are identified by performing further computation (curve fitting) on this set of measurements [6]. These mode shapes approximates the predominant vibratory motion of the structure at each resonant frequency and hence provide a further insight into the problem. At this point, it must be decided whether the excitation source should be reduced or eliminated, or whether the structural dynamics must be changed to control the problem. Many a times, it is not feasible to reduce the level of excitation or alter its frequency content. Therefore the problem should be solved by altering its structural behaviour.

Frequency Response Function (FRF)

The FRF (Frequency Response Function) is a fundamental measurement that isolates the inherent dynamic properties of a mechanical structure The FRF describes the input-output relationship between two points on a structure as a function of frequency [5].

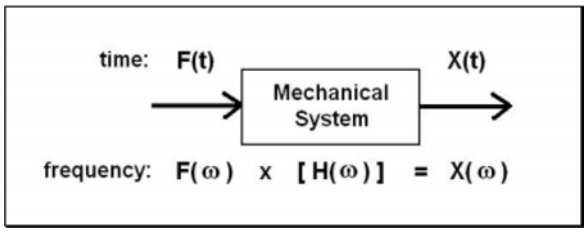

Equation 1

Equation 1 above also indicates that an FRF is defined as the ratio of the Fourier transforms of an output response (X (w)) to the input force (F (w)) that caused the output.

Problem Definition

In this paper, three differently styled hatchback vehicles (Model A, Model B & Model C) were selected wherein cabin booming noise was observed to be a problem. Very often, the vehicle Backdoor in hatchback style passenger vehicles is observed to be one of the main contributors to booming noise so study of the same becomes important. A study was done to carry out experimental modal analysis of the vehicle backdoor of all three models - A, B & C and establish the resonant frequencies of the same. Further, interior cabin noise measurements were taken during driving condition and a correlation with the Modal Parameter data obtained previously was studied for identification of the dominant modal frequencies to be targeted for further design improvements during concept & vehicle design stage.

Backdoor Panel Modes Measurement

The experimental modal analysis was conducted in two major phases - the panel mode testing and the modal analysis. The panel mode testing aims to measure the frequency response functions and the modal analysis involves the extraction of mode shapes by analyzing these frequency response functions (FRF's), coherence and the response phases of the structure [5]. A Data Acquisition System along with the piezo-electric acceleration sensors and a Low frequency Sound Generator was used for the Panel Mode Testing.

Test Setup

The following is the pictorial representation of the connections in the test setup (Figure 1). The transducers are mounted on the test structure. The transducers are then connected to the DAQ system. The low frequency sound generator is also connected to the DAQ system. The input module is connected to the PC through the LAN wire.

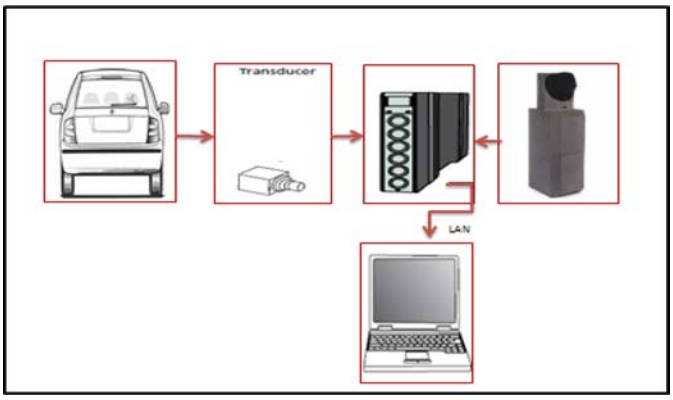

Figure 1. Layout of the Project Set-up

Test Methodology

The vehicle Backdoor of each of the three selected vehicles - Model A, B & C was divided into an evenly spaced grid size depending upon the size of the backdoor of each vehicle. The sound generator, capable of producing a noise signal from 20 Hz ~ 800 Hz frequency of uniform energy, was placed at the front cabin location and was excited by a random white noise signal and the vibration responses were measured on the backdoor using accelerometers. FRF functions (accelerance) were subsequently calculated. The step-by-step process of the EMA measurement is explained as follows:

1. First, the backdoor was divided into a finite number of evenly spaced grid points and the coordinates of these grid points were measured using the Global coordinate System (Figure 2).
2. Next the acceleration responses at these points are recorded via piezo-electric accelerometers mounted on the panel surface using adhesive (Figure 4). Care is taken to avoid

adding the weight of the transducer cables on the backdoor for accuracy purposes.

3. All the sensors were calibrated using Industry Standard Transducer Calibrator before carrying out the experiment. More importantly, directions of the acceleration sensors were correctly adjusted to match the axis of the geometric model for accurately capturing the modal behavior of the structure.
4. Using the Data Acquisition software PULSE LABSHOP 14.1.1, a random white noise signal of 20 ~ 200 Hz frequency band was produced and fed into the sound generator. Sufficient number of averages was taken during measurement to avoid any digital signal processing errors and increase accuracy of the measurement.
5. The procedure was repeated for other points and the FRF and Coherence data was acquired during the measurement for all the grid points.

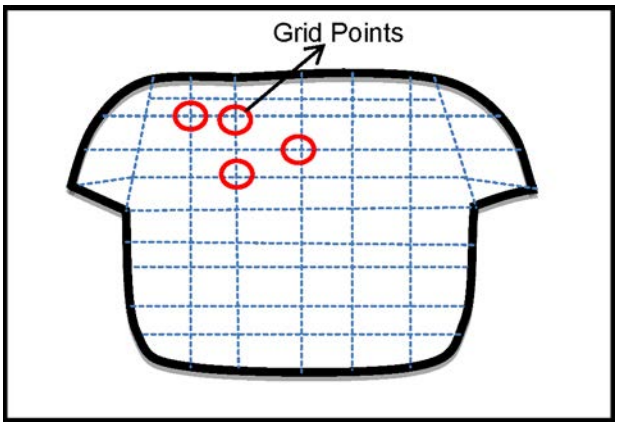

Figure 2. Grid Point Distribution on backdoor panel

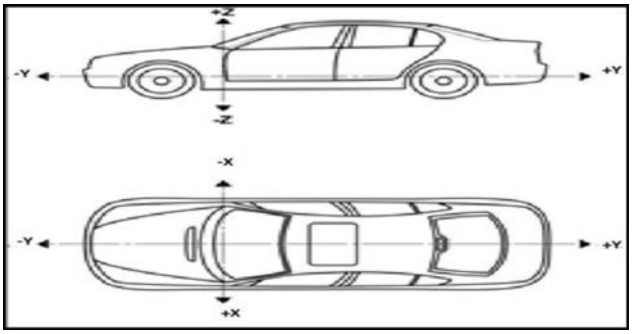

Figure 3. Global Coordinate System-Arrows pointing towards the Coordinate Axes.

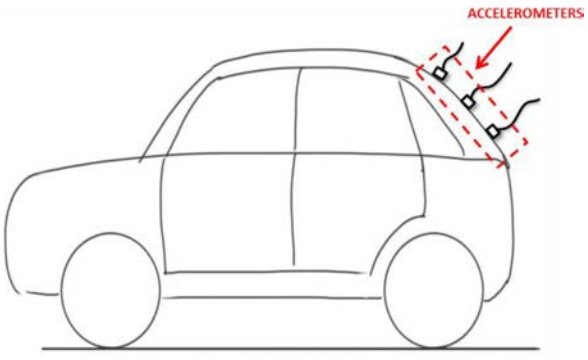

Figure 4. Mounting of accelerometers - side view

For each set of FRF data acquisition, it was ensured that the energy of the sound source generated was as uniform as possible throughout the frequency band and the coherence function of the response points with respect to the sound source is close to 1.

UFF files of the FRF functions were extracted in PULSE LABSHOP for analysis of the Mode shapes in the LMS Test.Lab software platform.

The coordinates of each grid point was measured in three dimensions as measured during the measurement according to the Global Coordinate System (Figure 3) and the geometry was created in LMS using these coordinate points.

Data Analysis

The coordinate points measured in each direction X, Y and Z respectively are used to create a CAD geometry of the backdoor of the three vehicles namely, Model A, B and C in LMS Test.Lab software. The following images depict the geometries of the backdoor of the 3 vehicles as created in LMS Test Lab. Figure 5, Figures 6 & Figure 7 denote the backdoor geometries created for Model A, B & C respectively. The figures 5,6 & 7 help in identifying the differences in the overall shape of the backdoor.

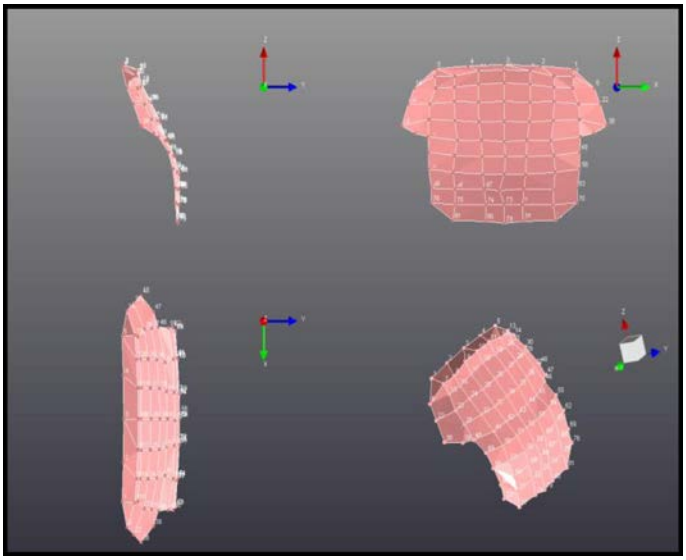

Figure 5. Geometry of Model A Backdoor.

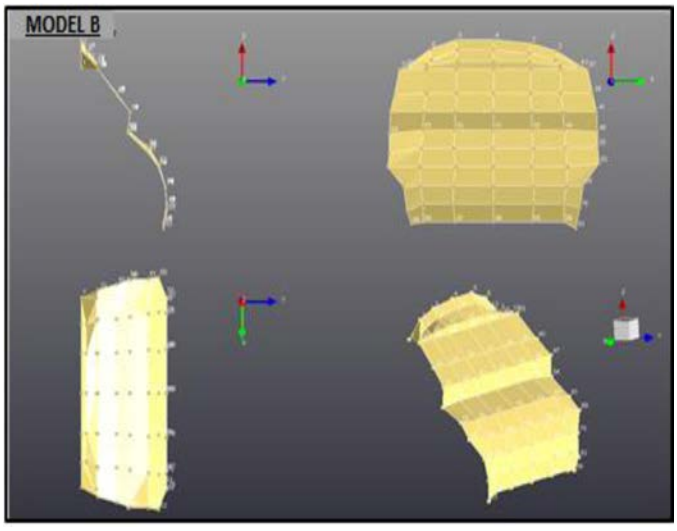

Figure 6. Geometry of Model B Backdoor.

After the geometries of the backdoor are created in the software, the FRF measurements captured in the test are imported into the POLYMAX Modal Analysis module in LMS Test.Lab.

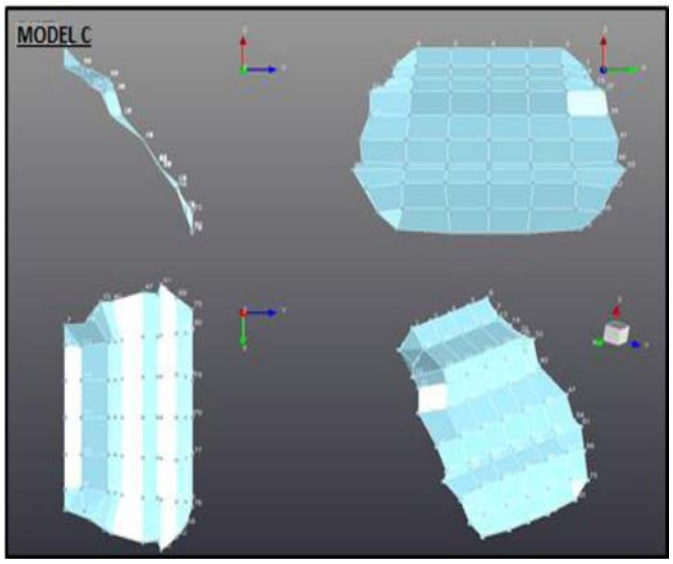

Figure 7. Geometry of Model C Backdoor.

PolyMAX Modal Analysis

The LMS PolyMAX method is a further evolution of the original LSCF estimation method, which was introduced to find initial values for the iterative maximum likelihood method. The main benefits of the PolyMAX algorithm, or poly-reference version of the LSCF Method was developed are that the SVD step to decompose the residues can be avoided and that closely spaced poles can be separated [7]. This method yields very clean Stabilization Diagrams easing the problem of selecting the model order and the best structural system poles [7].

A Stabilization Diagram is obtained after calculation of the FRF functions in the Modal Matrix. Figure 8 shows the stabilization diagram of the Front Cabin for one of the three test vehicles. A similar Stabilization Diagram is obtained for the other backdoor models too. The interpretation of the stabilization diagram yields a set of poles which are also called the eigen frequencies. The peaks highlighted in red appeared to be the most stable peaks where the eigen frequencies show a very strong modal behavior [5]. These stable peaks were only considered for further processing to obtain the mode shapes.

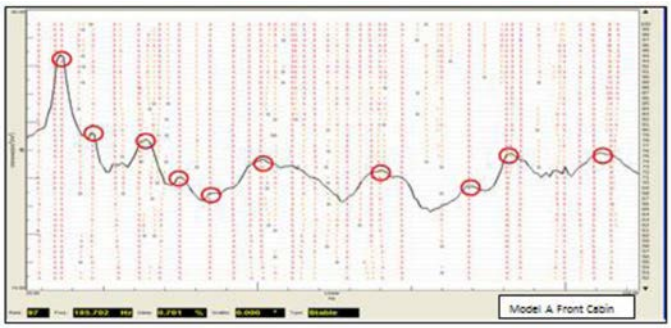

Figure 8. Stabilizing Diagram for Model A Front Cabin

Observations

Graph1 shows the SumFRF curve of all the grid points for the front cabin excitation for Model A. Graph 2 shows the SumFRF curve for Model B and Graph 3 shows the SumFRF curve for Model C. Two major Eigen frequencies at 36 Hz and 65 Hz are observed. The mode shape of these two major frequencies was analyzed further. Mode 1 at 36Hz is seen to be the First Bending Mode while the Mode 2 at 65 Hz is observed to the First Torsion Mode of the Backdoor. Table 1 shows the mode shapes obtained for the all the three vehicle backdoor models.

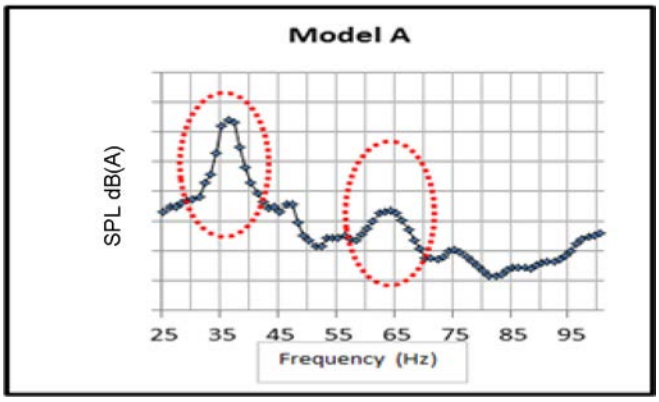

Graph 1. Sum FRF for Model A: Front Cabin

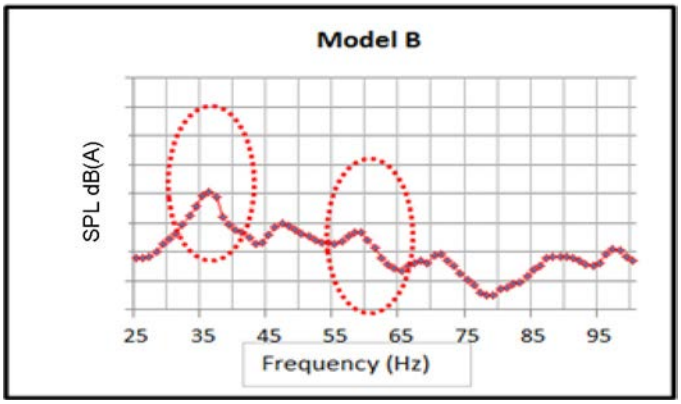

Graph 2. Sum FRF Curve for Model B: Front Cabin

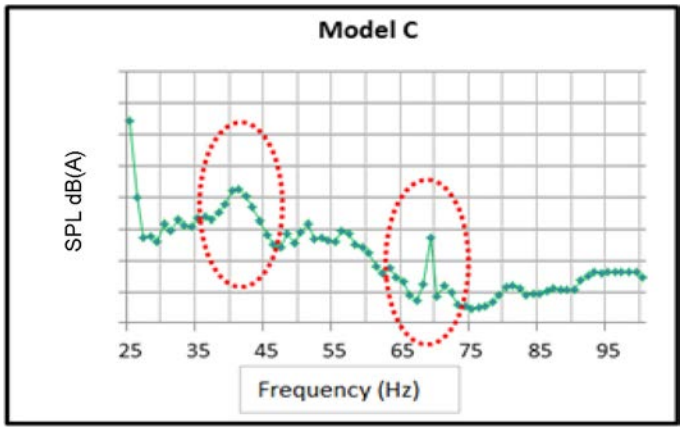

Graph 3. Sum FRF Curve for Model C: Front Cabin

- In Model A, First Bending Mode is observed at the Backdoor at 35 Hz, while the First Torsion Mode occurs at 65 Hz (Graph 1).

- In Model A, First Bending Mode is observed at the Backdoor at 35 Hz, while the First Torsion Mode occurs at 60 Hz (Graph 2).
- In Model A, First Bending Mode is observed at the Backdoor at 40 Hz, while the First Torsion Mode occurs at 67 Hz (Graph 3).

Table 1. Comparison between frequencies of all three models- Front Cabin

FRONT CABIN NOISE			
	Model A	Model B	Model C
First Bending (Hz)	35	35	40
First Torsion (Hz)	65	60	67

The following graphs show the SumFRF graphs for the Rear Cabin for all three hatchback models - Graph 4 for Model A, Graph 5 for Model B & Graph 6 for Model C respectively.

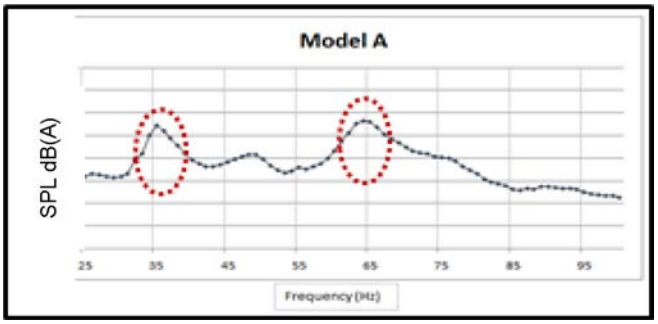

Graph 4. Sum FRF Curve for Model A - Rear Cabin

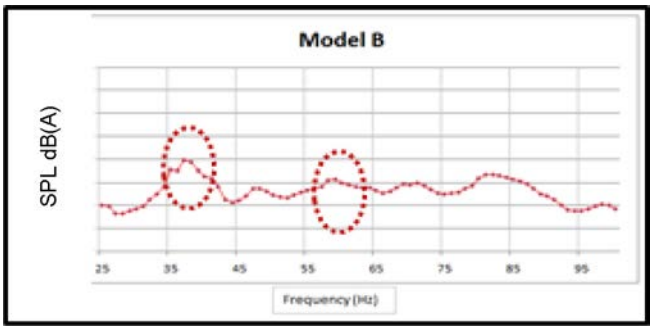

Graph 5. Sum FRF Curve for Model B - Rear Cabin

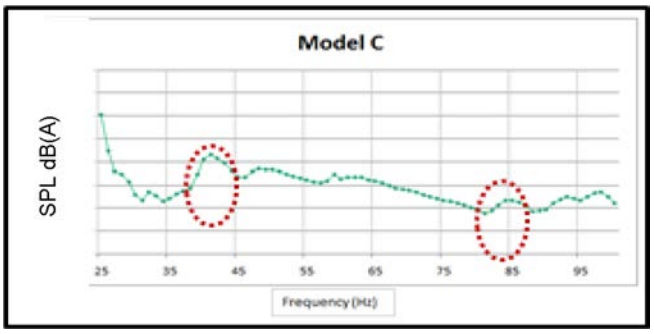

Graph 6. Sum FRF for Model C - Rear Cabin

Table 2 shows the Eigen Frequencies obtained for the three models by placing the Sound Generator in the Rear Cabin.

Table 2. Comparison between frequencies of all three models- Rear Cabin

REAR CABIN NOISE			
	Model A	Model B	Model C
First Bending (Hz)	35	37	42
First Torsion (Hz)	65	60	85

- In Model A, First Bending Mode is observed at the Backdoor at 35 Hz, while the First Torsion Mode occurs at 65 Hz (Graph 4).
- In Model A, First Bending Mode is observed at the Backdoor at 37 Hz, while the First Torsion Mode occurs at 60 Hz (Graph 5).
- In Model A, First Bending Mode is observed at the Backdoor at 42 Hz, while the First Torsion Mode occurs at 85 Hz (Graph 6).

Operational Data

It was previously observed that each of the three selected vehicles used for this study project (Model A, Model B, Model C) had an issue of booming noise at a particular engine RPM band. Cabin noise data at the Front Cabin and Rear Cabin at the human ear location was recorded during full load acceleration condition. A relationship between the operational measurement of cabin noise in operational condition and the extracted modal parameters of the back door was established. Mode shapes were extracted for each node for the three models. The order data for front and rear cabin noise was referred for identifying the dominant frequencies, and hence the possible contribution of back door towards this phenomenon.

Graph 7, 8 and 9 represent the 1st engine order data recorded at the Front Cabin & Rear Cabin during 5th gear acceleration condition for Model A, B and C respectively.

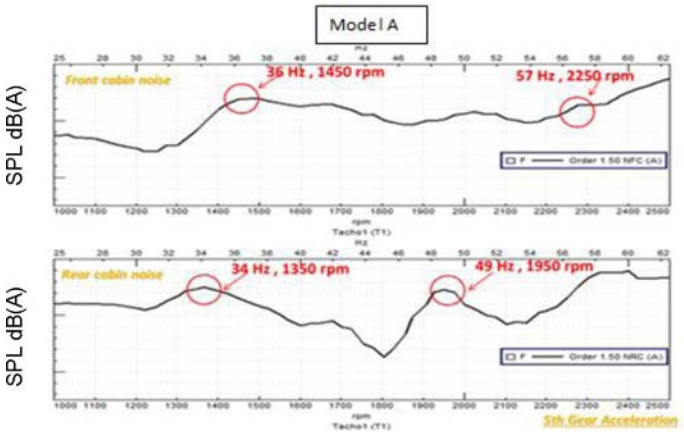

Graph 7. Order data for Model A

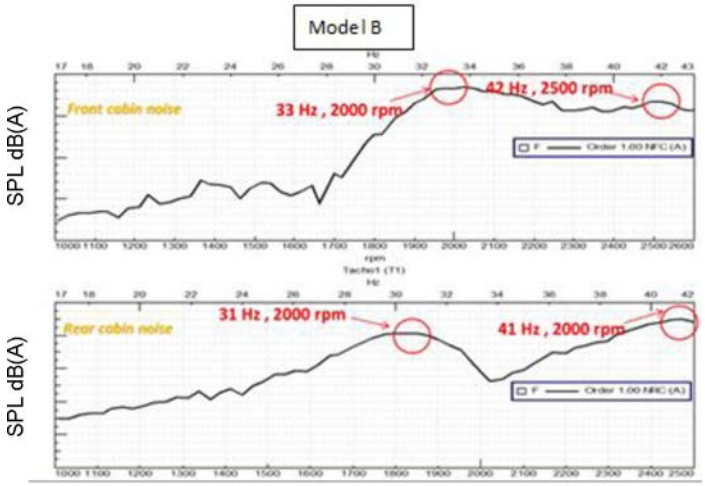

Graph 8. Order data for Model B

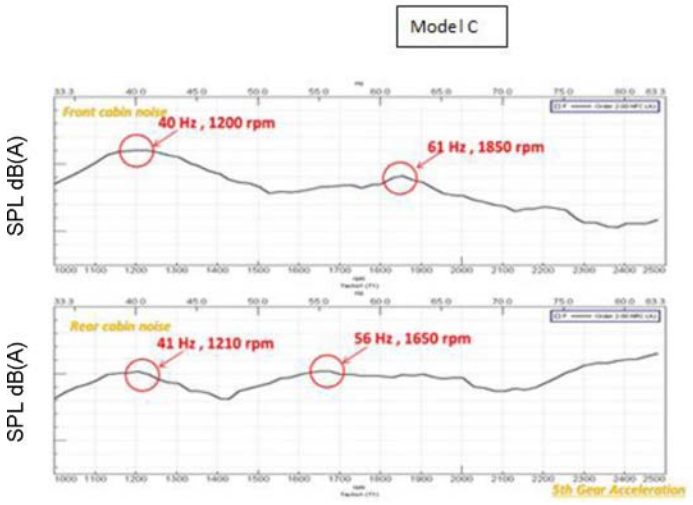

Graph 9. Order data for Model C

Summary/Conclusion

On studying the operational data and analyzing the mode shapes obtained through modal analysis, it could be established that high levels of response (or peaks) in the operational data are closely corresponding with the structure resonance of the vehicle Backdoor, or in other words - the natural frequency of the back door is getting excited due to an amount of drive-line excitation force.

Figure 11, 12 &13 shows the Mode shapes at the frequency excited during the operational condition for Model A, B and C respectively along with their corresponding operational data. These mode shapes approximates the predominant vibratory motion of the structure at each resonant frequency, and provides further design insight into the problem. It could be seen that the mode shapes obtained experimentally are in good co-relation with the frequencies extracted from the operational data for front cabin and rear cabin excitation experimentally. The frequencies highlighted in red are the frequencies corresponding to the natural mode shapes of the backdoor as obtained from the operational run up data.

The contribution of structure resonance of back door to the booming noise problem has been studied and it has been observed that the problem is getting amplified due to resonance of the back door panel near the problem frequencies.

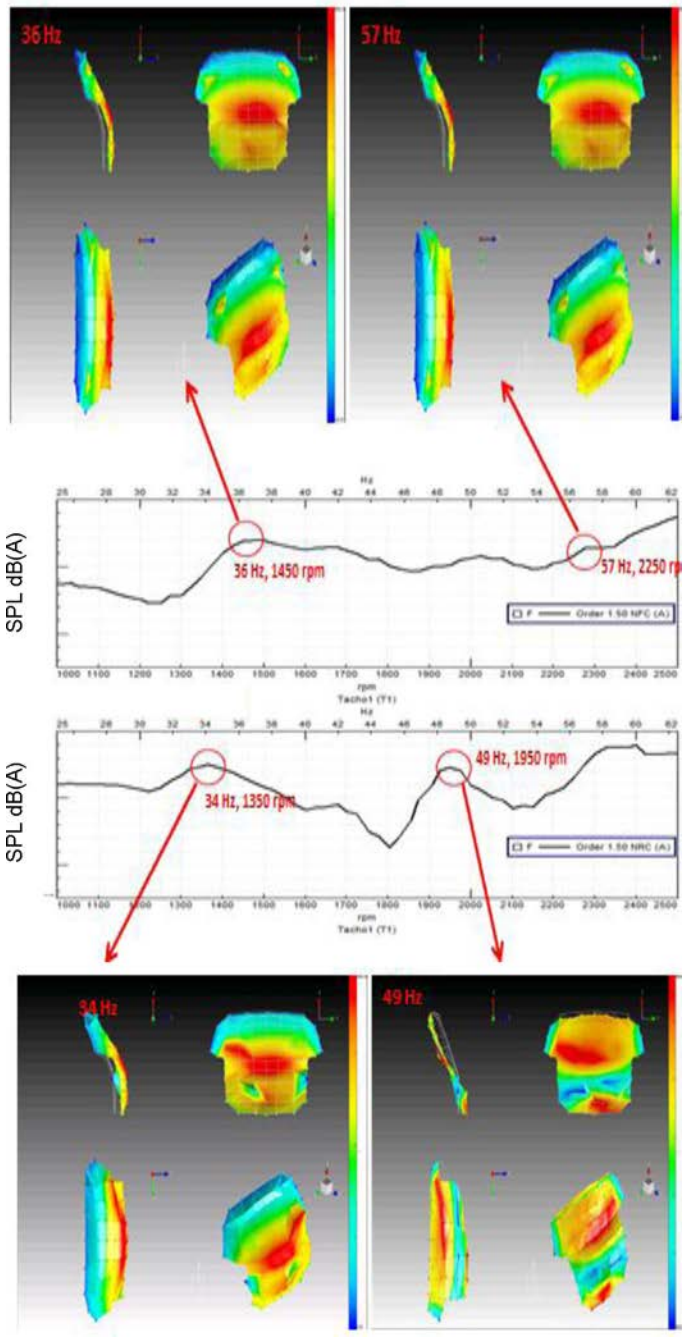

Figure 9. Mode Shape Correlation with Run Up data for Model A

Recommended modifications that were identified to improve the structural behavior are improving the damping of the structure for attenuating the amplitude of the troublesome resonance, increase in the panel stiffness which will alter the characteristic response of the

structure and shift the resonance to a higher or lower frequency to avoid the excitation. Feasibility of adding a dead block mass at certain location(s) can also be explored to alter the structural behavior.

Future Scope

During the early phases of vehicle conceptualization, a well correlated CAE model of the full vehicle structure to study the effect of backdoor resonance and further carry out design changes to negate any such resonance behavior, keeping the overall styling aspect of the product similar.

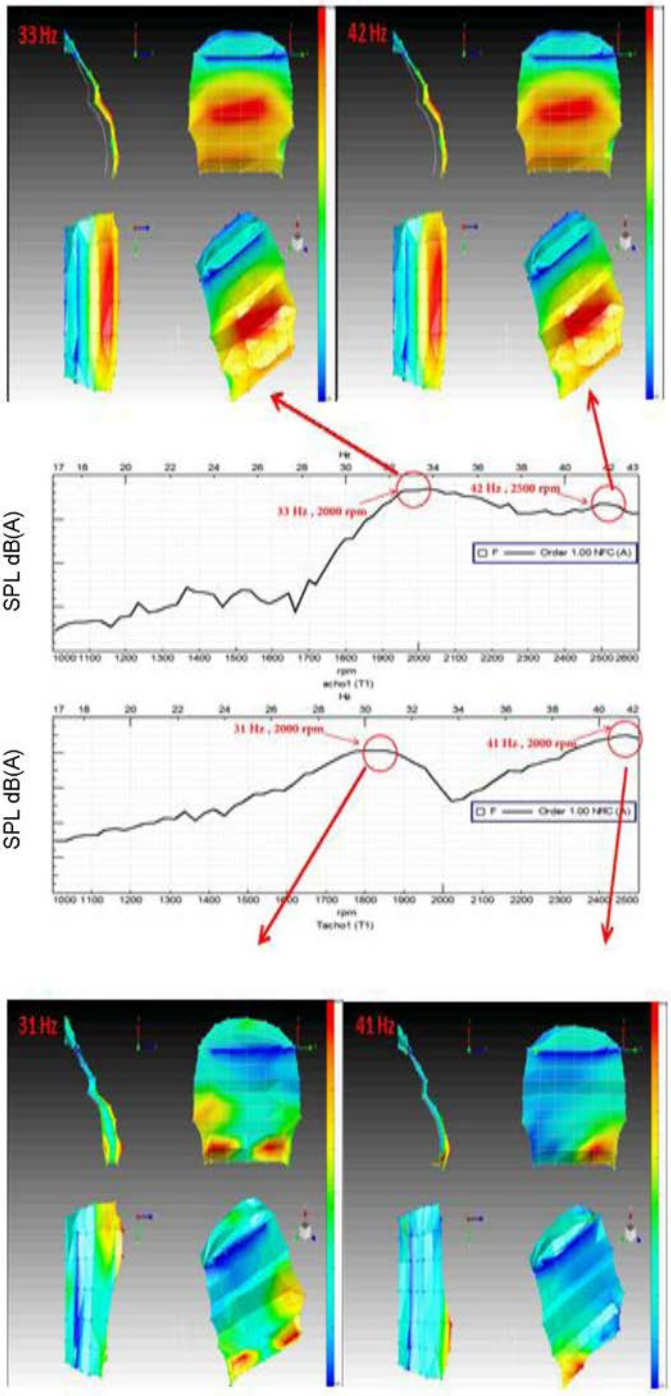

Figure 10. Mode Shape Correlation with Run Up data for Model B

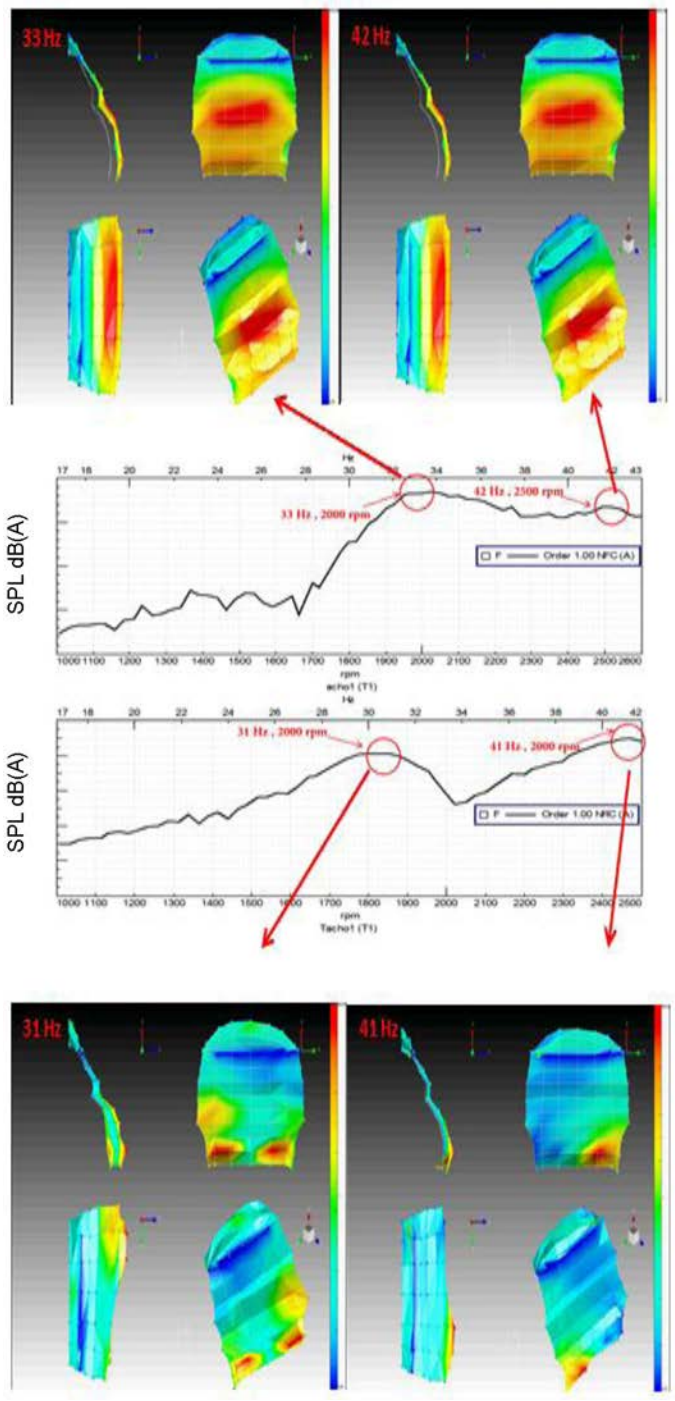

Figure 11. Mode Shape Correlation with Run Up data for Model C

References

1. Huston, R., and Liu, C. Q., “Principles of Vibrational Analysis with Applications in Automotive Engineering”, SAE International, Warrendale, PA, ISBN 978-0-7680-3339-7, 2011, doi:10.4271/R-395.
2. Harrison, M., “Vehicle Refinement, Controlling Noise and Vibration in Road Vehicles”, Society of Automotive Engineers, Inc., Warrendale, PA, ISBN 978-0-7680-1505-8, 2004, doi: 10.4271/R-364.
3. Lee, D., Hwang, W., and Kim, M., "Booming Noise Analysis in a Passenger Car Using a Hybrid-Integrated Approach," SAE Technical Paper 2000-01-0723, 2000, doi:10.4271/2000-01-0723.

4. University of Cambridge, “Dynamics and Vibration Research Group; Prediction of Vehicle Interior Noise”, http://www-mech.eng.cam.ac.uk/dynvib/research/rsl/v_noise.html, accessed Aug. 2015
5. Schwarz Brian J. & Richardson Mark H., “Experimental Modal Analysis”, Vibrant Technology, Inc. Jamestown, California 95327, Oct. 1999
6. Ramsey Kenneth A., “Experimental Modal Analysis, Structural Modifications and FEM Analysis on a Desktop Computer”, Structural Measurement Systems, San Jose, California, Sound and Vibration, Feb. 1983
7. Peeters Bart, Lowet Geert, Van Der Auweraer HermanAnd Leuridan Jan, A New Procedure For Modal Parameter Estimation, LMS International, Leuven, Belgium, SOUND AND VIBRATION / JANUARY 2004

Contact Information

Joydeep Chatterjee
Deputy Manager, Vehicle Testing (NVH)
Maruti Suzuki India Ltd
India
Joydeep.chatterjee@maruti.co.in

Acknowledgments

The authors would like to thank the team of senior Mr. Sunil Malhotra and Mr. C.V. Raman for their continuous support and encouragement throughout the duration of this study.

Definitions/Abbreviations

NVH - Noise, Vibration & Harshness

EMA - Experimental Modal Analysis

FRF - Frequency Response Function

RPM - Revolutions Per Minute

Hz - Hertz

CAD - Computer Aided Design

OEM - Original Equipment Manufacturer

DAQ - Data Acquisition

LAN - Local Area Network

PC - Personal Computer

UFF - Universal File Format

LSCF - Least Squares Complex Frequency

SVD - Singular Value Decomposition

SPL - Sound Pressure Level

dB(A) - Decibel in A-Weighted Scale

The Engineering Meetings Board has approved this paper for publication. It has successfully completed SAE’s peer review process under the supervision of the session organizer. The process requires a minimum of three (3) reviews by industry experts.

ISSN 0148-7191

http://papers.sae.org/2016-28-0198

Analysis of the Effective permittivity and Effective permeability of a grid of ferromagnetic microwires

Tarun Kumar
Department of Electronics Engineering
University of Petrolium and Energy Studies(UPES)
Dehradun, Uttarakhand 248007
Email: tkumar@ddn.upes.ac.in

***Abstract*—A novel method of analysis for the evaluation of effective permittivity and effective permeability of a ferromagnetic microwire grid consist of an infinite number of microwires is presented in this paper. The analysis is carried out through the evaluation of unknown scattering field coefficients of the reference microwire for a uniform plane wave incident normal to the surface of microwire. Evaluation of the unknown scattering field coefficients is obtained through boundary value type solution available in the literature. The current induced in each microwire is shown to be related to the scattering field coefficient. Average polarization over a unit cell is calculated with the help of current induced in the microwire. Finally, effective permittivity and effective permeability are evaluated with the help of average polarization over a unit cell. Numerical results are obtained for TM_z and TE_z polarizations in terms of the variation in effective permittivity and effective permeability with respect to the operating frequency.**

I. Introduction

Wire-based metamaterials (MTMs) have become a key research area in the recent past [1] [2] [3]. In [3], Pendry et al. has proved that a 3-D mesh of conducting wires can act like solid plasma and negative permittivity can be produced beyond the plasma frequency with the structure like this. Ferrites are known for the ferromagnetic resonance(FMR) inside the ferrite medium. The real part of permeability Re[μ_e] of the ferrite medium becomes negative beyond FMR frequency [4] [5]. Hence, Ferrites are reported to be found suitable for designing wire-based double negative (DNG) metamaterials. The effective permittivity and of the ferromagnetic microwire grid structure is reported in [6] for the normally incident uniform plane wave. In [6], effective medium properties are evaluated by assuming the grid as an impedance loaded sheet with equivalent current density. In this paper, effective permittivity of the ferromagnetic microwire grid structure as proposed in [6] is evaluated with the help of scattering field coefficients. The analysis of two dimensional scattering has been done already by many authors using various techniques [6]–[10]. A boundary value type solution is far more accurate [8] among all of them. The analysis of scattering field coefficient for a ferromagnetic microwire is available in the literature for normal incidence as well as oblique incidence case [4] [11] [12] [13]. Scattering from a ferromagnetic microwire grid containing an infinite number microwires has been reported recently in [14] for the generalized case. In this paper, the boundary value type solution for the scattering field coefficients is directly used as given in [14]. The current induced in each microwire is well known to be related to the scattered field [15]. Hence, the scattering field coefficient is shown to be related to the induced current in each microwire. Further, average polarization over a unit cell is calculated with the help of current induced in the microwire [6]. Finally, effective permittivity and effective permeability is evaluated with the help of average polarization over a unit cell [6]. Numerical results are obtained for and TE_z polarizations in terms of the variation in effective permittivity and effective permeability with respect to the operating frequency in the range of 5-15 GHz.

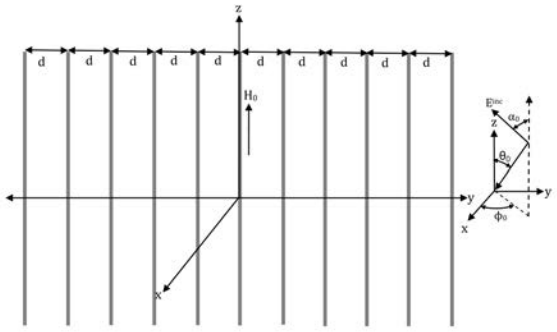

Fig. 1: Geometry of the problem

II. Formulation

As proposed in [6] [14], the microwires of infinite length, each with radius a and having applied internal axial magnetization H_0 are placed parallel to each other in y-z plane with the uniform spacing d as shown in Fig. 1. The reference microwire is assumed to be placed along the z-axis and impinged by uniform plane wave with polarization angle α_0 and incident angle θ_0. The effective permittivity and permeability of the medium are defined as

$$\varepsilon_{eff} = \frac{\varepsilon_0 \overline{E} + \overline{P}}{\overline{E}}, \tag{1}$$

$$\mu_{eff} = \frac{\varepsilon_0 \overline{H} + \overline{M}}{\overline{H}} \tag{2}$$

978-1-4673-8507-7/15/$31.00

where, $\overline{E}$ and $\overline{H}$ are the average local electric field and magnetic fields respectively in a unit cell. $\overline{P}$ and $\overline{M}$ are the average electric and magnetic polarizations respectively given as [6]

$$\overline{P} = \frac{1}{j\omega V}\int J(r')d^3r', \tag{3}$$

$$\overline{M} = \frac{1}{j\omega V}\int r \times J(r')d^3r'. \tag{4}$$

and J is the equivalent sheet current induced in a layer of microwires. As it is proved in the literature that the field of a line current source is equivalent to that of a microwire for $'n = 0'$, J can be obtained through the comparison to the scattered field obtained through boundary value type solution and a line current scatterer as

$$E_s^z = a_0^s H_0^{(2)}(\beta_0\rho), \tag{5}$$

$$E_s^z = -\frac{\mu_0\omega I_e}{4}H_0^{(2)}(\beta_0\rho) \tag{6}$$

$$, \tag{7}$$

$$J = \frac{-4a_0^s}{d\mu_0\omega} \tag{8}$$

where d is the spacing between the microwires, η and β are the intrinsic impedance and propagation constant of the free space respectively. It has been shown in [6] that the effective permeability for a ferromagnetic microwire grid is given as

$$\frac{\mu_{eff}}{\mu_0} = 1 + \frac{P}{(\mu_e - 1)^{-1} - NP} \tag{9}$$

where, N represents the demagnetization factor, equal to 0.5 for a cylinder, and $M(\mu_e - 1)h^{loc}$ is the density of the magnetic dipole moments inside the wire for a microwire with permeability,μ_e.

III. Numerical Results

In this section, numerical results are obtained for a 'Co' based ferrite microwire grid (see in Fig.1) with the following specifications [6] [14]: radius, $a = 20\mu m$, conductivity, $\sigma = 6.7 \times 10^5 S/m$, gyromagnetic ratio, $\gamma = 2 \times 10^{11} T^{-1}s^{-1}$, saturation magnetization, $\mu_0 M_s = 0.55T$, loss factor, $\delta = 0.02$, internal magnetization, $H_0 = 113.45kA/m$ along the z-coordinate and an operating frequency band of 5-15 GHz is assumed. Simulation results are plotted for the ϵ_{reff} and μ_{reff} against the operating frequency for two different polarization angles, $\alpha_0 = 0^\circ$ and 90°(i.e.,TM_z and TE_z polarizations respectively at normal incidence) (i.e. $\theta_0 = 90^o$).

A. ϵ_{reff}

Fig.2 and Fig. 3 shows the numerical results for effective permittivity for TM_z and TE_z polarizations respectively. The value of spacing between the microwires is considered to be d=3mm. It can be seen from figures that the real part of effective permitivitiy is negative in both the cases of TM_z and TE_z polarizations. In case of TM_z polarization, it shows resonance at 10 GHz (see in Fig. 2) due to the Ferromagnetic resonance(FMR). While in case of TE_z polarization, no such resonance is present because FMR takes place only for TM_z polarization.

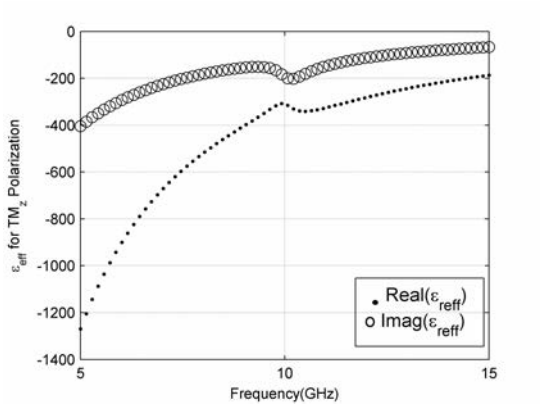

Fig. 2: Real and imaginary parts of effective permittivity for the considered ferromagnetic microwire grid for TM_z polarizations for spacing d=3 mm.

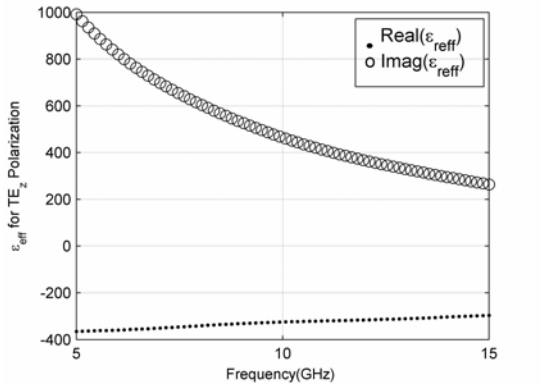

Fig. 3: Real and imaginary parts of effective permittivity for the considered ferromagnetic microwire grid for TE_z polarizations for spacing d=3 mm.

B. μ_{reff}

Fig.4 shows the effective permeability for TM_z and TE_z polarizations which is found to be same in both of the cases. As suggested in [6], It has real part equals to 1 (i.e. relative permeability of free space) irrespective of the radius and spacing among the microwires. This is because FMR occurs inside the ferrite medium only and it does not have any remarkable impact upon the surrounding medium which is air in this case. Hence the effective permeability of the air remains unaffected.

IV. Conclusion

The work discussed in the paper presents the theoretical analysis of the evaluation of effective permittivity and permeability with the help of scattering field coefficients of a planar grid of ferromagnetic microwires. The method available in the literature evaluated the effective permittivity by assuming the microwire grid as an impedence loaded surface and then calculated the equivalent current density. That approach is able to evaluate the effective permittivity only for the case of TM_z

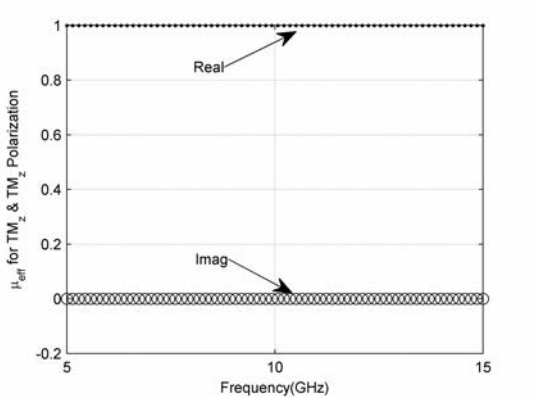

Fig. 4: Real and imaginary parts of effective permeability for the considered ferromagnetic microwire grid for TM_z and TE_z polarizations for spacing d=3 mm.

polarization. While, the method proposed in this paper has not made any such assumption and effective permittivity can be evaluated for both TM_z and TE_z polarizations. Furthermore, the approach can be extended for the evaluation of effective medium properties for any arbitrary polarization and incident angle. The numerical results are simulated through MATLAB and shows that the medium formed by a microwire grid (i.e. spacing d= $3\mu m$) can behave as a ENG (Epsilon Negative Medium). The medium can only offer negative permittivity and the value of effective permeability remains equal to that of free space.

REFERENCES

[1] Carignan, Louis-Philippe and Yelon,Arthur and Ménard,David,"Ferromagnetic Nanowire Metamaterials: Theory and Applications", IEEE Trans Microwave Theory Techn,vol. 59,no.10,pp. 2568-2586,Oct.2011, DOI: 10.1109/TMTT.2011.2163202.

[2] J. Carbonell, H. G.-Miqule, and J. S.-Dehsa,"Double Negative Metamaterials Based on Ferromagnetic Microwires ",Physical Review B,vol. 81, pp. 024401, 2010.

[3] J. Pendry, A. Holden, W. Stewart, and I. Youngs, "Extremely low frequency plasmons in metallic mesostructures",Phys. Rev. Lett., vol. 76, no. 25, pp. 4773-4776, 1996.

[4] Liberal,Iñigo and Ederra,Iñigo and Gómez-Polo,Cristina and Labrador, Alberto and Pérez Landazábal, Jose Ignacio, Gonzalo and Ramón,"Theoretical Modeling and Experimental Verification of the Scattering From a Ferromagnetic Microwire",IEEE Trans Microwave Theory Techn, vol.59, no.3,pp.517-526, Mar. 2011, DOI: 10.1109/TMTT.2010.2098037.

[5] Pozar,D.M., "Microwave Engineering", New York: Wiley, 4th edition, 2012, Chapter 9.

[6] I. Liberal, I. S. Nefedov, I. Ederra, R. Gonzalo, and S. A. Tretyakov, "Electromagnetic Response and Homogenization of Grids of Ferromagnetic Microwires", J. Appl. Phys., vol. 110, pp. 064909,2011.

[7] M. Polewski andJ. Mazur,"Scattering by an array of conducting,Lossy Dielectric, Ferrite and Pseudochiral Cylinders",Progress In Electromagnetics Research, PIER 38, 283-310, 2002.

[8] Atef Z. Elsherbeni "A comparative study of the two dimensional multiple scattering techniques"Radio science, Vol.24, No. 4, pp.1023-1033, Jul-Aug. 1994.

[9] Christos G. Christodoulou and J. Frank Kauffman,"On the Electromagnetic Scattering from Infinite Rectangular Grids with Finite Conductivity", IEEE Trans. on Antenna and Propg., Vol. AP-34, No. 2, Feb. 1986.

[10] B. H. Henin, A. Z. Elsherbeni, and M. Al Sharkawy "Oblique incidence of plane wave scattering from an array of circular dielectric cylinders",Progress In Electromagnetics Research, PIER 68, 261-279, 2007.

[11] Eggimann,W.H.,"Scattering of a Plane Wave on a Ferrite Cylinder at Normal Incidence,"IEEE Trans Microwave Theory Techn", vol. 8, no. 4, pp 440-445,Jul. 1960, DOI: 10.1109/TMTT.1960.1124754.

[12] R. A. Waldron, "Electromagnetic Wave Propagation in Cylindrical Waveguides Containing Gyromagnetic Media",Journal of the British Institution of Radio Engineers, vol.18, no.10, pp.597-612, Oct. 1958.

[13] Ahmed M. Attiya and Majeed A. Alkanhal,"Generalized Formulation for the Scattering from a Ferromagnetic Microwire",ACES Journal, vol. 27, No. 5, May 2012.

[14] T. Kumar, N. Kalyanasundaram, and B. K. Lande,"Analysis of the generalized case of scattering from a ferromagnetic microwire grid", Progress In Electromagnetics Research M, Vol. 35, 1-10, 2014.

[15] Balanis, C.A., "Advanced Engineering Electromagnetics", John Wiley and Sons, 2nd edition, 2012,Chapter 11.

Analytical Study on the Effect of Dimension and Position of Slot for the Designing of Ultra Wide Band (UWB) Microstrip Antenna

Ranjan Mishra[1,3], Raj Gaurav Mishra[1], Piyush Kuchhal[2]
[1]*Department of Electronics, College of Engineering Studies, UPES, Dehradun, India,*
[2]*Department of Physics, College of Engineering Studies, UPES, Dehradun, India.*
[3]*rmishra@ddn.upes.ac.in*

***Abstract*—This research paper presents a simple design consideration of Ultra-Wide Band (UWB) Microstrip antenna using a centrally loaded rectangular slot. An analytical study of the effects ofdifferent size and shapes of slots on the performance characteristic of UWB Microstrip antenna is presented. Insertion of slot and the changes in dimension of ground plane has a high impact on the behavior and parameter of the patch antenna. To improve the bandwidth of the patch antenna, proper insertion of slot on the planer patch structure has been used. In the paper 12mm by 15.6 mm rectangular patch antenna carved on FR4 substrate is presented. Both the simulated and the measured result show the operation of the antenna in the entire UWB range. This parametric study would be of a great interest in the designing of compact antennas for wireless communications operating in UWB.**

***Index Terms*—UWB, Microstrip Antenna, Bandwidth, Slot, Ground Plane, Impedance.**

I. INTRODUCTION

Antenna is the most fundamental block of the wireless communication. Recently, the growth of wireless systems leads to a lot of innovations in the Microstrip antenna designs. Microstrip patch antenna has become an integral part of these devices working in ultra to super high frequency ranges. The patch and slot are the two parameters which affect the overall antenna's performance.

Microstrip patch antennas are useful in various applications having requirements like broader bandwidth, smaller in size, lighter in weight, lower in cost and compatibility with integrated circuits [1-2]. A variety of wireless communication engineering applications, such as wireless links, remote sensing, cellular mobile phones and internet are in extensive demand and have witnessed a tremendous growth recently. The microstrip antenna has narrow bandwidth of the order upto 5%. This low bandwidth is not useful for many wideband wireless applications. Previously published literature has reported several possible techniques to improve bandwidth of the microstrip antenna [3-8]. Utility based applications opened the way for research in the design and development of Microstrip antennas.

Federal Communication Commission (FCC), in 2002, defined and drafted a frequency range from 3.1 GHz to 10.6 GHz for commercial ultra-wide band (UWB) communication [9]. In addition to this impedance bandwidth requirement, UWB antennas are required to radiate nearly isotropic along the entire bandwidth, with an acceptably low range of gain variation over this band. Since the bandwidth allocation of the UWB systems, the design of antennas for these systems is gaining a lot of interest.

In its simple form, a Microstrip patch antenna is consisting of a radiating patch on front side of a dielectric substrate, and a ground plane on the back side. The general basic shape of the radiating patch includes rectangular, square, circular and triangular for the simplification in the analysis and characteristic performance. A symmetrical diagram of a microstrip antenna is shown in figure 1.

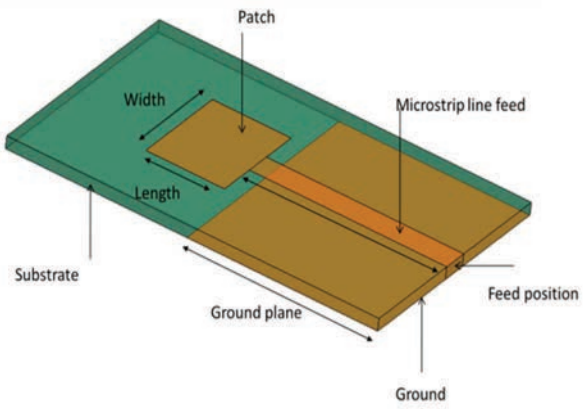

Figure 1: Rectangular Microstrip Patch Antenna

The slot is a cut on the front patch of the antenna. The shape of slot can be of any geometrical shape. The diagram for the slot loaded structure of the patch antenna is shown in figure 2. The length and width of the rectangular slot is *Ls* and *Ws*, and the distance of the slot form the junction of patch and line is denoted as *p*.

Incorporating a slot is easy in the design process and also it leads to an improvement in the bandwidth without increasing the volume of the antenna structures. Many research papers have verified the antenna's performance using these slots of various possible shapes such as U-slot, L-slot, C-slot, stepped U-slot, half stepped U-slot, W-shaped, M-slot folded slot, E-H shaped patch, and V-shaped slots [10-15]. Recently researchers introduced notches [16-17] to get UWB. Others use some variation in slots [18-21] to achieve the results.

This work was supported **University of Petroleum and Energy Studies**, Dehradun (Uttarakhand) India.

978-1-5090-2029-4/16/$31.00 @2016 IEEE

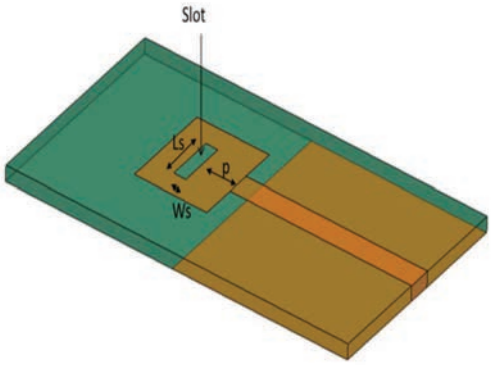

Figure 2: Slot loaded microstrip antenna

This paper emphasizes on the influence of slot in getting the desired UWB. The orientation of the paper is as follows. The result and discussion are presented in section II and III. Section II deals with the antenna structure and the factors influence it. Section III presents the impact of slot and ground plane, and the quality factor analysis. The simulation was performed in HFSS. Conclusion is summarized in section IV.

II. Antenna Structure and Design

The three important parameters which are required for designing of a microstrip patch antenna includes operating frequency (*f*), permittivity of the substrate (ε_r), and height of the substrate (*h*). In case of rectangular patch, all dimensions are exclusively dependent on these parameters. The resonant length and width of a microstrip patch can be achieved by employing the three aforesaid parameters [22]. The dimension of the slot is given in a complex analytical presentation [23]. These two references act as a primary source in selecting the dimension of the patch and slot. For the analysis presented in this paper the selected resonant frequency is6.0 GHz, the substrate material is epoxy FR4 having a permittivity of 4.4 and the height is 1.6 mm.

The length (L) and width (W) of the substrate are given as:

$$L = L_{eff} - 2\Delta L = \frac{c}{2f\sqrt{\varepsilon_{eff}}} - 2\Delta L \quad (1)$$

$$W = \frac{c}{2f} \times \sqrt{\frac{2}{(\varepsilon_{r+1})}} \quad (2)$$

The length extension ΔL is given as

$$\Delta L = 0.412h \frac{(\varepsilon_{eff} + 0.3)(\frac{W}{h} + 0.264)}{(\varepsilon_{eff} - 0.258)(\frac{W}{h} + 0.8)}$$

The effective permittivity (ε_{eff}) is related to the permittivity (ε_r) as:

$$\varepsilon_{eff} = \frac{\varepsilon_r + 1}{2} + \frac{\varepsilon_r - 1}{2} \sqrt{\left[1 + 12\frac{h}{W}\right]} \quad (3)$$

As the dimensions are inversely proportional to the dielectric constant, a substrate having high permittivity reduces the dimensions of the antenna. The analysis of dimensions with respect to the frequencies (2 GHz to 12 GHz) for three different substrates is shown in figure 3. The three substrates used are FR4, RT duroid, RO duroid. They have the permittivity of 4.4, 2.2 and 3.0 respectively.

The height of the substrate is chosen on the higher side (selected at 1.6 mm) to add the volume to the antenna and for enhancing its bandwidth. With this value the length and width of the antenna is to be 11.3 mm and 15.2 mm, as calculated from the various sets of equations taken from [10, 11]. Keeping the impedance matching into considerations of the microstrip antenna with the feed line, its length and width is selected at 12 mm and 15.6 mm. The length of the Microstrip line is selected as 30 mm.

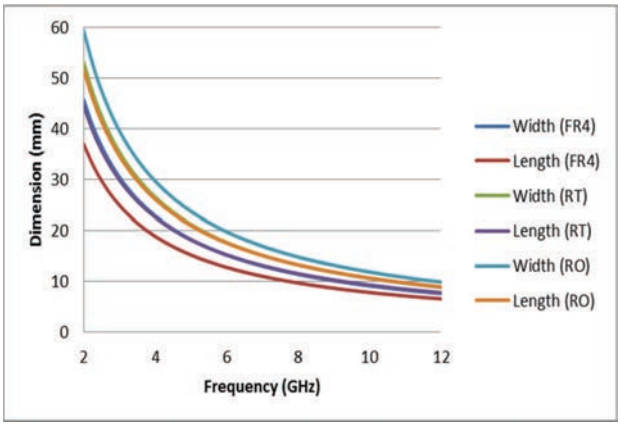

Figure 3: Dimensions of patch with different substrates

The impedance bandwidth of microstrip antennas can be improved with the use of substrate having low permittivity or by increasing the thickness of the substrate. The substrate thickness and lower permittivity increases surface wave, which results in lesser distortion in the radiated field pattern. It can be reported [24] that both the return loss and bandwidth increases with the height of substrate, and it is attaining a maximum value at a height of 1.6 mm. So, in the subsequent design the height of the substrate in this study is kept at 1.6 mm. as height increases, more volume is added to substrate. This will leads to better fringing effect.

III. Impact of Slot and Ground

The approximate length of the slot is determined by a complex set of slot line equation [17], and the maximum length is given as:

$$L_{slot} = \frac{0.45\,c}{f\sqrt{\varepsilon_{eff\_slot}}} \quad (4)$$

$$\text{where, } \varepsilon_{eff\_slot} = \frac{\varepsilon_r + 1}{2} \quad (5)$$

For a patch length of 12 mm, the maximum selective length of the slot would be near to 10 mm.

Equivalent circuit of the transmission line for a microstrip antenna having slots is shown in figure 4.

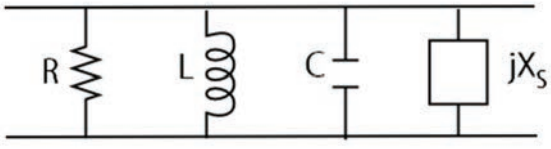

Figure 4: Equivalent circuit of slot loaded antenna

The input impedance of the antenna without the slot is

$$Z_{in} = \frac{1}{\frac{1}{R}+j\omega C+\frac{1}{j\omega L}}$$

On simplifying,

$$Z_{in} = \frac{R(\omega L)^2}{(\omega L)^2+R^2(\omega^2 LC-1)^2} - j\frac{R^2\omega L(\omega^2 LC-1)}{(\omega L)^2+R^2(\omega^2 LC-1)^2} \quad (6)$$

R, L and C are the resistance, inductance and capacitance of the circuit.

Equation (6) is expressed as:

$$Z_{in} = R - jX \quad . \quad (7)$$

Here R is the real and X is the imaginary part of the impedance.

In terms of the parameter of the antenna, the characteristic impedance is given as

$$Z_c = \frac{120\pi/\sqrt{\varepsilon_{eff}}}{\frac{W}{h}+1.393+0.667\ln(\frac{W}{h}+1.444)} \quad (8)$$

With reference to equation (6) and (7), the input impedance of slot loaded antenna is given as:

$$Z_{inS} = \frac{(R-jX)(jX_S)}{R-jX+jX_S}$$

Simplifying it yield

$$Z_{inS} = \frac{X.X_S+jRX_S}{R-j(X+X_S)} \quad .. \quad (9)$$

The value of X_S is given as

$$X_S = 30[2S(kL_S)+ coskL\{2S(kL_S) - S(2kL_S)- SinkL_S\{2Ce(kL_S) - Ce(2kL_S) - Ce(kW_S/2L_S)^2\}] \quad (10)$$

L_S is the length and W_S is the width of the slot respectively.
k $(=2\pi/\lambda)$ is the propagation constant in the free space,
Ce is the Euler's constant.

In the first set of simulations and their observations, a full ground plane is used along with different slot positions. The position of the slot is taken from the junction of the patch and line. The plot with different positions having significant values is plotted in figure 5. It is observed from the figure that the best result is obtained when the position of slot is selected at 6 mm.In the antenna design without having slot, the resonant frequency shows a narrow banding around 8 GHz. Antenna design with the slots of 2 mm and 9 mm, simulation shows the narrow band around 10 GHz and 11 GHz respectively. From the plot shown in figure 5, antenna design having a slot with a distance of 6 mm from the non-radiating side good broad bandwidth in the range of 9 GHz to 12 GHz along with the high return loss of the order of -32 dB is obtained.

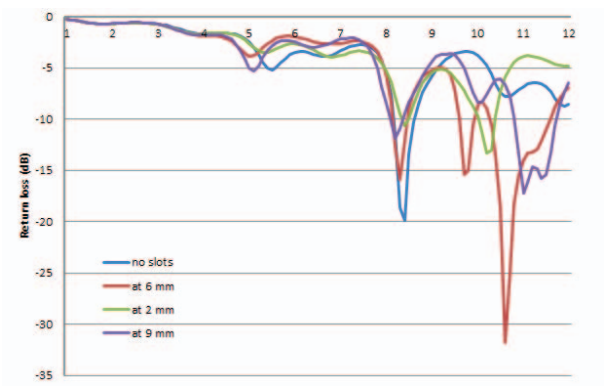

Figure 5: Performance for different positions of slot.

Then at this position (6 mm), the width of the slot is varied and the observations are made. The significant results obtained from three different widths selected and is plotted in figure 6. It observed from the figure 6 that the best result is obtained with the slot width of 2 mm in size. With this value of the slot width, broadening is observed near the frequency range of 9 to12 GHz. The achieved return loss having a maximum value of -32 dB is at 10.6 GHz. Any further increase in the width would result in subsequent decrease in the bandwidth and return loss.

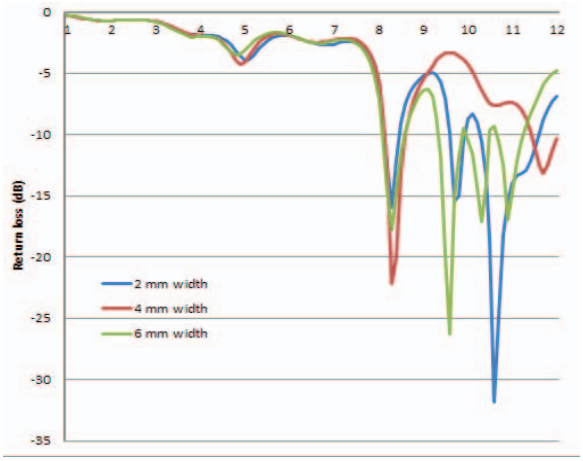

Figure 6: Performance for different widths of slot.

Next observation is made with variations in the length of the slot and the significant observation is plotted in figure 8. The most significant values are obtained with slot length of 8 mm in size. The slot intensifies the electric field on the suitable matching position on the patch. This leads to the enhancement of the performance of the antenna. With a slot length of 8 mm, the antenna shows a broadband resonance in the UWB range. Observing the plot in the figure 7, though the resonance pattern of the antenna with 6 mm and 10 mm size of slot resembles that of with 8 mm slot length, but the return loss in this two cases are not below the -10dB value in the entire range.

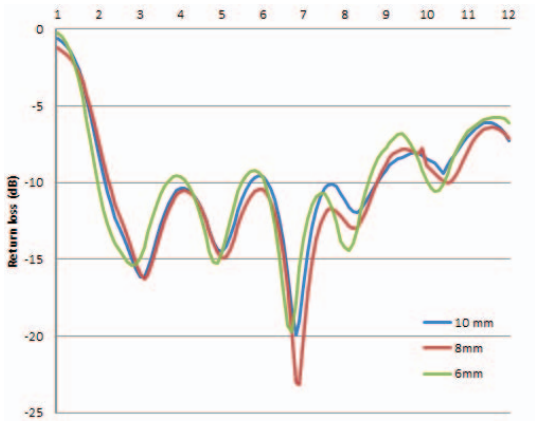

Figure 7: Performance for different lengths of slot.

Any change in the length and/or width of the slots affects the results/performance of the return loss and bandwidth of the proposed antenna. From the figure 5 to 7, it is observed that a wider and shorter length of slot produces the worst result. Equation (10) indicates that increasing the value of width of the slots result a reduction in the impedance.

Therefore a proper matching is obtained for a suitable dimension of the slot. This case also accounts for a significant back-reflection. The resonant frequency is shifted towards left, with the insertion of the slots as compared to the case without any slots.

In the next set of observations, the length of ground plane is varied and the significant values in the UWB ranges are observed. The plot for three significant ground plane sizes is shown in figure 8. The best result that completely covers the UWB range is obtained at a size of 30 mm.

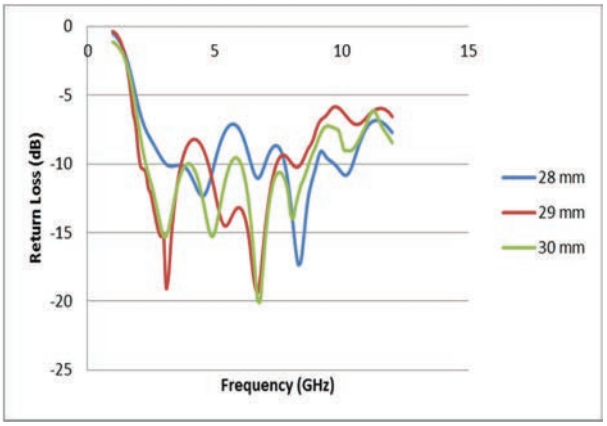

Figure 8: Performance in UWB range for different lengths of ground plane.

Return loss (S1 performance) of the best suited design after optimizing ground plane, slot position and slot dimensions are plotted. The antenna is showing a resonance in the UWB range with a slot length of 8 mm, slot width of 2 mm and ground plane of length 30 mm in size. The figure 9 shows the operating region for this dimension. The UWB performance has been obtained as the antenna resonates at four frequencies closer to each other. These frequencies are nearly at 3GHz, 5 GHz, 7 GHz and 8.5 GHz.

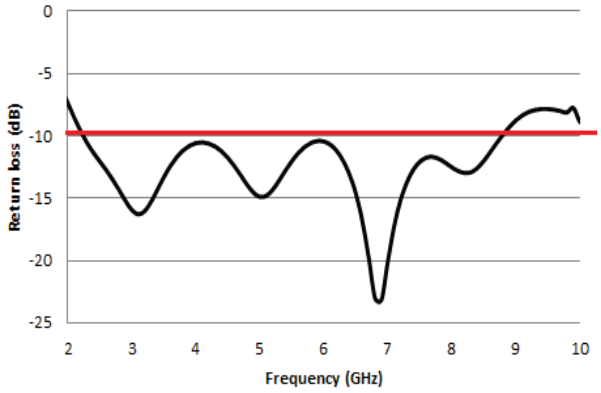

Figure 9: Operating region of antenna in UWB range

Taking into the result obtained the final dimension of the antenna is presented in table 1.

In the next step, the proposed antenna is fabricated on epoxy FR4 substrate by chemical etching method. The front and back side of the antenna are shown in figure 10(a) and (b) respectively.

TABLE I: GEOMETRICAL DIMENSION OF THE PROPOSED ANTENNA.

Length of the Patch	12 mm
Width of the Patch	15.6 mm
Length of Microstrip line	30 mm
Width of Microstrip line	3.6 mm
Length of slot	8 mm
Width of slot	2 mm
Length of Ground plane	29 mm
Length of Substrate	33 mm
Width of Substrate	29 mm

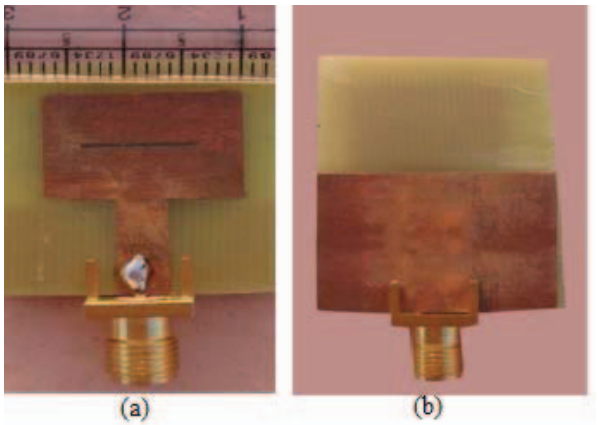

Figure 10: Front side (a) and back side (b) of the fabricated antenna.

To validate the result, the characterization testing of the antenna is done on vector network analyzer. The measured (experimental) values of the return loss at different frequencies ranging from 2 GHz to 11 GHz are recorded and it is plotted against the simulated (theoretical) values. The plot of the return loss at UWB frequency range of the two values (measured and simulated) is shown in figure 11.

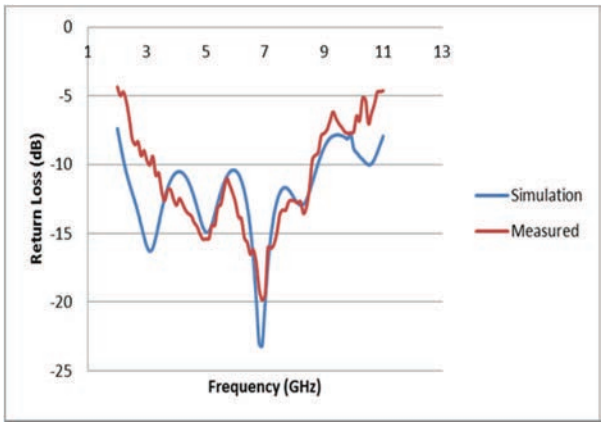

Figure 11: Comparison of the simulated and measured antenna

.

Also in the figure 12, VSWR of the fabricated antenna is plotted along with the results obtained in the simulation. . The VSWR is showing a good result (≤ 2) in the UWB range as per the specification of FCC.

The two dimensional radiation pattern at 6.8 GHz (prime resonant frequency) with $\Phi=0^{O}$ and $\Phi=90^{O}$ is shown in figure 13. The figure reveals a smooth uni-directional pattern with a max gain of 1.4 dB.

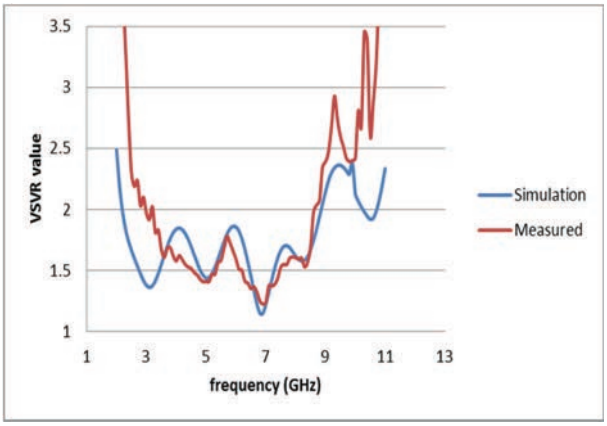

Figure 12: VSWR of the simulated and measured antenna.

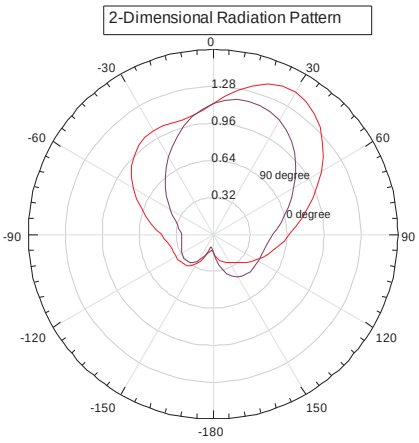

Figure 13: The back side of the fabricated antenna.

The radiation efficiency of the proposed antenna is shown in figure 14. Radiation efficiency is calculated from the gain and directivity of the antenna. More closely the two values better will be the efficiency.

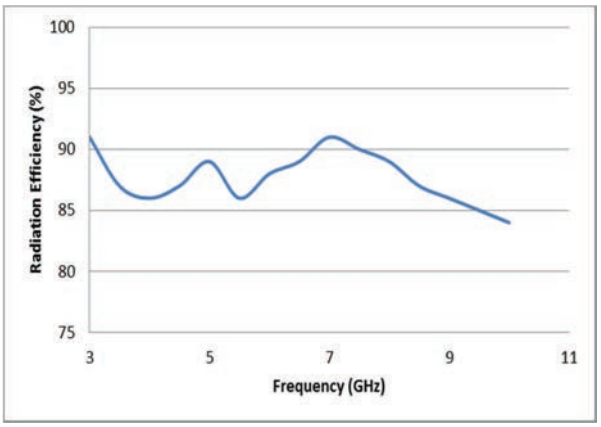

Figure 14: Radiation efficiency of the antenna

It is also clear from the figure 16 that the radiation efficiency is more than 80% near the four resonant frequencies. It has been observed from the figure 13 and figure 14 that the good result in the UWB band is obtained as the antenna resonates fairly in the entire UWB region. In the simulation result, the antenna resonates at four frequencies closer to each other (3.2GHz, 5.1 GHz, 6.9 GHz and 8.4 GHz). Also in the measured value of the fabricated antenna, there resonant frequencies (4.9 GHz, 6.9 GHz and 8.3 GHz) are observed. The last two resonant frequencies of both the simulated and measured result are same. This justifies a good validation of the result.

IV. Conclusion

With the above results and observation, a simple design of a wide band antenna is possible by the optimization of patch dimension for obtaining a proper feed impedance matching, along with the suitable slot geometry carved on a substrate having relative large thickness and low permittivity. Also a simple rectangular slot of proper size and at the proper matched distance on the radiating patch will provide a perfect matching and this yields a high bandwidth. The partial ground plane helps in the reduction of the quality factor and thus enhances the bandwidth further.

References

[1] K. R .Carver and J. W. Mink, “Microstrip antennatechnology,” IEEE Transaction on Antenna & Propagation, vol. 29, pp. 2-24, 1981.
[2] R. Gag, “Progress in Microstrip antennas”, IETE Technical Review, vol. 18, No. 2& 3 pp .85-98, 2001.
[3] S. Bhunia, D. Sarkar, S, Biswas, P.P.sarkar, B.Gupta, K.Yasumoto “Reduced Size Small Dual-Frequency Microstrip Antenna” Microwave & Optical Technology Letters. vol. 50, no.4, pp. 961-965, 2008.
[4] L. Guo, S. Wang, X. Chen, and C.G. Parini, “Study of compact antenna for UWB applications”, Electron Letter, vol. 46, 115–116, 2010
[5] K. G. Thomas and M. Sreenivasan, “Compact CPW-fed dual-band antenna”, Electron Letter, 46, pp 13–14, 2010
[6] C.Y.D. Sim, W.T. Chung, and C.H. Lee, “Compact slot antenna for UWB applications”, IEEE Antenna WirelessPropagationLetter, vol. 9, pp 63–66, 2010.
[7] Mohammad Tariqul Islam, Mohammed Nazmus Shakib, Norbahiah Misran, “High Gain Microstrip Patch Antenna”, European Journal of Scientific Research, vol.32 no.2, pp.187-193, 2009.
[8] Dimitrios Peroulis, Kamal Sarabandi, and Linda P. B. Katehi, “Design of Reconfigurable Slot Antennas”, IEEE Transactions on antennas and propagation, vol. 53, no. 2, pp 645-654, 2005.
[9] FCC, First report and order on ultra-wideband technology, Technical Report, 2002.
[10] A. A. Deshmukh and G. Kumar, Compact broadband U slot-loaded rectangular microstrip antennas, Microwave and Optical Technology Letters, vol. 46, no. 6, pp. 556–559, 2005.
[11] A. A. Deshmukh and K. P. Ray, Compact broadband slotted rectangular microstrip antenna, IEEE Antennas and Wireless Propagation Letters, vol. 8, pp. 1410–1413, 2009.
[12] A. A. Lotfi Neyestanak, F. Hojjat Kashani, and K. Barkeshli, “W-shaped enhanced-bandwidth patch antenna for wireless communication,”Wireless Personal Communications, vol. 43, no. 4, pp. 1257–1265, 2007.
[13] F. Jolani, A. M. Dadgarpour, and H. R. Hassani, Compact M – slot folded patch antenna for WLAN, Progress in Electromagnetics Research Letters, vol. 3, pp. 35–42, 2008.
[14] M. T. Islam, M. N. Shakib, and N. Misran, “Broadband E-H shaped microstrip patch antenna for wireless systems,” Progress in Electromagnetics Research, vol. 98, pp. 163–173, 2009.
[15] M. S. Nishamol, V. P. Sarin, D. Tony, C. K. Aanandan, P. Mohanan, and K. Vasudevan, “A broadband microstrip antenna for IEEE802.11.A/WIMAX/HIPERLAN2 applications,” Progress In Electromagnetics Research Letters, vol. 19, pp. 155–161, 2010.
[16] J. Wen, C. Wenquan,“A Novel UWB Antenna with Dual Notched Bands for WiMAX and WLAN Applications”, IEEE transaction on Antenna and Propagation, vol. 60, no 11, pp 293-296, 2012
[17] P. S. Bakariya, S. Dwari, M. Sarkar, “Printed Ultrawideband Monopole Antenna with Four Notch Band”, Wireless Personal Communications, vol. 84, Issue 4, pp 2989-2999, 2015
[18] Kang Woong, Kim Kangwook, Kim Woosu, “A Broad-Band Conductively-Loaded Slot Antenna for Pulse Radiation, A Broad-Band Conductively-Loaded Slot Antenna for Pulse Radiation, IEEE

transaction on Antenna and Propagation", vol. 62, no 1, pp-33-39, 2014.

[19] Jang Joon Won, Hwang Hee Yong, "An Improved Band-Rejection UWB Antenna With Resonant Patches and a Slot", IEEE transaction on Antenna and Propagation, vol. 57, no 8, pp 299-302, 2009

[20] Yingsong Li, Wenxing Li, "A Circular Slot Antenna with Wide Tunable and Reconfigurable Frequency Rejection Characteristic Using Capacitance Loaded Split-Ring Resonator for UWB Applications", Wireless Personal Communications, vol. 78, Issue 1, pp 137-149, 2014.

[21] G. Zheng, T. Huiping, W. Xudong, L. Qun, et al,"Bandwidth Enhancement of Monopole UWB Antenna With New Slots and EBG Structures", IEEE transaction on Antenna and Propagation, vol. 61, no 12, 2013, pp 1550-1553.

[22] C. Balanis, "Antenna Theory; Analysis and Design', second edition, Wiley and Sons, New York, 1982.

[23] K. C. Gupta, Ramesh Garg, Inder Bahl and Prakash Bhartia, "Microstrip Lines and Slotlines", second edition. Artech house, 1996.

[24] R. Mishra, P. Kuchhal, A. Kumar, "Effect of Height of the Substrate & Width of the Patch on the Performance Characteristics of Microstrip Antenna", International Journal of Electrical and Computer Engineering, vol. 5, no 6, pp 1441-45, 2015.

2015 1st International Conference on Next Generation Computing Technologies (NGCT-2015)
Dehradun, India, 4-5 September 2015

Assessment of Determinants Influencing Customers Adoption of Network Provider: An Empirical Study

Karanpal Singh*, Shivangnee Sharma† and Inder Singh‡

* Center for Information Technology, College of Engineering Studies,UPES, Dehradun, Uttrakhand, India, palsinghk@gmail.com
†Center for Information Technology, College of Engineering Studies,UPES, Dehradun, India, sharma.shivangnee@gmail.com
‡Assistant Professor, Center for Information Technology , UPES, India,inder@ddn.upes.ac.in

***Abstract*—In India cellular communication scenario, the term MNP or Mobile Number Portability is becoming more popular. The mobile operators are forced to adapt the Herbert Spencers theory on Survival of the fittest. MNP allows the customer to transfer their existing number from one mobile network provider to another. Thus, if a customer is dissatisfied by the services provided by a mobile operator the customer can now change to another operator without changing the existing number. This change is governed by some factors. Thus, to statistically evaluate the factors influencing MNP, a model has been developed using SEM in this paper.**

Keywords Mobile Number Portability, Structural Equation Modeling, Factor Analysis, Subscribers, Service Providers;

I. Introduction

India has the fastest growing telecom network market with Airtel, Vodafone, Idea, Uninor, Reliance, TATA DoCoMo, BSNL, Aircel, TATA Indicom and MTNL as the major network operators. Private operators hold 90.05% of wireless subscriber market share, whereas BSNL and MTNL, the two PSU operators hold only 9.95% market share according to TRAI.[1] Thus providing Indian users a wide range of selecting a network provider, either by changing his/her number or by the new concept of Mobile Number Portability.

A. History

Mobile Number Portability (MNP) enables mobile phone users to retain their mobile phone numbers when changing from one mobile network operator to another. [2] The customer wishing to port his/her number is required to contact the donor to obtain a Unique Porting Code (UPC) which is then showed to the recipient network to proceed. [1] In India out of approximately 950 million wireless subscribers, 800 million connections are active. Since 2009, approximately 200 million mobile number portability requests have been received till December 2014 as per the TRAIs annual report 2014.

Thus, there should be some factors influencing the customers to switch their number from one network provider to another. This research tends to identify and evaluate these factors and prepare a statistical model indicating how much these factors are contributing towards mobile number portability

B. Objectives

The objectives of this study are:

- To identify the determinants that influence the adoption of network provider by the customers;
- To assess the determinants to find out the direct and indirect effect on adoption of network provider.

II. Literature Review

- A study has been conducted in Hyderabad City of India to find out students preferred brand towards choosing a particular network providers. [3]
- A comprehensive study was conducted in National Capital Region of India on Mobile Number Portability. This study concluded that MNP when implemented will prove a sigh of relief to the customer in case of bad services provided by a particular telecom service provider. [4]
- A study was conducted in South Africa on how in South Africa the Telecommunication industry has introduced Mobile Number Portability (MNP) as new functionality. This study concluded that, a great opportunity was provided by MNP helping to increase acquisition and also inspire a healthy competition between mobile operators. [5]
- A study was conducted in Hyderabad City of India which focuses on vital aspects of Mobile Number Portability and found that its effectiveness among the students, working class and retired people. Considering attribute technology, brand image, quality network, tariff and other services. [6]
- A study was conducted to examine the customer preference and awareness about the Mobile Number Portability and try to find out factors that motivate the use of mobile number portability. [7]
- A study was conducted in Turkey to acquire the factors affecting the MNP and shows how specific model can be helpful for telecommunication managers in order not to be affected by mobile number portability. [8]
- A study was conducted on the Idea Cellular Ltd. to figure out impact of Mobile Number Portability on service providers and service users. [9]
- A study was conducted on Malaysian consumers to analyze the elements affecting the Mobile Number Portability using SEM. [10]

978-1-4673-6809-4/15/$31.00 ©2015 IEEE

- A study was done to provide introduction to structural equation modelling including the comparison between traditional statistical approach and structural equation modelling analysis. [11]
- A study was conducted on Bangladeshi consumers using structural equation modelling approach for knowing the factors affecting preference of mobile network providers. [12]
- A study was conducted on Ghanas Mobile Telecommunication industry which helps to understand the customers behavior towards mobile number portability. [13]
- A study was conducted on the Erode district of Tamil Nadu targeting on MNP on the mobile customers. [14]
- A survey was conducted which reveals customers reasons and preferences for shifting from one network provider to another. [15]
- A study was conducted on Nigerian Telecommunication
- A study was conducted on Gujarat Telecommunication Circle to understand the behavior of consumers after the mobile number portability. [17]
- A study was conducted in Ghana to examine the student selection of mobile phone services. [18]
- A study was conducted in Chennai to understand the consumers shifting behavior in mobile network providers. [19]
- A research was done to understand the components influencing the institution students mobile dependence and anxiety. [20]

Based on the literature review done following factors were identified and hypothesis were made:

1) External Environment
   - Because of Friends (having same network provider)
   - Because of Family (having same network provider)
   - Service guarantee by network provider

   H0 : External Environment has no significant effect on MNP
   H1 : External Environment has a significant effect on MNP
2) Tariff Plans
   - Tariff Plan suits customers budget
   - Tariff Plans are flexible
   - Tariff Plans are valued for money
   - Bogus Billing

   H0 : Tariff Plans has no significant effect on MNP
   H1 : Tariff Plans has a significant effect on MNP
3) Service Quality
   - Poor voice quality
   - Frequent call drops
   - Poor internet services

   H0 : Service Quality has no significant effect on MNP
   H1 : Service Quality has a significant effect on MNP
4) Customer
   - Inefficient customer care dealing services

   H0 : Customer Care has no significant effect on MNP
   H1 : Customer has a significant effect on MNP
   - Advertisements & Offers
   - Brand value of network provider
   - Attractive and innovative advertisements
   - Promotional offers

   H0 : Advertisements & Offers has no significant effect on MNP
   H1 : Advertisements & Offers has a significant effect on MNP

III. METHODOLOGY

For getting the desired objectives, the following methodology was followed:

- Identification of the determinants that influence the adoption of network provider
- Design of survey questionnaire by carefully selecting the direct factor effecting the adoption of network provider.
- Pilot testing of survey questionnaire (Cronbachs Alpha)
- Data Analysis - Scale reliability using Cronbachs Alpha - KMO and Bartletts Test (for checking the appropriateness of the factors)
- Factor Analysis - Exploratory Factor Analysis - Confirmatory Factor Analysis
- Descriptive Statistics of Latent constructs
- Testing Goodness-of-fit Model using IBM SPSS AMOS. and Evaluation of Hypotheses

A. Data Collection

The data collection done for this research can be categorized into the primary source of data, i.e. via Questionnaire. The questionnaire consisted of the identified factors on a 5-likert scale. 300 questionnaires were distributed, of which 286 were received. Also, 16 questionnaires among these were partially filled and were neglected. Thus, a 270 questionnaires were considered for the further analysis.
To sample the population an approach of Stratified Random Sampling was used. In this, strata were formed by diving population into smaller groups based on common characteristics. Here, age group from 21-30 years was considered to be under one strata, 31-40 another strata and so on.

TABLE I. GENDER VS AGE CROSS TABULATION

		Age					
		Below_Equal_20	21-30	31-40	41-50	Above 50	Total
Gender	Male	72	60	22	11	7	172
	Female	49	33	13	3	0	98
Total		121	93	35	14	7	270

TABLE II. GENDER VS CONNECTION CROSS TABULATION

		Connection		
		Pre-paid	Post-Paid	Total
Gender	Male	153	19	172
	Female	87	11	98
Total		240	30	270

IV. ANALYSIS PERFORMED

A. Cronbalchs Alpha

Given variable x1, , xk and $x0 = \sum_{j=1}^{k} x_j$ and Cronbachs alpha is defined to be [20]

$$\frac{k}{1-4}\sum_{i\neq j}^{k}\frac{con(x_i - x_j)}{var(x_0)} = \frac{k}{1-k}(1 - \sum_{j=1}^{k}\frac{var(x_j)}{x_)} \quad (1)$$

Cronbachs alpha provides a useful lower bound on reliability. Cronbachs alpha will generally increase when the correlations between the items increase. For this reason the coefficient measures the internal consistency of the test. Its maximum value is 1, and usually its minimum is 0, although it can be negative. [21]

B. Factor Analysis

Factor Analysis is a commonly used data variable reduction technique. This multivariate statistical technique is used for three primary reasons: - Reduce the number of variables, from large to small - Establish underlying dimensions between measured variables and constructs and - Provide construct validity evidence Factor Analysis include Exploratory Factor Analysis (EFA) and Confirmatory Factor Analysis (CFA). As the names suggest, EFA is used where the study is being conducted with no preconceived theories or expectations while CFA is used where the study is being conducted to test a proposed theory. [22]

C. Explanatory Factor Analysis

Exploratory Factor Analysis (EFA) is a statistical approach for determining the correlation among the variables in a dataset. This type of analysis provides a factor structure (a grouping of variables based on strong correlations). In general, an EFA prepares the variables to be used for cleaner structural equation modelling. An EFA should always be conducted for new datasets. The beauty of an EFA over a CFA (confirmatory) is that no a priori theory about which items belong to which constructs is applied. This means the EFA will be able to spot problematic variables much more easily than the CFA. [23]

TABLE III. STANDARD THRESHOLD VALUES FOR CRONBACHS ALPHA

Cronbach's alpha	Internal consistency
$\alpha \geq 0.9$	Excellent
$0.7 \leq \alpha < 0.9$	Good
$0.6 \leq \alpha < 0.7$	Acceptable
$0.5 \leq \alpha < 0.6$	Poor
$\alpha < 0.5$	Unacceptable

Source: Essentials of Psychological Testing by Lee J. Cronbach

KMO-Bartletts Test of Sphericity KMO Bartletts Test of Sphericity is a measure of sampling adequacy that is recommended to check the case to variable ratio for the analysis being conducted. In most academic and business studies, KMO Bartletts test play an important role for accepting the sample adequacy. While the KMO ranges from 0 to 1, the worldover accepted index is over 0.6. Also, the Bartletts Test of Sphericity relates to the significance of the study and thereby shows the validity and suitability of the responses collected to the problem being addressed through the study. [22]

Rotation Factor Matrix Another important aspect that needs mention is the Rotated Component Matrix. While deciding how many factors one would analyze is whether a variable might relate to more than one factor. Rotation maximizes high item loadings and minimizes low item loadings, thereby producing a more interpretable and simplified solution. There are two common rotation techniques - orthogonal rotation and oblique rotation. While orthogonal varimax rotation that produces factor structures that are uncorrelated, oblique rotation produces factors that are correlated. [22]

Irrespective of the rotation method used, the primary objectives are to provide easier interpretation of results, and produce a solution that is more parsimonious.

D. Confirmatory Factor Analysis

Confirmatory Factor Analysis (CFA) is the next step after exploratory factor analysis to determine the factor structure of your dataset. In the EFA we explore the factor structure (how the variables relate and group based on inter-variable correlations); in the CFA we confirm the factor structure we extracted in the EFA. [24]

Model Fit It means how strongly the suggested model explains the correlations between variables in the data. For getting a good fit model, one needs to see if the explanation is being done for all the major correlations inherent in the data. If the explanation does not show any major correlations, it means that there is a significant ”discrepancy” a between the correlations proposed and the correlations observed, and the model is said to have a poor model fit.

Metrics There are clear-cut measures that can be used to show the goodness of fit for the model suggested. The metrics along with their adequate threshold values are listed below, sample size is inversely of related to the Goodness of fit and the number of variables in the model.

V. RESULTS AND DISCUSSIONS

Cronbachs Alpha The following table represents the case processing summary for the Cronbachs Alpha test. Here, the

TABLE VI. CASE PROCESSING SUMMARY

Cronbach's Alpha	N of Items
.763	17

TABLE VII. KMO AND BARTLETT'S TEST

Kaiser-Meyer-Olkin Measure of Sampling Adequacy.		.714
Bartlett's Test of Sphericity	Approx. Chi-Square	1044.802
	df	136
	Sig.	.000

TABLE VIII. ROTATED FACTOR MATRIXA

	Factor				
	F1	F2	F3	F4	F5
Poor_quality	.777				
Call_Drops	.737				
Poor_Internet	.571				
Ineffecient_CC	.536				
Bogus_Billing					
Tariff_Suits		.754			
Tariff_valued		.626			
Tariff_Flexible		.624			
Service_guarantee					
Attractive_Ads			.807		
Promotional_Offer			.599		
Brand_Value					
Family				.849	
Friends				.624	
Conect_MNP					.668
Easy_Process					.525
Cust_demo					

Extraction Method: Principal Axis Factoring.
Rotation Method: Varimax with Kaiser Normalization.

TABLE IX. CMIN

Model	NPAR	CMIN	DF	**P**	**CMIN/DF**
Default model	24	21.042	21	**.456**	**1.002**
Saturated model	45	.000	0		
Independence model	9	533.302	36	.000	14.814

TABLE X. RMR, GFI

Model	RMR	**GFI**	**AGFI**	PGFI
Default model	.024	**.984**	**.965**	.459
Saturated model	.000	1.000		
Independence model	.206	.671	.588	.536

TABLE XI. BASELINE COMPARISONS

Model	NFI Delta1	RFI rho1	IFI Delta2	TLI rho2	**CFI**
Default model	.961	.932	1.000	1.000	**1.000**
Saturated model	1.000		1.000		1.000
Independence model	.000	.000	.000	.000	.000

TABLE XII. RMSEA

Model	**RMSEA**	LO 90	HI 90	**PCLOSE**
Default model	**.003**	.000	.052	**.940**
Independence model	.227	.210	.244	.000

TABLE IV. STANDARD THRESHOLD VALUES FOR GOODNESS-OF-FIT

Measure	**Threshold**
Chi-square/df (cmin/df)	<3 good; <5 sometimes permissible
p-value for the model	>0.5
CFI	>0.95 great; >0.90 traditional; >0.80 sometimes permissible
GFI	> 0.95
AGFI	> 0.80
SRMR	<.09
RMSEA	<0.05 good; 0.05-0.10 moderate; >0.10 bad
PCLOSE	> 0.05

Source: statwiki.kolobkreations

TABLE V. CASE PROCESSING SUMMARY

		N	%
Cases	Valid	60	100.0
	Excluded[a]	0	.0
	Total	60	100.0

a. Listwise deletion based on all variables in the procedure.

test was performed on first 60 questionnaires. Out of which, none of the questionnaire was excluded.

Explanatory Factor Analysis The following table represents the results given by the KMO and Bartletts Test. As per the standard threshold i.e. over 0.6, the sampling Adequacy for this dataset is 0.714, which is considered to be good, indicating that the factors are valid and suitable according to the study being done.

The following represents the most important aspect of Factor analysis. It can be seen, that the valid variables are clubbed into 5 major factors namely F1, F2, F3, F4 and F5. These new factors, will be used for conducting further analysis.

Extraction Method: Principal Axis Factoring. **Rotation Method:** Varimax with Kaiser Normalization.

Goodness-of-fit In reference to the Table: 4.2, depicting the standard threshold values, Table: 5.6, Table: 5.7, Table: 5.8 and Table: 5.9 for model fit, it can be concluded that this model is excellent fit.

VI. CONCLUSION

Tariff Plan and Service Quality are two major constructs which are influencing the customers adoption of network provider as they are influencing mobile number portability 22% and 9% respectively. Also the Covariance between F1 - F2

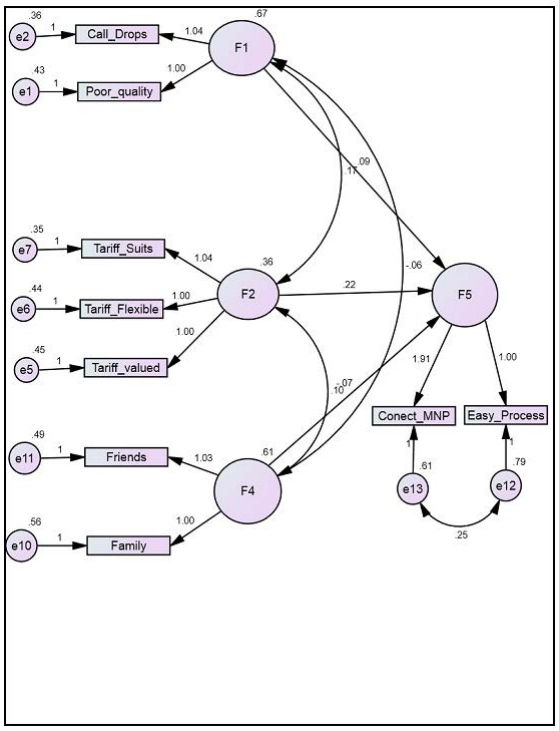

Fig. 1. SEM

and F2 - F4 is 0.17 and 0.10 respectively. Positive covariance is showing that both determinants tend to increase or decrease together. Covariance between F1 - F4 is -0.06 showing that one determinant tends to increase as the other decreases. So, null hypothesis for all measurable variables of Tariff Plan and Service Quality latent constructs are rejected.

ACKNOWLEDGMENT:We are indeed grateful to many groups of people who have helped us directly and indirectly with various aspects of this study. We take this opportunity to thank Dr. Krishan Kumar Pandey, Assistant Professor, Department of QT, RM Operations, College of Management & Economics Studies, University of Petroleum & Energy Studies, Dehradun for guiding us. His knowledge and experience about various statistical techniques and ongoing trends influenced us in overcoming many hurdles.

REFERENCES

[1] Telecom Regulatory Authority of India, "Telecommunication Mobile Number Portability (Sixth Amendment) Regulations," TRAI, New Delhi, 2015.

[2] D. R. Arora and D. A. Chawla, "Mobile Number Portability: A New Feather In Telecom," International Journal of Research in Finance and Marketzing, vol. 4, no. 3, pp. 75-88, 2014.

[3] S. A. Odunaike, "The Impact of Mobile Number Portability on TUT students On-line Connectivity," in ISECON Proceedings, Nashville Tennessee,USA, 2010.

[4] C. S. Yadav, "An Empirical Study of Customers Perception Towards Mobile Number Portability (MNP) With Special Reference To India," International Journal of Marketing, Financial Services Management Research, vol. 5, pp. 86-89, 2012.

[5] P. S. Vaghela, "Customer Preference for Mobile Number Portability," International Journal of Management and Social Sciences Research, vol. 1, no. 3, pp. 71-75, 2012.

[6] B. Kutlu, "Effects of Mobile Number Portability: Case of Turkey," International Journal of Business and Social Science, vol. 4, no. 14, pp. 120-124, 2013.

[7] R. K. Yadav and N. Dabhade, "Effects of Mobile Number Portability in Telecom Sector - A Case," Indian Journal of Economics and Development, vol. 1, no. 2, pp. 49-59, 2013.

[8] S. Rahman, A. Haque and M. I. S. Ahmad, "Exploring influencing factors for the selection of mobile phone service providers: A structural equational modeling (SEM) approach on Malaysian consumers," African Journal of Business Management, vol. 4, no. 13, pp. 2885-2898, 2010.

[9] A. Haque, S. Rahman and M. Rahman, "Factors Determinants the Choice of Mobile Service Providers: Structural Equation Modeling Approach on Bangladeshi Consumers," Business and Economics Research Journal, vol. 1, no. 3, pp. 17-34, 2010.

[10] S. G. Nimako, B. A. Ntim and A. F. Mensah, "Effect of Mobile Number Portability Adoption on Consumer Switching Intention," International Journal of Marketing Studies, vol. 6, no. 2, pp. 117-134, 2014.

[11] K. Kumaresh and S. Praveena, "An Empirical Analysis Of Consumer Switching Behavior Towards Mobile Number Portability," National Monthly Refereed Journal Of Reasearch In Commerce Management, vol. 1, no. 11, pp. 10-22.

[12] D. D. Dave and M. C. Vyas, "Mobile Number Portability: Challenges And Opportunities For Network Service Providers".

[13] W. Olatokun and S. A. Nwone, "Influence of Socio-Demographic Variables on Users' Choice of Mobile Service Providers in Nigerian Telecommunication Market," nternational Journal of Computer and Information Technology, vol. 2, no. 5, pp. 888-894, 2013.

[14] B. Suthar, D. J. K. Sharma and D. A. Gwal, "A Study on Consumer Behaviour After Mobile Number Portability With Reference To Gujarat Telecom Circle," BAUDDHIK, vol. 3, no. 2, pp. 1-7, 2012.

[15] S. A. Keelson, "FACTORS AFFECTING CONSUMER CHOICE OF MULTIPLE MOBILE SERVICES," GLOBAL JOURNAL OF BUSINESS RESEARCH, vol. 6, no. 4, pp. 59-67, 2012.

[16] M. Sathish, K. Kumar, K. Naveen and V. Jeevanantham, "A Study on Consumer Switching Behaviour in Cellular Service Provider: A Study with reference to Chennai," Far East Journal of Psychology and Business, vol. 2, no. 2, pp. 71-81, 2011.

[17] H.-J. Yang and Y.-L. Lay, "Factors Affecting College Students Mobile Phone Dependence and Anxiety," in Proceedings of the World Congress on Engineering and Computer Science, WCECS 2011, San Francisco, USA, 2011.

[18] B. RAMULU and D. S. SINGH, "BRAND PREFERENCE OF STUDENTS TOWARDS CHOOSING CELLULAR SERVICE PROVIDERS IN HYDERABAD CITY," Asia Pacific Journal of Marketing Management Review, vol. 2, no. 5, pp. 17-29, 2013.

[19] D. Suhr, "The Basics of Structural Equation Modeling," University of Northern Colorado, Northern Colorado

[20] R. Develles, "Scale Development," Sage Publications, pp. 24-33, 1991.

[21] L. J. Cronbach, in Essentials of Psychological Testing, Haper Row, 1970, p. 161.

[22] S. Peri, "Business Analytics," 05 August 2012. [Online].Available: http://www.badmforum.blogspot.in/2012/08/factor-analysis-kmo-bartletts-test.html

[23] Statwiki, "Exploratory Factor Analysis," [Online].

[24] Statwiki, "Confirmatory Factor Analysis," [Online]. Available:http:// statwiki.kolobkreations.com /wiki/Confirmatory_ Factor_Analysis.

Chroma Haptic System Enabling Color Cognition for the Visually Impaired

Siddharth Kalra[1], Sarika Jain[2], Amit Agarwal[3]

[1,2]Amity University Uttar Pradesh, Noida, India
[3]University of Petroleum and Energy Studies, Dehradun, India
[1]siddharthkalra@gmail.com [2]ashusarika@gmail.com,[3]coer.info@gmail.com

Abstract: **As human sight corresponds to the maximum amount of sensory data consumption with respect to visual information input. The loss of visual cognition is a great loss in terms of "data lost in acquisition/transit". Amongst other things, the loss of chromatic or colour data is a considerable loss for the visually impaired subject. This paper proposes a novel approach towards enabling the cognition of colours for the visually impaired users. It is done as a practical approach towards fulfilling multiple practical applications. This elusive goal is achieved by virtue of creating a family of 16 basic colours based on the CGA palette and converted to families. These colour families in turn are mapped to a glove with micro tactile vibration actuators mapped to the fulcrum points of the joints of each finger of one hand (total 15 actuators). Each finger corresponds to a colour family and its intensity is mapped on its respective finger joints based vibrators. Thus providing a very intuitive and least neural load based colour cognition. All the computation happens on a smart device which is wirelessly connected to the glove and a camera that translates the live input image and pre-processes the image into 16 colour palette based "blobs" which when overlapped by the hand, sends equivalent vibration signals to the glove, enabling an instantaneous access to colour data and that too very naturally.**

Keywords: **haptic glove, filter, visually impaired, colour family.**

I. INTRODUCTION

When anyone is impacted by visual impairment, the loss of vision actually is just not limited to seeing and recognizing objects and people, rather there is a host of visual cues that get lost in the process. When we "see" an image, we comprehend a lot of attributes, such as shapes, outlines, colours, people, objects landscapes, threats etc. While the loss is immense, this paper tries to compensate the loss of colour cognition to a certain extent.

Colour constitutes a large part of the visual cognition data, and if it can somehow be compensated, the visually impaired subject can really benefit and be enabled in multiple situations, for example, knowing the colour of the traffic lights, a RED coloured post box, the yellow coloured sun, or a light source, colour of a particular type of bus/vehicle, etc. A system thus, which is accurate, easy to use and economical could prove to be of immense utility for the visually impaired individuals.

The colour cognition for visually impaired has been attempted and auxiliary systems implemented by many researchers in the past, however there has been a need to overcome challenges and limitations for an effective implementation of a system in terms of natural perception, minimal neural load, intuitiveness, discreteness, speed and real time data, accuracy, practical usability and long distance applicable.

The concept behind this system is that, we humans are not machines, and our brains tend to quickly generalize things that we see, especially colour. For example there may be more than thousands of the colour pink, in a digital image ecosystem, however we as humans may like to address the colour in perhaps, light pink, or dark pink, or just Pink. In some specialized tasks there may be a need to very accurately differentiate between shades of a same colour, however under normal and practical usage, users may not need exact colour information in terms of many shades, and their respective RGB values, for generic day to day task. Aggregation of multiple shades of a colour in to a larger colour family, reduces lot of unnecessary data processing, and lets the system focus on the basic values that are needed and can simply aggregate the other colour values, creating lesser sample space to act upon, intrinsically enhancing the efficiency and accuracy. So the proposed system basically tries to provide the user a basic broad sense of colour of his surroundings.

In order for things to be practical, fast for instant cognition, a two factor approach is utilized. One is at the Glasses levels which are enabled by camera, Bluetooth, earplugs, WiFi and microcontroller/microprocessor. The second component is a Haptic-Vibro-Tactile, Glove, which is tracked by the Glasses and it houses number of micro vibration motors as depicted later in this paper. The system also deploys pixilation and blurring filters on the image that defocuses the colour and high contrast points to a minimum. Post the above step the blobs in the image are grouped and converted to a simple family of colours. e.g. all shades of green are converted and tagged as just "Green", so on and so forth. While the glove is moving within the viewport of the camera, it continuously tries to locate the middle finger tip of the glove, and subsequently tries to recognize the colour tag adjacent to the glove middle finger".

II. RELATED WORK

Woźniak et al. [1] proposed a novel haptic glove with color sensing capabilities utilizing an illuminating color sensor that's positioned in the palm. Once the color sensor is activated it

propagates pulse width signals to actuators which thus impart hues of the difference in chromatic hues.

Giannopoulos et al. [2] uses Microsoft Kinect camera and sdk to implement a vibrotactile interactivity with 3D virtual objects through a haptic glove with a number of haptic actuators for vibratory feedback. This system uses a virtual reality model and 3D virtual objects simulation.

Díaz [3] also utilizes the Microsoft Kinect sensor, to interact with 3D virtual scenes using spatial locations of the object which are mapped to the work volume of the user utilizing kinect sensor. The hand and its location is also marked which is thus tracked by the sensor and the interactivity is implemented by the vibrating elements deployed by virtue of tactors placed on the user glove.

Rantal et al. [4] have taken this system a bit further implementing interactivity with real object in the real world, using a very sensitive vibrotactile feedback on the glasses worn by the user. These glasses house a subtle vibrotactile feedback on three separate locations on the glasses stimulating three separate regions of the forehead.

The eyewear is also sensitive towards gaze and can interact with real life objects using user gaze as input, for ex, turning on the ceiling fan by gazing at it for a few seconds. This is achieved by a combination of haptic glasses and a camera.

Tapson et al [5] implements as similar predication, where they try and capture the primary colors. They propose that the primary colors can be accurately assimilated by utilizing electronic means, and thus they propose a system of getting the same deployed. They use a few short range color sensors placed on the palm of a user wearable glove which is connected to a belt with vibrotactile actuators that vibrate at different frequencies assimilating the presence of primary colors. This is a very useful system for the visually impaired.

Schwerdt et al. [6] extends on earlier investigations by Tapson et. al. [5] that successfully demonstrated the capability of accurately identifying colours through haptic feedback. Here Schwerdt et al. proposes using a vibro tactile glove instead of a belt with tactors that translate color data to haptic signals processed in the microprocessor.

Hamilton-Fletcher & Ward [7] proposes a visual sensory substitution devices (SSDs) for the visually impaired subjects to understand the world around them, this system basically tries to codify a grayscale version of the image and low resolution color images to provide spatial cues for scene and object recognition.

Dipietro & Sabatini [8] describe the data acquisition and analytics of the hand movement, recognizing and working with gestures, pinch grip etc. in the virtual digital space. The range of motion and other data are captured through this experiment. Numerical measurements have been done by acquiring mechanical data and the critical numbers generated during the task. It's a very good system for skilled therapists and clinical practitioners.

III. PROPOSED METHOD

This paper uses multiple mechanisms to achieve the above stated goal. The core workflow works as given in Fig. 1.

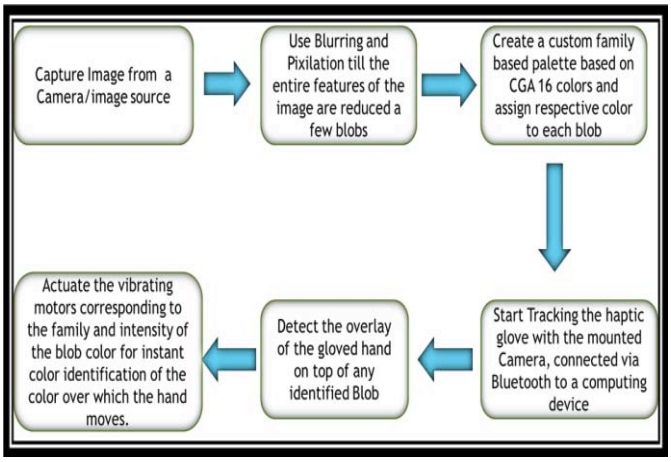

Fig 1: The workflow of the algorithm

However, the detailed steps are as follows:

STEP 1: Capture image from a head mounted camera: The proposed design consists of a wearable eyeglass equipped with CMOS camera for visual input and earplugs for the harmonic acoustic feedback, which consists of polycarbonate frame, earplugs, LiPo battery pack, Infra-Red filters: used in solid state (CCD or CMOS) cameras to filter out Infra-Red light, microcontroller module: to control the onboard hardware and manage the communications between the eye gear and the computing system, bluetooth transceiver module: to transmit and receive data to and from a connected computing device that processes all image input data and returns feedback information, Fig. 2.

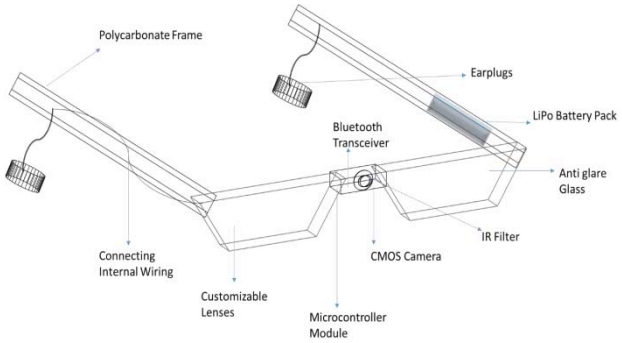

Fig. 2. A wearable eyeglass equipped with CMOS camera

STEP 2: Image preprocessing:

Once the image is captured, the image is thus required to be simplified. The initial goal of the paper is to produce a system for the visually impaired for colour cognition in the day to day life, so that it is easier for the user to comprehend colours quickly and with minimal neural load. Thus, for the system to work, the captured image needs to undergo the three critical steps: i) Image simplification using pixilation, ii) pixilated components grouping, iii) assigning colour families to the groups.

Image Simplification using Pixilation: Proposed methodology is the modification in arithmetic mean filter. The arithmetic mean filter works on the centre pixel of the rectangular subimage, whereas proposed system replaces all the values of rectangular subimage by the average of that subimage, i.e., filter works on a matrix /subimage rather than working on the centre pixel and moves matrix to matrix. In other words,

$$\hat{f}(x,y) = \frac{1}{mn}\sum_{(s,\ t)\in M_{xy}} g(s,\ t)\ \forall\ (x,\ y) \in g(x,\ y),$$

where $\hat{f}$ is the restored intensity at (x, y), M_{xy} represent the set of coordinates of the filter of size m x n, $g(s,t)$ is the original intensity. Moreover, if the size of the image is not divisible by the size of the subimage, then the proposed system changes the size of the filter according to the remainder.

1st Pass: The original image (Fig. 3) is divided into a set of 3 x 3 matrices. Then applying a 3 x 3 averaging filter which replaces all the values of a particular matrix by the average of that matrix. This creates a homogenous pixilation of 3x3 matrix, and normalizes colour gradient, refer Fig. 4.

2nd Pass: Similarly on the image obtained from Pass 1, the image is divided into a set of 5 x 5 matrices and applying a 5 x 5 averaging filter which replaces all the values of 5 x 5 matrix with average. This creates a homogenous pixilation of 5x5 matrix and further normalizes colour gradient starts creating uniforms blobs, Fig. 5.

3rd Pass: The image is divided into a set of 7 x 7 matrices and applying a 7 x 7 averaging filter which replaces all the values of 7 x 7 matrix with average. This creates a homogenous pixilation of 7x7 matrix, and further normalizes colour gradient starts creating even more uniforms blobs, Fig. 6.

Fig. 3. Original Image as seen by the wearable camera

Fig. 4. Image after 1st Pass

Fig. 5. Image after 2nd Pass

The proposed system also works dynamically, i. e., the size of the filters could be changed according to the dimensions of the image.

Fig. 6. Image after 3rd Pass

Pixilated Components Grouping: This procedure isolates the blobs which are in the range of ± 15 % of the average colour blobs, creating a large areas of similar colours. The above pixilation helps in normalizing and getting rid of spikes in the image pixels. For, a 3x3 filter is used and if the 8 neighborhood pixels fall within the ± 15% deviation, then those pixels are the parts of the blob, and this blob is thus

named numerically. This procedure creates a map of edges where the colour blobs are created.

Assigning colour families to the groups: When all the blobs are assimilated, they are assigned standard colour family codes which are strategically designed for the use of 16 generic colours and at the same time conducive for implementation of the haptic glove. Based on the CGA palette, all 16 colours have been further divided in 5 families, namely: black family, blue family, red family, magenta family, green family and white, Fig. 7.

Fig. 7. Colour families

Once the colour families are assigned to the blobs, we get an image map, Fig. 8.

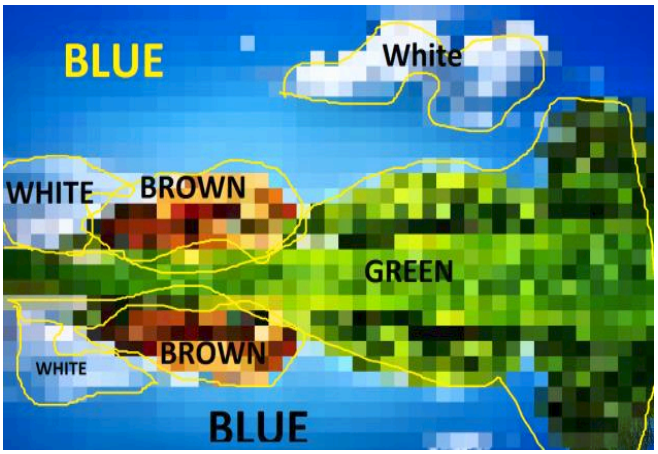

Fig. 8. Image map with pixilation and colour family assignment

STEP 3:

The Haptic Hand: The haptic hand is a glove that is to be worn by the visually impaired subject, and to use it, the subject needs to move his hand in front (over the scene) and as soon as it overlaps a blob, the corresponding actuator is triggered, and in practical application the user will very easily remember that five fingers corresponding to five simple colours, viz black, blue, red, magenta, and black. All inner finger actuators are the lighter versions of the base family colour. So a very quick and instantaneous mechanism is in place for a simple, easy and intuitive colour cognition system for the visually impaired. Fig. 9 shows the haptic glove and its inner constituents with colour family encoded actuators.

Fig. 9. The Haptic glove

Fig. 10. the haptic hand overlaying a blobbed image

IV. RESULTS AND DISCUSSION

Fig. 3 is the original image on which preprocessing steps are applied. Fig. 4-6 depicts the three passes of preprocessing step. In each pass, homogenous pixilation and normalization of colour gradient starts creating uniforms blobs of similar colours. At the end, each blob represents a colour family (Fig. 8) according to the scheme given in Fig.7. In step 3, the haptic glove with micro tactile vibration actuators is moved over the scene. Actuators are triggered as soon as the glove (Fig. 9) encounters a colour blob. In Fig. 10, the haptic hand overlaying a blobbed image, and the camera sees the overlay, actuating the thumb.

V. CONCLUSION

The paper discusses about a haptic glove with micro tactile vibration actuators. Each finger corresponds to a colour family and its intensity is mapped on its respective finger joints based vibrators. This system creates a great ease for the

"generalized" colour cognition of the environment for a visually impaired subject. The user can now very intuitively and with a very small learning curve can use the system and implement the same instantly. Rather than relying on memorizing multiple stimulations, and vibrational amplitudes, now the user just needs to remember 5 colours, and their gradient families, and the user shall be able to comfortably traverse through the environment, with a near real time colour comprehension.

The device being a portable and wearable system, enables the users to use it in the real life and not just particular lab setting. The pixilation of the image simplifies the input image, and thus converting the same into colour blobs, reduce so many irrelevant details, and simplifies the processing of the system to a great extent.

Future application: The system can be enhanced to greater distances, which otherwise is difficult for the sighted individuals also. For example, the camera fitted with a zoom/telephoto lens can help the user to "feel" colours even when far off. Similarly all advancements, such as shake filter, image stabilization system, despeckle filter etc. in the camera ecosystem are bound to enhance the capabilities of our chroma haptic system in a great way.

REFERENCES

[1] Paweł Woźniak, Kristina Knaving, Mohammad Obaid, Marta Gonzalez Carcedo, Ayça Ünlüer & Morten Fjeld, (2015), "ChromaGlove: a wearable haptic feedback device for colour recognition", In 6th Augmented Human International Conference, 219-220

[2] Elias Giannopoulos, Ausias Pomes & Mel Slater, (2012), "Touching the void: exploring virtual objects through a vibrotactile glove", The International Journal of Virtual Reality, 11(3), 19-24.

[3] Carlos Díaz, "An experimental study of remote multi-modal interface in robotic systems", (2014), thesis, Simon Fresor University.

[4] Jussi Rantala, Jari Kangas, Deepak Akkil, Poika Isokoski & Roope Raisamo, (2014), "Glasses with haptic feedback of gaze gestures", Proceeding CHI '14, ACM DL, 1597-1602.

[5] Jonathan Tapson, Netta Gurari, Javier Diaz, Elisabetta Chicca, David Sander, Philippe Pouliquen & Ralph Etienne-Cummings, (2008), "The feeling of colour: a haptic feedback device for the visually disabled", IEEE Conference on Biomedical Circuits and Systems Conference, 381 – 384.

[6] Schwerdt, H.N. ; Tapson, J. ; Etienne-Cummings, R. (2009), "A colour detection glove with haptic feedback for the visually disabled", IEEE conference on Information Sciences and Systems, 681-686.

[7] Giles Hamilton-Fletcher, Jamie Ward, (2013), "Representing colour through hearing and touch in sensory substitution devices", Multisensory research, 26 (6), 503-32.

[8] Laura Dipietro, Angelo M. Sabatini, (2008), "A survey of glove-based systems and their applications", Ieee Transactions On Systems, Man, And Cybernetics—Part C: Applications And Reviews, Vol. 38, No. 4.

2016 IEEE/RSJ International Conference on Intelligent Robots and Systems (IROS)
Daejeon Convention Center
October 9-14, 2016, Daejeon, Korea

Incremental Real-Time Multibody VSLAM with Trajectory Optimization Using Stereo Camera

N Dinesh Reddy[1,2], Iman Abbasnejad[2,3,4], Sheetal Reddy[1], Amit Kumar Mondal[5] and Vindhya Devalla[5]

Abstract— **Real-time outdoor navigation in highly dynamic environments is an crucial problem. The recent literature on real-time static SLAM don't scale up to dynamic outdoor environments. Most of these methods assume moving objects as outliers or discard the information provided by them. We propose an algorithm to jointly infer the camera trajectory and the moving object trajectory simultaneously. In this paper, we perform a sparse scene flow based motion segmentation using a stereo camera. The segmented objects motion models are used for accurate localization of the camera trajectory as well as the moving objects. We exploit the relationship between moving objects for improving the accuracy of the poses. We formulate the poses as a factor graph incorporating all the constraints. We achieve exact incremental solution by solving a full nonlinear optimization problem in real time. The evaluation is performed on the challenging KITTI dataset with multiple moving cars.Our method outperforms the previous baselines in outdoor navigation.**

I. INTRODUCTION

Outdoor navigation in dynamic environments is a challenging task for autonomous driving assistance systems (ADAS). It has wide applications in various areas like collision avoidance, path planning and scene understanding. Inference of highly dynamic scenes accurately is crucial for such systems. A robot navigating in such environments needs a fast and accurate localization of the moving objects and their trajectories. In the past decade, a lot of literature is available for static SFM or SLAM [1], [2] pipeline, where they utilize the static landmarks to build an accurate map and trajectory. These methods treat the moving objects as outliers. These methods fail when there are multiple moving objects in the scene like a congested urban scene due to wrong inlier fitting.

Dynamic object segmentation and trajectory optimization is relatively new field of research with sparse literature. The few solutions to this problem present in the literature can be categorized into Decoupled and Joint Methods. Joint approach like [3] use monocular cameras to jointly estimate the depth maps, do motion segmentation and motion estimation of multiple bodies. Decoupled approaches like [4], [5] have a sequential pipeline where they segment motion and independently reconstruct the moving and static scenes. Our approach is a real-time incremental approach, and differs from the other methods due to the simultaneous optimization of multiple moving cars. The algorithm is easily scalable to multiple cars and highly traffic scenarios.

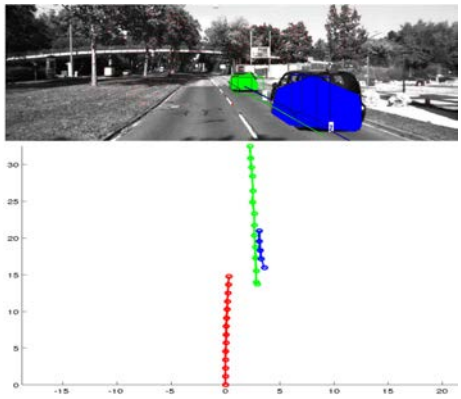

Fig. 1. The top images depicts the real time segmentation of moving objects. The top view of the trajectories of moving objects and the camera odometry are depicted. The Red trajectory represents the camera odometry. The blue and green represents the moving car odometry.Best viewed in color.

Our approach emphasis on a real time approach for moving object trajectory optimization. We obtain our real time motion detection and segmentation from the sparse motion segmentation algorithm [6]. The moving object trajectories are initialized using the triangulation of the moving objects in the current frame and then transforming the trajectories with respect to the world coordinate frame. These trajectories are initialized as poses of a factor graph. The factor graph is included with additional constraints like the relationship between the camera motion and moving object. We also incorporate the motion model of the moving objects for more accurate localization. The main contribution in this paper is the optimization for the moving object trajectory and the camera trajectory simultaneously in real-time. We introduce the concept of anchor nodes for moving object trajectory estimation. The anchor nodes initialize each moving object as a new pose optimization problem and solves for the complete trajectory of the moving object.

II. RELATED WORK

A lot of research in the area of computer vision and robotics has been focused on motion segmentation and SLAM, but limited literature focuses on improving the localization of moving objects and their reconstruction using vision based feedback. Motion segmentation has been approached using geometric priors mostly from a video. General paradigm involves using geometric constraints [12],

[1] International Institute of Information Technology, Hyderabad, India
[2] Max Planck Institute For Intelligent Systems, Tübingen, Germany
[3] The Robotics Institute, Pittsburgh, PA, USA
[4] Queensland University of Technology, Brisbane, QLD, Australia
[5] University of Petroleum and Energy Studies, Dehradun, India

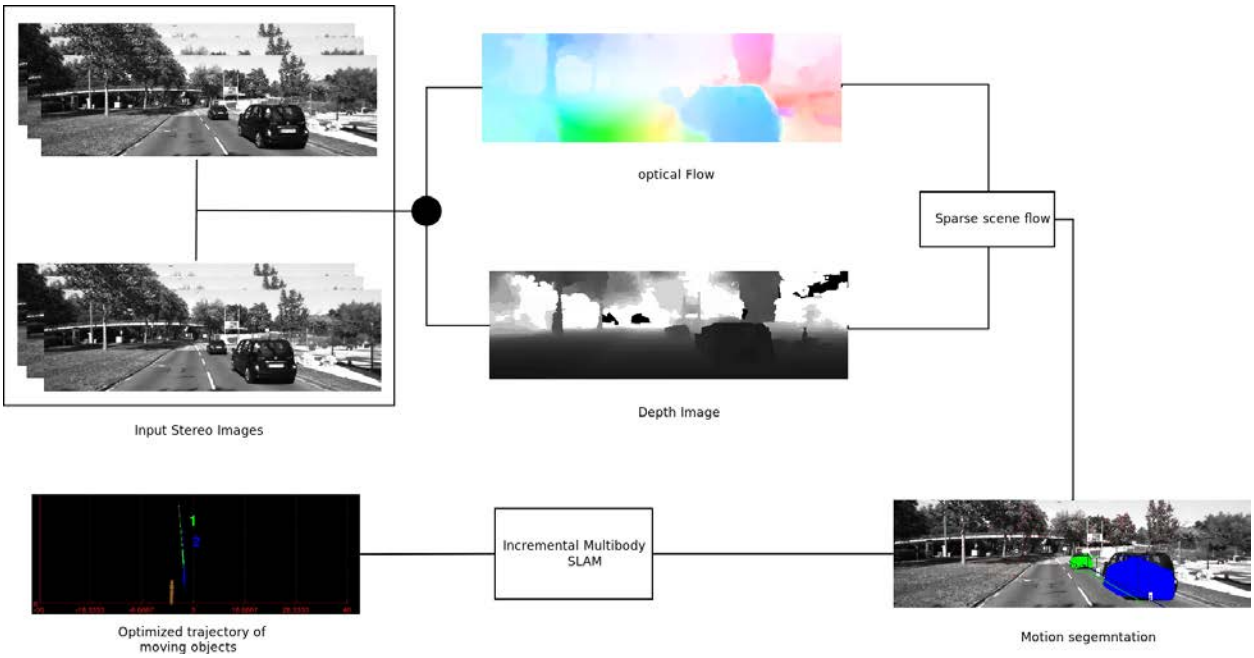

Fig. 2. Illustration of the proposed method.The system takes a sequence of rectified stereo images from the tracking dataset of KITTI (A).Our formulation computes the sparse scene flow (D) using disparity map(B) and optical flow(C).These are used to segment the multiple moving cars in the scene(E).For each segmented car, we estimate the trajectory separately and put them into a joint formulation. The optimized moving object trajectories are displayed in world coordinate frame. Best viewed in color.

[14], reducing the model to affine to cluster the trajectories into subspaces [15] or semantic constraints [13].

A variety of approaches have been proposed to recover the Trajectories of static indoor and outdoor scenes. In contrast, here we propose a method that is able to extract accurate 3d information by reasoning jointly about static and dynamic scene elements as well as their complex interplay using semantic information. Recent advances in static SFM involve adding semantic and geometric constraints to Bundle Adjustment [16]. Jianxiong et al. have shown results on indoor sequences with very high accuracy. Factor graphs[10] have shown considerable improvement in static robot localization. An incremental version of the smoothing and mapping [9] has been shown a improvement in the Static incremental SLAM algorithms.

The moving object localization has recently been a widely researched area for Automated Driver Assistance Systems (ADAS). Song et al. [17] use the object detection and SFM cues for improving the 3D object localization. Dinesh et al.[19] have used semantic constraints for accurate localization of moving objects. The accurate localization of the moving objects in dynamic environments helps in better understanding for outdoor navigation.

Our work closely resembles [8] in problem formulation. They exploit the relationship between two moving robots in the environment and solve the SLAM problem in an incremental formulation. We differ from the above method in terms of the constraints we exploit. We formulate our problem as a factor graph over moving object trajectories. This allows us to model smooth trajectories without employing hard geometric constraints. We also use these trajectories to fuse dynamic and static objects which can be used in robot navigation.

III. OUR APPROACH

We present a probabilistic formulation of the multi-body SLAM problem based on pose graphs. Pose graphs are a common solution for single robot localization and mapping, in which all current and past robot poses form a Markov chain connected by odometry measurements. We have implemented the incremental smoothing and mapping (iSAM) for optimizing the pose graph because it provides an efficient solution without need for approximations and allows effective access to the estimation uncertainties. The implementation exploits constraints between the different poses.

A. Motion Detection and segmentation

We consider a sequence of images from a stereo camera rig. Interest points are detected in two consecutive and rectified stereo images and checked for mutual consistency. The interest points are generated using the SIFT feature detection algorithm. Each feature is matched with their stereo rig and the disparity is computed for each interest point. The 3d location of each Interest point is computed from the disparity. Since ,the mounting and pitching of the stereo rig is unknown, we detect the ground plane for better understanding of the environment. The ground plane computation gives a good prior for the computation of moving and stationary point clusters. All the cluster of points on the ground plane are segmented as stationary. These interest points are tracked over multiple frames and the scene

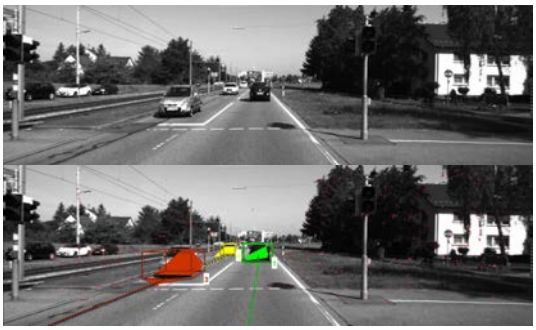

Fig. 3. The results for the motion segmentation algorithm on the KITTI2 sequence is depicted in the image.Each moving car is segmented and labelled with different color, the red point represent the stationary landmarks used for odometry computation. Best viewed in color.

flow is computed using finite difference approximation to yield derivatives. The scene flow stores the information of the motion of the interest point in the world frame.

A graph-like structure connecting all detected interest points in the image plane is generated using Delaunay triangulation. The resulting edges are removed according to scene flow differences exceeding a certain threshold with respect to the uncertainty of the computed 3D position of every interest point. We have added additional geometric constraints for accurate segmentation as proposed in the [14]. We use the ground plane computed earlier for excluding the false positive solutions. The remaining connected components of the graph describe moving objects in the scene. Detected objects are tracked over time using a global nearest neighbor (GNN) approach. The GNN algorithm searches the closest object in distance from its location and tracks the object over multiple frames.

B. Moving object trajectories in global frame

We first formulate the problem of the multibody mapping problem using one pose graph for each moving object trajectory. We show a typical moving object scenario with two moving objects in front of the camera in Fig.4. The pose variables are shown as coloured circles , and measurements as small black discs. In Fig.4 each moving object is represented with different color. For M moving objects, the trajectory of the moving object $m \in \{0....M-1\}$ in the scene is given by $N_m + 1$ pose variables $\{z_i^m\}_{i=0}^{N_m}$. As each moving object trajectory is computed from the stereo triangulation, the trajectories by themselves are underconstrained. We fix the gauge freedom by introducing a prior P^m for each trajectory m. Measurements between poses of a single trajectory are of two types. Where the successive poses are connected based on the camera readings, the other kind of measurements is the connection of arbitrary poses i.e readings of the poses between the cars from the depth information of the stereo cameras.

We have discussed about the moving car trajectory as an independent entity , We now introduce the relationships between the moving objects and the camera trajectories. An encounter **e** between the moving object and the camera odometry exploits the relationship between the camera motion and the moving object motion ,depicted in Fig. 5.Similarly, an encounter **e** between two moving objects m_1 and m_2 is a measurement that connects the two moving objects in a scene $z_i^{m_1}$ and $z_i^{m_2}$. An example is shown in the Fig. 6, with the relation between the measurements and poses. Since we have a setup where the observations are the same time instance, all our measurements **e** connect poses taken at the same instance.

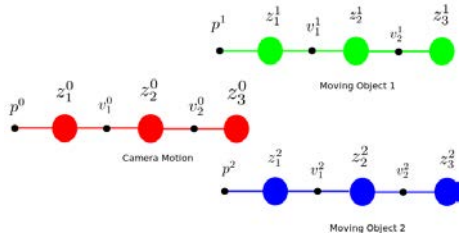

Fig. 4. This depicts the formulation of the dynamic iSAM problem. The red represents the camera odometry, while the green and blue represent the moving objects predicted from the III-A.

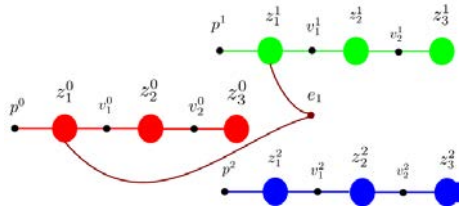

Fig. 5. Here we depict the relationship between the moving object pose and the camera trajectory. The pose of the moving object and the camera is exploited by this constraint.

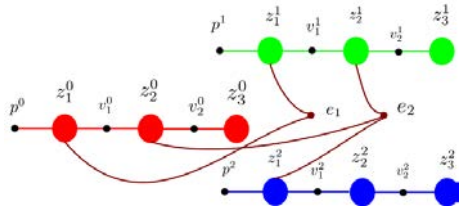

Fig. 6. Here we depict the relationship between the moving object pose m_1 and another moving object m_2. This exploits the relationship between the moving object motions.

We take a probabilistic approach for estimating the moving object trajectory based on all the measurements.We formulate a joint probability for all the poses $Z = \{z_i^m\}_{i=0,m=0}^{N_m}$,measurements and priors $Y = \{v_i^m\}_{i=0}^{N_m} \cup \{p^m\}_{i=0}^{N_m}$ and L encounters $E = \{e_i^m\}_{i=0,m=0}^{N_m}$:

$$P(Z,Y,E) = \prod_{m=0}^{M-1} \left(P(z_0^m|p_0^m) \prod_{i=1}^{N_m} P(z_i^m|z_{i-1}^m, v_i) \right) \prod_{j=1}^{L} P(z_{i_j}^{m_j}|z_{i'_j}^{m'_j}, e_j) \quad (1)$$

The number of encounters L is equal to to the number of frames in the sequence. The data association between the encounters i_j, i'_j, m_j, m'_j is computed for each frame

from the motion segmentation and localization algorithm as discussed in section III-A. The noise is assumed to be gaussian as proposed in multiple SLAM systems.

$$z_i^m = f_i(z_{i-1}^m, v_i^m) + w_i^m \tag{2}$$

This describes the moving object localization in the current frame of reference computed from the disparity computation. The w_i^m is a normally distributed noise with covariance matrix ξ_i^m. We model the encounters within the moving objects and between the moving objects and the camera as :

$$z_{i_j}^{m_j} = h_j z_{i'_j}^{m'_j}, e_j + k_j \tag{3}$$

Similar to the successive poses interactions the noise for the measurement model of the moving objects is computed from the disparity computation. Here, k_j is a normally distributed noise with covariance of Γ_j.

We formulate the problem as a maximum a posterior (MAP) estimate for the moving object trajectory. This leads to the following nonlinear least squares problem:

$$\begin{aligned} Z^* = arg\ min\Bigg\{ & \sum_{r=0}^{M-1} \Big(||p^m - z_0^m||_\Sigma^2 \\ & + \sum_{i=1}^{N_m} ||f_i(z_{i-1}^m, v_i^m) + w_i^m||_{\xi_i^m}^2 \Big) \\ & + \sum_{j=1}^{L} \Big|\Big| h_j z_{i'_j}^{m'_j}, e_j + z_{i_j}^{r_j} \Big|\Big|_{\Gamma_j}^2 \Bigg\} \end{aligned} \tag{4}$$

Here $||a||_\Sigma^2 = a^T \Sigma^{-1} a$ is the squared Mahalanobis distance with covariance matrix Σ.

We solve the non-linear least squares problem using the incremental smoothing and mapping (iSAM) algorithm. Since the error in object localization of the moving object is modelled as a gaussian and the constraint functions are non-linear , nonlinear optimization methods are used. We can use the methods like gauss-newton, Levenberg-marquardt or the Powell's Dog-leg algorithm , which use succession of linear approximations to reach a minimum.All the components can be written in a standard least squares problem of the form :

$$\Theta^* = argmin_\Theta ||A\Theta - b||^2 \tag{5}$$

where the vector $\Theta \in R^n$ consists of all the moving object poses and the robot pose, where n is the number of variables. The matrix $A \in R^{mxn}$ is a large , but sparse measurement jacobian , with m the number of measurements, and $b \in R^m$ is the right-hand side vector. We solve this using the method of QR factorization of the A matrix.

$$A = Q \begin{bmatrix} H \\ 0 \end{bmatrix} \tag{6}$$

where $H \in R^{nxn}$ is an nxn upper triangulation matrix , 0 is an $(m-n)xn$ zero matrix , Q is an mxn orthogonal matrix. The vector b is modified accordingly during the QR decomposition to obtain $d \in R^n$. The solution is obtained by back substitution.

$$R\Theta = d \tag{7}$$

To avoid refactoring an increasingly large measurement jacobian each time a new measurement is computed, we have followed the method of iSAM to update the new measurement rows. The key to efficiency is to keep the square root information matrix sparse, which requires choosing a suitable variable ordering. iSAM periodically reorders the variables according to some heuristic and performs a batch factorization that also includes relinearization of the measurement equations.

The initialization of the moving object trajectories is done using the stereo triangulation of all the points in the segmentation. The pose is initialized as the transformation between the set of 2d points. The motion detection algorithm is used for accurate prediction of the prior p^m, therefore we have very less gauss freedom and a very good initialization of the moving object trajectories.

IV. EXPERIMENTAL RESULTS

We have used the KITTI tracking dataset for evaluation of the algorithm , as the ground truth localization of moving objects per camera frame is available. It consists of several sequences collected by a car-mounted camera in urban,residential and highway environments, making it a varied and challenging real world dataset. We have taken two sequences consisting of 30 images and 212 images for evaluating our algorithm. The first sequence contains two cars which are over-taking the current car and the second sequence is a highway sequence of multiple moving cars. We chose these 2 sequences as these sequences pose challenge to motion segmentation algorithm as the moving cars lie in the subspace as the camera. These sequences also has a mix of multiple cars visible for short duration and whole sequence tracked cars which allows us to test our robustness of localization and trajectory reconstruction on both short and long sequences.

A. Trajectory Evaluation

We compare the estimated trajectories of the moving objects to the extended Kalman filter based object tracking VISO2 (Stereo). VISO2 S(Stereo) has reported error of 2.44% on the KITTI odometry dataset, making it a good baseline algorithm to compare with. As proposed by Sturm et al. [11], we compare the two sequences based on ATE for root mean square error (RMSE), mean, median and ARE. We use their evaluation algorithm which aligns the 2 trajectories using SVD. We show the three statistics as mean and median are robust to outliers while RMSE shows the exact deviation from the ground truth. We also evaluate RE which is the relative error $\%$ of RMSE: $(ATE_V - ATE_O)/ATE_V$ and signifies the error change relative to VISO2. The trajectory for each moving object is computed using the KITTI tracking dataset's Ground truth. The location of each moving object in individual frame is transformed to the world reference frame using the odometry of the VISO2.

Car Num	P	VISO2				OUR APPROACH				
		ATE R(m)	ATE M(m)	ATE Me(m)	ARE (deg)	ATE R(m)	ATE M(m)	ATE Me(m)	ARE (deg)	**RE(%)**
1	28	0.731	0.513	0.330	3.659	0.317	0.277	0.299	2.589	**36.63**
2	28	0.391	0.212	0.079	2.235	0.193	0.174	0.141	1.356	**50.51**
Cam	28	0	0	0	0	0.10	0.09	0.08	1.238	

TABLE I

STATISTICS OF VISO2 AND OUR APPROACH FOR **KITTI 2** DATASET. **P** IS #POSES. **ATE R** IS ABSOLUTE TRAJECTORY ERROR RMSE, **ATE M** IS ABSOLUTE TRAJECTORY ERROR MEAN,**ATE ME** IS ABSOLUTE TRAJECTORY ERROR MEDIAN, **ARE** IS AVERAGE ROTATION ERROR AND **RE** IS RELATIVE POSE ERROR.

Car Num	P	VISO2				OUR APPROACH				
		ATE R(m)	ATE M(m)	ATE Me(m)	ARE (deg)	ATE R(m)	ATE M(m)	ATE Me(m)	ARE (deg)	**RE(%)**
1	212	2.371	2.222	2.009	5.272	2.146	1.822	1.307	3.594	**9.4**
2	**9**	0.900	0.744	0.733	3.685	0.519	0.446	0.436	2.976	**42.33**
3	**8**	0.962	0.749	0.595	4.522	0.378	0.300	0.296	2.684	**60.7**
4	**8**	0.381	0.324	0.307	2.354	0.259	0.217	0.214	1.343	**32.02**
5	**9**	0.559	0.489	0.445	3.254	0.473	0.341	0.239	2.378	**38.99**
Cam	212	0	0	0	0	2.02	1.84	1.56	5.256	%

TABLE II

STATISTICS OF VISO2 AND OUR APPROACH FOR **KITTI 1** DATASET. **P** IS #POSES. **ATE R** IS ABSOLUTE TRAJECTORY ERROR RMSE, **ATE M** IS ABSOLUTE TRAJECTORY ERROR MEAN,**ATE ME** IS ABSOLUTE TRAJECTORY ERROR MEDIAN, **ARE** IS AVERAGE ROTATION ERROR AND **RE** IS RELATIVE POSE ERROR.

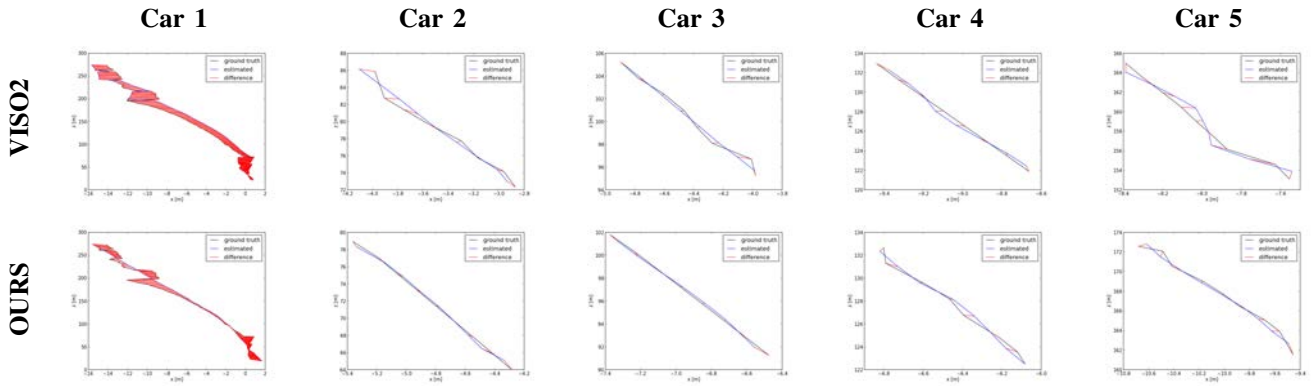

Fig. 7. Comparison plots for 5 moving cars in the KITTI 1. The black plot represents the ground truth trajectory of the moving car in the world frame. Blue plot represents the estimated trajectory of the moving car. Red lines represent the error in the estimate with respect to ground truth for the trajectories. The error comparison is computed between OUR method and VISO2.

KITTI 1 Sequence is a 212 image sequence with in total 13 moving cars. We have showed results for 5 moving cars (due to space constraints). The car in front of the camera is tracked for 212 images while others are 5-10 images long. As seen from Table II we can clearly observe that VISO 2 accumulates drift leading to higher RMSE and Median error over the long sequence. Our approach shows considerable robustness to drift and has average reduction error of 36.688 %. Car 2-5 show on small sequences average error reduction of 42.5 % which is due to the smoothness constraints.

KITTI 2 Sequence is a 28 image sequence with 2 cars overtaking the camera, this poses challenge to motion segmentation leading to noisy initial estimates. Our approach here too does better than VISO2 as shown in Table I with average error reduction of 43.57%. This shows our method is able to handle both long and short sequences. Fig III-B shows the comparison of the trajectories relative to VISO2.

The KITTI 2 sequence is an good example of localization error of the robot. The motion of the cars lie in the flow vector direction leading to error propagation into the camera localization. Our formulation incorporates the motion of the moving objects into the formulation causing improvement in the localization of the camera concurrently more accurate localization of landmarks and moving objects. Using our current formulation, we propose an improvement in the odometry and moving object localization when the ransac based SLAM systems fail. We can attribute this to the joint formulation of the odometry and moving object trajectories. The prior from the moving object adds to the localization of the camera.

V. CONCLUSIONS

This paper presents an approach for accurate localization of moving objects in a highly dynamic environment. This

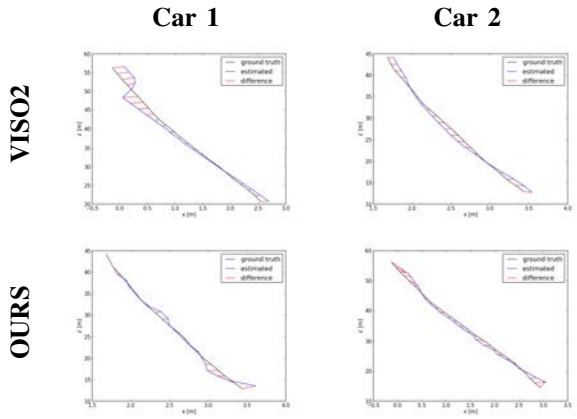

Fig. 8. Comparison plots for 2 moving cars in the KITTI 2 sequence. The black plot represents the ground truth trajectory of the moving car in the world frame. Blue plot represents the estimated trajectory of the moving car. Red lines represent the error in the estimate with respect to ground truth for the trajectories. The error comparison is computed between OUR method and VISO2.

is an incremental real time algorithm and can be used in both indoor and outdoor environments. The algorithm solves the full multibody VSLAM optimization algorithm in real time. We have proposed a new algorithm for moving object localization. We show an improvement in the camera trajectory computation compared to the standard camera trajectory computations. An extensive evaluation of trajectories for long sequences has been compared. We propose a novel method of evaluation of moving object trajectories. The accurate localization of the moving objects is useful in ADAS systems.

We plan on releasing the GT trajectories for the moving objects and the evaluation script for cross comparison. We plan on improving the motion segmentation using additional semantic constraints for better localization of the moving objects. Incorporating additional constraints into the Factor graph will be exploited. We are also investigating the trajectory planning for the robot navigation in dynamic environments.

REFERENCES

[1] C. Kerl and J. Sturm and D. Cremers,Dense Visual SLAM for RGB-D Cameras, International Conference on Intelligent Robot Systems (IROS), 2013.

[2] J. Engel and T. Schops and D. Cremers ,LSD-SLAM: Large-Scale Direct Monocular SLAM ,In International Conference on computer vision (ICCV) , 2014.

[3] Roussos, Anastasios and Russell, Chris and Garg, Ravi and Agapito, Lourdes,Dense multibody motion estimation and reconstruction from a handheld camera, IEEE International Symposium on Mixed and Augmented Reality (ISMAR), 2012

[4] Chang Yuan and Gerard G. Medioni,3D Reconstruction of Background and Objects Moving on Ground Plane Viewed from a Moving Camera, Conference on Computer Vision and Pattern Recognition (CVPR), 2006.

[5] Kundu, Abhijit and Krishna, K. Madhava and Jawahar, C.V.,Realtime Multibody Visual SLAM with a Smoothly Moving Monocular Camera, IEEE International Conference on Computer Vision (ICCV), 2011.

[6] Philip Lenz and Julius Ziegler and Andreas Geiger and Martin Roser,Sparse Scene Flow Segmentation for Moving Object Detection in Urban Environments,Intelligent Vehicles Symposium (IV),2011 .

[7] Michael Kaess and Frank Dellaert. Covariance Recovery from a Square Root Information Matrix for Data Association , in Journal of Robotics and Autonomous Systems (RAS) ,2009.

[8] Been Kim and Michael Kaess and Luke Fletcher and John Leonard and Abe Bachrach and Nicholas Roy and Seth Teller , Multiple Relative Pose Graphs for Robust Cooperative Mapping ,in IEEE Intl. Conf. on Robotics and Automation (ICRA) ,2010.

[9] Michael Kaess and Hordur Johannsson and Richard Roberts and Viorela Ila and John J. Leonard and Frank Dellaert ,iSAM2: Incremental Smoothing and Mapping with Fluid Relinearization and Incremental Variable Reordering, In IEEE Intl. Conf. on Robotics and Automation (ICRA), 2011

[10] Frank Dellaert ,Square Root SAM: Simultaneous Location and Mapping via Square Root Information Smoothing,In Robotics: Science and Systems (RSS), 2005.

[11] J. Sturm and N. Engelhard and F. Endres and W. Burgard and D. Cremers. A Benchmark for the Evaluation of RGB-D SLAM Systems, International Conference on Intelligent Robot Systems (IROS), 2012.

[12] R.K. Namdev, K.M. Krishna, and C. V jawahar. Motion segmentation of multiple objects from a freely moving monocular camera, International Conference on Robotics and Automation (ICRA), 2012.

[13] N.Dinesh Reddy, Prateek Singhal and K. Madhava Krishna,Semantic Motion Segmentation Using Dense CRF Formulation,Indian Conference on Computer Vision, Graphics and Image Processing (ICVGIP),2014.

[14] Victor Romero-Cano and Juan I. Nieto,Stereo-based motion detection and tracking from a moving platform,Intelligent Vehicles Symposium(IV),2013.

[15] E.Elhamifar and R.Vidal. Sparse subspace clustering, International Conference on Computer Vision and Pattern Recognition (CVPR), 2009.

[16] Jianxiong Xiao, Andrew Owens, Antonio Torralba, "SUN3D: A Database of Big Spaces Reconstructed Using SfM and Object Labels", International Conference on Computer Vision(ICCV), 2013,pp. 1625-1632.

[17] S. Song and M.K. Chandraker, Joint SFM and Detection Cues in 3D Object Localization for Autonomous Driving ,In International Conference on Computer Vision and Pattern Recognition(CVPR) 2015.

[18] N. Dinesh Reddy, Prateek Singhal, Visesh Chari, K. Madhava Krishna , Dynamic Body VSLAM with Semantic Constraints , In International Conference on Intelligent Robot Systems (IROS) 2015.

[19] Chhaya, Falak and Reddy, N Dinesh and Upadhyay, Sarthak and Chari, Visesh and Zia, M Zeeshan and Krishna, K Madhava , Monocular Reconstruction of Vehicles: Combining SLAM with Shape Priors, In International Conference on Robotics and Automation (ICRA) 2016.

[20] Chieh-chih Wang and Charles Thorpe and Martial Hebert and Sebastian Thrun and Hugh Durrant-whyte,Simultaneous localization, mapping and moving object tracking,In International Journal of Robotics Research ,2004.

2015 1st International Conference on Next Generation Computing Technologies (NGCT-2015)
Dehradun, India, 4-5 September 2015

Intelligent Custom Dictionary Based Encryption/Decryption Scheme

Abhineet Anand*, Ankur Dumka†, Ravi Tomar‡ and Ankit Khare§

* Center of Information Technology, University of Petroleum and Energy Studies, Dehradun, abhineet.mnnit@gmail.com
†Center of Information Technology, University of Petroleum and Energy Studies, Dehradun
‡ Center of Information Technology, University of Petroleum and Energy Studies, Dehradun
§ Center of Information Technology, University of Petroleum and Energy Studies, Dehradun

***Abstract*—Message are send through encrypter, no one can read the text without having the encrypted software and key that has been used. If any user intends to send a open massage to many people(family, friends, colleagues, etc.) and if it being read by many people at other end too(public mail server, ICQ, etc.), discussed method will come in to play. Experiences of using encryptors and steganographers for security has led to arise many questions as to why there are so many softwares still very few are used. with discussed methodology the opportunity to explore the world of algorithms, security, Java and encryption to nd out the answers to questions. The learning process is being improved on development of the each term of development and curve steeper than previous work. From the theoretical aspect, many researcher are doing a lot of work in this domain of encryptions decryption and its related areas.**

A new security protocol has been proposed implemented by encoding it in Java based environment, which prove to be more secure provide reliable transmission from sender to receiver. This implementation uses a unique key generated requested by user for secure transmission over the network.

Keywords: Cryptography, Security, RSA, AES, DES

I. INTRODUCTION

It is very challenging that the Internet and other information technology eld are making the change at very high speed and the ways, in which communication is changing also. When digital revolution comes, it also brings new challenges with the speed, accuracy, and effective benets, these challenges of the security information transporting over the open communications scenario[1].

Earlier we were using the traditional black and white paper based media for communication and wooden cabinets for storing important data and information, those are now being replaced by the wired and wireless communication means. Basic security measure which can be used for securing new ages of data communication may be suggested as Identication, authorization & authentication rst. With that suggestion can be made for various robust and complex algorithm for encryption & cryptographical techniques. These encryption techniques were using various arithmetical process which involve various mathematical and logical techniques, which were mainly used by different defense agencies for difference purpose. But when the more smart device come into the picture i.e. Computer, and its revolution with the changes that are part of change in the eld of encryption, a new era for secure and safe means of data communication has been introduced.

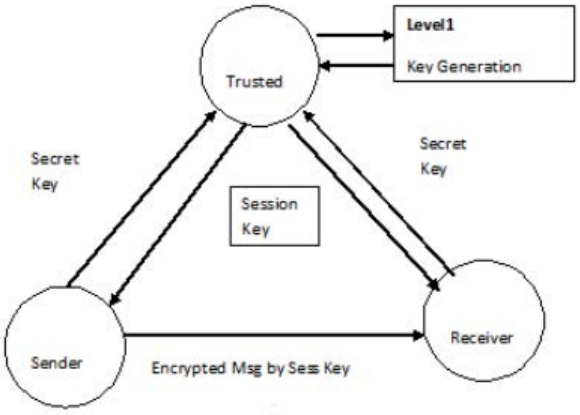

Fig. 1. Proposed Methodology

The new economical changes in the world lead by electronic revolution has changed the way of thinking of a common man and the changed the need of social and economical way of taking things in their life. [2] Now, the calculating device is used for storing personal, nancial, medical, research, and many more type data for future use and analysis. And they are being exchanged and shared among all in a very restricted as well as shared manner. As the data was shared and exchanged with a open media, the need of privacy enabled technology is increasing with the time.

II. RELATED STUDIES

Perhaps the need of the hour is security and this could be achieved by the use of encryption. Take for example, in the business word, the information that a business owns is invaluable to its productive operation. Therefore, the protection of this information is absolutely necessary and one they best way to protect such information and data are through encryption[3]. For people working in small ofces and home ofces, the most practical use of the encryption for data protection are le and email encryption[2]. Our objective is cleared with the above captioned lines. Here. is the outline of work process how this is going to be implemented.

- Changing the data in other form so that it is possible to send it through unsecured media.
- Code the process in some advanced programming environment.
- Using various required calculation including arithmetic as well as logical computations.
- Efcient implementation with the digital verication using digital signature. For the sake of easy environment, it should be Graphical based.
- Now, the nal step should be for storing the data into some web based environment to provide easy accessibility and handling.

III. NECESSITY OF DATA ENCRYPTION

Information Super Highway has become a common phrase now a days. Now, it is the need and necessity for a common man. People are always talking about the sharing data and information through various communication media. So, the need of application and gateways are also increasing with the time. The characteristic required in these application are to be fast, easy and secured. A common man is using these type of application very regularly and constantly. But, to keep them secured is the highest challenge for developers and administrators and it is become more complex and difcult with the time also. The security issue is being raised all the time. Stories about hackers with malicious intents penetrating computer systems are abundant. Various cases of fraud, hacking and stealing of data and information are in news all the time. Some cases are so vital that they are effecting the normal life also. A common man is trying to become more cautious and alert while using their ATMs, Bank accounts for transferring money, in paying bill through credit cards and at various more occasions. There is always threat of stealing of their data or information.

This is where data encryption and cryptography comes into play. Encryption techniques can be used to mask electronic information and make it unreadable. Only by doing the decryption techniques can the information be converted back to readable format.

A. *Below are the example of the seriousness of electronic theft*

1) In United States during 2001, the Internet fraud complaint center organized by the United States Department of justice and the FBI, received 49,711 complaints relating to Internet fraud, 16,775 of which were referred to other authorities for further action. The average monetary loss per referee complaint was USD 435,000 with 43 percent of complaints relating to action fraud.[8]
2) The federal trade commission fraud database consumer sentinel which compiles identity theft and consumer fraud data from United States and Canadian agencies, recorded over 200,00 complaints in 2001.This compare with 18,600 complaints in 1999 and 8,000 in 1998.[9]

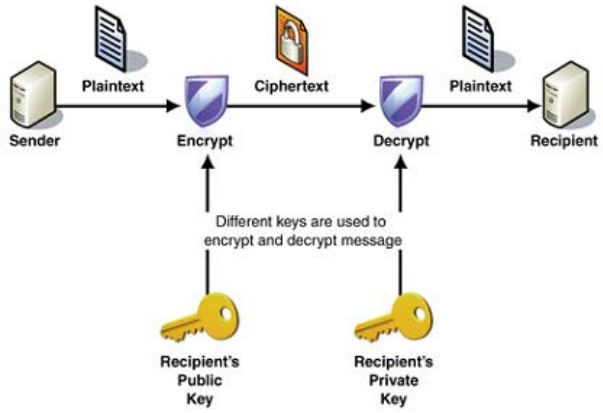

Fig. 2. Different keys are used to encrypt and decrypt message

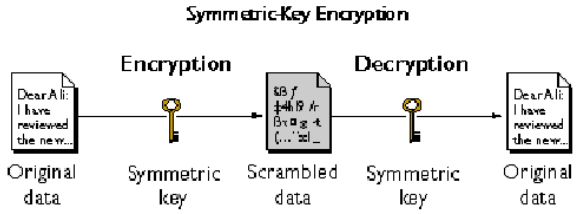

Fig. 3. Symmetric-Key Encryption

IV. DESIGN BASIS

Various algorithm and technique has been proposed with the time to make the data exchange secure, fast and easy. In one the environment Symmetric Key Cryptography has been used. In this algorithm same key is used at the senders side and receivers side. This common key is being shared at both end.which makes, it very easy guess/calculate the common key used in this environment, which makes its very weak technique for sending highly valued data over unsecured media. There are various other technique/algorithm to implement the secure medium for exchanging data. Here, in this paper three of them has been discussed.

1) RSA Algorithm
2) Advanced Encryption Standard
3) Data Encryption Standard

A. *RSA Algorithm*

The RSA algorithm uses the idea of that it is not possible to have factor of huge numbers like 100 - 200 digits integer. RSA is the one of the very rst algorithm to implement data encryption technique which is using different keys at the senders side and receivers side. This senders side key is known to all, but the key at receivers side is made private. So it is the combination of public and private key. This algorithm is named after its inventors Ron Rivest, Adi Shamir, and Lenard Adleman in 1977. This algorithm was declassied until 1997. There are further calculation also which makes this algorithm very popular and guided various other researcher for their work. Here is a go through of this algorithm. The data encrypted with the public key at senders side, can only be evaluated at receivers side in a reasonable amount of time

using the key, not known to other. Now, lets see how the scientist have designed the keys for encryption.

Encryption: The process of encryption for encryption key(e,n) will follow the following steps:

- Take the data to be transmitted in the form of 0 and n-1. If it is a big number then divide it into smaller parts.
- Every part should be shown using the integer of the same range.
- Translate the massage by taking it eth power of module n. , this output of the process is the converted text which will be C.
- To nd the cipher text data C, we have to get the power d of mod n. massage Key(e,n) is known to all, but the dycryp- tion key(d,n) is not known to any one except user.

Decryption: A can recover m from c by using her private key exponent d by calculating

$$mc^d(modn) \tag{1}$$

Given m, she can recover the original message M by reversing the padding scheme. (In practice, there are more efcient methods of calculating cd using the precomputed values below.)

B. Find suitable values for e, d and n

Finding suitable value of e, d and n is also a tedious task, as they will be key of whole process. Following steps are being followed for getting values of these nos.

- Select two large nos such that the length of these no should be more than hundred digits.
- Denote numbers as x and y.
- Find z = x * y.
- Get any big number, g, such that, , GCD(g,((x-1)*(y-1))=1
- Get, e*d=1(mod(x-1)*(y-1))

RSA gives the very productive and cost effective procedure for all the step of these algorithm in very efcient manner.

C. Advanced Encryption Standard

Advanced Encryption Standard(AES) is an encryption technique which uses block cipher technique to convert the plain text to cypher text and its uses length as 128 bits.The AES algorithm does not use the DES algorithm standard, rather its use substitution-permutation Network. It is in three different length version which are: 128, 192 or 256 bits version. The conversion process is having 10 different cycles of conversion for 128-bit keys. Usually it is of 12 cycle - 192 bit keys 14 cycle for 256 - bits. Last cycle for all the conversion is same.

For all cycle of calculation, it should have following steps

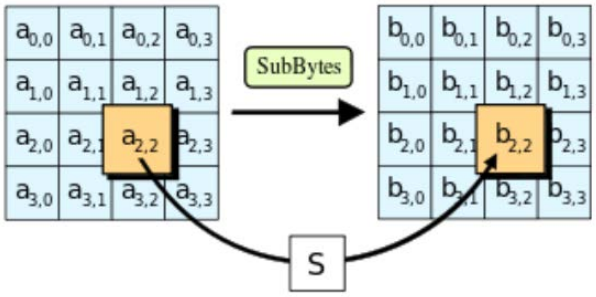

Fig. 4. The SubBytes Step

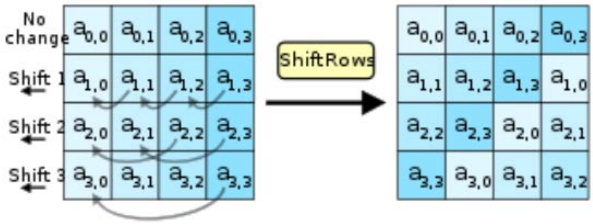

Fig. 5. The ShiftRows Step

1) *Sub Byte Step:* In this step each byte is combined with a block using a logical xor operation.
2) *Shift Row Step:* Each byte is substituted with other as discussed in the table used in the process.
3) *Mix Column Step:* Column of the state are mixed as the operation in this step. Its combines four different bytes to each column.

1) **The SubBytes Step:** In the very step of the this encryp- tion the byte ai,j is changed by SubByte s(a,b) as discussed in the Rijndael S-box as shown in the g. 4. The S-Box is taken from the Multiplicative Inverse. The s-box is cerated by adding the inverse function and invertible afne transformation. In the decryption phase the reverse of subbytes step is used to tak the afne transfermation for getting the multiplicative inverse. That is just the reverse of this step.
2) **The ShiftRows Step:** This step follows the step of shifting the bytes of each roes to its left which results in shifting the bytes in all row by certain offset value. In this particular algorithm the bytes of rst row will not be changed and all the rows next to rst row will be shifted to its left. This is done because it will not allow to create columns linearly independent, which produce four independent block ciphers. The step can be easily demonstrated by gure 5.
3) **The MixColumns step:** This step is used for mixing of column as the name suggests. The four bytes of the all column are added by invertible liner transformation. Its takes 4 bytes as input and produces 4 bytes as output. Diffusion technique is used to for getting the cipher. During this operation, each column is multiplied by a xed matrix shown in matrix - 1.

In the matrix multiplication, the different no represents the shifting of the value by the no of column.

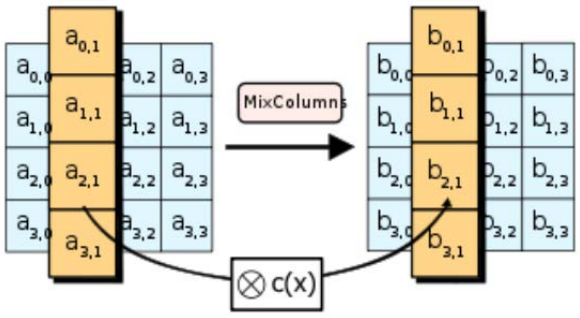

Fig. 6. The MixColumns Step

$$\begin{bmatrix} 2 & 3 & 1 & 1 \\ 1 & 2 & 3 & 1 \\ 1 & 1 & 2 & 3 \\ 3 & 1 & 1 & 2 \end{bmatrix}$$

Fig. 7. Matrix - 1

As shown in the gure that if the multiplication is done with 1 that will not changed. If the multiplication is done by 2 means the data will be shifted by two columns and if its 3 then it will by shifted by 3 columns. Then, the function of xor will be performed. But that will be done only done if the shifted value is more than 0xff. The MixColumns step can also be viewed as a multiplication by the shown particular MDS matrix in the nite eld GF(28). This process well dened in the Rijndael mix columns.[14]

4) **The AddRoundKey Step:** This step involves the combi- nation of the state with the subkey. In each round, a key is generated by the main Rijndeals Key of the same size as in the state. The subkey is combined with the bytes of state of the corresponding byte of the subkey in the bitwise xor operation.

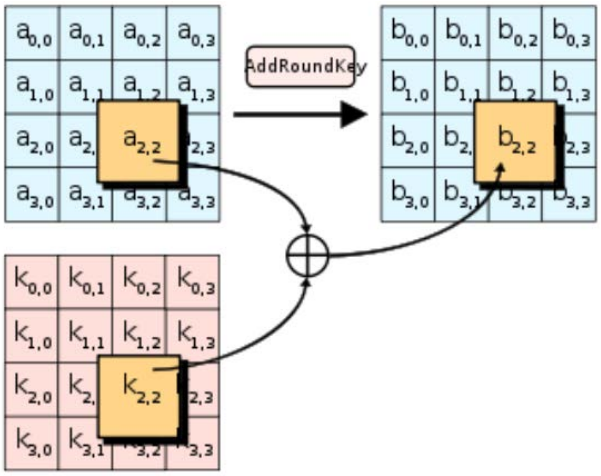

Fig. 8. The AddRoundKey Step

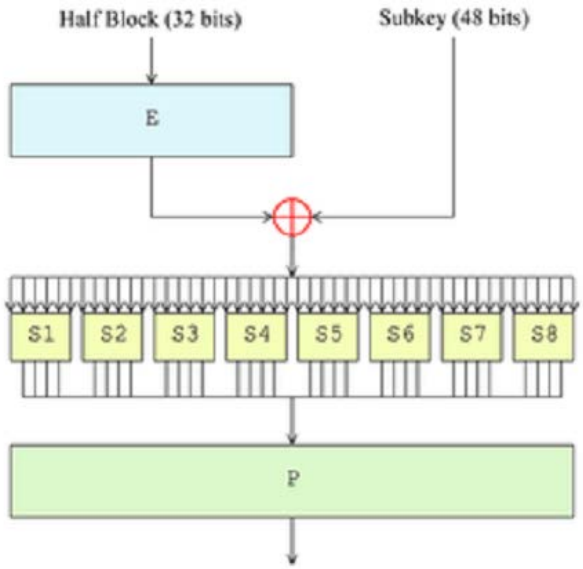

Fig. 9. The Feistel (F) function

D. Data Encryption Standard Algorithm

The Data Encryption Standard(DES) is ofcially designed by IMB and Government of US. The main purpose of was to communicate safely and secured environment.

The encryption procedure was divided in to 16 different cycles. The data which was entered was use to generate a 16 different 48 bits keys. These 16 codes was for 16 different cycle. In each cycle, eight different S boxes are used. Now this S-boxes are used for 6-bit are mapped to group of four bits. These s box are designed by U.S. National Security Agency. Now the block of the massage is divided into two halves.

1) **The Feistel (F) function:** The F-function, as shown in the picture g.8., calculates half a block (32 bits) at a time and which have of four different stages:
   - Expansion: As it is being said that the block is divided in to two halves, the 32-bit half is made to 48 bits by the expansion permutation, Shown as E in the fig.8, by coping half of the bits. The result is having 8, 6 pieces, all of it have a duplicate value of 4 corresponding input bits, plus a duplicate value of the immediately adjacent bit from each of the input pieces to either side. Now the following step are applied for getting the expansion
   - Key mixing: The final outcome is added with sub key and xor operation is applied for this combination. Different 16, 48-bit sub key are generated from the main key using the key schedule.
   - Substitution: After substituting and mixing in the subkey, the block is further departed into 8, 6-bit parts before executing by the substitution boxes. The S boxes gives the main part of the security of DES.
   - Permutation: Finally, the 32 outputs from the S-boxes are rearranged according to a fixed

permutation, the P box. This is designed so that, after permutation, each S-boxs output bits are spread across 4 different S boxes in the next round.

The alternation of substitution from the S-boxes, and permuta tion of bits from the P-box and E-expansion provides so-called confusion and diffusion respectively, a concept identified by Claude Shannon in the 1940s as a necessary condition for a secure yet practical cipher.

2) **key Schedule:** Figure illustrates the key schedule for en cryption the algorithm which generates the sub-keys. Initially, 56 bits of the key are selected from the initial 64 by Permuted Choice 1 (PC-1) the remaining eight bits are either discarded or used as parity check bits. The 56 bits are then divided into two 28-bit halves; each half is thereafter treated separately. In successive rounds, both halves are rotated left by one or two bits (specified for each round), and then 48 subkey bits are selected by Permuted Choice 2 (PC-2) 24 bits from the left half, and 24 from the right. The rotations (denoted by in the diagram) mean that a different set of bits is used in each subkey; each bit is used in approximately 14 out of the 16 subkeys. The key schedule for decryption is similar the subkeys are in reverse order compared to encryption. Apart from that change, the process is the same as for encryption. The same 28 bits are passed to all rotation boxes.

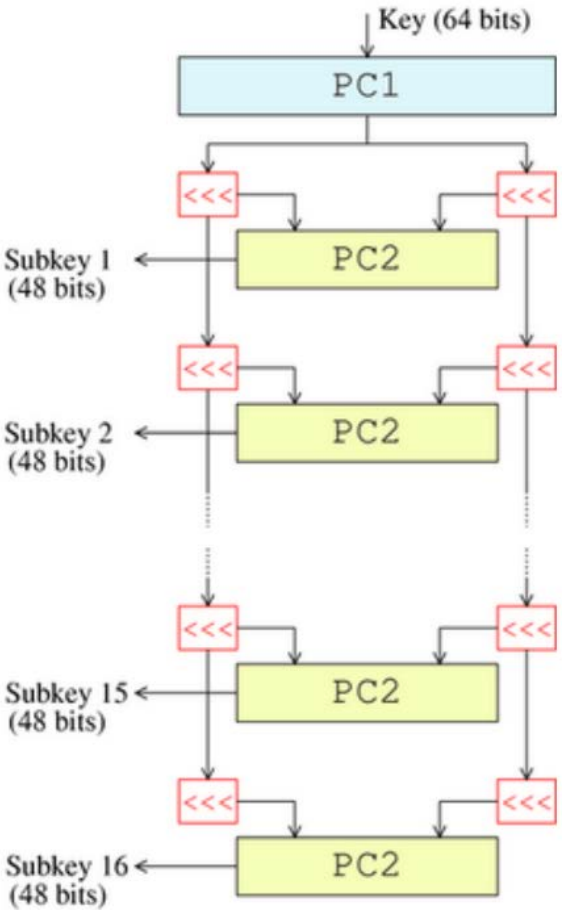

Fig. 10. Key Schedule Step

V. PROPOSED METHOD

Intelligent Custom Dictionary Based Encryp tion/Decryption Scheme This text security algorithm works on the custom dictionary system that enriches itself as the user tends to use the system more . It stores the new words and patterns used by the user in a database that is located in the System of the user itself , hence not sending any vunerable information over the network . Even if a hacker tends to get hold of the data that is being transmitted over the network all he gets is a combination of and * which is useless without the custom dictionary that is used by the user to encrypt the data . The same dictionary is available with the recipient who then uses it to decrypt the sent string . The beauty of this security scheme is the custom dictionary which is enhanced and enriched in accordance to the users vocabulary. The scheme develops the encryption codes of new words on the go without any interference from the user hence providing a seamless way to encrypt and decrypt data . User can can use multiple dictionaries while communicating with different people whereas all the other users will only need to maintain only one dictionary that Is specific to their conversation.

A. *Encryption Scheme*

1) Take input from the user.
2) Invoke the copy() function , this function dynamically creates a new array(SAY ARRAY1) that will contain the words and the encoding patterns form the base array as well as from the database that is saved in the memory. The beauty of this function lies in the fact that it is able to take data from the memory , split it into substrings , with each word and its encoding pattern stored as a different substring and then append them to the last of the new array that previously contains the values from the base array.
3) Ask the user how many times does he want to shuffle the encoding pattern in the database. After the user inputs this value , the shuffle() function is invoked that in turn shuffles the encoding pattern in ARRAY1 only while leaving the text values intact and in their previous position.
4) Split() function is invoked , which takes the inputed string , breaks in into smaller substrings of individual words and puts them in an array (SAY ARRAY2).
5) search() function is invoked , this function compares all the values in ARRAY2 with all the values in ARRAY1 . There are two possible solutions ;
   - A value in ARRAY2 matches a value in ARRAY1 , then its encoding format is saved.
   - A value in ARRAY2 does not match with any value in ARRAY1 , the word is kept as it is , but after the execution is done the new word is added to the database along with the automatically generated encoding pattern which will return a positive result when the word is next used.
6) The final encoded string is displayed to the used which is a combination of and * and is absolutely

safe to be transmitted over a network.

B. Decryption Scheme

1) Take input from the user , which is a string comprising of a sequence of and *.
2) Invoke the copy() function , this function dynamically creates a new array(SAY ARRAY1) that will contain the words and the encoding patterns form the base array as well as from the database that is saved in the memory. The beauty of this function lies in the fact that it is able to take data from the memory , split it into substrings , with each word and its encoding pattern stored as a different substring and then append them to the last of the new array that previously contains the values from the base array .
3) Ask the user how many times does he want to shuffle the encoding pattern in the database. After the user inputs this value , the shuffle() function is invoked that in turn shuffles the encoding pattern in ARRAY1 only while leaving the text values intact and in their previous position.
4) Split() function is invoked , which takes the encoded string , breaks in into smaller substrings of individual combinations of , the * in the original input string are removed in this step as they are used to separate different encoded patterns and puts them in an array (SAY ARRAY2).
5) search() function is invoked , this function compares all the values in ARRAY2 with all the values in ARRAY1. There are two possible solutions
   - A value in ARRAY2 matches a value in ARRAY1 , then its decoded string is saved
   - A value in ARRAY2 does not match with any value in ARRAY1 , then the word is saved in the database along with the automatically generated encryption pattern which will be exactly the same as the one generated by the encryption scheme of the sender because of the use of similar algorithms.
6) The user is able to see the final decoded string.

VI. CONCLUSION

A new protocol is proposed & implemented which changes the massage received from user by invoking function & change the message by embedding certain character & translate whole messages in form of &*. Thus, make this algorithm secure ‘ from intrudes & at the receiving end invoking the same func tion & applying same concept translated message converted to original message ready to be read by receiver. Thus, make it efficient as instead of embedding, it translate whole embedded message to certain format which is highly secure & free from intruders.

REFERENCES

[1] Wavelength conversion and deflection routing in all-optical packet-switched networks through contention resolution: a survey, A Anand, VK Sihag, SN Gupta Proceedings of the CUBE International Information Technology Conference, 155- 159.

[2] Improving Convergence of Congestion Control Algorithm, Abhineet Anand PSVS Sridhar, International Journal of Computer Applications 81 (2), 1-4.

[3] Multiprotocol Label Switching Feedback Protocol for Per Hop Based Feedback Mechanism in MPLS Network, Dumka Ankur and Mandoria HardwariLal, Emerging ICT for Bridging the Future - Proceedings of the 49th Annual Convention of the Computer Society of India (CSI) Volume 1.

[4] Privacy on the Line, The Politics of Wiretapping and Encryp tion Whitfield Diffie and Susan Landau, The MIT Press, 1998 ISBN 0-262-04167-7.

[5] Technology and Privacy: The New Landscape Philip Agre and Marc Rotenberg, The MIT Press, 1997 ISBN 0-262-01162-x.

[6] Building in Big Brother, The Cryptographic Policy Debate edited by Lance Hoffman, Springer Verlag, 1995 ISBN 0-387- 94441-9.

[7] The Unwanted Gaze - The Destruction of Privacy in America Jeffrey Rosen, Random House, 2000 ISBN 0-679-44546-3. [8] Database Nation Simson Garfinkel, OReilly Associates, 2000 ISBN 0-596-00105-3.

[8] The Official PGP Users Guide Philip Zimmermann, The MIT Press, 1995 ISBN 0-262-74017-6. (Out of date with current PGP software, but still politically interesting)

[9] Practical Cryptography Niels Ferguson and Bruce Schneier, John Wiley Sons, 2003 ISBN 0-471-22357-3. (If you can only read one book on crypto, this is it)

[10] Applied Cryptography, 2nd edition Bruce Schneier, John Wiley Sons, 1996 ISBN 0-471-12845-7. (Before Practical Cryptog raphy came out, this was the one book you needed)

[11] Handbook of Applied Cryptography Alfred Menezes, Paul van Oorschot, and Scot Vanstone, CRC Press, 1996 ISBN 0-8493- 8523-7.

[12] Journal of Cryptology International Association for Crypto logic Research (IACR) See www.iacr.org.

[13] Advances in Cryptology (Conference proceedings of the IACR CRYPTO conferences) published yearly by Springer-Verlag. See www.iacr.org.

[14] Cryptography and Data Security Dorothy Denning, Addison Wesley, 1982 ISBN 0-201-10150-5. (A good introduction to crypto for beginners, but no longer in print)

[15] Protect Your Privacy - A Guide for PGP Users William Stallings, Prentice Hall, 1995 ISBN 0-13-185596-4. (Out of date with current PGP software, but technically comprehensive)

[16] PGP: Pretty Good Privacy Simson Garfinkel, OReilly As sociates, 1995 ISBN 1-56592-098-8. (Good technical info on PGP of that era, with mostly correct history of PGP) See also

[17] Cryptography for the Internet Philip Zimmermann, Scientific American, October 1998 (introductory tutorial article)

2016 International Conference on Internet of Things and Applications (IOTA)
Maharashtra Institute of Technology, Pune, India 22 Jan - 24 Jan, 2016

IoT based Smart Parking System

Abhirup Khanna
University of Petroleum and Energy Studies (UPES)
Dehradun, Uttarakhand
abhirupkhanna@yahoo.com

Rishi Anand
University of Petroleum and Energy Studies (UPES)
Dehradun, Uttarakhand
rishi.anand0@gmail.com

***Abstract*— In recent times the concept of smart cities have gained grate popularity. Thanks to the evolution of Internet of things the idea of smart city now seems to be achievable. Consistent efforts are being made in the field of IoT in order to maximize the productivity and reliability of urban infrastructure. Problems such as, traffic congestion, limited car parking facilities and road safety are being addressed by IoT. In this paper, we present an IoT based cloud integrated smart parking system. The proposed Smart Parking system consists of an on-site deployment of an IoT module that is used to monitor and signalize the state of availability of each single parking space. A mobile application is also provided that allows an end user to check the availability of parking space and book a parking slot accordingly. The paper also describes a high-level view of the system architecture. Towards the end, the paper discusses the working of the system in form of a use case that proves the correctness of the proposed model.**

Keywords*— *Internet of Things; Cloud Computing; Smart Parking; Smart City; Cloud of Things

I. INTRODUCTION

The concept of Internet of Things (IoT) started with things with identity communication devices. The devices could be tracked, controlled or monitored using remote computers connected through Internet. IoT extends the use of Internet providing the communication, and thus inter-network of the devices and physical objects, or 'Things'. The two prominent words in IoT are "internet" and "things". Internet means a vast global network of connected servers, computers, tablets and mobiles using the internationally used protocols and connecting systems. Internet enables sending, receiving, or communicating of information. Thing in English has number of uses and meanings. Dictionary meaning of 'Thing' is a term used to reference to a physical object, an action or idea, situation or activity, in case when we do not wish to be precise. IoT, in general consists of inter-network of the devices and physical objects, number of objects can gather the data at remote locations and communicate to units managing, acquiring, organizing and analyzing the data in the processes and services. It provides a vision where things (wearable, watch, alarm clock, home devices, surrounding objects with) become smart and behave alive through sensing, computing and communicating by embedded small devices which interact with remote objects or persons through connectivity. The scalable and robust nature of Cloud computing is allowing developers to create and host their applications on it. Cloud acts as a perfect partner for IoT as it acts as a platform where all the sensor data can be stored and accessed from remote locations[11]. These factors gave rise to the amalgamation of both technologies thus leading to the formation of a new technology called Cloud of Things(CoT). In CoT the things(nodes) could be accessed, monitored and controlled from any remote location through the cloud. Due to high scalability in cloud any number of node could be added or removed from the IoT system on a real time basis. In simple terms IoT can be explained in form of an equation stating:

Physical Object + Controller, Sensor and Actuators + Internet = Internet of Things

The ideal of creating a Smart City is now becoming possible with the emergence of the Internet of Things. One of the key issues that smart cities relate to are car parking facilities and traffic management systems[3]. In present day cities finding an available parking spot is always difficult for drivers, and it tends to become harder with ever increasing number of private car users. This situation can be seen as an opportunity for smart cities to undertake actions in order enhance the efficiency their parking resources thus leading to reduction in searching times, traffic congestion and road accidents. Problems pertaining to parking and traffic congestion can be solved if the drivers can be informed in advance about the availability of parking spaces at and around their intended destination. Recent advances in creating low-cost, low-power embedded systems are helping developers to build new applications for Internet of Things. Followed by the developments in sensor technology, many modern cities have opted for deploying various IoT based systems in and around the cities for the purpose of monitoring. A recent survey performed by the International Parking Institute [6] reflects an increase in number of innovative ideas related to parking systems. At present there are certain parking systems[8] that claim to citizens of delivering real time information about available parking spaces. Such systems require efficient sensors to be deployed in the parking areas for monitoring the occupancy as well as quick data processing units in order to gain practical insights from data collected over various sources.

The smart parking system that we propose is implemented using a mobile application that is connected to the cloud. The system helps a user know the availability of parking spaces on a real time basis. The rest of the paper is organized as follows: Section II talks about the factors responsible of Cloud-IoT

integration. Section III presents the state-of-the-art in smart parking system. Section IV describes the implementation and working of the system. Section V concludes the paper.

II. NEED FOR IOT-CLOUD INTEGRATION

Cloud computing and IoT have witnessed large evolution. Both the technologies have their advantages, however several mutual advantages can be foreseen from their integration. On one hand, IoT can address its technological constraints such as storage, processing and energy by leveraging the unlimited capabilities and resources of Cloud[4]. On the other hand, Cloud can also extend its reach to deal with real world entities in a more distributed and dynamic fashion by the use of IoT. Basically, the Cloud acts as an intermediate between things and applications, in order to hide all the complexities and functionalities necessary for running the application. Below are some of the factors that led to the amalgamation of Cloud and IoT.

- *Storage capacity*: IoT comprises of a large number of information sources (things), which produce huge amounts of non-structured or semi-structured data. As a result IoT requires collecting, accessing, processing, visualizing and sharing large amounts of data[14]. Cloud provides unlimited, low-cost, and on-demand storage capacity, thus making it the best and most cost effective solution to deal with data generated by IoT. The data stored on the Cloud can be accessed and visualized from anywhere through standard APIs.

- *Computation power*: The devices being used under IoT have limited processing capabilities. Data collected from various sensors is usually transmitted to more powerful nodes where its aggregation and processing can be done[18]. The computation needs of IoT can be addressed by the use of unlimited processing capabilities and on-demand model of Cloud. With the help of cloud computing, IoT systems could perform real-time processing of data thus facilitating highly responsive applications.

- *Communication resources*. The basic functionality of IoT is to make IP-enabled devices communicate with one another through dedicated set of hardware. Cloud computing offers cheap and effective ways of connecting, tracking, and managing devices from anywhere over the internet[16]. By the use of built-in applications IoT systems could monitor and control things on a real-time basis through remote locations.
- *Scalability*: Cloud provides a scalable approach towards IoT. It allows increase or decrease in resources in a dynamic fashion. Any number of "things" could be added or subtracted from the system when cloud integration is provided[22]. The cloud allocates resources in accordance with the requirements of things and applications.

- *Availability*: Any time any where availability of resources becomes very easy with cloud integration. Many of the cloud providers assure 5 nine availability. With cloud, the applications are always up and running and continuous services are being provided to the end users.

- *Interoperability*: IoT involves the use of devices that are heterogeneous in nature. These devices may have different hardware or software configurations as a result causing compatibility issues. It becomes very difficult in an IoT environment to ensure interoperability among these devices[19]. Cloud helps in addressing this problem as it provides a common platform where various devices can connect and interact. Devices are allowed to share and exchange data in a format that is acceptable to them.

III. SYSTEM ARCHITECTURE

This section describes the high level architecture for the smart parking system along with a mathematical model. The parking system that we propose comprises of various actors that work in sync with one another. Below is the mathematical model that defines our smart parking system.

Table 1: Nomenclature Table

SYMBOL	**MEANING**
T	Parking time
C	Driver's car number
P	Amount paid
U	User ID
S	Parking slot
M_i	Driver
O	Occupancy rate
X()	Input function
Y()	Output function
F()	Computation function
I()	Identity function

$M_i \rightarrow X(T,C,P,U,S)$ // Driver provides input to the input function

$X() \rightarrow F(S,T)$ // Input function notifies the computation function

$X() \rightarrow I(P,C,U)$ // Input function notifies the identity function

$O_i = F(S,T) \rightarrow Y()$ // Computation function notifies the output function and the resultant is stored in form of the occupancy rate.

$O_i = 0 \mid 1$ // Occupancy rate can either be 0 or 1. Where 0 specifies occupied and 1 means vacant.

The following figure gives an outlined view of the complete system.

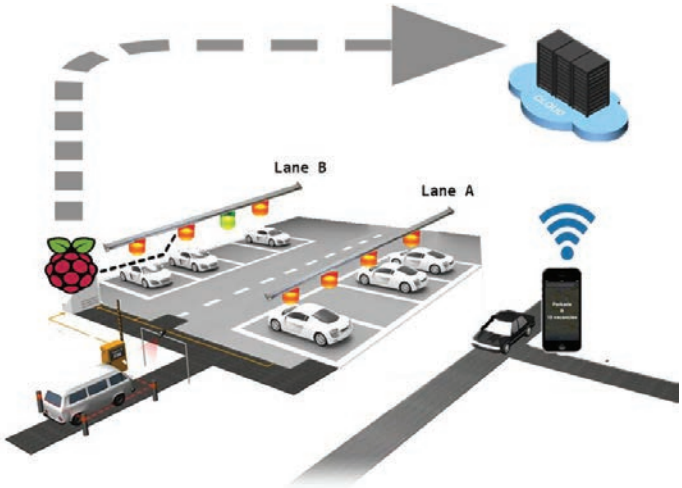

Figure 1: Smart Parking System

Talking of the above mentioned figure, it depicts a parking area where our parking system is implementation along with the way in which communication happens between various actors. The primary actors that constitute the parking system are:

- *Parking Sensors*: For our parking system we have made use of sensors like Infrared, Passive Infrared(PIR) and Ultrasonic Sensors. The work of these sensors is the same i.e. to sense the parking area and determine whether a parking slot is vacant or not. In this case we are using ultrasonic sensors to detect the presence of a car. The ultrasonic sensors are wirelessly connected to raspberry pi using the ESP8266 chip. An ESP8266 WiFi chip comprises of a self contained SOC with integrated TCP/IP protocol stack that allows any microcontroller to access a WiFi network. The sensors are connected to a 5V supply either from raspberry pi or an external source. External source being more preferable.

- *Processing Unit*: It comprises of Raspberry pi which is a processor on chip. The processing unit acts like an intermediate between the sensors and cloud. All the sensors are wirelessly connected to the processing unit. A single raspberry pi unit comprises of 26 GPIO pins i.e. 26 different sensors can be connected to it. However we can increase this number by attaching a multiplexer (MUX) to it. It is essential that the ground of raspberry pi and sensors must be connected in order to transfer data using the GPIO pins. There is a python script running on the chip that checks the status of various GPIO pins and updates this information onto the cloud. Data collected from various sensors is sent to the raspberry pi through the esp8266 chip. The raspberry pi then transmits this data to the IBM MQTT Server through MQTT protocol over a channel. MQTT[15] (Message Queue Telemetry Transport) Protocol is a publish-subscribe based "light weight" messaging protocol that is used on top of the TCP/IP protocol. It is designed to establish connections across remote locations where limited amount of data needs to be transferred or in cases of low bandwidth availability.

- *Mobile application*: The mobile application acts like an interface for the end users to interact with the system. The application is developed in Apache Cordova and Angular Js framework using Javascript as a programming language. The purpose of using Apache Cordova is to create applications that can run on both android and iOS platform with the same source code. The application is connected with the IBM MQTT server through a secure channel and a 2 factor authorization. The purpose of this mobile application is to provide information regarding availability of parking spaces and allowing the end user to book a slot accordingly. Transfer of data takes place in JSON format between IBM MQTT server and the mobile application. In order to ensure proper communication both the Raspberry pi and mobile application must be subscribed to a particular channel on IBM MQTT server.

- *The Cloud*: The IBM MQTT server is hosted on cloud. Cloud acts as a data base to store all the records related to parking areas and end users that have access to the system. It keeps a track of every user connected to the system and maintains information such as time at which the car was parked, time duration for parking a car, amount paid by the user and mode of payment. It is due to the flexible nature of cloud which permits the system to add any number of users at any time of the day. Continuous backup is made of the data stored on cloud in order to ensure easy and quick recovery of data in case of any kind of system failure.

  On closely looking at the figure one gets to see that empty parking spaces are indicated by red light in Lane A whereas green light in Lane B. This is due to the fact that in case of Lane A although there is no car currently parked but there still is a red light because the slot has already been booked by some user. On the other hand, the parking slot in Lane B shows green light because it neither has a booking nor a car parked in it.

IV. IMPLEMENTATION & WORKING

In the previous section we discussed about the architecture and technical stack related to the smart parking system. In this section we talk about the implimtation and working of the system in a real world scenario. The complete process of booking a parking slot, parking a car in that slot and leaving the parking area is explained with the help of the following flow chart.

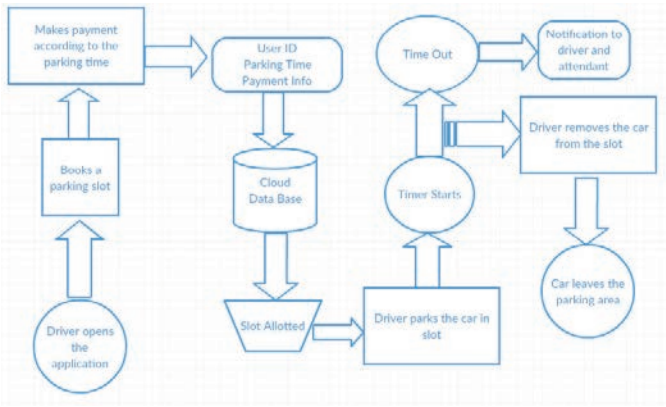

Figure 2: Flow chart of the system

We conducted an experiment in order to depict the working of our system at every stage from checking the availability of parking space to actually park a car in a vacant parking slot. This is done by implementing the smart parking system in the parking area of a shopping mall. Below are the steps that a driver needs to follow in order to park its car using our parking system.

- **Step 1**: Insall the smart parking application on your mobile device.
- **Step 2**: With the help of the mobile app search for a parking area on and around your destination.
- **Step 3**: Select a particular parking area.
- **Step 4**: Browse through the various parking slots available in that parking area.
- **Step 5**: Select a particular parking slot.
- **Step 6**: Select the amount of time (in hours) for which you would like to park your car for.
- **Step 7**: Pay the parking charges either with your e-wallet or your credit card.
- **Step 8**: Once you have successfully parked your car in the selected parking slot, confirm your occupancy using the mobile application.

The above mentioned procedure for booking a slot and parking a car in that very slot is explained with the help of the following screenshots.

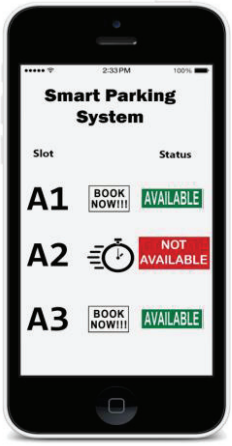

Figure 3: Booking a parking slot

The above figure depicts the presence of vacant and occupied parking slots. In this case parking slots named A1 and A3 are vacant whereas slot A2 is occupies. The driver chooses the A1 parking slot.

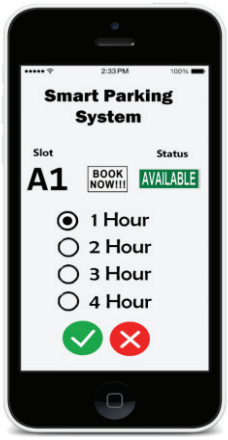

Figure 4: Selecting the amount of time

The above figure depicts the scenario when a driver needs to specify the amount of time for which it needs the selected parking slot. In this case the driver selects the 1 hour option.

Figure 5: Occupancy check

Once the driver has parked its car in the selected slot it needs to confirm its occupancy. Figure 5 depicts this very scenario in which the driver has to specify its presence. This feature is added so that only a genuine driver can park its car in a particular parking slot. If a driver fails to confirm his occupancy in the next 30 seconds of parking its car, an alarm would start ringing causing the authorities to know that a car has been parked in the wrong place. If by any chance a genuine driver fails do so he can stop the alarm any time by confirming his occupancy.

In case the driver over shoots its parking time, a notification stating this scenario would be sent to the driver as well as to the parking attendant. The driver would then have an option of extending its parking time and pay accordingly for the extra time. In case the driver fails to do so, the parking attendant would make a note of this and charge money for the extra time in form of a fine. This fine would be collected from the driver at the time when the car would be leaving from the parking area.

V. CONCLUSION

The concept of Smart Cities have always been a dream for humanity. Since the past couple of years large advancements have been made in making smart cities a reality. The growth of Internet of Things and Cloud technologies have give rise to new possibilities in terms of smart cities. Smart parking facilities and traffic management systems have always been at the core of constructing smart cities. In this paper, we address the issue of parking and present an IoT based Cloud integrated smart parking system. The system that we propose provides real time information regarding availability of parking slots in a parking area. Users from remote locations could book a parking slot for them by the use of our mobile application. The efforts made in this paper are indented to improve the parking facilities of a city and thereby aiming to enhance the quality of life of its people.

REFERENCES

[1] Rico, J., Sancho, J., Cendon, B., & Camus, M. (2013, March). Parking easier by using context information of a smart city: Enabling fast search and management of parking resources. In Advanced Information Networking and Applications Workshops (WAINA), 2013 27th International Conference on (pp. 1380-1385). IEEE.

[2] Zheng, Y., Rajasegarar, S., & Leckie, C. (2015, April). Parking availability prediction for sensor-enabled car parks in smart cities. In Intelligent Sensors, Sensor Networks and Information Processing (ISSNIP), 2015 IEEE Tenth International Conference on (pp. 1-6). IEEE.

[3] Zhou, F., & Li, Q. (2014, November). Parking Guidance System Based on ZigBee and Geomagnetic Sensor Technology. In Distributed Computing and Applications to Business, Engineering and Science (DCABES), 2014 13th International Symposium on (pp. 268-271). IEEE.

[4] Botta, A., de Donato, W., Persico, V., & Pescapé, A. (2014, August). On the Integration of Cloud Computing and Internet of Things. In Future Internet of Things and Cloud (FiCloud), 2014 International Conference on (pp. 23-30). IEEE.

[5] Ji, Z., Ganchev, I., O'droma, M., & Zhang, X. (2014, August). A cloud-based intelligent car parking services for smart cities. In General Assembly and Scientific Symposium (URSI GASS), 2014 XXXIth URSI (pp. 1-4). IEEE.

[6] International Parking Institute, “2012 Emerging Trends in Parking”.

[7] Ballon, P., Glidden, J., Kranas, P., Menychtas, A., Ruston, S., & Van Der Graaf, S. (2011, October). Is there a Need for a Cloud Platform for European Smart Cities?. In eChallenges e-2011 Conference Proceedings, IIMC International Information Management Corporation.

[8] FastPark System website, http://www.fastprk.com.

[9] Chen, S. Y., Lai, C. F., Huang, Y. M., & Jeng, Y. L. (2013, July). Intelligent home-appliance recognition over IoT cloud network. In Wireless Communications and Mobile Computing Conference (IWCMC), 2013 9th International (pp. 639-643). IEEE.

[10] Dash, S. K., Mohapatra, S., & Pattnaik, P. K. (2010). A survey on applications of wireless sensor network using cloud computing. International Journal of Computer science & Engineering Technologies (E-ISSN: 2044-6004), 1(4), 50-55.

[11] Fox, G. C., Kamburugamuve, S., & Hartman, R. D. (2012, May). Architecture and measured characteristics of a cloud based internet of things. InCollaboration Technologies and Systems (CTS), 2012 International Conference on (pp. 6-12). IEEE.

[12] Han, D. M., & Lim, J. H. (2010). Smart home energy management system using IEEE 802.15. 4 and zigbee. Consumer Electronics, IEEE Transactions on, 56(3), 1403-1410.

[13] Parwekar, P. (2011, September). From Internet of Things towards cloud of things. In Computer and Communication Technology (ICCCT), 2011 2nd International Conference on (pp. 329-333). IEEE.

[14] Rao, B. B. P., Saluia, P., Sharma, N., Mittal, A., & Sharma, S. V. (2012, December). Cloud computing for Internet of Things & sensing based applications. In Sensing Technology (ICST), 2012 Sixth International Conference on (pp. 374-380). IEEE.

[15] Wikipedia website, https://en.wikipedia.org/wiki/MQTT.

[16] Suciu, G., Vulpe, A., Halunga, S., Fratu, O., Todoran, G., & Suciu, V. (2013, May). Smart cities built on resilient cloud computing and secure internet of things. In Control Systems and Computer Science (CSCS), 2013 19th International Conference on (pp. 513-518). IEEE.

[17] Ye, X., & Huang, J. (2011, December). A framework for cloud-based smart home. In Computer Science and Network Technology (ICCSNT), 2011 International Conference on (Vol. 2, pp. 894-897). IEEE.

[18] Zaslavsky, A., Perera, C., & Georgakopoulos, D. (2013). Sensing as a service and big data. arXiv preprint arXiv:1301.0159.

[19] Doukas, C., Capra, L., Antonelli, F., Jaupaj, E., Tamilin, A., & Carreras, I. (2015, January). Providing generic support for IoT and M2M for mobile devices. In Computing & Communication Technologies-Research, Innovation, and Vision for the Future (RIVF), 2015 IEEE RIVF International Conference on (pp. 192-197). IEEE.

[20] Tsirmpas, C., Anastasiou, A., Bountris, P., & Koutsouris, D. A new method for profile generation in an Internet of Things environment: An application in ambient assisted living.

[21] Kafle, V. P., Fukushima, Y., & Harai, H. (2015, April). ID-based communication for realizing IoT and M2M in future heterogeneous mobile networks. In Recent Advances in Internet of Things (RIoT), 2015 International Conference on (pp. 1-6). IEEE.

[22] Sarkar, C., Uttama Nambi SN, A., Prasad, R., Rahim, A., Neisse, R., & Baldini, G. (2012). DIAT: A Scalable Distributed Architecture for IoT.

Interacting metallic disc-antennas as metamaterial absorber in the NIR frequency

P. Mandal

Citation: AIP Conference Proceedings **1731**, 140025 (2016); doi: 10.1063/1.4948191
View online: http://dx.doi.org/10.1063/1.4948191
View Table of Contents: http://aip.scitation.org/toc/apc/1731/1
Published by the American Institute of Physics

Interacting Metallic Disc-antennas as Metamaterial Absorber in the NIR frequency

P. Mandal

Department of Physics, University of Petroleum and Energy Studies, Dehradun-248007, India
Email: pmandal@ddn.upes.ac.in

Abstract. Interacting subwavelength metallic disc-antennas are important class of metamaterials that can be used for perfect metamaterial design at a specific frequency domain. The present study describes the design and demonstration of metamaterial perfect absorber in the spectral window of 0.8 to 2 micron. Two disc-antennas of different size show interaction induced absorption at NIR frequency. This absorption band is observed to be sensitive to input light polarization orientation.

Keywords: Metamaterial, Perfect absorber, NIR frequency, Interacting disc-antennas.
PACS: 42.25.Bs, 81.05.Xj

INTRODUCTION

Plasmonic manmade metamaterials consisting of subwavelength engineered structures are very exciting material systems that have been exploiting for novel applications such as, negative refraction and perfect lensing [1, 2], optical filters and modulators [3-4], perfect absorber for spectroscopy [5], and sensor applications [6]. Out of these applications, recently, metamaterial perfect absorbers have attracted tremendous attentions due to potential for thermo-photovoltaics [7], thermal imaging and sensing [8-10], therapy [11], microwave communication systems [12]. Various designs of metamaterial perfect absorbers are available in a wide spectral range of giga hertz to optical regimes [13-16]. In most of the cases, planar structures with single or stacked multilayers have been investigated to demonstrate multi-resonant broadband absorption [17-18]. Depending upon the structural symmetry these structures may be polarization sensitive or insensitive. Polarization sensitive perfect absorption has important implication where a specific polarized light to be detected efficiently.

It is a great challenge to design ultra-compact and polarization sensitive plasmonic perfect absorber with planar structures. Interacting plasmonic disc-antennas may be considered as promising candidates to manipulate optical properties and tuning the absorption band in the specific frequency window.

The present study describes the design and theoretical demonstration of metamaterial perfect absorber in the NIR window of 0.8 to 2 microns. Two disc-antennas of different size show interaction induced absorption at NIR frequency sensitive to the input light polarization orientation.

EXPERIMENTAL

Interacting disc-antenna planar metamaterial absorber consists of two Au layers separated by a dielectric layer (figure 1). The bottom Au layer is flat film whereas; the top Au layer is structured. Optical absorption ($A(\lambda)$) properties of subwavelength interacting metallic disc-antennas are studied using finite difference time domain (FDTD) simulation. The interacting discs of different size (thickness 30 nm) are placed periodically on the top of a SiO_2 spacer layer of

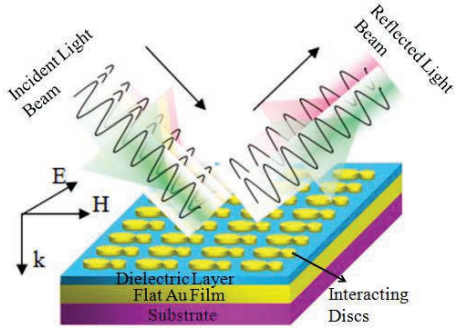

FIGURE 1. Interacting disc-antennas as metamaterial perfect absorber.

DAE Solid State Physics Symposium 2015
AIP Conf. Proc. 1731, 140025-1–140025-3; doi: 10.1063/1.4948191
Published by AIP Publishing. 978-0-7354-1378-8/$30.00

fixed refractive index (*RI*) of 1.5 (40 nm thick layer) as shown in figure 1. There is a ground gold film of 100 nm thickness underneath the SiO_2 layer. The sequential layers are placed on the top of a supportive bottom substrate (200 nm thick layer made of SiO_2 of *RI* = 1.5). The top structures have a typical periodicity of 500 nm in either direction. The discs have size of 200 nm and 100 nm and are placed without a gap between them (until unless specified). Gold film is considered to have Lorentz–Drude dispersion in the spectral range of interest. Periodic boundary conditions (*PBC*) are applied along X– & Y–directions, while in the Z–direction (along the growth direction) anisotropic perfectly matched layers (*APML*) are used. A linearly polarized (X–pol, E field along X) plane wave is launched normally, and the output spectra in the form of reflection (*R*), transmission (*T*) are obtained.

RESULTS AND DISCUSSIONS

Absorption $A(\lambda)$ spectra are obtained from the simulated reflection ($R(\lambda)$) and transmission ($T(\lambda)$) spectra using the relation $A(\lambda) = 1-R(\lambda)-T(\lambda)$. The absorption spectra for different metamaterial systems are plotted in the figure 1 in the spectral range of 0.5 microns to 1.85 microns. For the metamaterial with 200 nm disc (big) the spectrum shows two absorption bands at ~1.025 μm (P2) and ~0.7 μm (P7). The P2 band shows about 95% absorption, whereas P7 band shows about 80% absorption. For small disc metamaterial the spectrum also shows two absorption bands which are located at ~0.74 μm (P4) and ~0.625

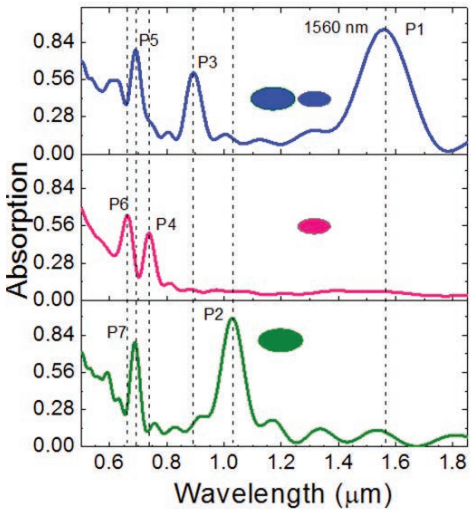

FIGURE 2. Absorption spectra of interacting metallic disc-antennas in the visible to NIR spectral window.

μm (P6). The absorption strengths are found to be ~ 55% and 65%, respectively. When these two discs are arranged to design metamaterials with interacting elements, such as, as in the figure 2 (top row), we observed three distinct absorption bands. The bands are located at ~ 1.56 μm (P1), ~0.9 μm (P3) and ~0.7 μm (P5) with the absorption strengths of about 90%, 55% and 0.75%, respectively. While P3 and P5 bands arise due to the antisymmetric and symmetric modes, the P1 band arises due to the interaction between the two interacting discs. The full width at half maximum (FWHM) of this band (P1) is very broad (~0.2 μm).

In order to elucidate the origin of the interaction induced absorption, a gap dependent absorption has been studied. The interacting disc-antennas and their corresponding absorption spectra are shown in figure in figure 3. For the case when the two particles merged (as shown in the second case of figure 3, from

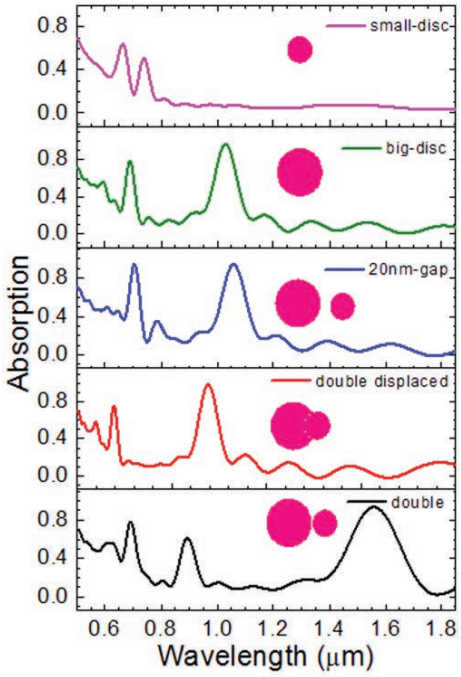

FIGURE 3. Absorption spectra of interacting metallic disc-antennas in the visible to NIR spectral window for various gap between the discs. For comparison, the absorption spectra for big and small discs are also shown in the figure.

bottom), the spectrum shows no interaction induced absorption band, instead the symmetric (0.625 μm) and antisymmetric (0.975 μm) modes shifted to blue as compared to the metamaterial spectrum obtained from the array of disc of bigger size (spectrum in 4th row from the bottom, as in figure 3). However, an inverse situation occurs when the discs are separated by 20 nm

gap. Both the bands shifted to red (spectrum in 4th row from the bottom, as in figure 3). It is also observed that the high frequency absorption is enhanced which can be attributed to the contribution from the small size disc. For the case when there is no gap between the discs, the spectrum shows the symmetric and antisymmetric bands at 0.7 μm and 0.9 μm, respectively, as mentioned earlier (during the description of figure 2). The interaction induced absorption at ~1.56 μm clearly shows the distance dependent sensitivity.

Polarization dependent optical absorption properties are studied on the interacting discs system when there is no gap between them. The spectra are shown in figure 4. For the y-pol case (top row) the spectrum shows similar features as observed for the case of metamaterial consisting of the array of big disc (figure 2, bottom row spectrum is referred). It is clear that the interaction induced absorption arises when the incident electric field has component along x-direction or the component electric field can be treated as x-pol.

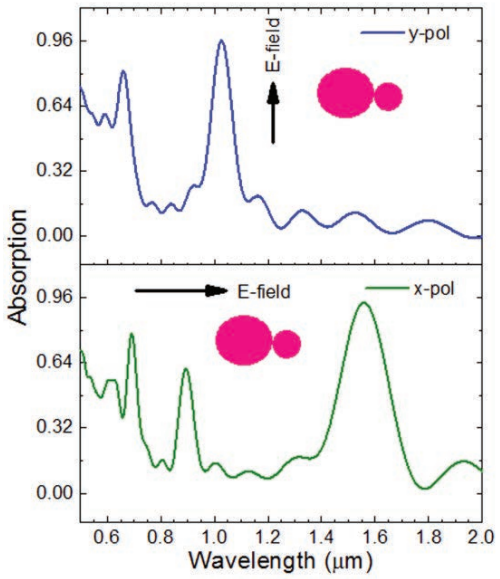

FIGURE 4. Polarization dependent optical absorption spectra of interacting metallic disc-antennas in the case of input polarization state as x-pol (bottom row) and y-pol (top row).

CONCLUSIONS

A metallic disc-antenna metamaterial is designed and its optical absorption properties are studied in the spectral window of 0.8 to 2 micron. Interaction induced absorption is observed when two disc-antennas of different size placed together side by side, without any gap between them. The interaction induced perfect absorption at a desired frequency can be achieved by manipulating the size and the positional arrangement of the subwavelength disc antennas, and the choice of the input light polarization orientation.

ACKNOWLEDGMENTS

Author is thankful to Prof. S. A. Ramakrishna, Department of Physics, IIT Kanpur, for providing the access to computational facility.

REFERENCES

1. V. M. Shalaev, Nat. Photonics **1** 41-48 (2007).
2. J. B. Pendry, Phys. Rev. Lett. **85** 3966 (2000).
3. S. Yokogawa, S. P. Burgos and H. A. Atwater, Nano Lett. **12** 4349-4354 (2012).
4. J. –Y. Ou, E. Plum, L. Jiang and N. I. Zheludev, Nano Lett.**11** 2142-2144 (2011).
5. P. Mandal, Plasmonics doi: 10.1007/s11468-015-0038-8 (2015).
6. P. Mandal, Plasmonics **10** 439-445 (2015).
7. O. Neumann, A. S. Urban, J. Day, S. Lal, P. Nordlander and N. J. Halas, ACS Nano **7** 42-49 (2012).
8. T. Maier and H. Brückl, Opt Lett. **34** 3012 (2009).
9. A. Tittl, A. K. U. Michel, M. Schäferling, X. Yin, B. Gholipour, L. Cui, M. Wuttig, T. Taubner, F. Neubrech and H. Giessen, Adv. Mater. 2015, doi:10.1002/adma.201502023.
10. W. Padilla and X. Liu, Spie Newsroom: doi:10.1117/2.1201009.003137, 2010.
11. K. Aydin K, V. E. Ferry, R. M. Briggs and H. A. Atwater, Nat. Commun. **2** 517 (2011).
12. P. K. Singh, K. A. Korolev, M. N. Afsar, and S. Sonkusale, Appl. Phys. Lett. **99** 264101 (2011).
13. Q.-Y. Wen, H.-W. Zhang, Y.-S. Xie, Q.-H. Yang and Y.-L. Liu, Appl. Phys. Lett. **95** 241111 (2009).
14. H. Tao, C. M. Bingham, D. Pilon, K. Fan, A. C. Strikwerda, D. Shrekenhamer, W. J. Padilla, X Zhang and R. D. Averitt, J. Phys. D: Appl. Phys. **43** 225102 (2010).
15. J. A. Mason, S. Smith and D. Wasserman, Appl. Phys. Lett. **98** 241105 (2011).
16. J. Hao, J. Wang, X. Liu, W. J. Padilla, L. Zhou and M. Qiu, Appl. Phys. Lett. **96** 251104 (2010).
17. J. Wang, C. Fan, P. Ding, J. He, Y. Cheng, W. Hu, G. Cai, E. Liang and Q. Xue, Opt Exp. **20** 14871 (2012).
18. G. Dayal and S. A. Ramakrishna, J. Opt. **15** 055106 (2013).

2015 Workshop on Research, Education and Development of
Unmanned Aerial Systems (RED-UAS)
November 23-25, 2015. Cancun, Mexico

Performance Analysis of a Powered Parafoil Unmanned Aerial Vehicle Using Open Loop Flight Test Results and Analytical Results

Vindhya Devalla
Aerospace Engineering Dept.
University of Petroleum and Energy Studies
Dehradun, India
vindsdevalla@yahoo.com

Amit Kumar Mondal
Electronics Instrumentation and Control Engineering Dept.
University of Petroleum and Energy Studies
Dehradun, India
akmondal1603@gmail.com

Om Prakash
Aerospace Engineering Dept.
University of Petroleum and Energy Studies
Dehradun, India
omprakash@ddn.upes.ac.in

***Abstract*— This paper presents an approach to design and develop an Unmanned Powered Parafoil Aerial Vehicle (UPPAV) to surveillance an area. The paper discusses in detail about the relation between Parafoil size and payload weight. Analytical calculations are done to understand the UPPAV performance. The performance results are then compared with open loop flight test results.**

Keywords—UPPAV; Performance; Parafoil Payload Sizing; Data Acquisition System, Flight Test

I. INTRODUCTION

The U.S Department of Defense (DOD) defines an unmanned aircraft as follows [1]:

A powered vehicle that does not carry a human operator, can be operated remotely or autonomously, can be expendable or recoverable and can carry a lethal or non lethal payload. Ballistic or semi ballistic vehicle, cruise missiles, artillery projectiles, torpedoes, mines, satellites and unattended sensors are not considered unmanned vehicles. Unmanned vehicles are the primary component of unmanned system.

This definition covers multiple forms of unmanned systems including Unmanned Air Systems (UASs), unmanned ground vehicles (UGV), unmanned surface vehicles (USVs), and unmanned underwater vehicles (UUVs).

The definition excludes sensors with no form of propulsion. This exclusion is likely intended to eliminate son buoys and unattended ground sensors (UGS). Non-powered aircraft, known as gliders, can perform many useful missions and are generally considered to be UASs. They have flight controls which are capable of navigation, and carry payloads. One could argue that a glider's propulsion is the conversion of potential to kinetic energy [2].

UASs have taken many names and forms over their long history can be called in many ways:

- Remotely piloted vehicle
- Unmanned aerial vehicle
- Uninhabited combat aerial vehicle
- Organic aerial vehicle
- Uninhabited combat aircraft system
- Remotely piloted aircraft
- Remotely piloted helicopter
- Aerial robotics
- Micro aerial vehicle

General attributes of unmanned aircraft are following:

- Smaller size potential
- High versatility
- Greater performance than manned aircraft

A problem of interest is to device methodologies and innovative ways of developing PAV for surveillance because of its unique characteristics which include components like GPS for finding the location, Ultrasonic Sensors for obstacle detection and IMU for direction control.

II. ABOUT POWERED PARAFOIL UNMANNED AERIAL VEHICLE

The Powered Parafoil is an aircraft which derives lift from a ram-air inflated canopy, under which the fuselage is suspended [3]. The parachute is inflated by the dynamic pressure of the air flowing into the canopy which has a cross section in the shape of an airfoil. This process helps the vehicle to create lift. This feature differentiates these parafoils from conventional parachutes which are used to simply create drag. Powered parachutes have been utilized mostly for recreation activities, but some of the special properties make them a suitable platform for unmanned aerial vehicle (UAV) and remote sensing applications. Powered parafoils have existed since 1981 [4]. The concept was introduced at the Sun & Fun aviation event by the ParaPlane Corporation [5].

Figure 1. Para Plane Concept

They represent aircraft that are somewhere between balloons and fixed wing aircraft when control is considered as shown in Fig 4.

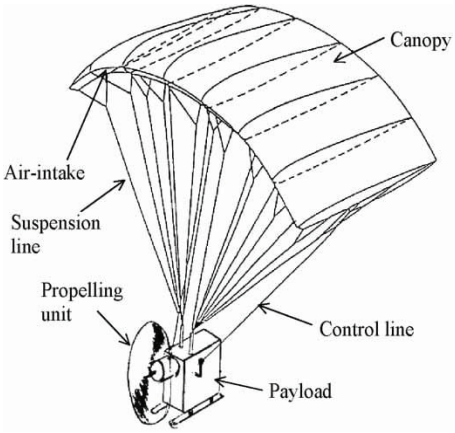

Figure. 2. Control Of Powered Parafoil Aerial Vehicle

The direction of a powered parachute is controlled by the pilot pushing on either a left or right steering bar that pulls down on a line attached to the trailing edge of the canopy.

The increased drag causes the aircraft to turn. The control lines connected to the canopy are pulled down together, which will drop both trailing ends of the canopy at a time and cause a sudden increase in lift. This maneuver is done during landing, when the pilot wants a smooth touchdown. A different steering configuration which is used on some small-scale aircraft is known as a "fly-bar." In this design, the Parafoil is connected to the ends of a bar, as seen in figure 5.

This bar can be pulled either side of the aircraft, changing the direction of the lift and making the aircraft turn. Aircraft using each of the two steering systems behave identically in response to thrust inputs. Powered parafoils have the tendency to fly at a constant airspeed [6]. A powered parafoil will climb, cruise and descend somewhere around the speed of 26 – 32 MPH. These Aircrafts have pendulum stability and oscillations as shown in the figure 6, because of the mass of the airframe suspended significantly below the canopy. This feature allows the aircraft to achieve directional control rather than rolling motion [7]. The applications powered parafoil in surveillance and imaging has benefit of a low-speed, low-cost, and stable platform which is capable of lifting payloads of up to 600 lbs. These platforms are very stable and must only get disturbed with gusts that would change the flight trajectory.

The addition of a propelling unit makes the paraglider an Unmanned Aerial Vehicle (UAV). A Powered parafoil consists of a Parafoil and a payload equipped with an engine or motor and a propeller. From the view of dynamics and control, the configuration provides the following unique characteristics, as compared to traditional wing aircraft [3].

- The separation between the centers of gravity of the canopy and the payload produces a swinging motion.
- Changing the thrust induces a considerable pitching motion.
- Relative pitching and yawing motions exists between the canopy and the payload.
- Canopy is a tailless flying wing.
- Directional control is mainly achieved through yawing motion, rather than through rolling motion.
- The apparent mass of the canopy must be taken into account, as in case of an airship.

III. VEHICLE CONSTRUSTION

The UPPAV is a concept which consists of a Parafoil and a powered payload. The Parafoil is connected to the payload at two joints using flexible lines. The vehicle is fully stable and requires only two controls, one for direction control and one for take-off and landing. The vehicle has numerous advantages and applications ranging from aerial delivery to remote sensing. The vehicle was developed for remote sensing purpose. The vehicle is a small unmanned powered Parafoil vehicle with payload carrying capability of 2.5 – 4.5 Kg including the electronics, battery and sensors. The vehicle was developed with only two controls. This section discusses in detail about the payload concept which includes various parts of the payload, Parafoil Performance which includes the Parafoil size with respect to the payload calculation and the sensors and control unit used in detail. The above mentioned systems are prime requirements to full fill the autonomous remote sensing task.

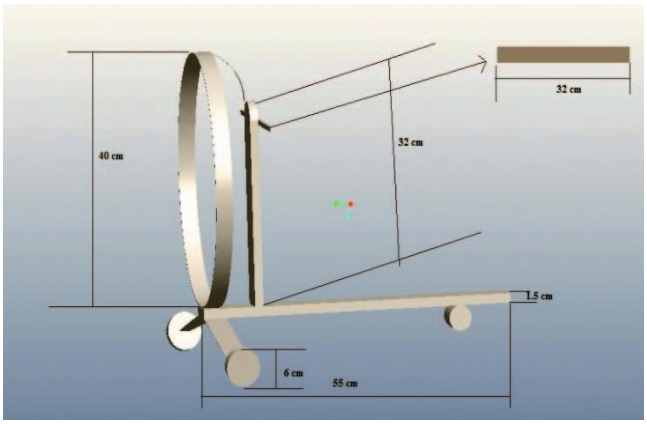

Figure .3. Physical Dimensions of the Vehicle

The payload generally consists of the following parts

- Nose
- Main frame
- Propeller guard
- Back landing gears
- Front landing gear
- Control rod
- Sensors and control Unit

The above mentioned parts are discussed in detail in this section. The sensors and control unit is placed on the payload.

A. Nose to Main Frame Ratio

The nose is made up of balsa wood. It is generally considered to be long compared to the main frame in a ratio of 7:5. The length of the nose is 55cm. It is observed that if the nose is taken short the vehicle tends to stall.

B. Main Frame

The mainframe is also made up of balsa wood. The mainframe acts as a house for propulsion unit and the control unit. The propulsion system (motor and the propeller) is placed exactly at the center so that the propeller does not touch the surface of the nose when rotating.

C. Propulsion unit

The propulsion unit consists of an out-runner Brushless DC Motor (BLDC). The motor selection is done by the power calculation. The power required can be calculated by multiplying volts and amps.

- Input watts per pound gives the power requirement based on the weight of the model.
- If the model weight is considered to be x, and power required is 100 watts then then 100x input watts per pound is the minimum power required to achieve the desired performance.
- The input power the motor can handle is determined by

Average voltage X continuous current = input watts

Therefore for a 3 kg payload, 6 Cells, Continuous Power Capability: 19.8 Volts (6 x 3.3) x 40 Amps = 792 Watts. The size propeller attached to the model depends on the motor selected.

D. Propeller Guard

The propeller guard is made of aluminum which is bent in the form of a circle to give protection to the strings. The diameter of the propeller guard is 32cm.

E. Front and Back Landing Gears

The front landing gear has one wheel and the back landing gear has two wheels giving the shape of a triac. All the wheels are made of balsa wood. Each wheel is of 6cm diameter

F. Control Rod

The control rod is hinged to the main frame at the center, and is connected to a servo through a push pull rod. The control rod made of an aluminum rod, and is 32cm.

G. Sensors and Control Unit

The complete set of electronics and the controller used is discussed in detail in the later sections of the chapter (3.6 - Data acquisitions and control system). The toal weight of the sensors system is 20 grams.

IV. PARFOIL SIZING

A. Size of the Parafoil

The mass of the payload may range in between 1kg to 8000kg which can be observed in figure 5. Change in the weight of the payload increases the size of the parachute [8]. The general requirements for calculating the size of the parachute are:

- Payload mass (W)
- Horizontal flight velocity (w)
- Vertical flight velocity (u)
- Lift (L)
- Drag (D)
- Aspect ratio (A)
- Chord length (B)
- Span (B)
- Density (d)

Figure 4. Parafoil Used in PAV

Size

The size of the parachute will be determined by the mass of the payload to be delivered. Therefore the velocity of the parachute is also calculated.

The velocity of the parachute is square root of horizontal flight velocity and vertical flight velocity.

$$v = \sqrt{u^2 - w^2} \tag{1}$$

The horizontal flight velocity (w) is calculated by, the L/D is assumed to be 3.

$$w = \frac{u}{L/D} \tag{2}$$

Using these values the size of the parachute is calculated, which is given by:

$$S = \frac{W}{10\sqrt{(C_l^2 + C_d^2)(0.5V^2\rho)}} \tag{3}$$

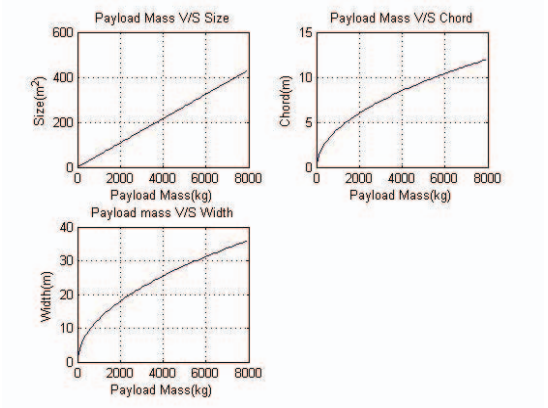

Figure 5. Parafoil Size to the Payload

Span

The span of the parachute is given by

$$b = \sqrt{S / A} \tag{4}$$

Cord

The cord of the parachute is calculated using Aspect Ratio and the span of the parachute

$$c = bA \tag{5}$$

Since our operation has to be performed using a small Parafoil the following table was again calculated to the approximate size of the Parafoil which should be capable of lifting a payload of maximum 5 Kg, which includes the discussed payload components.

S.No.	Weight (kg) (maximum)	Span (m)	Chord (m)	Area (m^2)
1	1	0.84	0.28	0.24
2	2	1.2	0.4	0.48
3	3	1.47	0.5	0.73
4	4	1.68	0.56	0.97
5	5	1.89	0.63	1.2

Table 1 Parafoil Payload Relationship

Keeping the Payload components, Parafoil Performance and Parafoil sizing, the Parafoil that was selected is capable of lift 5 Kgs (Maximum), the following is the specification of the vehicle.

Payload mass	3-4 kg (Including electronics)
Cord	0.65m
Span	2m
Area	1.3 m^2
Velocity	10 m/s
Density	1.22
Aspect Ratio	3

Table 2. UPPAV Specifications

V. PERFORMANCE PARAMETERS

Performance Parameters include the basic L/D concept and lift and drag coefficient calculation and glide performance [8].

A. Parafoil L/D Ratio

The L/D ratio of Parafoil changes according to the angle of attack, thereby getting different L/D ratios at different flight conditions. L/D ratio is also used to determine the drag coefficients it is taken as 3 initially.

B. Parafoil Lift and Drag Coefficient Calculation

The requirement of lift coefficient acting on UPPAV is determined as following from the estimated flight velocity [11]

$$L = \frac{1}{2}\rho V^2 S C_l \tag{6}$$

$$L = W \tag{7}$$

$$C_l = \frac{2W}{\rho S V^2} = 0.5 \tag{8}$$

For the drag coefficient, the lift to drag ratio can be determined by the gliding flight

$$C_d = \frac{C_l}{L/D} = 0.16 \tag{9}$$

The total drag that is acting on the Parafoil is given as the sums of the parasite drag and drag due to lift.

$$C_d = C_{d_p} + C_{d_i} \tag{10}$$

The δ = 0.018 for Aspect Ratio 3 taken

$$C_{d_i} = \frac{C_l^2(1+\delta)}{\pi A} = 0.046 \tag{11}$$

Parasite drag can be calculated by subtracting the Drag due to the lift from the total drag

$$C_{d_p} = C_d - C_{d_i} = 0.104 \tag{12}$$

These estimates suggest that the parasite drag is 50.6 % of the total drag and drag due to the lift is 49.37%.

C. Payload and Lines Drag Calculation

Surface Area of the main frame = 0.46mX 0.015mX0.05m
Surface Area of the Nose = 0.55mX 0.015mX0.05m
Surface Area of the Width = 0.32mX0.015X0.05m
Therefor total drag area of the payload = 0.05m^2
For which the drag coefficient is 0.057, the drag coefficient for the lines comes out to be 0.01.
Therefore the total drag of the vehicle comes out to be C_d= 0.21.

D. Lift to Drag Ratio of the Complete System (PAV)

$$E = \frac{C_l}{C_d} = 2.5 \tag{13}$$

Where, E is known as the lift to drag ratio.

E. Level Flight and Gliding Flight Performance of PAV

Velocity of the vehicle during gliding flight is given as

$$V = \sqrt{\frac{2XW}{\rho S C_l}} = 10 m/s \tag{14}$$

Gamma (glide angle) is given by

$$\gamma = -\frac{1}{E} = -0.4 radians = -22 \text{degrees} \tag{15}$$

During the level flight lift to drag ratio is zero, which make glide angle 0.

F. Thrust Performance

The motor used for the developed UPPAV if E Flite 60 which generates a power of 1200 Watts which comes out to

be 1.6 bhp. The motor used is capable of lifting a payload upto 5 Kgs.

Thrust required by UPPAV can be estimated from the following formula [3]

$$T = \frac{VW}{L/D(motor(bhp))} = 8N \quad (16)$$

VI. System Harware

A. PAV

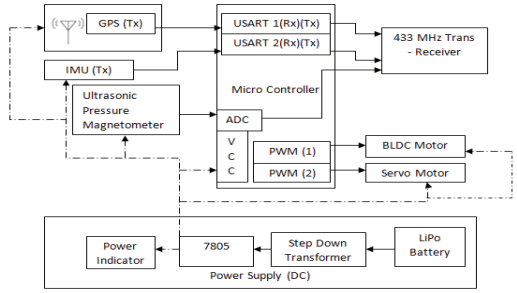

Figure 6. On board Hardware

The block diagram of transmitting and receiving sections (system with the aerial vehicle and ground station) are given above. The on board Embedded system is basically placed on the aerial vehicle. The system is interfaced with three sensors GPS, IMU and Ultrasonic sensors. GPS measures the vehicle speed, latitude, longitude and altitude whose values are used to control the vehicle direction also, are transmitted to the ground station using 433 MHz Transmitter Receiver for the operator.

The ground station receives the signal from the onboard embedded system and displays all the sensor information to the user.

B. Ground station

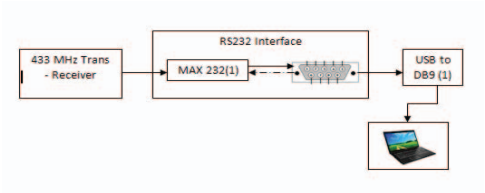

Figure. 7. Ground station Hardware

VII. Open loop flight test plan

The Open Loop Flight Test is helpful to demonstrate that the flight can be carried out with a single servo Most of the developed vehicles use two servos to control the direction of the vehicle, but in UPPAV a single servo is used which has advantages in terms of power and control algorithm design

To check the take off

This test would help us in determining the power required for takeoff, which is generally in full throttle condition.

To analyze the turn performance

Before the closed loop system is designed, the turn rate, turn radius with respect to the servo tilt must be known. Therefore, the turn performance analysis is done

Gliding test

This test would help us understand the AOA, Glide angle and pitch angle performance. This test would also help us in estimating the landing distance and throttle condition.

VIII. Open loop Flight Test Results

As discussed Section VII, open loop flight tests were done to understand the system behavior. Flight tests were done for take-off, landing and turn performance analysis.

These results would give an insight about the attitude of the Powered Parafoil Aerial Vehicle. This will help us in interpreting the controller gain values.

A. Take-Off Mode

During the take-off mode the pitch angle observed is about 20 degrees. These variations are due to vibration of the motor.

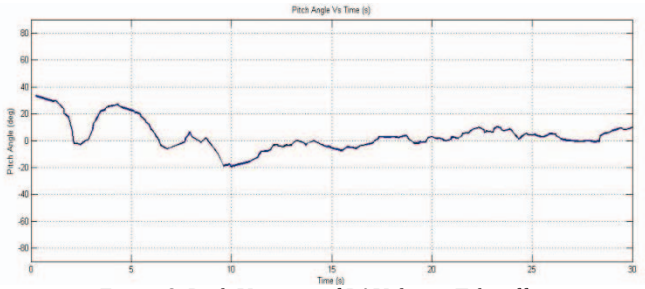

Figure. 8. Pitch Variation of PAV during Take off

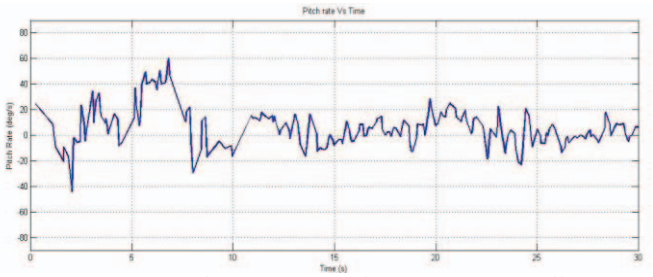

Figure.9. Rate of Pitch Variation of PAV During Take Off

The pitch angle tends to increase indicating that the vehicle tends to climb for 7 seconds. After 7 seconds the PAV tried achieve a level flight decreasing the pitch angle. The rate of pitch also is also maintained about zero. This can be observed in figures 8 and 9.

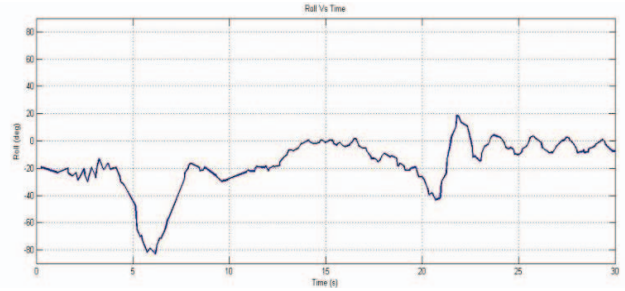

Figure 10. Roll Variation of PAV During Take Off

The roll variation is about -20 degrees initially. This initial angle is due to the turn as seen in the latitude lomgitude graph. The variations are due to the vibrations due to the motor attached on the payload. Figure 10 and 11 replictes the same. The roll rate is also about zero degrees due to the static stability of the vehicle. The oscillation are about +/- 20 degrees. The vibrations are observed due to the large motor propeller. It can be highlighted that due to the vibrations a variation in the values are observed. The range of the variations tends to be very small. In figure 12 it can be observed that the PAV take off and the takes a left turn.

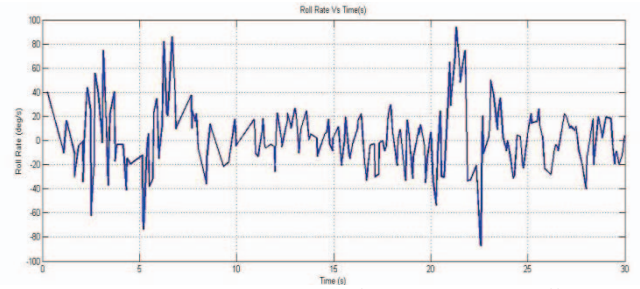

Figure 11. Roll Rate Variation of PAV During Take Off

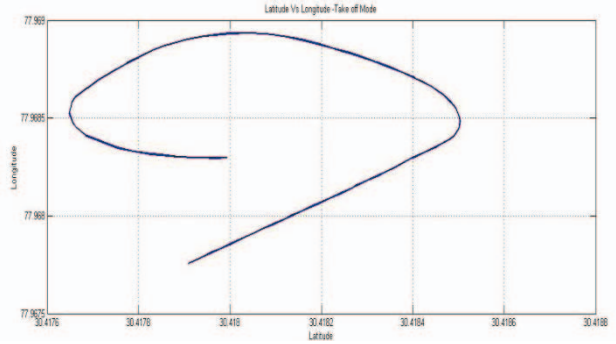

Figure 12. PAV Latitude and longitude Positions During Take-Off.

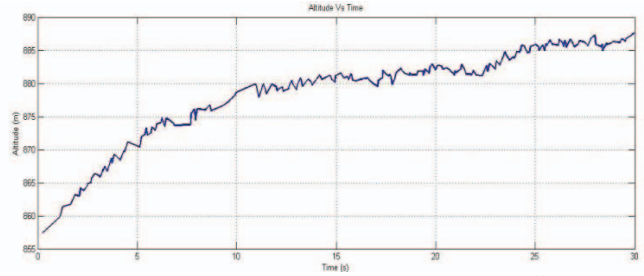

Figure 13. PAV Altitude variation during the takeoff

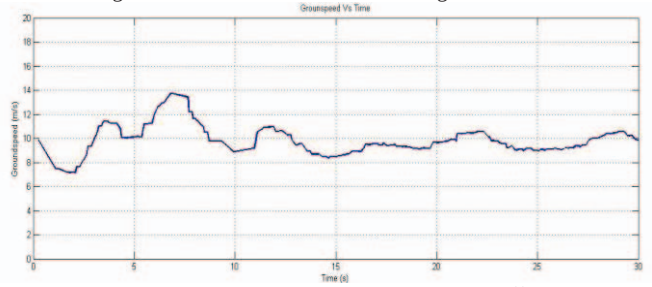

Figure 14. PAV Ground Speed during Take-Off

Figure 12 and 13 shows the PAV position with respect to latitude, longitude and altitude. The PAV tends to gain an altitude of 30m in 250ms.

The ground speed remains to be approximately 10m/s during take-off which can be seen in figure 14.

B. Landing

During the landing mode the pitch angle observed is about -2.5 degrees. These variations are due to vibration of the motors. The pitch angle tends to decrease indicating that the vehicle is tending to climb down. The rate of pitch also is also maintained about zero. The same can be seen figure 15 and 16.

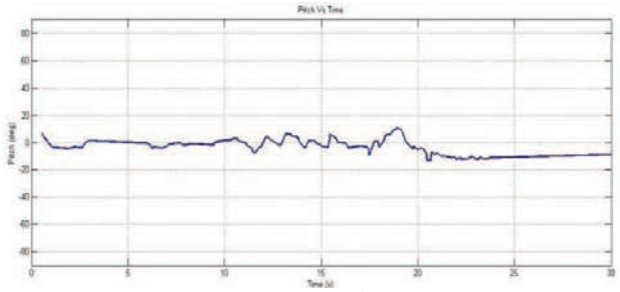

Figure 15. Pitch Variation of during Landing

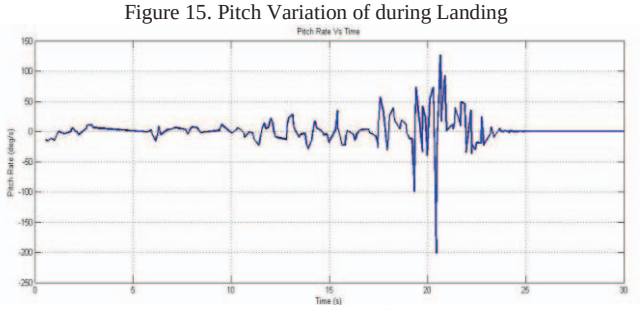

Figure 16. Pitch Rate Variation of during Landing

The roll variation is about 11 degrees. The variations are due to the vibrations due to the motor attached on the payload. Figure 17 and 18 replictes the same.

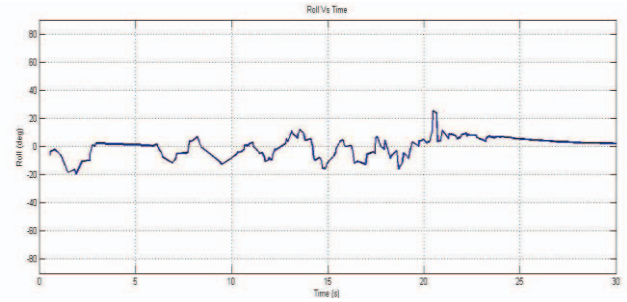

Figure 17. Roll Variation of PAV during Landing

The roll rate is also about zero degrees due to the static stability of the vehicle. The oscillation are about +/- 5.7 degrees.

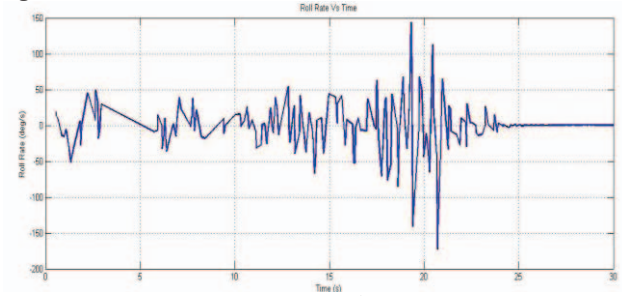

Figure 18.Roll Rate Variation of PAV during Landing

The Yaw Pitch and Roll values are plotted while take off the. The vibrations are observed due to the large motor propeller. A lot of oscillations are found in pitch rate, roll rate and yaw rate during touch down. These oscillations are due to the flare maneuver. Figure 19 shows the PAV position with respect to latitude, longitude and altitude.

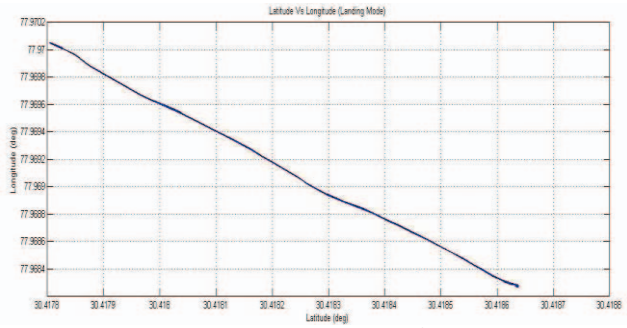

Figure 19. Latitude and Longitude variation of PAV during Landing

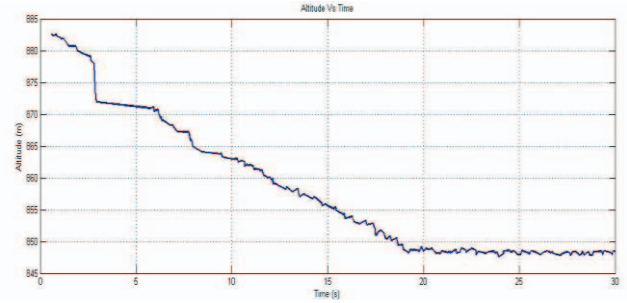

Figure 20. Altitude Variation during Landing

PAV loses an altitude of 40 meters in 20 seconds with a minimum thrust provided as seen in figure 20.

The ground speed value of the vehicle remains to be 10 m/s, as discussed in chapter 3; theoretically the velocity of the vehicle tends to be in 10m/s, as seen figure 21.

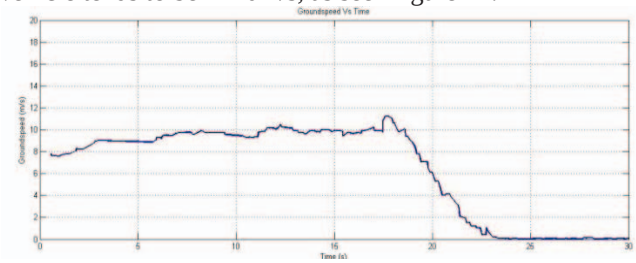

Figure 21. PAV Groundspeed during Landing

C. Turn Flight

During the take-off mode the pitch angle observed is about zero degrees. The variation in roll is about zero degrees which is very less.

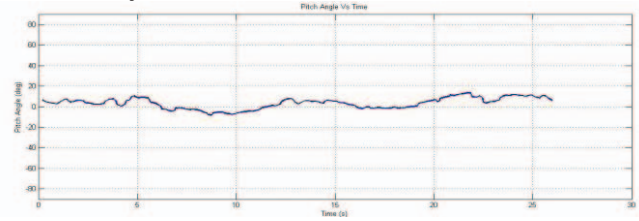

Figure 22. Pitch Variation During PAV Turning Flight

These variations are due to vibration of the motors. The pitch angle tends to be around zero indicating that the vehicle tends to maintain level flight. The rate of pitch also is also maintained about zero. The same can be seen figure 22 and 23.

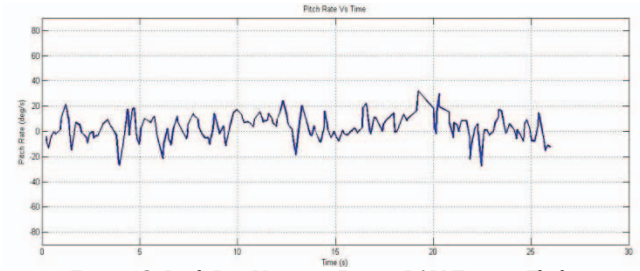

Figure 23. Pitch RateVariation During PAV Turning Flight

The roll variation is about zero degrees which is again negligible. The variations are due to the vibrations due to the motor attached on the payload. Figure 4.29 and 4.30 replictes the same.

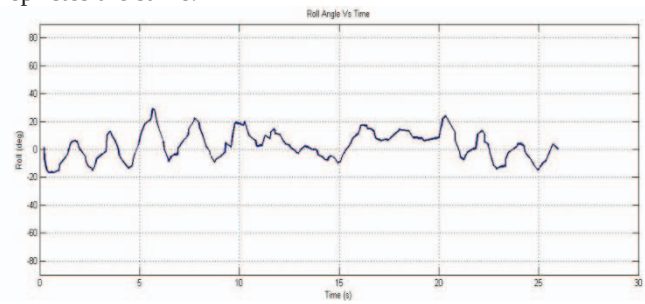

Figure 24. Roll Variation During PAV Turning Flight

The roll rate is also about zero degrees due to the static stability of the vehicle. The oscillation are about zero degrees which again very low. It can be observed from figure 24 that during the turn (from 14 seconds to 19 seconds) there was a cnage in roll angle of about 10 degrees due to the turn.

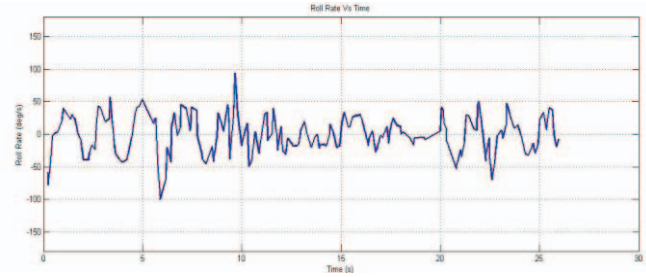

Figure 25. Roll Rate Variation During PAV Turning Flight

Figure 26 shows that the glide angle for the level flight is 0. When seen from altitude lost with respect to the horizontal distance covered. Since the PAV is in level flight as discussed in the open loop simulation result the glide angle is zero. Figure 26 shows the PAV position with respect to latitude, longitude and altitude. There is no altitude change and the vehicle is maintaining a turn rate of 18 deg/s.

Analytically, as discussed in earlier section, the velocity is 10 m/sec using the empirical formula, and from the figure 4.33 it can be seen that the velocity is maintained at 12 m/s. It can also be seen from figure 27 that the PAV

maintains a velocity of 10 m/s for level flight and during the turn the velocity goes up to 12 m/s.

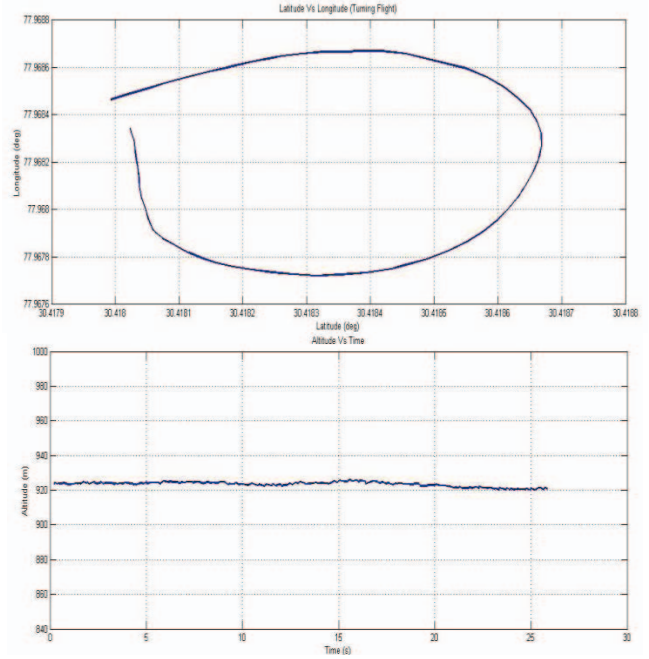

Figure 26. Latitude, Longitude and Altitude Variation During PAV Turning Flight

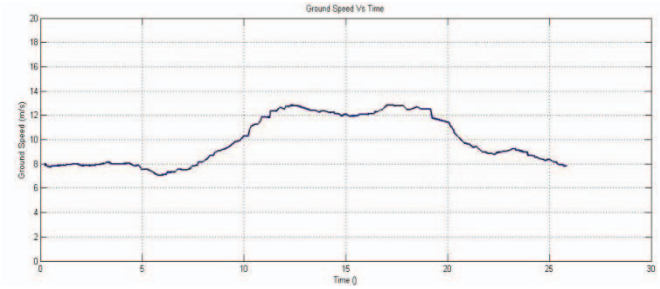

Figure 27. Velocity During PAV Turning Flight

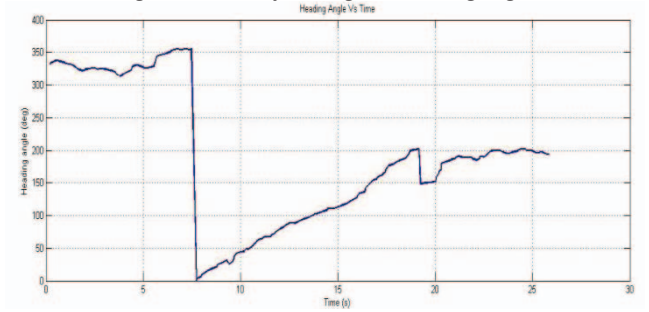

Figure 28. Heading Angle During PAV Turning Flight

From the figure 28, in the heading angle graph, it can be observed that the PAV is taking turn from 14 seconds to 19 seconds, at the turn rate of 18 deg/s with a bank angle of 10 degrees.

IX. CONCLUSION AND FUTURE WORK

This paper shows that the flight test results and the analytical results of the Unmanned Powered Parafoil Aerial Vehicle match within the range. The initial section of the paper discussed about the construction of the vehicle. The vehicle shape is in the triac shape having a nose fitted with the electronics and control unit. A single servo is used for controlling the direction of the UPPAV and BLDC motor used is used to take off, land and to maintain a level flight. The total weight of the payload is 3.8 kg. The next section gives the relation between size of the Parafoil and the payload weight. For a 4 kg payload the size of the Parafoil is taken as 2X0.65 m Parafoil. The system performance is also calculated where the lift and drag of the system is calculated. The Parafoil flight velocity is determined and turn performance is also determined. Three types of flight tests were performed and the flight test were compared with the analytical results and concluded the vehicle was performing as desired. It can be observed that during the level flight, while the vehicle is turning it there are less number of oscillations, while the vehicle is climbing up the oscillations are more.

All the observations in this section are done on Payload. A lot of oscillations/ vibrations are seen in the graphs as the sensors are placed on the Payload. The vibrations on the Parafoil would be comparatively lesser. Pitch angle, Glide Angle, heading angle, latitude, longitude, altitude and ground speed give the performance analysis of the complete system. The above mentioned graphs would help us in understanding the Parafoil performance.

These flight tests helped us in understanding the system performance which will be a great help in developing the autopilot. A flight stability system would be developed to reduce the pendulum effect of the payload. Lateral heading controller and longitudinal altitude hold controllers will also be designed to achieve way point navigation by making the system completely autonomous.

References

[1] Dept. of Defense, Unmanned Systems Road map 2007- 2032, office of Secretary of Defense, Washington D. C., 10 Dec. 2007.

[2] Jay Gundlach, "Design of Unmanned Aircraft Systems, A comprehensive approach" AIAA Education Series.

[3] John R. Chambers, "Longitudinal Dynamic Modeling and Control of Powered Parachute", Thesis Report, Department of Mechanical Engineering, Rochester Institute of Technology, New York.

[4] US Department of Transportation, Federal Aviation Administration, Flights Standard Service "Powered Parachute Flying Handbook", Aircraft Technical Book Company, http://www.actechbooks.com, 2007.

[5] Phil Dietro, "History of Paraplane", Adirondack Chapter Newsletter, EAA Sprit of Aviation, August 2012.

[6] V Devalla and Om Prakash, "Developments in Unmanned Powered Parachute Aerial Vehicle: A Review", IEEE Aerospace and Electronics system society magazine, November 2014.

[7] Y Ochi and m Watanabe, "Modeling and Simulation of the Dynamics of a Powered Paraglider", proceedings in IMechE, Vol.225, Part G.

[8] Hale, Francis J. "Introduction to aircraft performance, selection and design." John Wiley & Sons, Inc., 605 Third Ave. New York, NY 10158, USA, 1984, 416 (1984).

Privacy of Patient Information

Implementation and Security Analysis of a Secure Three Tier Patient Information System based on QR Code

Narendra Panwar
Dept. of Computer Science & IT
Uttarakhand Technical University
UK, India
naren.rishikesh@gmail.com

Dr. Manmohan Singh Rauthan
Dept. of Computer Science & Eng.
HNB Garhwal University
UK, India
mms_rauthan@rediffmail.com

Dr. Amit Agarwal
Dept. of Computer Science & Eng.
Univ. Of Petroleum & Energy Stud.
UK, India
core.info@gmail.com

***Abstract*— In the era of technology data security and information sharing is always a hot topic to talk on. There are lot of methods that are being used in security for secret information sharing such as cryptography, steganography, watermarking etc. another technology that is being used by people is QR code based information sharing but this technology is not enough to provide privacy in information sharing. Therefore, there is need of a better security algorithm which can be used for secure communication and have better efficiency and accuracy than others. In this paper author proposed a QR code based cryptographic technique which can be applied for security patient information.**

Keywords— Stenography, QR code, image encoding, DES, encryption.

I. INTRODUCTION

It is extremely dangerous to handle the internet against intruders. When sender sends a message to an authorized person than it can also be seen by an intruder. So the technology needs a better way to share information securely. QR (Quick Response) codes are a technology that desperately wants our attention. They appear everywhere from supermarket shelves and magazines to online shopping. The one dimensional barcodes used on general products are mechanically extracted by scanners. A barcodes scanner read data by physically penetrating a narrow beam of infrared light onto the barcode image, which can be interpreted using the pattern of infrared light reflected off the white area between the two barcode lines. Quick response codes can hold 100 times more data than 1D barcodes and they can also be scanned digitally more fast. QR codes provide an intelligent way to share information but it can be viewed by anyone easily by scanning it. To overcome this problem, the paper introduced a new way of information sharing using three tier security with QR code. The proposed work present the information sharing as scheme as –

- Message Encryption
- QR code generation
- QR code encoding.

By doing this the author added three tier of the security in this scheme. The further work can be done by adding a secure way to transmit this encoded image to the receiver.

A. Technique Used

1) Quick Response Code (QR Code): Data Coding

QR code can be used for sharing information securely and immediately. QR code is the trademark name for the 2D barcode systems. In 1994 QR codes was originally invented at Denso Wave which is a Toyota subsidiary, as a technique to track vehicles on assembly line, and to quickly scan vehicle components. Denso Wave has granted free license on QR code technique. The Quick Response code work by recognizing some point in QR code image. In this technique a smartphone image sensor can be used to scan small block of Black/White squares and then it is interpreted by system processor. The smaller black and white squares are used to normalize size and angle of scanned image while 3 large black and white squares are used to align the image with image sensor. QR code is not enough alone to provide complete privacy on information sharing. So author uses cryptography in proposed work with QR code for enhanced security of electronic patient information system (EPIS) data.

TABLE I. COMPARISON OF QR CODES WITH BARCODES

Features	QR Code	Barcode
Data representation capacity	Up to 7089 digit support	10-20 digit support
Reading Capability	Up to 30% damaged	Impossible to read damaged code
Space used	40 digit numeric on 5mm x 5mm space	10 digit numeric on 50mm x 20 mm space
Reading angle	Support 360 degree reading	Only horizontal reading

2) Data Encryption Standard: Cryptography Technique

Cryptography is the science of changing over the messages that are planned to be mystery into some other structure, such that it is not justifiable to anyone other than the proposed sender and beneficiaries. In the current work author uses DES Algorithm to achieve the goal. The DES is a secure modern block cipher scheme. In this scheme a cryptographic key and algorithm are applied to a block of user data bits simultaneously. In encryption phase, DES processes a 64-bit

978-1-5090-3411-6/16 $31.00 © 2016 IEEE
DOI 10.1109/ICMETE.2016.130

plaintext data with the help of cryptographic key and generates a 64-bit cipher text data.

In the decryption phase, DES takes a 64-bit cipher text data as input and generates a 64-bit plaintext data with the help of symmetric cryptographic key. The encryption process uses feistal structure and S Boxes in 16 rounds. In DES, the symmetric 56-bit cryptographic key is used for both encryption and decryption process.

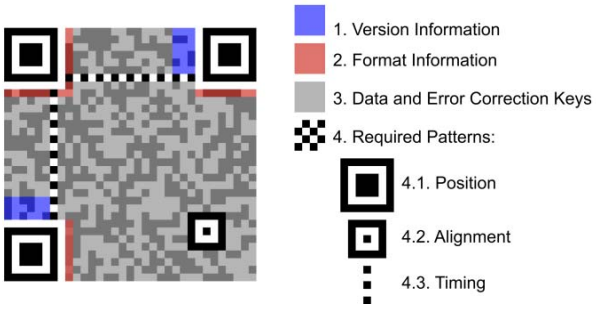

Fig. 1. QR Code Component

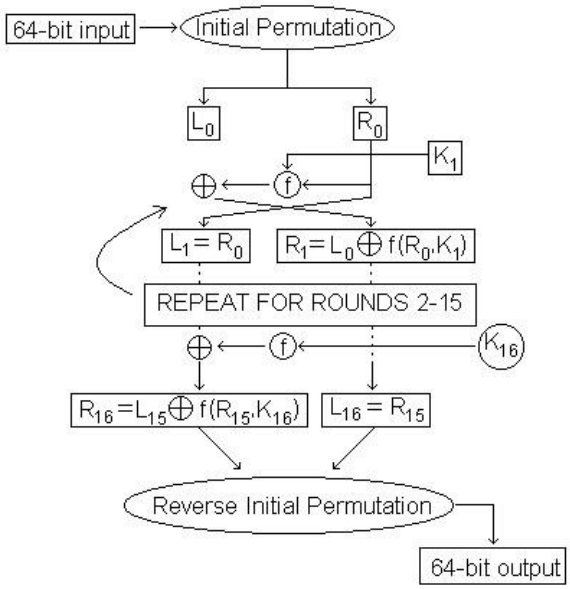

Fig. 2. DES Algorithm

II. Related Work

Previously many authors contribute in the field of secret information sharing using watermarking and Quick Response code based information sharing techniques [4-11].

In 2008, a watermarking based novel scheme was proposed by Zhang et al. [14]. Further, In 2012, Rungraungsilp et al. [12] proposes QR code embedded technique for invisible watermarking. Their result shows the comparison between mid-band coefficients and low-band coefficients. A geometric invariant watermarking technique have been explained and enlisted by Lakshmi et al. [13].

In 2013, Islam et al. [3] present a novel DWT-SVD based stenographic technique, A QR-code payload guides the alternation of the singular-values of DWT blocks. Their proposed method can be implemented in smart phones and smart video-cameras for consumer and business applications. In 2014, Ramaya et al. [1] examines the various imperceptibility characteristics such as Peak Signal to Noise Ratio, Average Difference, Maximum Difference, Mean Square Error, Normalized Absolute Error based on pixel value based information hiding.

By examining the QR code author gives best image quality measures between the Cover QR and the stenographic QR, as the secret data has been embedded to its best matching pixel value of the cover QR code. In 2015, Maheswari et al. [2] introduced a frequency domain steganography based information hiding technique using Fresnelet transform (FT), in this scheme author uses fresnelet coefficient of the least significant bit at high frequency sub-band to embed the QR code secret message.

The remainder of paper is as follows: In section III we have presented our proposed scheme and section IV describes result and discussion of paper. Finally, section V conclude the paper with merits and future work.

III. Proposed Technique

In this work we use a QR code based system for patient information sharing. For sharing information securely author uses QR code of encrypted private message and encode that QR code with C# .NET.

A. *Encoding Process*

1) Encryption process:

- A1: Input patient personal information.
- A2: Divide patient information into the block of 64 bits.
- A3: Apply DES algorithm on individual blocks.
- A4: Store cipher text

2) QR code generation process

- Next, we uses a program which creates QR code from the encrypted message.
- A5: Input stored cipher text
- A6: Generate QR code of cipher text (encoded image)
- A7: Now we send this encoded image to the receiver who can recover the secret message by decryption process.

B. *Decoding process*

- Receiver receives the encoded image by secure communication medium and then performs decoding process of image by the same pre-shared program and generates the QR code.

- B1: Extract the encrypted cipher text from QR code by QR code scanning application.
- B2: Apply DES algorithm on individual blocks for decryption.
- B3: Receives patient information securely.

IV. RESULTS AND DISCUSSION

As the secret patient information is hidden in encrypted form so it is important that the message remains unchanged even after QR code encoding and decoding. The proposed work consist of the process to check the alteration in image after encoding. It confirms the reliability and accuracy of the work in message sharing. For this author uses simple C#.NET code to check alteration in original QR code and the decoded QR code. By adopting this scheme a sender can send secret message more securely and in future this work can be enhanced by providing secure transmission system for image transfer.

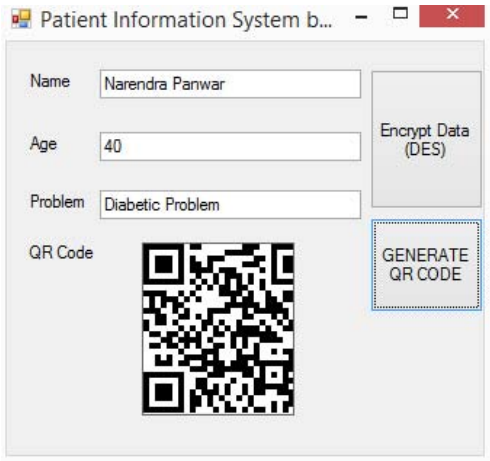

Fig. 3. Patient Information Encoding

Fig. 4: Patient Information Decoding using QR Code

V. CONCLUSION

In the present work we try to embed encrypted secret message in the form of QR code. Then we encode the QR code with image encoding technique. We proposed a secret message sharing algorithm which combines steganography and cryptography for achieving better security in message sharing. In principle it will be infeasible for attacker to decrypt the encoded message without knowing the cryptographic key. The method can be used for better security.

REFERENCES

[1] V. Ramya and G. Gopinath, "Review On Quick Response Codes in the Field Of Information Security",IEEE - International Conference on Advances in Engineering and Technology-(ICAET2014), ISBN No.:978-1-4799-4949-6

[2] Uma Maheswari, D. Jude Hemanth, "Frequency domain QR code based image steganography usingFresnelet transformS.", International Journal of Electronics and Communications (AEÜ)2015, 1434-8411

[3] Md. Wahdeul Islam, and Saif al Zahir, "A Novel QR Code Guided Image Stenographic Technique" IEEE International Conference on Consume Electronics(ICCE), 2013

[4] Shikha and Vidhu Kiran Dutt," Steganography: The Art of Hiding Text in Image using Matlab", International Journal of Advanced Research in Computer Science and Software Engineering, Volume 4, Issue 9, September 2014, pp: 822-828

[5] Z. V. Patel1 and S. A. Gadhiya," A Survey Paper on Steganography and Cryptography", RESEARCH HUB – International Multidisciplinary Research Journal (RHIMRJ), Volume-2, Issue-5, May-2015, pp: 1 of 5.

[6] W. Bender, D. Gruhl, N. Morimoto, and A. Lu, "Techniques for data hiding", IBM Systems , vol. 35, Issues 3&4 1996 Journal, pp. 313-336.

[7] Kor Ashwini N, Prof. N.M.Kazi," A Survey of Water Mark Technique", International Journal of Advanced Research in Electrical,Electronics and Instrumentation Engineering, Vol. 3, Issue 2, February 2014, pp: 7126-7131.

[8] Omprasad Deshmukh and Shefali Sonavane," Multi-Share Crypt-Stego Authentication System", International Journal of Computer Science and Mobile Computing IJCSMC, Vol. 2, Issue. 2, February 2013, pg.80 – 90.

[9] Wojciech Mazurczyk and Luca Caviglione," Steganography in Modern Smartphones and Mitigation Techniques", IEEE 2014, pp:1-25.

[10] Jitha Raj.T, PG Scholar and E.T Sivadasan, Asst. Professor," A Survey Paper on Various Reversible Data Hiding Techniques in Encrypted Images", 2015 IEEE, pp: 1139-1143.

[11] Mehdi Hussain and Mureed Hussain," A Survey of Image Steganography Techniques", International Journal of Advanced Science and Technology Vol. 54, May, 2013, pp: 113- 124

[12] Suppat Rungraungsilp, Mahasak Ketcham, Virutt Kosolvijak, and Sartid Vongpradhip, ‖data hiding method for QR code based on watermark by compare DCT with DFT domain‖, International Conference on Computer and Communication Technologies (ICCCT'2012), May 26-27, 2012.

[13] Shanjun Zhang and Kazuyoshi Yoshino, ―DWT-Based Watermarking Using QR code‖, Science Journal of Kanagawa University Vol. 19, 2008.

[14] Lakshmi Chetana Vemuri, Gogineni Krishna Chaitanya, Narasimham, Geometric Invariant Digital Image Watermarking Techniques for QR code‖, (IJCSIT) International Journal of Computer Science and Information Technologies, Vol. 3 (1) , 2012, 3037 – 3041

2016 International Conference on Internet of Things and Applications (IOTA)
Maharashtra Institute of Technology, Pune, India 22 Jan - 24 Jan, 2016

Reliable Communication for Sustainable Energy Efficient Low Power Smart Home Application (SELSA)

Rishi Anand
University of Petroleum and Energy Studies (UPES)
Dehradun, Uttarakhand
rishi.anand0@gmail.com

Himanshu Raj
University of Petroleum and Energy Studies (UPES)
Dehradun, Uttarakhand
hraj3116@gmail.com

***Abstract*— Technology has played a vital role in our living lifestyle. Today Technology is monotonically increasing our comfort level. Using very much efficient Technology that could save energy is what we are looking for. SELSA (Sustainable Energy Efficient Low Power Smart Home Application) is a solution to cut off Energy Wastage and provide users with multiple benefits like Remote Management, Intrusion Detection, Safety Solution and much more. At the same time SELSA uses ESP8266 which is extremely low power consuming hardware and MQTT which is very much lightweight publish-subscribe based messaging protocol to connect to Internet, this makes it very much reliable solution to cut off Energy Wastage and provide other benefits like Remote Management etc. Thus SELSA saves more energy and delivers secure, smart and connected solutions for a home.**

Keywords*— *Internet of Things; Remote Management; Smart Home; ESP8266; MQTT Protocol

I. INTRODUCTION

Everybody in this world wants to live in a fantasy world and of course that needs a great technologies, innovations and ideas. While all particular innovations might remain beyond our grasp, we can still enjoy a bit of "the future" today with smart home automation. Home Automation [1] is way to create an environment of smart home where everything, electrical devices such as light, fan, AC, refrigerator, can also be controlled remotely. Making it simple, home automation allows you to access and control critical systems and appliances from a remote or centralized location.

SELSA is a way ahead from smart home automation in terms of energy consuming and energy saving. SELSA uses hardware that requires comparatively very much less power for functioning. This makes it more convenient and reliable, if we are looking for energy saving solutions. SELSA also provides many more functions like a few taps on a touchscreen panel or a couple of voice commands in your home (or even your smartphone! Or web-app) one can set temperatures, turn off lights, and tweak their home's security among other options. Home automation is not only the next big demand in future but SELSA enriches the ecosystem in all aspects (commercially, economically, environmentally, socially etc.).

The home of a person is an important place in its life where he/she wants to get all kind of comfort. The home has many parts such as rooms, balcony, hall, kitchen, bathroom etc. Each and every part of the room consist of several electronic devices such as lights, AC, refrigerator, oven, fans, television etc. Apart from these, we have our garage where we keep our vehicles [2] and some houses also have gardens. There are different kind of users in the home such as small kids, old grandparents and very busy parents. SELSA provides the ease to use these devices in an efficient way so that energy can be saved and provides notification of everything, this makes monitoring home very much easier and comfortable. One can control the devices from anywhere. There are several devices which need to be switched on and off at a routine time on a fixed day or daily basis, while there are devices which need to be controlled on a particular events. SELSA makes the home such automated that the devices can be controlled on events and time basis and it could be beneficial for every group of users. Apart from these, the major concern in today's time is the security of the home. Automated home provide us real time notification for the threat or intrusion detection in our home on our mobile or desktop devices. For example, time based devices can be electric heater which need to be on for a particular duration to warm the room, event based devices are switching on the cooler when a person comes from office, switch on the light when a person move in the room or switch off the television when everybody has slept. We can control all these devices without worrying about the time, SELSA will do it all for us in just a click from the mobile app or web app. This paper tells us about such an automated environment, how we can create such an environment, what technologies and devices we will use in SELSA and what is the importance of these kind of environment in one's life and how it can bring a drastic change in the ecosystem.

SELSA implements Energy Efficient Low Power Application using efficient [3] and new hardware chips. SELSA communicates with sensors through ESP8266 (E-12) chip. ESP8266 has very much less power requirement for operation. It can be operated over battery for more than 1 years. It has 8 GPIO pins to take input from sensors and trigger some event based on threshold value of sensors. SELSA has one controller unit which is connected to ESP's. Controller [4] connects to ESP8266 through WiFi communication and Controller connects to Cloud over MQTT protocol. MQTT is very much light weight protocol designed for 'Internet of Things'. Using MQTT protocol ensures reliable communication from Cloud to Home Controller.

978-1-5090-0044-9/16/$31.00 ©2016 IEEE

SELSA reduces internet data usage by using a local server at home controller. So that, request from devices inside home network needs not to be processed from Internet [5]. This make communication fast and also reduces cost of Data. Incase if any home do not have internet for remote communication, then SELSA uses GSM module [6] to accept instruction from Remote Devices. Using of GSM module makes it more reliable to have it in home.

The rest of the paper is structured as follows. In section II we discuss related work. In section III we have mentioned about all technologies and hardware's we have used. In section IV we have described home automation systems which covers all modules that are included in SELSA. In section V we have described about SELSA applications. In section VI we have mentioned about benefits of SELSA. Section VII is about Conclusion and section VIII contains references.

II. Related Work

A. Principles of Smart Home Control

Seeking to be sensitive to users, smart home researchers have focused on the concept of control. They attempt to allow users to gain control over their lives by framing the problem as one of end-user programming. But families are not users as we typically conceive them, and a large body of ethnographic research shows how their activities and routines do not map well to programming tasks. End-user programming ultimately provides control of devices. But families want more control of their lives. In this paper, we explore this disconnect. Using grounded contextual fieldwork with dual-income families, we describe the control that families want, and suggest seven design principles that will help end-user programming [7] systems deliver that control.

B. Applications, Systems and Methods in Smart Home Technology

Smart Home technology started for more than a decade to introduce the concept of networking devices and equipment in the house. According to the Smart Homes Association the best definition of smart home technology [8] is: the integration of technology and services through home networking for a better quality of living. Many tools that are used in computer systems can also be integrated in Smart Home [9] Systems. In this paper, we present the Technologies and tools that can be integrated or applied in Smart Home systems.

C. Smart Homes and Home Automation

Smart homes and home automation are ambiguous terms used in reference to a wide range of solutions for controlling, monitoring and automating [10] functions in the home. Berg Insight's definition of a smart home system requires that it has a smartphone app or a web portal as a user interface. Devices that only can be controlled with switches, timers, sensors and remote controls are thus not included in the scope of this study. Smart home systems can be grouped into five primary categories: (1) energy management and climate control systems, (2) security and access control systems, (3) lighting, window and appliance control systems, (4) home appliances, and (5) audio-visual.

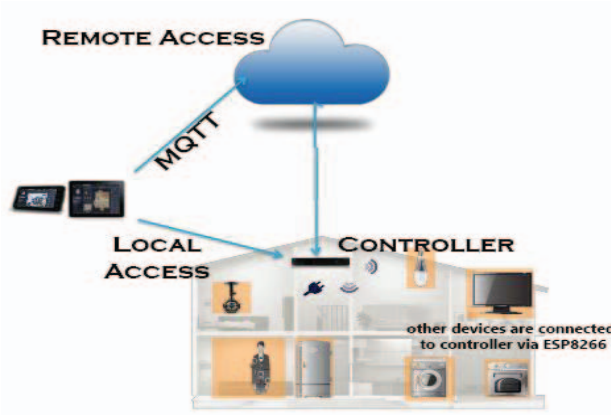

III. SELSA Automation Technology

Fig. 1. SELSA Architecture

SELSA uses new technologies to provide robust and efficient home automation solution. Some technologies and hardware that SELSA comprises of includes:

A. Raspberry Pi

Raspberry Pi is a small (ATM-card) sized, low cost and Linux based computer with a Broadcom BCM 2835 SoC, 256MB to 1024MB of RAM, USB ports, GPIO pins, Ethernet, HDMI out, camera header and an SD card slot [11]. Raspberry Pi supports programming in all languages. We can program it to get request from web and control GPIO pins accordingly. We can set our own local server on the raspberry pi which will help us to control devices when there is no internet. Even the installation of Raspberry Pi is a threat compared to other devices of this category. The boot time of pi, when the light gets on and off, is greater than other devices.

B. Arduino

Arduino is a micro-controller. It is an open-source prototyping platform. The most important feature is its easy-to-use hardware and software [12]. Arduino boards are able to read inputs – lights on a sensor, a finger on a button, or a Twitter message – and turn it into an output – activating a motor, turning on a LED, publishing something online. One can use the Arduino programming language (based on Wiring), and the Arduino Software (IDE), based on Processing.

Arduino is considered a major tool in Home Automation. The major benefit of Arduino is that the booting time is negligible and installation is very easy but at the same time it cannot be use for a wide variety of reasons, it has limited memory, it supports limited languages like C.

C. ESP8266

ESP8266 is a hardware which provides low cost wifi module functionality to any microcontroller such as Arduino via a serial connection. ESP8266 is also a 32 bit micro controller with an integrated WiFi chipset and TCP/IP stack. The major benefit of using ESP8266 is that by merely adding power, the wifi module can be reprogrammed to act as a standalone WIFI connected device.

It includes following features:

- soft-AP Integrated TCP/IP protocol stack
- Wi-Fi Direct
- 802.11 b/g/n protocol

D. *ZigBee*

ZigBee is a hardware developed by the IEEE. It supports ample of current protocol technologies. It is a low cost, low-power and wireless mesh technology. The best features in ZigBee is that it can connect to the internet using low-power and low-cost ZigBee radios. The main use of the ZigBee [13] is to leverage the ZigBee radio send and receive IPv6 packets to enable applications to send data back to the user via the Internet. Thus ZigBee has become a huge potential for home automation and sensor applications. The major drawback of ZigBee is that it is unable to communicate easily with other IP protocols.

E. *MQTT Protocol*

MQTT Protocol stands for Messaging Queue Telemetry Transport Protocol. It is a machine-to-machine (M2M) or Internet of Things (IOT) connectivity protocol. The most important feature of this protocol is that it is very light weight that means it can operate in a very small network connectivity. It is useful where connections is required in remote locations or where network bandwidth is a concern.

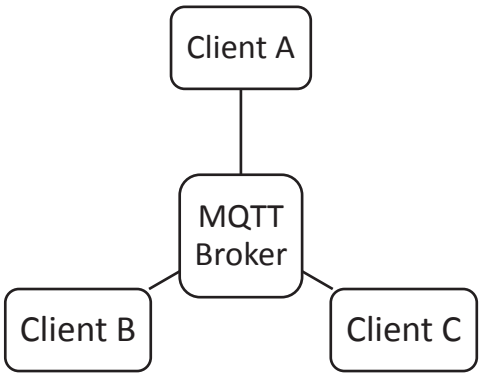

Fig. 2. Publishing and subscribing message in MQTT Protocol

It is a publish/subscribe based messaging transport protocol. It is suitable for mobile application because of its small size, low power usage, minimized data packets, and efficient distribution of information to one or many receivers.

IV. SELSA AUTOMATION SYSTEM

The Home Automation field is expanding rapidly as electronic technologies converge and especially in developing countries. The home network encompasses communications, entertainment, security, convenience, comfort and information systems. SELSA has Raspberry Pi as a Controller and ESP8266 is used to connect sensors to controller over WiFi.

The different modules included in SELSA are:-

A. *Controlling Devices from anywhere (through internet)*

In this module we are using an MQTT broker as an intermediate. Our mobile app or the web app communicates through the microprocessor in the house through the MQTT protocol. Whenever a user sends a command through the app, the app publishes a command on a particular topic .The devices are subscribed to that particular topic which receives the message at that topic and accordingly controls the devices. This module has two factor authentication.

1) *The MQTT broker authenticates the user*
2) *The other server (server of company) authorizes the user*

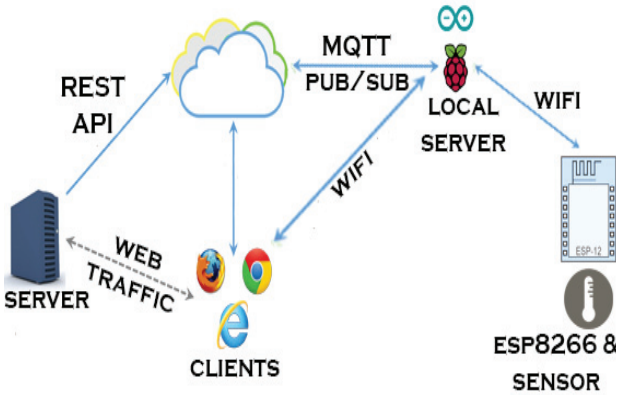

Fig. 3. SELSA Devices and their connection with Internet.

The user can only publish if it is authorized on both channels. The devices are connected to the app using web socket and the backend server can communicate to the MQTT broker server through the REST API's.

B. *Controlling devices locally from home (through local server)*

This system is a beneficial when the user is not connected to the internet. The device (Raspberry Pi) has a server deployed on to it, the user can connect to it when he is in the home and can then send the commands. The server can be Apache server or the server created through NodeJS, anything.

1) Client-Server Architecture: Here microcontroller is server and the devices connected to it are clients. The clients continuously pings to the server and tries to get the message. Whenever the user send the command to the server from the app it is stored in the local file on the server and the after a while the devices checks the file and implements the changes.

2) Publish – Subscribe: NodeJS is a JavaScript framework which is made for the server side programming. It is highly used for its callback features and events emitter. In this module when the user sends a command the command goes to the server and an event is generated which run asynchronously and

accordingly the changes are implemented. Similarly, for the acknowledgement of changes an event is generated and all the connected devices are informed.

C. Controlling devices from anywhere through SMS

This is useful when SELSA is not connected to Internet. In this approach end devices sends instructions inside SMS to GSM module attached in Raspberry Pi.

D. Controlling devices locally from home (through local server)

The best feature is that it doesn't ignore the manual part. If a change is made manually, the acknowledgement is send from the Raspberrypi or related devices to the subscribed devices and all the devices are updated accordingly.

V. SELSA Applications

Technology is the wheel of Revolution. Technology has drastically changed in last few years. Internet has connected us to every corner of Globe. SELSA harness internet to make human life simpler and easier like never before. SELSA controls sensors using intelligent microprocessor which uses MQTT (Message Queue Telemetry Transport) protocols to publish and subscribe to a topic over internet. It is "light weight" messaging protocol for use on top of the TCP/IP protocol. MQTT is very much light weight and so it works at very less internet speed and consumes very less data.

SELSA includes many energy and time saving applications:

A. Lighting Control

Controlling Lights in Home or in any building is basic application of SELSA. It makes easier and convenient to control lights from mobile or web application [14] when you are not home. It gives us more control over devices. Devices can be turned off using mobile and application whether we are at home or somewhere away.

B. Intelligent Thermostat Tuning (ITT)

Sustainable Development is key to successful resource utilization and resource management. As cost of resources are going high and pressure of Sustainable Development increases, this makes us to think narrow on Intelligent Energy Utilization Methodology. Heating and cooling our homes consumes on an average 50% yearly energy costs. SELSA makes cooling and heating efficient based on learning our preferences. It can reduce cooling and heating when no human is present in home. It uses Passive Infrared (PIR) sensor to sense human presence in home. If presence is not detected for a duration of time then SELSA intelligently turns it off saving a lot of energy and reducing cost over thermostat.

C. Automatic Lawn Irrigation

A lush and healthy lawn is a source of pride for almost all homeowners. But irrigating it without knowing humidity of soil can adversely affect plants and nearly half of that amount of water is wasted due to inefficiency. SELSA uses appropriate soil sensors to gather information about soil humidity and sprinkles water only when soil needs it. Thus saving water and ensuring healthy growth of plants.

D. Smart LPG Leakage Detection

LPG is a cooking gas that most of us use in our kitchen to cook food. LPG can cause explosions if not handled properly. SELSA uses high quality LPG gas leakage sensor to avoid accidents and help people to take action before any unwanted situation. It triggers alarms and switch on exhaust fan to clean air in kitchen.

E. Glass Break Detection Sensor

SELSA includes smart glass break detection sensor that detects breaking of glass based on frequency of sound produced which is caught by high quality microphone. It helps to know about any breach or in intrusion detection in smart house.

F. Advanced Light Control in Darkness

It is one of challenging task for peoples to track wall switches in darkness. It becomes more difficult for old people to light on bulb in night. It becomes a danger situation if somebody is searching for wall mounted [15] switch in night and gets hurt. SELSA uses sensors to track human motion in night and thus switches on light if it is darkness to avoid any unwanted accidents. If people gets up from bed in darkness and takes one step forward then light automatically glows. SELSA uses PIR motion sensor to analyze motion.

VI. SELSA Benefits

A Smart Home Automation system allow you to save money and even save the environment.

A. Convenience

Ability to control all your lights without getting out of the bed is no less than magic. This saves you lot of trouble in winters. Switching all electric appliances on and off from any remote place over internet can help save energy.

B. Timer based Control over Appliances

Control all your electric appliances based on timer. Electric appliances will automatically turn off on specific times.

C. Home Automation is easy to use

SELSA's Mobile Application makes controlling homes easy like never before. Home Automation makes it easier to power on and off appliances from remote place.

D. It increases Safety Levels

SELSA includes many sensors to keep an eye on home activities even if someone is not at home. LPG Sensor helps people to know about LPG leakage. It instantly triggers alarms and send notification to people in case of LPG [16] leakage. Glass Break sensor lets people know about any glass break in home. It will help people to know about any breach activity.

SELSA uses light weight protocol thus ensuring high reliability of message delivery even if there is network congestion. Using hardware that uses low power also makes it energy efficient. Thus SELSA is a smart solution for home automation.

VII. CONCLUSION

In this paper, we have presented insight about smart home and how SELSA can turn smart home, smarter. We have emphasized more on sustainable growth by saving energy. SELSA saves energy by cutting off extra power usage when nobody is at home. SELSA makes the home such automated that the devices can be controlled on events and time basis and it could be beneficial for every group of users. Apart from these, the major concern in today's time is the security of the home. Automated home provide us real time notification for the threat or intrusion detection in our home on our mobile or desktop devices. SELSA provides the ease to use these devices in an efficient way so that energy can be saved and provides notification of everything, this makes monitoring home very much easier and comfortable. One can control the devices from anywhere. There are several devices which need to be switched on and off at a routine time on a fixed day or daily basis, while there are devices which need to be controlled on a particular events. SELSA takes care of all such events and generates notification on each event.

REFERENCES

[1] F. K. Aldrich. Smart homes: Past, present and future. In R. E. Harper, editor, Inside the Smart Home, pages 17–39. Springer, 2011

[2] G. Coulouris, J. Dollimore, T. Kindberg, and G. Blair. Distributed Systems. Concepts and Design (Fifth Edition). Addison Wesley, 2011.

[3] N. Dipsis and K. Stathis. Ubiquitous agents for ambient ecologies. Pervasive and Mobile Computing, 8(4):562–574, aug 2012.

[4] A. Fensel, S. Tomic, V. Kumar, M. Stefanovic, S. V. Aleshin, and D. O. Novikov. Sesame-s: Semantic smart home system for energy efficiency. Informatik-Spektrum, pages 1–12, 2012.

[5] G. Fortino and A. Guerrieri. Decentralized management of building indoors through embedded software agents. Computer Science and Information Systems, 9(3):1331–1359, 2012.

[6] C. Gomez and J. Paradells. Wireless home automation networks: A survey of architectures and technologies. IEEE Communications Magazine, 48(6):92–101, june 2010.

[7] X. Jiang, S. Dawson-Haggerty, P. Dutta, and D. Culler. Design and implementation of a high-fidelity ac metering network. In Proceedings of the International Conference on Information Processing in Sensor Networks (IPSN), pages 253–?264, Washington, DC, USA, 2009.

[8] J. Gubbi, R. Buyya, S. Marusic, and M. Palaniswami. Internet of Things (IoT): A Vision, Architectural Elements, and Future Directions. Future Generation Computer Systems: pp.1645-660.

[9] D. Evans, The Internet of Things: How the Next Evolution of the Internet Is Changing Everything. https://www.cisco.com/web/about/ac79/docs/innov/IoT_IBSG_0411FINAL.pdf. 2011.

[10] Rohit D. Gawade and Dr. S. L. Nalbalwar. Mac Protocol Based Low Energy Operations In Wireless Sensor Networks. International Journal of Electronics and Communication Engineering & Technology, 5(3), 2014, pp. 79 - 93.

[11] D. Evans, The Internet of Things: Raspberry Pi https://www.raspberrypi.org/ 2011.

[12] G. Coulouris, J. Dollimore, T. Kindberg, and G. Blair. Distributed Systems. Concepts and Design (Fifth Edition). Addison Wesley, 2011.

[13] N. Dipsis and K. Stathis. Ubiquitous agents for ambient ecologies. Pervasive and Mobile Computing, 8(4):562–574, aug 2012.

[14] C. Reinisch, M. J. Kofler, F. Iglesias, and W. Kastner. Thinkhome: Energy efficiency in future smart homes. EURASIP Journal on Embedded Systems, 2011(1):18, 2011.

[15] ZigBee Alliance, "ZigBee Home Automation Public Application Profile", 2010.

[16] Jahnke, J.H., d'Entremont, M., & Stier, J. (2002) Facilitating the programming of the smart home, IEEE Wireless Communications, 9(6): 70-76.

2015 International Conference on Soft Computing Techniques and Implementations- (ICSCTI)
Department of ECE, FET, MRIU, Faridabad, India, Oct 8-10, 2015

Star Shaped Cluster Deployment in Triangular Grid for Monitoring Forest Fires

Chhavi Gupta
Centre for Information Technology
University of Petroleum & Energy Studies
Dehradun, India
Chhavigupta.cs@gmail.com

Ankit Khare
Centre for Information Technology
University of Petroleum & Energy Studies
Dehradun, India
Ankit.khare86@gmail.com

Abstract— As the technology is advancing, a tiny device called sensor is proving its worth and applications in vast areas. These areas may include medical field, agriculture, environment monitoring, smart city projects and many more. These sensors works by forming a network called Wireless Sensor Networks (WSNs) which is very vivid and encouraging field of research in itself. But the bottleneck of this technology is the energy constraint as nodes are limited battery operated. Hence, in this paper, a star shaped deterministic deployment of the sensor nodes has been proposed. This technique will optimize the energy consumption as all nodes in the cluster will be only one node apart from the cluster-head. This is because we know the fact that maximum energy dissipates in sending information from one node to another. This technique will also result in minimum delay in taking decision. At the same time it will cover the maximum region by keeping the number of nodes low. Accuracy is again an important factor for WSNs for this support Vector Machine has been applied. Furthermore, cluster- head will keep changing after fixed time interval to balance the energy consumption of different nodes in the network.

Keywords— Wireless Sensor Networks, Event Detection, Deterministic Deployment, Support Vector Machine, Clustering, Energy Optimized Routing.

I. INTRODUCTION

Forest is one of the basic element for human survival on the earth. Forest fires are the biggest challenge to deal to avoid any mis-happening which can cause disaster in terms of asset and lives. It has been recorded [21] that 77,500 forest fires burned 6,790,000 acres in United State of America (USA) in year 2004. To monitor environmental problems like forest fires, military surveillance, service monitoring, smoke detection etc. is a biggest challenge and especially in such areas where fire brigade is difficult to reach like hilly regions. So to detect such events and provide an immediate solution we require an accurate mechanism.

Wireless Sensor Networks (WSNs) is a technology which can provide the solution for this problem and can be applied in real time for prediction and detection such events.

WSNs are an organization of sensor nodes, and these nodes can be deployed in any particular area randomly or in manual fashion and these nodes can sense environmental conditions such as temperature, pressure, vibration, motion, sound, and pollutants and then finally send this information data to the base station.

A sensor node is capable to sense, compute and communicate but a node has a limited communicating range and sensing scope over the network. Sensor node consists of the following parts a) battery (an external energy source) b) microcontroller (for computing the sensed information) and c) a radio transceiver with an external antenna.

Event Detection in WSNs is a critical issue as it can effect on property as well as lives of human being. So, event detection in specific time constraint in WSNs becomes the essential area which is to be research and analyzed. WSNs consist of large number of sensor nodes deployed at distributed location to sense the environmental conditions. These Sensor nodes send the data to the cluster head and cluster head send collaborative information to base station. Base station makes the final decision on the basis of this collected information and past experiences.

We have proposed an architecture which is energy efficient and giving better accuracy. Star shape of cluster maintains direct communication between head and node hence it improving efficiency. In case of failure of cluster head is being handled by frequently change cluster head hence it improves lifetime of the network.

One of the major challenges of WSNs are energy consumption and deployment strategy and so this deterministic deployment provide uniform coverage and also this is less complex as compare to other deployment strategies. Deployment in triangular fashion minimizes overlapped area

and covers the entire region with minimum number of nodes as compare to rectangular and hexagonal deployment.

The proposed algorithm changes the position of cluster head after fixed time interval in such a fashion that every node will become cluster head. A sensor node within the cluster send sense data to respective cluster head and then head process all the collected data and delivers this information to base station. For a better lifetime of the network this is necessary to frequently change the position of cluster head.

Furthermore, we have compared our algorithm with existing algorithm D^2CH (Deterministically deployed cluster head selection algorithm). Result section will show the comparative study and analysis of the proposed algorithm. We have analyzed time complexity of our algorithm as well.

II. RELATED WORK

Vast research is taking place in the field of Wireless Sensor Networks and in its wide areas. Many researchers contributed a marking work in the history and gave the path to young researchers to carry forward their work in future. Some of the researches are discussed here which is based on the parameters like network Lifetime, Energy Consumption, Clustering Techniques, Minimum delay and coverage area.

Alemdar in [11], described various applications and challenges in the field of WSNs like Military applications, replacement of minefields, precision agriculture, habitat monitoring including forest fires, earthquakes, Tsunamis etc. As every technology has its own pros and cons, so has WSNs has. With vast application it has challenges too like battery power, routing, communication, integrated circuits and security etc. are also been discussed in this paper.

In 2012 Barfunga, S.P. et al [10] present a cluster-based routing protocol for WSNs. And routing in WSNs is very challenging task. In WSNs Major critical aspects are lifetime of the network, sensing the data and communication between sensor nodes. Communication consumes energy and therefore power management and scheduling are the important factors that can effectively extend operational time.

In 2005, Cardei, M. et al [5], the author has proposed an efficient method for extending operational time of the sensor network by organizing the sensors into a maximal number of disjoint set covers that are activated successively.

In [1,12] Ankit Khare et al (2012,2013) the author has used deterministic deployment technique and also proposed cluster head selection algorithm to continuously change the position of cluster head , and therefore, it can enhance the lifetime of the network and energy efficient.

In these days number of approaches has been proposed by various researchers which deal in distributed event detection by using WSN. The idea behind the event detection is to define a threshold value for specified parameters like temperature, pressure etc. When major difference is recorded between threshold value and sensor recorded value an alarm or signal is generated.

Above discussed Approaches addresses the problem of collecting data for processing offline from different sensor nodes located at remote locations and introduced the techniques for storing data online for later use.
Our proposed approach is different, as this algorithm is more accurate and simpler and has the minimum delay in disseminating information in the network. Based on the above-explained approaches, we have proposed our algorithm and framework to enhance the lifetime of WSNs.

III. SUPPORT VECTOR MACHINE

Support Vector Machine (SVM) is well known classification techniques used mainly in data mining and machine learning areas. SVM classifies data through building N-dimension hyper plane that divides the data into two categories in best possible way [22]. SVM models are very similar to the tradition model of multilayer perception neural networks. SVM is becoming hot choice for classifying data as it offers following advantages [23]-

- It does not need any comprehensive statistical approach
- It provides best classification solution by increasing the marginal scope of decision boundaries
- It ignores dimensionality complexities.

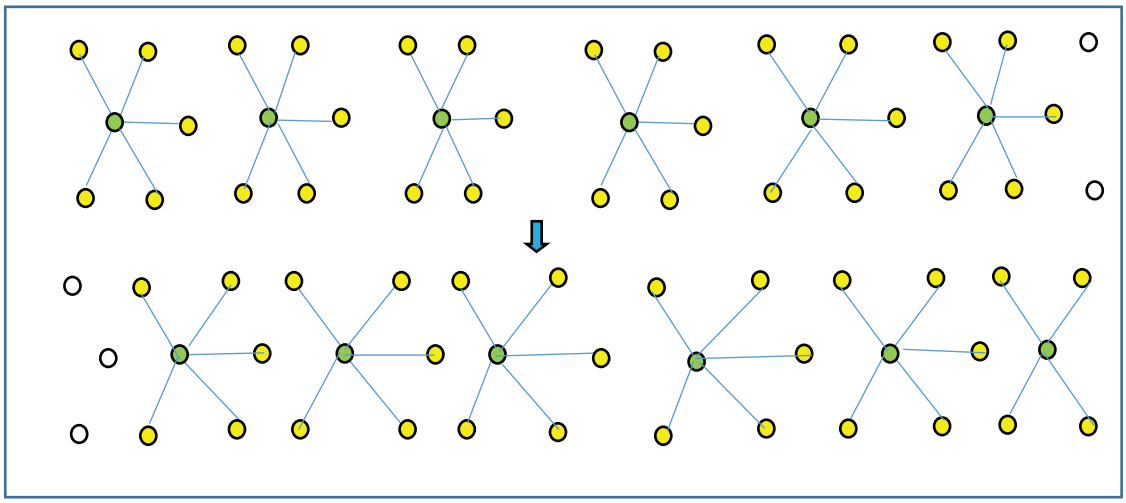

Fig. 1 Cluster head changing scenario

IV. PROPOSED WORK

In this paper, an architecture for monitoring and detecting forest fires has been proposed. Basic objectives of this paper are –

- Optimize the energy consumption.
- Coverage of maximum area with minimum sensor nodes.
- Detection of Forest fires with minimum delay.
- Accuracy

Instead of taking five nodes in a cluster [1], we are taking five nodes in a cluster. Due to which, number of cluster will be less. Hence, base station will get more structured data.

In our approach, we are applying unsupervised learning model support vector machine at base station which is known for its accuracy when we deal with such large database. Now in our architecture for monitoring forest fires, we have these components-

- Deployment scheme
- Clustering scheme
- Cluster head selection and data transmission to base station

V. DEPLOYMENT SCHEME

In this section, we will discuss the scheme for deployment of sensors. We have opted a deterministic deployment scheme in triangular fashion [1]. Decision of deploying sensors also plays a significant role as network performance will also be affect by this decision. Main objectives for this type of deployment are-

- If the sensor nodes are placed in triangular fashion, then power consumption will be same for all the three nodes as all three nodes will be equidistant.
- Deployment scheme is deterministic that is in fixed fashion. One of the most important advantage of this scheme is minimized packet collision.
- Sensor nodes should cover the region efficiently in order to detect forest fire with minimum delay.
- Triangular deployment covers the region effectively with minimum number of nodes.

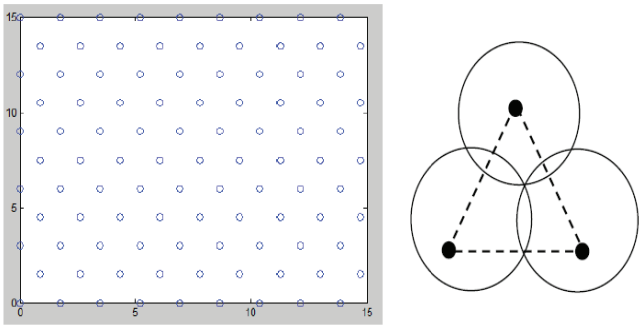

Fig. 2 Triangular Deployment

We have proposed the scheme to form the cluster in star shape in which the central node will behave as a cluster-head. This technique will reduce the energy consumption as all the sensor nodes of the cluster will be at single hop distance. Maximum interaction takes place between cluster-head and the nodes. So, the energy consumption will be less as the data transmission distance is less.

VI. CLUSTERING SCHEME

In our architecture, we are making cluster of six nodes such that central node will always be the cluster head and will make the shape of star. Basic idea behind this type of clustering is that first of all, cluster head will be on one hop distance. Thus, Communication time will be optimum and information about any time critical event can be communicated with minimum delay. Secondly, number of nodes is comparatively less due to which cluster head will have precise and structured data. Cluster design will be like-

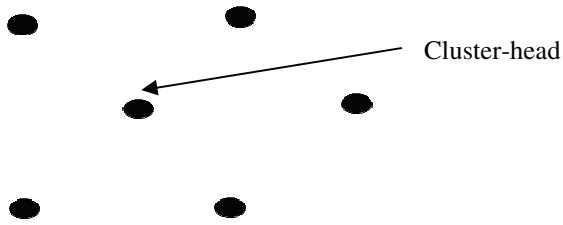

Fig. 3 Cluster View

Central node will always behave as cluster-head and after time interval t cluster haed will shift to right hand side and will form new cluster in the same manner.

VII. PROPOSED ALGORITHM

In this section, Algorithm is defined for proposed work as follows-

1. Sensor nodes will be placed deterministically in a triangular grid.
2. Six nodes will form a cluster in star shape and central node will behave like a cluster-head.
3. These sensor nodes will continuously sense the parameters like temperature, humidity, CO_2 and CO and send the data to the respective cluster head.
4. Cluster-head will apply one pass clustering method to form the clusters of large evolving data.
5. Cluster-head will send the clustered data to the base station.
6. SVM will be applied on the received data at base station and base station will detect the event.

7. After threshold time t, perform right shift on the position of cluster head.
   \\ Repeat step 2 to 7.

In this approach, we have deterministically deployed sensors and declared central node as cluster head. Idea behind this is if cluster head will be at exactly one hop distance, there will be less dissipation of energy in data has to travel less now. Secondly, there will be minimum delay as all the information in our scenario is life critical.

All these nodes will continuously sense the parameter like temperature, humidity CO2 and CO etc. This collated data will be sent to cluster head continuously where one pass clustering technique will be applied on large evolving data. There are many techniques for large clustering data but we have chosen one pass clustering technique. This is because firstly, it is very simple in working. Secondly, Energy is very limited with the cluster head. So, applying complex method will not be a good idea.

Now, this structured data will be transmitted to base station where SVM will be applied. We will have prior experiences stored at base station. Using cluster sampling, SVM will classify collected data and will extract the useful data. Now, more precise decisions can be taken as false alarms or delayed alarms can cost to unbearable loss in depicted scenario.

Threshold time t has been set. After waiting time t, right shift operation on the cluster head will be applied. This is because we know the fact that cluster head consumes energy at very fast pace. Thus, thought behind making balance between energy present with all nodes is to give a chance to every node to be a cluster head.

VIII. RESULT AND COMPLEXITY ANALYSIS

We have simulated proposed work as well as D^2CH (Deterministically deployed cluster head selection algorithm) on the basis of following defined values-

Table 1 Parameters

Parameters	Value
Network Size	100×100
Number of nodes	Maximum 250
Number of cluster	Maximum 40
Base station position	100× 150
Number of Rounds	3200

In below chart, we have shown comparison of proposed work with D^2CH algorithm in regard of Energy consumption over rounds. The graph is indicating at every level of rounds proposed algorithm is showing better results.

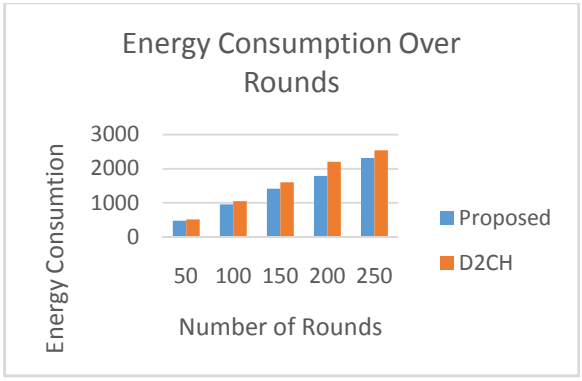

Fig. 4 Energy Consumption

In this graph, we have taken exact parameters as of D^2CH that is we have taken number of nodes as 169 and number of rounds as 3200. According to the shown graph, at point 3200 we have still 104 nodes alive while in case of D2CH only 96 nodes were alive.

Furthermore, if we talk in terms of complexity analysis of this algorithm, it is quite good. Time complexity of support vector machine approach is O (n^a) where a=1+x and x>0. If there are p processors, it will take O (p*n) time in sequence. If we execute it in parallel on multiple p machines it will take linear time.

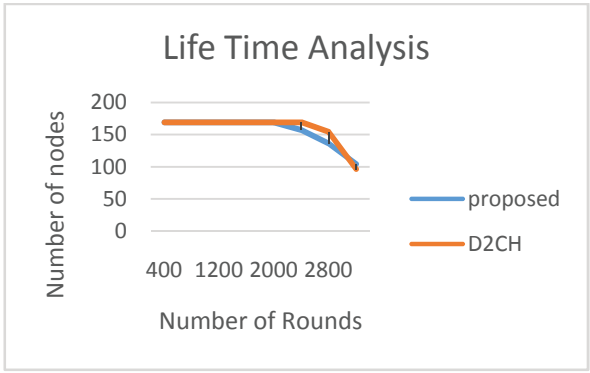

Fig. 5 Network Life Time Analysis

So complexity of algorithm will be O (n^a). If can replace this technique by any other simpler method, but will affect other parameters.

ACKNOWLEDGEMENTS

In this paper, we have deployed a star shaped cluster deterministically for event detection for forest fires. In this architecture, all sensor nodes are placed deterministically in triangular deployment method. Six nodes are forming a cluster

of star shape in which central node will be cluster head. These sensors will convey all the sensed information to the cluster head and cluster head will further transfer the information to base station in structured form. Base station will detect the event on the basis of past experiences as well as collected data. This architecture is minimizing the delay in communication, giving more accurate results or say minimizing false alarms and reducing the energy consumption. Hence, it is improving the network lifetime. We have also compared our results with existing algorithm D^2CH. According to the results, proposed algorithm is working better. We have analyzed time complexity of algorithm that is O (n^a). Inter cluster communication is also one of the issue whose study can give new dimensions to the research.

REFERENCES

[1] Ankit Khare and Nitin, "Radioactive Pollution Monitoring Using Triangular Deployment in Wireless Sensor Networks", Proceedings of the International Conference on Advanced Computing, Networking, and Informatics, India, June,2013.

[2] Ming Ma and Yuanyuan Yang, "Adaptive Triangular Deployment Algorithm for Unattended Mobile Sensor Networks", IEEE Transactions on Computers, Volume 56, Issue: 7, 946 – 847, 2007.

[3] M. Cardei, J. Wu, M. Lu, and M. Pervaiz, "Maximum network lifetime in wireless sensor networks with adjustable sensing ranges". In Proceedings of the IEEE International Conference on Wireless and Mobile Computing, Networking and Communications (WiMob), 2005.

[4] M. Cardei, M. Thai, L. Yingshu, W. Weili, "Energy-efficient target coverage in wireless sensor networks", INFOCOM 2005. 24th Annual Joint Conference of the IEEE Computer and Communications Societies. Proceedings IEEE, Vol. 3, 1976- 1984, 2005.

[5] M. Cardei and D. Du, "Improving Wireless Sensor Network Lifetime through Power Aware Organization", Wireless Networks, Vol. 11, Issue: 3, 2005.

[6] K. Flouri et al., "Training_A_SVM-Based Classifier in Distributed Sensor Network", In proceedings of 14th European Signal Processing Conference, 2006.

[7] Chhavi Gupta et al., "Fault Tolerant Event Detection in Distributed WSN via Pivotal Messaging", International journal of Computers and Technology, vol. 7, issue no. 1, 2014.

[8] Yashwant Singh, Sumah Saha, Urvashi Chugh, Chhavi Gupta, "Distributed Event Detection in WSN for Forest Fires", Internation Conference of Computer Modelling and Simulation (UKSIM'13), 2013.

[9] Chhavi Gupta, Ankit Khare and Manish Prateek, " Energy Efficient Fault Tolerant Architecture for Distributed Event Detection", Elsevier International Conference on Emerging Research in Computing, Information, Communication and Applications (Ercica), 2014.

[10] Sonam Palden Barfunga; Rai, Prativa; Sarma, Hiren Kumar Deva, "Energy Efficient Cluster Based Routing Protocol for Wireless Sensor Networks", Computer and Communication Engineering (ICCCE), International Conference, pp. 603 – 607, 2012.

[11] A. Alemdar and M. Ibnkahla, "Wireless sensor networks: applications and challenges," ISSPA, pp 1-6, 2007.

[12] Ankit Kumar Jain, Ankit Khare, Kaushlendra Kumar Pandey, "Developing an efficient framework for real time monitoring of forest fire using wireless sensor network", Second IEEE International Conference on Parallel, Distributed and Grid Computing at Jaypee University of Information Technology, Waknaghat, Solan, Himachal Pradesh, India , pp 811 – 815, 2012.

[13] Ankit K Jain, N Purohit, K K Pandey, Akshansh Jain, Harsh Bansal and Harshit, "An Efficient Clustering Technique for Deterministically Deployed Wireless Sensor Network", International Journal of Computer Applications, pp 0975 – 8887, Vol. 59 – No.6, 2012.

[14] Majid Bahrepour, Nirvana Meratnia, Mannes Poel, Zahra Taghikhaki and Paul J. M. Havinga, "Distributed event detection in wireless sensor network for disaster management", International Conference on Intelligent Networking and Collaborative Systems (INCOS), pp. 507-512, 2010.

[16] W..Heinzelman et al., "Energy-Efficient Communication Protocol for Wireless Microsensor Networks", 33rd Hawaii international Conference on System Sciences, vol. 2, pp.1-10, 2000.

[17] M. Haenggi, "Energy-Balancing Strategies for Wireless Sensor Networks", IEEE International Symposium on Circuits and Systems , Bangkok, Thailand, May 2003.

[18] Chee-Yee Chong, and S. P. Kumar, "Sensor Networks: Evolution, Opportunities, and Challenges", Proceedings of IEEE, Vol. 91, No. 8, 2003.

[19] F. García-Hernández, P. H. Ibargüengoytia-González, J. García-Hernández, and J. A. Pérez-Díaz, "Wireless Sensor Networks and Applications: a Survey", International Journal of Computer Science and Network Security (IJCSNS), Vol.7, No.3, 2007.

[20] I.Akyildiz, W. Su, Y. Sankarasubramaniam, and E. Cayirci, "A survey on sensor networks", IEEE Communications Magazine, Vol.40, No. 8, pp 102–114, 2002.

[21] http://www.wrh.noaa.gov/sew/fire/olm/nfdrs.htm, "National Fire Danger Rating System".

[22] M. Mohamed Sathik et al., "Fire Detection Using Support Vector Machine in Wireless Sensor Network and Rescue Using Pervasive Devices", International Jounal of Advanced Networking & Applications, Vol. 2, issue 2, pp, 636-639, 2010.

[23] M. Syed Mohamed et al., "Outlier Detection Using Support Vector Machine in Wireless Sensor Network Real Time Data", International Journal of Soft Computing & Engineering, ISSN 2231-2307, Vol.-1, Issue-2, 2011.

Synthesis of carbon nanotubes over 3D cubical Co-KIT-6 and nickel decorated graphene by Hummer's method, its application as counter electrode in dye sensitive solar cell

Sunu Subramanian and Arumugam Pandurangan

Citation: **1724**, 020121 (2016); doi: 10.1063/1.4945241
View online: http://dx.doi.org/10.1063/1.4945241
View Table of Contents: http://aip.scitation.org/toc/apc/1724/1
Published by the American Institute of Physics

Synthesis of Carbon Nanotubes Over 3D Cubical Co-KIT-6 and Nickel Decorated Graphene by Hummer's Method, its Application as Counter Electrode in Dye Sensitive Solar Cell

Sunu Subramanian[a] and Arumugam Pandurangan[b]

[a]*Research Scholar , Department of Chemical Engineering, College of Engineering Studies, University of Petroleum and Energy Studies, Dehradun. Email Id: sunusubramanian11@gmail.com*
[b]*Head of the Department, Department of Chemistry, College of Engineering Guindy, Anna University, Chennai*

Abstract. The challenges on carbon nanotubes and graphene are still the subject of many research works due to its unique properties. There are three main methods to synthesis carbon nanotubes in which chemical vapor deposition (CVD) method can use for large scale production. The principle of CVD is the decomposition of various hydrocarbons over transition metal supported catalyst. KIT-6 molecular sieve was used as a support to prepare cobalt catalyst for CVD method using metal impregnation method to produce cobalt loadings of 2, 4 and 6 wt%. The catalysts were characterized by XRD, FTIR &TEM. Carbon nanotubes (CNTs) synthesized on Co-KIT-6 was also characterized by XRD, TGA, SEM & Raman spectra. Graphene was synthesized by Hummers method, which is the most common method for preparing graphene oxide. Graphene oxide was prepared by oxidation of graphite using some oxidizing agents like sulphuric acid, sodium nitrate and potassium permanganate. This graphene oxide is further treated with hydrazine solution to convert it into chemically converted graphene and also decorated with nickel metal and characterized. Hummer's method is important for large scale production of graphene. Both Graphene and carbon nanotubes are used in different fields due to its unique properties. Both Graphene and carbon nanotubes are fabricated in counter electrode of Dye sensitized solar cells (DSSC). By cyclic voltammetry study, it confirms that both materials are good and efficient to replace platinum in the DSSC.

Keywords: Carbon Nanotubes, Graphene, CVD, Hummer's Method, DSSC, Cyclic voltammetry

INTRODUCTION

In this century, the main challenges of researchers are to develop a system that helps to converse energy. Due to the depletion of non-renewable energy resources, it is necessary to utilize the renewable resources as in different forms that it can be done. In response to the energy crisis, it is important to have storage devices that can convert solar energy which is an abundant resource for billions of years. Dye sensitized solar cells DSSCs revealed as a new class of low cost energy conversion devices with simple manufacturing procedures. The sensitizing dye in a DSC is anchored to a wide-band gap semiconductor such as TiO_2, SnO_2 or ZnO. When the dye absorbs light, the photo-excited electron rapidly transfers to the conduction band of the semiconductor, which carries the electron to one of the electrodes. A red-ox couple, usually comprised of iodide/triiodide ($I–/I^{3-}$), then reduces the oxidized dye back to its neutral state and transports the positive charge to the platinized counter-electrode In semiconductor p-n junction solar cell charge separation is taken care by the junction built in electric field, while in dye sensitizes solar cell charge separation is by kinetic competition as in photosynthesis [1-2].

DSSC consists of dye molecules, nanocrystalline titanium dioxide (TiO_2), electrolyte containing a redox couple and counter electrode. A porous network of TiO_2 particles act as a charge transport medium on which monolayer of dye molecules is chemically adsorbed. Dye acts as a light absorbing medium and electrons were injected from the photo excited anode into the conduction band of TiO_2. While holes shuttle towards the counter electrode through iodide/triiodide (I^-/I_3^-) redox electrolyte. In this process, the electron reaches the counter electrode and reduced the I_3^- ion and also reacts with dye to go to normal state. Thus the electric circuit is completed. Normally a thin layer of Platinum catalyst on fluorine-doped tin oxide (FTO) is used as counter electrode. But there are main problems like dissolution of Pt film in the corrosive electrolyte, high temperature heat treatment etc occurs in the electrode, so there is a need of stable cost effective counter electrode materials for optimum performances. Now-a-days different forms of carbon materials have studied as a cost effective and stable catalyst for I_3^- reduction reaction in DSSCs. Here we are using carbon nanotubes and graphene as counter electrode materials [3-5].

2nd International Conference on Emerging Technologies: Micro to Nano 2015 (ETMN-2015)
AIP Conf. Proc. 1724, 020121-1–020121-14; doi: 10.1063/1.4945241
Published by AIP Publishing. 978-0-7354-1371-9/$30.00

Carbon nanotubes (CNTs) are unique nanoscale objects with several advantages like large surface area, high electrical & thermal conductivity and chemical & environmental stability. CNTs can be classified in many ways: according to number graphene sheets as Single walled carbon nanotubes (SWCNTs) and multi walled carbon nanotubes (MWCNTs), according to their structure as Zig-Zag, Chiral and armchair. The fast electron transfer kinetics and large surface area of MWCNTs made it to use in several electro catalytic applications. CNTs can be synthesized using various methods, including laser-ablation, arc-discharge and chemical vapour deposition (CVD. In which CVD method is moderately simple, economical, operates at temperatures around 800^0C and easy to scale up the production level. One of the main reasons to promote CVD method is its reaction conditions can be controlled easily [6-7].

Synthesis of CNTs by CVD method is essentially a two-step process consisting of an initial catalyst preparation step followed by the real reaction for which the presence of catalyst is vital. Careful selection of the catalyst and support improves the process yield significantly. Strong metal-support interactions will improve dispersion of active metal species and result in narrow size distribution. CNTs synthesis requires metal support with high surface area, high temperature, interaction between metal particles and the support material. KIT-6 exhibits an interesting 3D cubic (Ia3d symmetric) structure with interpenetrating bi-continuous network of channels. The monometallic Co-KIT-6, Fe-KIT-6 have been reported as catalyst for the CNTs growth [8-11]

Graphene is an another carbon allotropes which also has several unique properties like large surface area, high electrical and thermal conductivity, biological properties like drug delivery agent and high tensile strength. There are different methods to synthesize graphene like epitaxial growth on metal substrates, micromechanical and chemical exfoliation, pyrolysis of sodium ethoxide, unzipping of CNTs, DVD burner method and Hummers method. Among these methods, Hummer's method is moderately easy, economical and large scale production of graphene. In this method, graphene is synthesized by reducing graphene oxide, which is synthesised by oxidation of graphite flakes using strong oxidizing agents like sulphuric acid, sodium nitrate, potassium permanganate and hydrogen peroxide. Chemical reduction of graphene oxide is normally done using hydrazine. The reduced Graphene oxide is decorated with nickel and palladium metal [12-14].

Here, we represent well graphitized MWCNTs synthesized over mesoporous novel 3D monometallic Co-KIT-6 and nickel & palladium decorated reduced graphene oxide are successfully fabricated onto transparent conducting oxide glass (Fluorine doped tin oxide, FTO) and implemented as efficient low-cost, platinum free counter electrode in DSSCs, featuring notably good electro catalytic activity towards I^-/I_3^- red-ox electrolyte.

MATERIALS AND METHODS

2.1 Materials Used

Materials used for the synthesis of KIT-6 are P123 (a triblock copolymer named as Pluronic P123 [poly(ethylene glycol)-poly(propylene glycol)-poly(ethylene glycol)] $EO_{20}PO_{70}EO_{20}$,are known generally as poloxamer, 35% HCl, n-butanol and TEOS (tetraethyl orthosilicate). Materials used for the synthesis of catalyst are metal nitrates and prepared KIT-6. Cobalt nitrates, nickel nitrates and tetra-ethyl-orthosilicate (TEOS) were purchased from Aldrich and used as the source for cobalt, nickel and silicon, respectively. Triblock copolymer (Pluronic P123; M_{av} = 5800) was purchased from Aldrich and used as a structure-directing agent. For synthesis of graphene, materials used are graphite flakes, sulphuric acid, sodium nitrates, potassium permanganate, hydrochloric acid, hydrogen per oxide, ammonia and hydrazine solution. For fabrication of DSSC materials like Titanium dioxide, acetic acid, ethanol, terpineol and ethyl cellulose were used. Redox electrolyte used for DSSC is lithium per chlorite, iodine and Lithium iodide in acetonitrile solution. Graphite flakes, ethyl cellulose, terpineol, lithium per chlorite, lithium iodide and acetic acid are purchased from Aldrich fine chemicals limited. Hydrochloric acid, sulphuric acid, sodium nitrate, iodine, acetonitrile solution, hydrogen per oxide, ethanol, ammonia, Acetone, Hydrofluoric acid, hydrazine solution, nitric acid and potassium permanganate are purchased from Merck chemicals limited. Transparent conducting Fluoride doped tin oxide (FTO) glass plates (sheet resistance 15 Ohm sq^{-1}) were purchased from Xinyan Technology Ltd., HK. Titanium dioxide was purchased from Ranbaxy fine chemicals limited.

2.2 Preparation of Catalyst Support

Mesoporous material KIT-6 was prepared by a reaction of P123 polymer, water, hydrochloric acid, n-butanol with tetraethyl orthosilicate. Procedure for the preparation of the catalyst supporting material "KIT-6" (Mesoporous

Materials). 4g of P123 was dissolved in 144ml of H_2O and 7.9g of 35% HCl in polypropylene bottles. The mixture was continuously stirred at 35°C for 3 hours until the copolymer was completely dissolved. Then 8.5g of TEOS and 4g of n-butanol was slowly added in drops. The mixture was then stirred for an additional 48 hours at 35°C. Subsequently, the samples were aged at 100°C in an autoclave for 24 hours. After cooling, the solids were washed and filtered with deionized water. Then the filtered materials were dried at 100°C for 12 hours. Then it was crushed and calcined at 550°C for 12 h in muffle furnace.

2.3 Preparation of Catalyst

The final calcined KIT-6 material was used as a support for the cobalt catalyst. Cobalt was introduced to the support by the slurry phase impregnation method using an aqueous solution of cobalt nitrate. Here first catalyst support material KIT-6 is dissolved in 25ml water and stirred for 1 hour. Then to this aqueous solution of cobalt nitrates were added dropwise and stirred for 2 hours. After impregnation (2, 4 and 6 wt.%) of cobalt, the catalysts were dried at 353 K and then calcined in flowing air at 823 K for 5 hours. Catalyst is prepared by means of metal impregnation method.

2.4 Synthesis of Carbon Nanotubes

Set Up Of CVD Equipment for Synthesis Of CNTs

CVD furnace was heated up to 800°C for 24 h before starting the experiment and allowed to cool. CVD was cleaned thoroughly using acetone. Weight of Quartz boat was measured before placing the catalyst and found to be 12.976 g, and then 0.1g of Co-KIT6 (catalyst) was added and spread uniformly to the boat and placed in the center of the CVD equipment. Now argon gas was passed at 110ml/min from room temperature to 700°C. Hydrogen gas was passed for half an hour at 700°C at the flow rate of 110 ml/min. From 700°C to 800°C, Argon gas was passed at same flow rate. At 800°C, acetylene (carbon source) was passed at a flow rate of 40 ml/min for half an hour. Temperature was reduced to room temperature by passing argon. Quartz boat was taken out next day and weighed with and without the product, found to be 13.278g and 12.991g. Hence 0.2g CNTs was synthesised by CVD method and purified by liquid phase oxidation method as described below. Likewise reaction was carried out by many times and amount of CNTs produced was measured.

2.5 Purification of CNT

The synthesized CNT was purified by liquid phase oxidation method. Initially acid treatment was done, followed by air oxidation method. In acid treatment, different concentration of acids like hydrofluoric acid, hydrochloric acid and nitric acid where used. 100 mg of sample is dissolved in 10 ml HF and 40ml H_2O in polypropylene bottle and stirred for 6 hours at room temperature. Then it was centrifuged and clear sample was dried for 6 hours. Dried sample was dissolved in 10 ml HCl and 40 ml H_2O and stirred for 6 hours. Then it was centrifuged and clear sample was dried for 6 hours. Dried sample was dissolved in 10 ml HNO_3 and 40 ml H_2O and stirred for 6 hours. Again the material was centrifuged and clear samples were dried for 6 hours.

2.6 Synthesis of Graphene Oxide

Graphene Oxide is formed by oxidizing crystalline graphite with a mixture of sodium nitrate, sulphuric acid, and potassium permanganate. The oxidation method is also known as the Hummers method. Structurally, the graphene oxide is similar to a graphene sheet with its base having oxygen-containing groups. Since these groups have high affinity to water molecules, i.e. graphene oxide is hydrophilic and can be easily dissolved in water. This property of solubility in water ensures that the thin film deposition of Graphene Oxide is very straightforward. Graphene Oxide is a poor conductor but when it undergoes treatment using heat, light, or chemical reduction, most of graphene's properties are restored. Chemical reduction is normally done using hydrazine. 1.5g Graphite flakes was dissolved in 34.5ml of H_2SO_4 and then 0.75g of $NaNO_3$ added. Mixture was cooled to 0°C (Ice Bath) and 4.5g $KMnO_4$ was added slowly in portions to keep the reaction temperature below 20 °C. The Reaction was warmed to 35 °C & stirred for 30 minutes. 138 ml water was added slowly (highly Exothermic) and reaction temperature is 98 °C. External heating was introduced to maintain the temperature at 98 °C for 15 minutes. Heat was removed and the

reaction was cooled using a water bath for 10 minutes. After cooling the mixture was purified by following process like Filtration, Multiple Washing by HCl, Centrifuging, Decanting & drying.

2.7 Metal Decoration of Graphene Oxide

Graphene oxide is reduced to Graphene and also decorated with nickel. Graphene oxide and double distilled water were mixed well using an ultra-sonication method. The pH value of graphene oxide is reduced using ammonia. Then it is decorated using nickel. Also the graphene oxide is reduced to graphene using hydrazine solution. 0.120g of Graphene oxide (GO) was dissolved in 240 ml of 2D H_2O by ultra-sonication method for 0.5 hours. Then transferred into 500ml beaker stirring for 0.5 h. Ammonia (NH_3) was added drop wise to the beaker and made the content into base. (pH ~10). Nickel nitrate (6mM & 8mM), 60ml of 2D H_2O and 75 µL Hydrazine hydrate were added and stirred for 0.5 hours. Contents were transferred into 500ml RB flask and refluxed at 100°C for 24 hours. Then the mixtures was filtrated and dried at 100°C for 24 hours. The material was then annealed in Nitrogen atmosphere at 500°C for 5 hours.

2.8 Purification of FTO Glass Plates

FTO glass plate was ultra-sonicated thoroughly in acetone, ethanol and double distilled water for 15 minutes each.

2.9 Fabrication of Working Electrode: TiO_2 thin film photo-anode

Titanium dioxide is mixed well with acetic acid, ethanol, terineopl and ethyl cellulose. It is made in a paste form. This paste is coated in FTO using simple coating technique, dried and annealed. This photo-anode is kept in ethanoic dye solution. The detailed procedure is as follows: 0.167 ml acetic acid and 1g TiO_2 powder were mixed in an agate mortar for 5 minutes. Then 0.833 ml double distilled water and 5 ml ethanol were introduced dropwise into the agate mortar. The mixture was transferred to beaker using 8.33ml ethanol and stirred for 1 hour followed by ultra-sonication for 30 minutes. Terpineol and ethyl cellulose in ethanol was added into the beaker. Then the mixture was kept for 6 h in a ultrasonic water bath at 28°C to obtain well dispersed TiO_2 paste. The TiO_2 paste was coated using spin coating techniques. Then this TiO_2 coated FTO glass plate kept for drying at 60°C for 10 min. Glass plate was immersed in ethanoic dye solution for 24 h in dark at room temperature. Then washed with ethanol and dried at 80°C for 10 min. TiO_2-Dye FTO glass plates was ready to use as a photo anode (working electrode) for DSSCs.

2.10 Fabrication of Counter Electrode

Nickel decorated graphene or Carbon nanotubes were made into a paste using terpineol and ethyl cellulose. This paste was coated in FTO glass plate. The procedure: 0.028g of Nickel decorated reduced graphene oxide or Graphene oxide or Carbon nanotubes were mixed with 1ml Terpineol and 0.1g Ethyl cellulose by ultra-sonication method for 15 minutes. Mixtures was coated on centre part (0.25cm x 0.25cm : Square) of FTO glass plate by spin coating techniques and dried at 60°C for 10 minutes in hot air oven. Then the Ni-rGO/GO/CNT coated FTO was annealed at 300°C for 15 minutes.

2.11 Characterization Techniques

The XRD patterns of all the samples were recorded with a Bruker D8 Advance diffractometer, using nickel-filtered Cu K alpha radiation (k = 1.54 Å) and liquid nitrogen- cooled germanium solid-state detector. The diffractogramms were recorded in the 2θ range of 0.5–10 for the catalyst, 5–80 for the MWCNTs and Graphene. The peaks were identified with reference to compilation of stimulated XRD powder patterns. Raman spectra were recorded with a BRUKER RFS 27: FT-Raman Spectrometer of spectral range 50 -4000 cm^{-1} laser excitation wavelength at 532 nm (Nd:YAG), 0.5–1 mW, with 1 lm focus spot in order to avoid photodecomposition of the samples. The Raman scattering was excited in infrared at 1064 nm with Nd:YAG laser, equipped with liquid nitrogen cooled charge-coupled array detector at 200 mV. TGA measurements were carried out under atmospheric air and nitrogen atmosphere using a high-resolution TA Instrument, SDT Q600 V8.0 Build 95 system. About 15 mg of the Graphene and MWCNTs were used in each experiment. The sample was heated in air/nitrogen atmosphere at the rate of 1°C/min in the temperature range from 35 to 1000°C. UV-vis DR spectra of the graphene oxide were

recorded in the scan range of 200 – 800 nm using UV-visible spectrophotometer (JASCO-V-650). FTIR spectra of the samples were recorded on a FTIR spectrometer (Nicolet Avatar 360). The electrochemical experiments were carried out using an electrochemical workstation (Autolab PGSTAT 302 N). Cyclic voltammogrames were recorded in the potential range from 0.5 to 1.5 V at different scan rates. Ni-rGO or GO or MWCNTs coated FTO, standard calomel electrode and Pt electrode were used as working electrode, reference electrode and counter electrode, respectively. The electrolyte was composed of 10 mM LiI, 1 mM I_2, and 0.1 M $LiClO_4$ in acetonitrile solution. For EIS measurement, a thin layer symmetric cell was fabricated by clamping two identical MWCNTs (or GO/Ni-rGO) coated FTO electrodes on each other with Surlyn thermosetting film as a spacer. The electrolyte was filled between the two electrodes before clamping. The measurement was carried out using AC impedance analyzer from 0.1 Hz to 100 kHz with perturbation amplitude of 10 mV. DSSC was fabricated by clamping a dye-sensitized TiO_2 electrode and MWCNTs (or Ni-rGO/GO) counter electrode. Surlyn thermosetting spacer was kept between photo-anode and counter electrode. Before clamping, the active area (1 cm^2) was filled with same electrolyte used in EIS measurement.

RESULTS AND DISCUSSION

3.1 Characterisation of Catalyst

The cobalt catalyst (Co-KIT-6) shows not only high dispersion and high reduction/thermal stability for Co^{2+} ions/cobalt metal particles similar to Co-MCM-41 and Co-SBA-15 but also has high cobalt loadings. Different characterization techniques were used including XRD and FTIR. XRD is used to identify the physical properties of the catalyst such as pore structure etc.

.

3.1.1 X-Ray Diffraction Analysis

Figure 1 show that the small angle powder XRD pattern of calcined Ia3d cubic KIT-6, monometallic 2 wt% Co-KIT-6, 4 wt% Co-KIT-6 and 6 wt% Co–KIT-6 catalysts molecular sieves. XRD analysis was done for the value of 2θ in the range of $0\text{-}10^0$ and it is low angle XRD. The high intensity peak observed in the 2θ range of 0.7–0.9 is due to (211) diffraction and a shoulder around at the range of 2θ = 1.0–1.1 due to (220) diffraction. The unit cell parameters are calculated from the reflection (211) using the formula, $a_0 = d_{hkl} * (6)1/2$ and they are shown in Table 1. The XRD pattern confirms the synthesized KIT-6 has highly ordered structure and well crystalline in nature. The pattern shows excellent structural order with symmetry commensurate to a body-centered cubic Ia3d space group, which matches the reported data. XRD patterns of the calcined material prove that there is no structural deformation or change of phase during calcination. This suggests that KIT-6 has good thermal and structural stability after calcinations.

Table 1 Structural properties of catalysts

Catalyst	2θ [degree]	d-spacing (nm)	Unit cell parameter, a_o (nm)
KIT-6	0.95	9.291	13.37904
2 wt% Co-KIT-6	1	8.827	12.71088
4 wt% Co-KIT-6	1.1	7.355	10.5912
6 wt% Co-KIT-6	1.5	5.884	12.9245

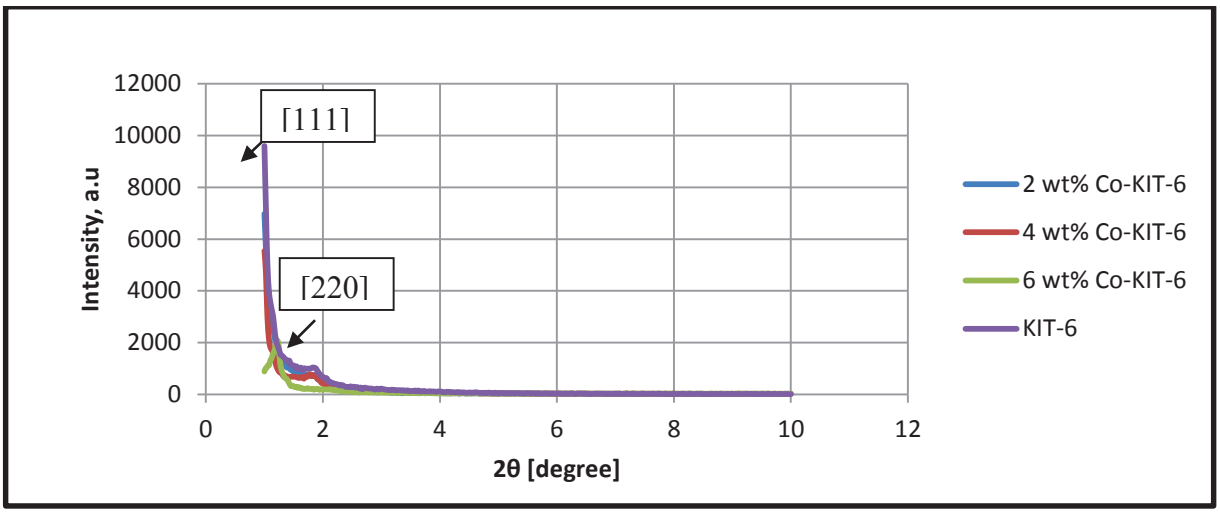

Figure 1 Low-angle X-ray diffraction pattern of catalysts

3.1.2 FTIR Spectroscopy

The broad band between 1300 and 1000 cm^{-1} is due to internal and external asymmetric Si-O-Si stretching modes. The band at 810 cm^{-1} is assigned to symmetric stretching of Si-O-Si. The bending mode of Si-O-Si occurs at 480 cm^{-1}. The band due to the stretching vibration of Si-O units bound to Co sites is observed around 960 cm^{-1} in Co-KIT-6 catalyst (Kochkar & Figueras 1997; Li and Lin 2004). The intensity of this band increases with the increase of cobalt content. A broad band around 3440 cm^{-1} is due to OH stretching of water.

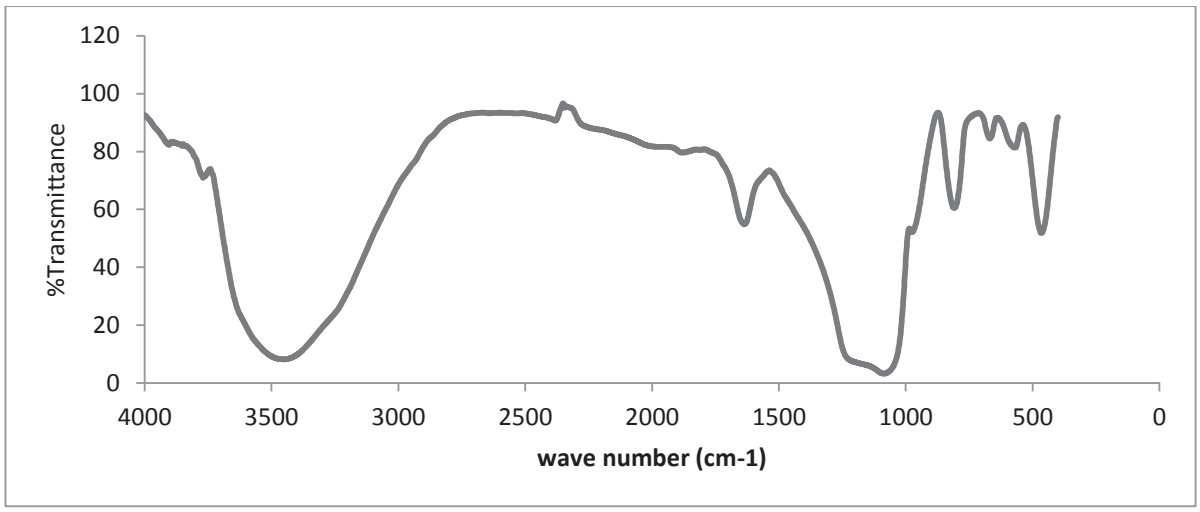

Figure 2 FT-IR spectrum of 6 wt% Co-KIT-6

3.2 Characterisation of Carbon Nanotubes

In order to identify the best catalyst, growth of MWCNTs was carried out using monometallic 2 wt%, 4 wt% and 6 wt% Co-KIT-6 catalysts with acetylene gas flow rate of 40 mL min^{-1} for 20minute at 800°C. The 6 wt% Co-KIT-6 catalyst provided higher carbon deposit yield compared to other catalysts. This may be due to greater stability of 6 wt% Co-KIT-6 catalyst to decompose acetylene precursor. Different characterization techniques were used including XRD, SEM, TGA and Raman spectroscopy.

3.2.1 X-Ray Diffraction Analysis

The XRD pattern of the MWCNT grown over the 6 wt% Co-KIT-6 at 850ºC is shown in Figure 3. As per the literature, we can confirm that the given material is pure CNT when its 2θ value from the graph is exactly at 26º. It indicates that the intensity of characteristic peak of the CNT is very close to an ideal graphite particles crystal with a higher graphitization degree.

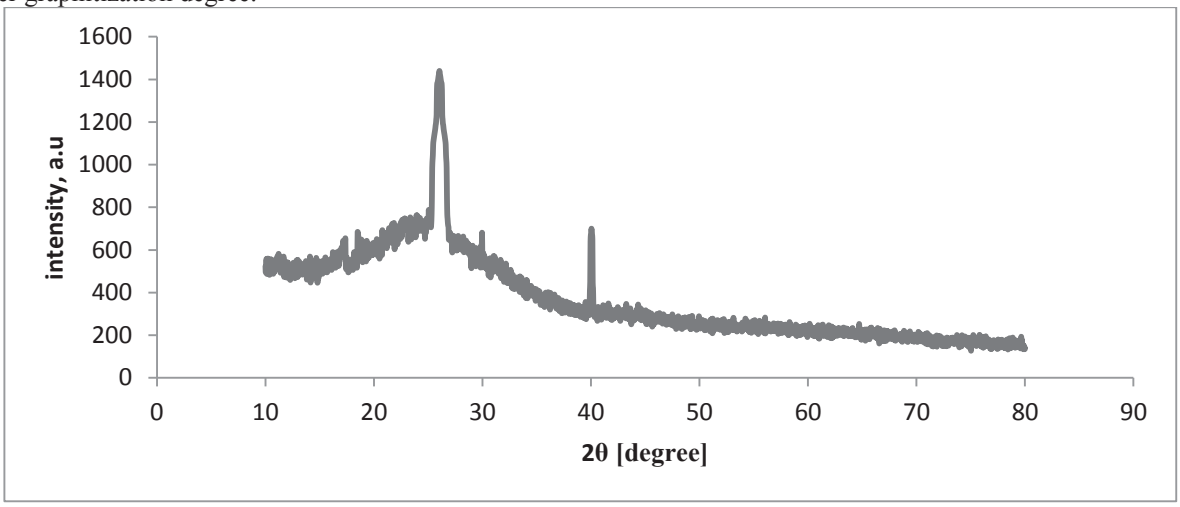

Figure 3 X-ray diffraction of CNTs

3.2.2 Scanned Electron Microscopy

SEM was used to characterize the microstructure of carbon nanotubes produced at 850^{0}C with the Co-KIT-6 mesoporous molecular sieve (Co: 6wt %) and the images were shown in Figure 4 (a) and 4 (b). The SEM shows the morphology of CNTs is composed of a large number of carbon nanotubes along with traces of catalytic particles and amorphous carbon present in the sample. The results showed that carbon nanotubes are well graphitization, and having diameters of 53.96 nm, 55.95 nm, 60.09 nm, 60.47 nm, 62.47 nm & 75.77 nm.

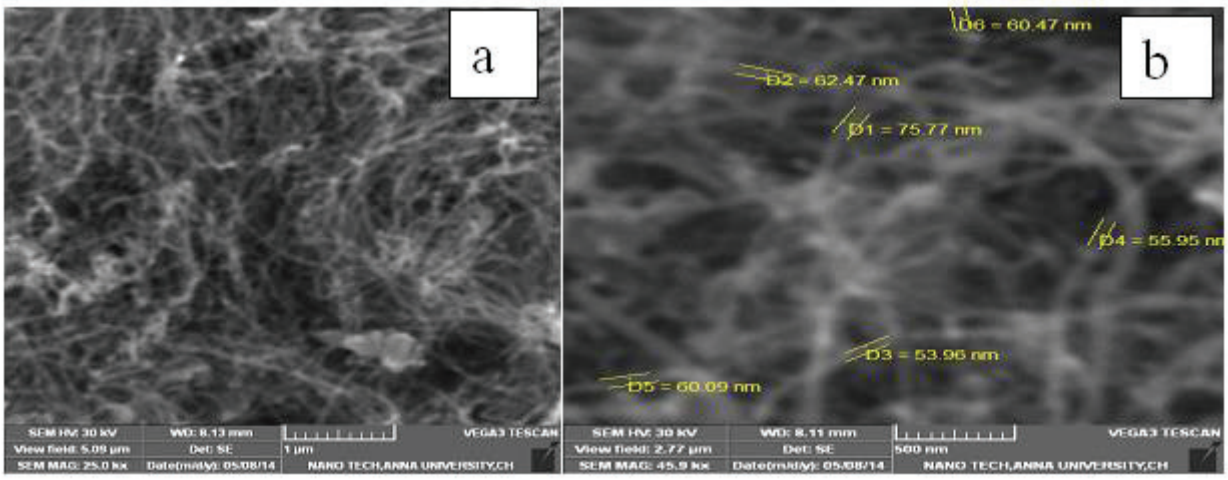

Figure 4 SEM images of MWCNTs

3.2.3 Raman Spectroscopy Analysis

The Raman band appearing in the range of 1500–1605 cm^{-1} region is noted as G band (graphite band) & Raman band appearing in the range of 1250–1300 cm^{-1} region is noted as D band (disorder band). The G band is related to the C–C vibration of the carbon material with a sp2 orbital structure, and the D band is contributed to the disorder

induced vibration of C–C bond. The relative intensity ratio of D band to G band is known as an index to determine the CNTs structure. Raman spectra of the synthesized MWCNT are shown in Figure 5. Only two Raman bands appearing in the high wave number region at 1298 cm^{-1} and 1581 cm^{-1} indicates that the CNTs are most likely to be MWCNTs. In addition, the intensity of G band is higher than the D band for the synthesized MWCNTs due to the high purity and well graphitization of the MWCNTs. The ratio of I_D/I_G reaches to a minimum ($I_D/I_G < 1$).

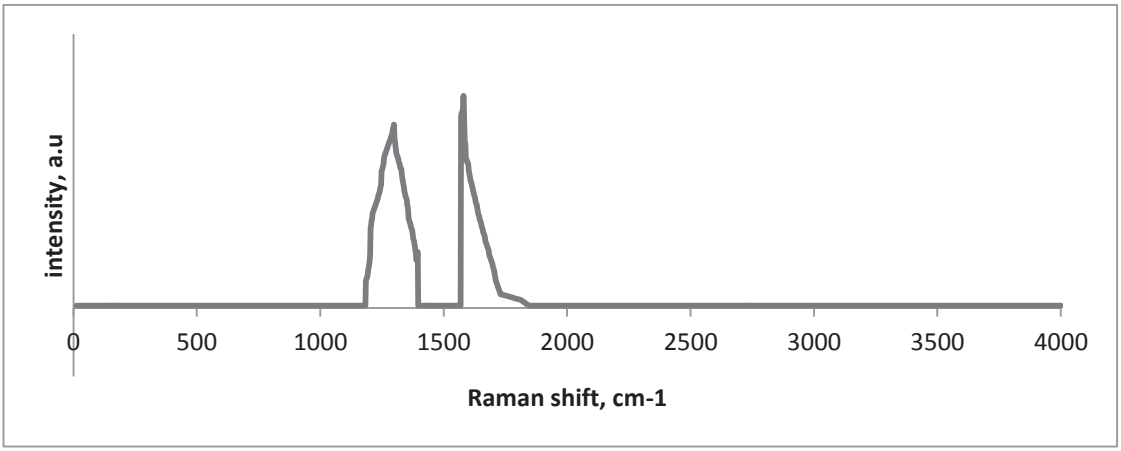

Figure 5 Raman spectra of CNT

3.2.4 Thermo gravimetric analysis

Thermo-gravimetric analysis (TGA) was performed using a SDT Q600 V8.0 Build 95 system at a ramp rate of 1 °C/min up to 1000 °C in air atmosphere. The initial weight loss (in trace amounts) observed between the temperatures 80 and 200 °C was due to desorption of physically adsorbed moisture on the CNTs. The steep fall in weight observed in the decomposition temperature range between range between 450 and 550 °C was attributed to the oxidation of the CNTs. It was noted that there was no weight loss below the temperature of 550 °C which proves the absence of carbonaceous impurities like amorphous carbon and microcrystalline carbon, since the combustion of amorphous carbon usually occurs below 400 °C. Additionally, there was no weight loss observed, since the synthesized CNTs were of high purity without any metallic particles. Therefore, CNTs have high thermal stability due to the presence of numerous well-graphitized walls.

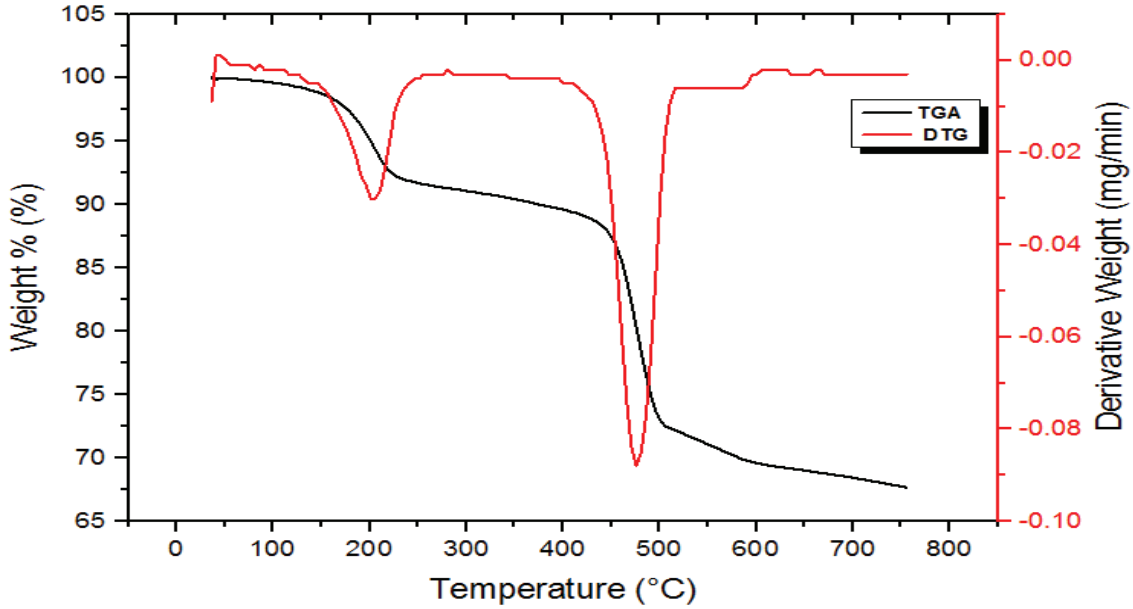

Figure 6 TGA-DTG analysis of carbon nanotubes

3.3 CHARACTERISATION OF GRAPHENE & GRAPHENE OXIDE

Graphene was synthesized using graphite flakes and some oxidation agents by hummers' method. Graphite was converted to graphene oxide and then was converted to reduced graphene. Different characterization techniques were used such as XRD, UV-Visible spectroscopy, Raman spectroscopy, SEM-EDAX, TGA and FTIR spectroscopy.

3.3.1 X-ray diffraction analysis

Although XRD is not a perfect tool for identifying single-layer graphene, it is very informative. Pristine graphite exhibits a basal reflection (002) peak at $2\theta = 26.6^0$ (d spacing = 0.335 nm) in the XRD pattern. Upon oxidation of pristine graphite, the 002 reflection peak shifts to a lower angle at $2\theta = 10^0$ (d spacing = 0.79 nm). This increase in d spacing is due to the intercalation of water molecules and generation of oxygen functionality in the interlayer spacing of graphite. When graphite oxide is completely exfoliated to a single layer of GO, a straight line with no apparent diffraction peak in the XRD pattern is obtained (Figure 7). The XRD pattern of single layer graphene is exactly the same to that of single-layer GO, indicating that the periodic structure of graphite has been eliminated and that it has been completely exfoliated into individual sheets.

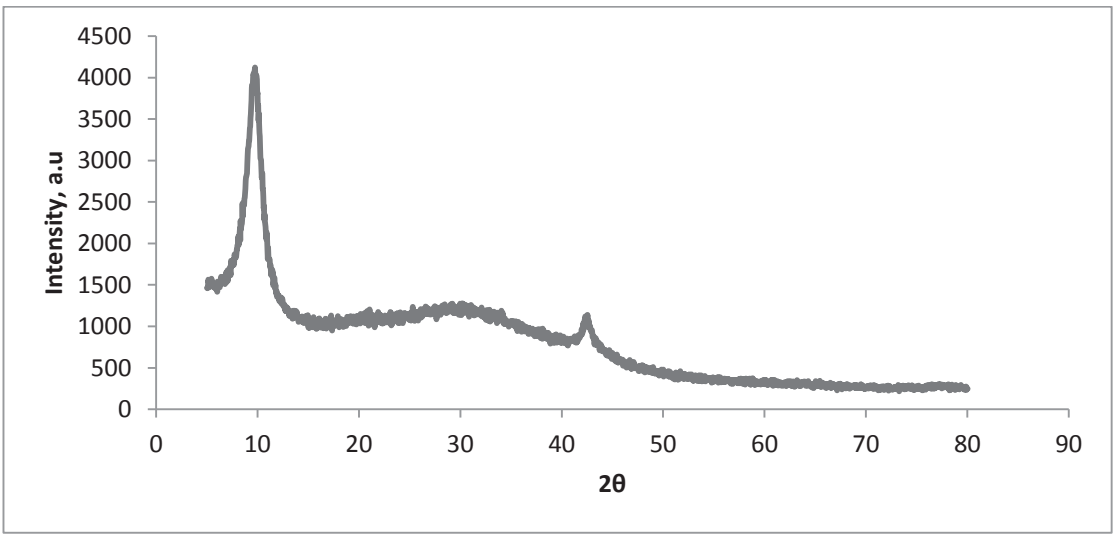

Figure 7 XRD of Graphene oxide

3.3.2 UV-Visible Spectroscopy

The strictly two-dimensional graphene oxide exhibits an absorption peak at 225 nm in the UV–visible spectrum. This is attributed to the π-π^* transitions of aromatic C=C bonds. Figure 8 shows that the transparency of GO. The transmittance originates from the recovery of sp2 carbons. This is an indication of the restoration of electronic conjugation in reduced graphene. In addition, the transparency of stacked graphene is much lower than that of the monolayer graphene. Sun et al. have reported that monolayer graphene shows transmittance of 97.1% at a wavelength of 550 nm. The transmittance (k = 550 nm) of bilayer graphene is 94.3%, which shows linear enhancement in the ultraviolet absorption. Graphene with six-layer thickness has a transmittance of 83% at a similar wavelength. Therefore, analysis of UV visible results provides both a tentative idea about graphene formation and the number of layers.

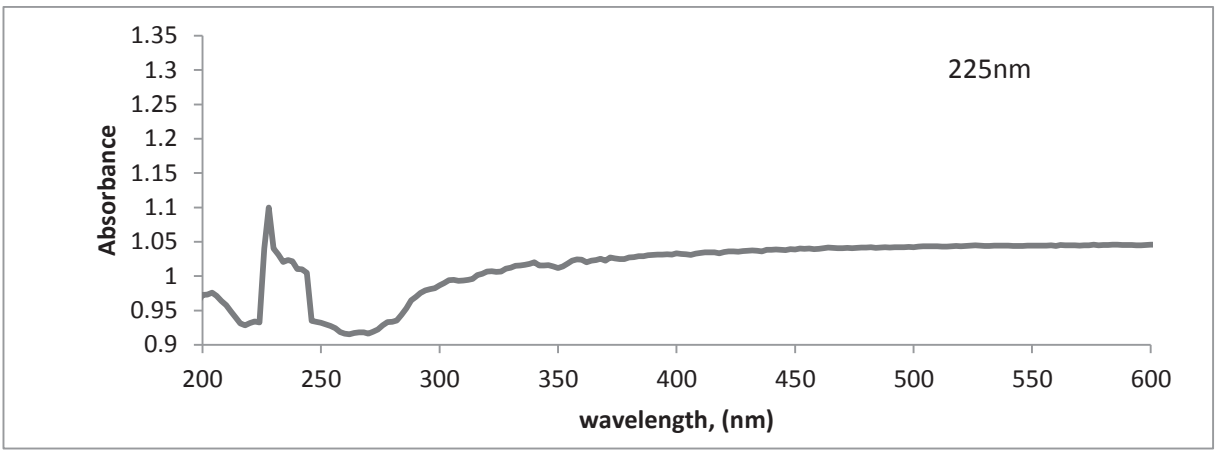

Figure 8 UV-Visible spectra of reduced graphene

3.3.3 Raman Spectroscopy

Raman spectroscopy provides a quick and simple structural and quality characterization of graphene. Graphene derived from the chemical oxidation–reduction method shows extensive defects, while graphene prepared by CVD, liquid phase production, and micromechanical cleavage of graphite exhibits no defects Chemically reduced graphene exhibits a peak at ca. 1576 cm^{-1} (G band) corresponding to the doubly degenerate zone centre. It is related to the vibration of sp2-bonded carbon atoms in a two-dimensional hexagonal lattice. However, the peak at 1326 cm^{-1} (D band) is characteristic of defects and disorders of chemically reduced graphene sheets. In contrast, Raman spectra of graphite and graphene prepared by other methods exhibit a band at ca. 1580 cm^{-1} (G band) and a band at 2700 cm^{-1} (2D band). The second order zone boundary phonon, 2D band, does not satisfy the Raman fundamental selection rule and is not seen in defect-rich graphene. Such phonons give rise to a peak at 1326 cm^{-1}. However, this type of D band is absent in the center of defect-free graphene. The 2D band of monolayer graphene shows a single sharp peak, while in graphite this band consists of two peaks. Moreover, the G band intensity of monolayer graphene is lower than that of bi-, tri-, or multi-layer graphene. G band intensity increases almost linearly with an increase in number of layers. It has been deduced that Raman spectroscopy could clearly distinguish between a single layer, bilayer, and several layers (<5 layers) [15-17].

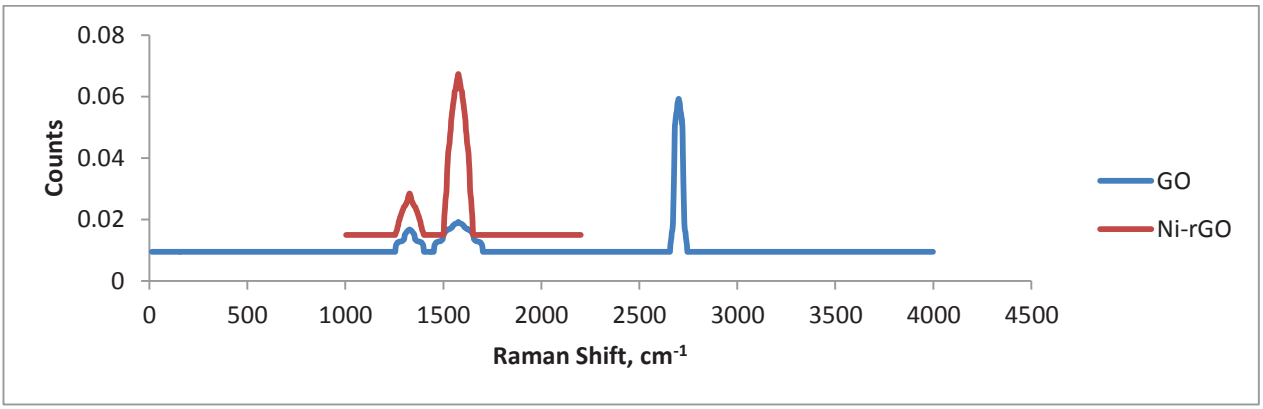

Figure 9 Raman spectrum of GO and Ni-rGO

3.3.4 Thermo gravimetric analysis

Thermo-gravimetric analysis (TGA) was performed using a SDT Q600 V8.0 Build 95 system at a ramp rate of 1 °C/min up to 1000 °C in Nitrogen atmosphere. The first 17.62% mass loss (approx 100 °C) it is due to water solvent

molecules absorbed into the GO bulk material, the following 5.350% decrease (400 ºC) stands for elimination of remaining functional groups, further decomposition take place up to 1000 ºC.

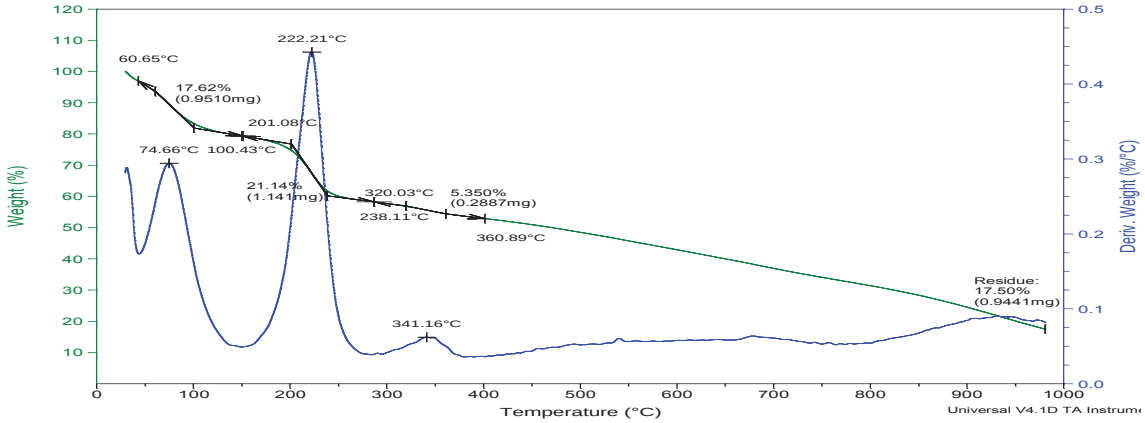

Figure 10 TGA of Graphene oxide

3.3.5 SEM-EDAX Analysis

Figure 11 a, b and c presents EDAX results and SEM images of nickel decorated reduced graphene oxide. SEM images revealed that the reduced GO material consists of randomly aggregated, thin, crumpled sheets closely associated with each other and forming a disordered solid. At the resolution limit of the instrument used, these data again suggest, but do not prove, the presence of individual sheets in reduced GO materials. The absence of charging during the SEM imaging indicates that the network of graphene-based sheets and the individual sheets are electrically conductive. This qualitative conclusion was further confirmed by DC electrical measurements. Fig 3.12.a gives that 6.06% Nickel is well distributed in the Graphene oxide which has 87.12% carbon and 6.82% oxygen.

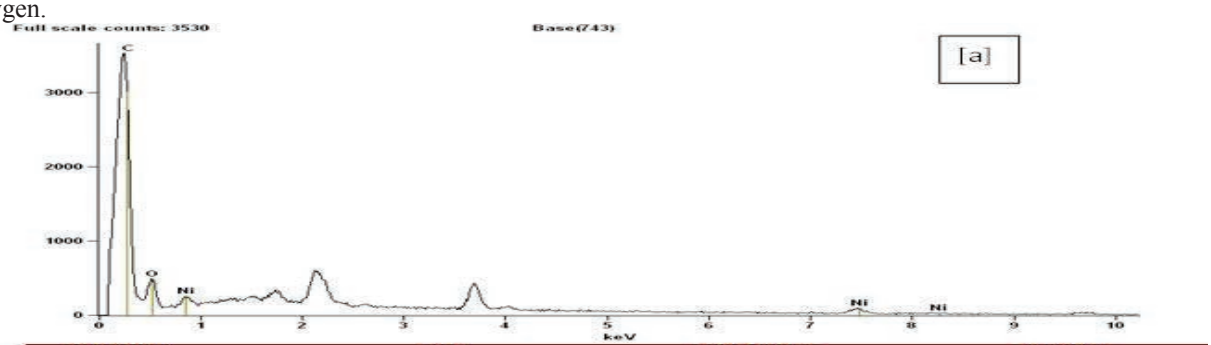

Element	Net Counts	Weight %	Atom %
C	30262	87.12	93.20
O	1957	6.82	5.48
Ni	1267	6.06	1.33
Ni	1472	---	---
Total		100.00	100.00

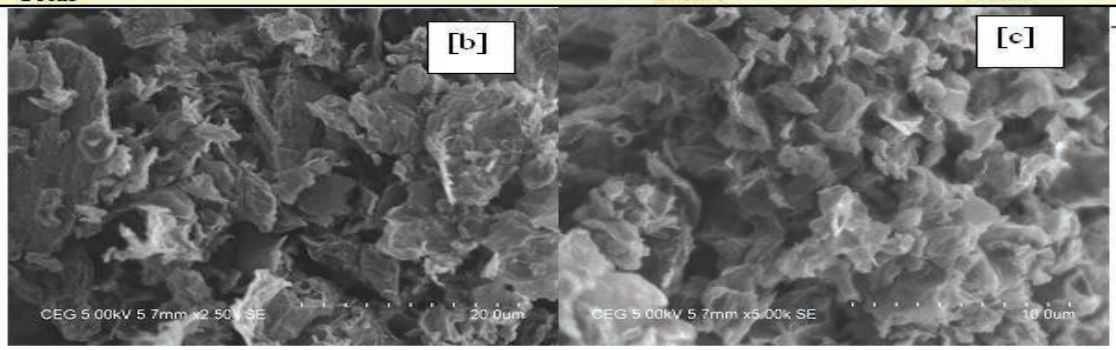

Figure 11 SEM-EDAX analysis of Nickel decorated reduced Graphene oxide

3.3.6 FT-IR analysis

FTIR analysis of Graphene oxide shows peaks at 3400 cm^{-1}(O-H stretching vibrations), at 1720 cm^{-1} (C=O), at 1600 cm^{-1} (unoxidized graphitic domain), at 1220 cm^{-1} (C-OH) and at 1060 cm^{-1} (C-O), whereas for reduced Graphene oxide FT-IR peaks will be only at 3400 cm^{-1} (significantly reduced due to deoxygenating O-H), 1720 cm^{-1} and at 1060 cm^{-1}.

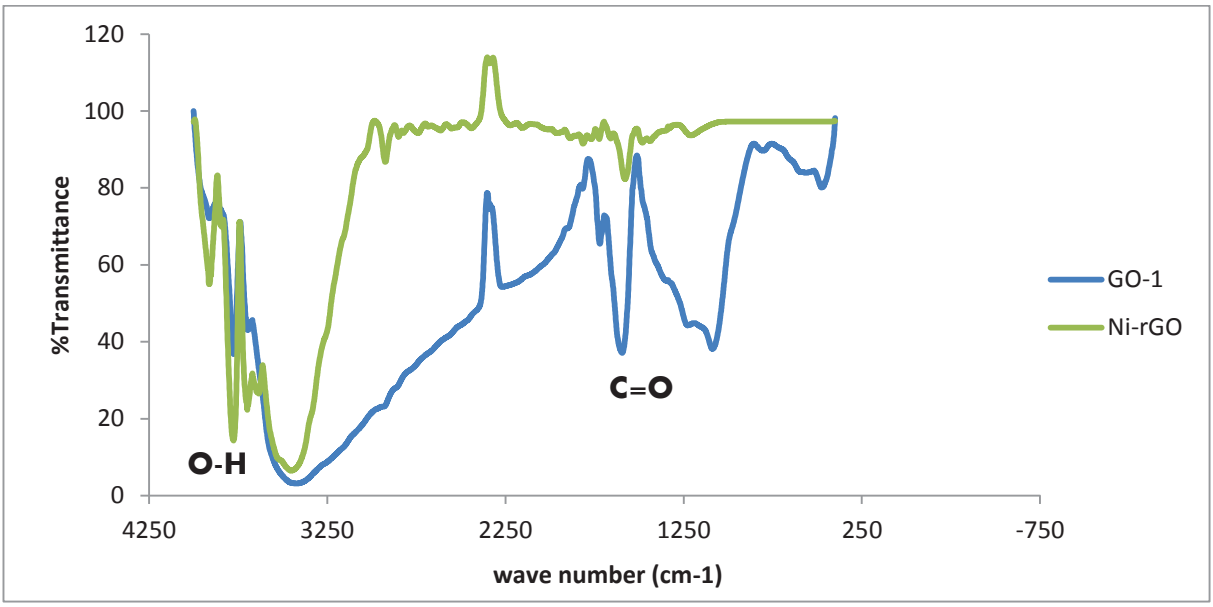

Figure 12 FT-IR spectra of GO and rGO

Figure 12 shows FT-IR spectra of graphene oxide and reduced graphene oxide. The presence of different type of oxygen functionalities in graphene oxide was confirmed at 3400 cm^{-1} (O-H stretching vibrations), at 1720 cm^{-1} (stretching vibrations from C=O), at 1600 cm^{-1} (skeletal vibrations from unoxidized graphitic domains), at 1220 cm^{-1} (C-OH stretching vibrations), and at 1060 cm^{-1} (C-O stretching vibrations).

3.4 Photovoltaic Performance of DSSCs

Figure 14 presents Cyclic voltammograms of bare electrode, Ni-rGO, and CNT in 10 mM LiI + I_2 in acetonitrile solution containing 0.1M $LiClO_4$ as supporting electrolyte. The datas were recorded from 1.5 to -1.5 V with scan rate of 50 mV s^{-1}. Comparing with Ni-rGO, and MWCNTs, MWCNT exhibits higher current densities and large electrode active surface and large current density can explain the high electro-catalytic activity. Most important is the DSSCs with these materials as electrode show good stability. The stability was confirmed by stability of the current voltage curves and also there is no detachment of materials from FTO glass occurred while doing the CV study by increasing the numbers of cycles. Figure 15 shows the electrochemical impedance spectrum (EIS) of CNTs, Ni-rGO and GO. The EIS is used to evaluate the catalytic activity of counter electrode towards the reduction of I_3^- to I^-. From EIS, the value of charge transfer resistance (R_{ct}) was determined which plays a significant role in the performance of the DSSCs. The R_{ct} values for CNTs, GO, Pd-rGO and Ni-rGO are 2.53 Ω cm^2, 5.45 Ω cm^2, 7.82 Ω $cm^2$and 8.95 Ω cm^2 [18-21].

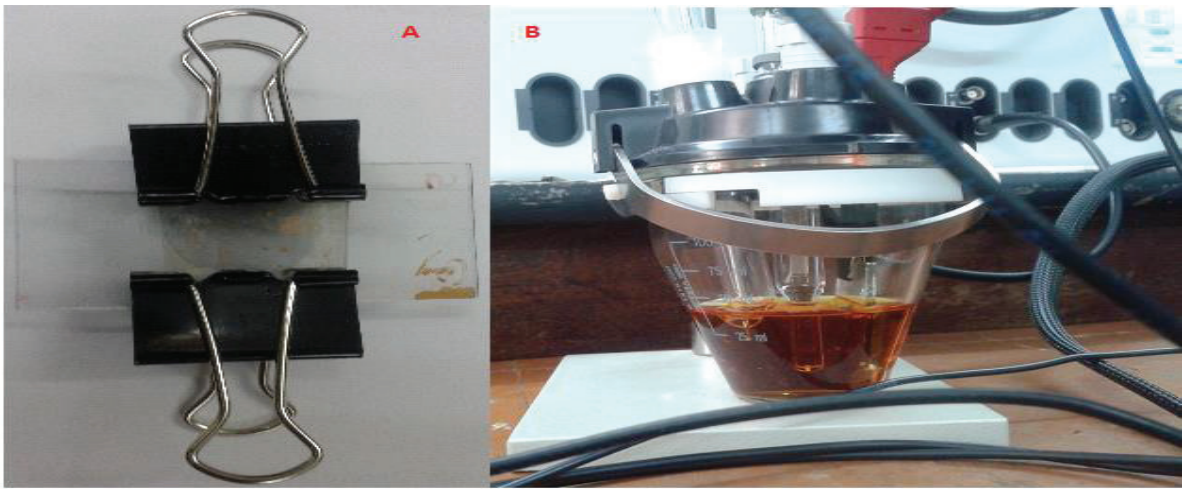

Figure 13 Representation of DSSCs A) DSSC with counter and working electrode coupled using a clamp. B) Cyclic voltammetry study of the counter electrode in acetonitrile solution containing 10 mM LiI, 1 mM I2, and 0.1 M LiClO4

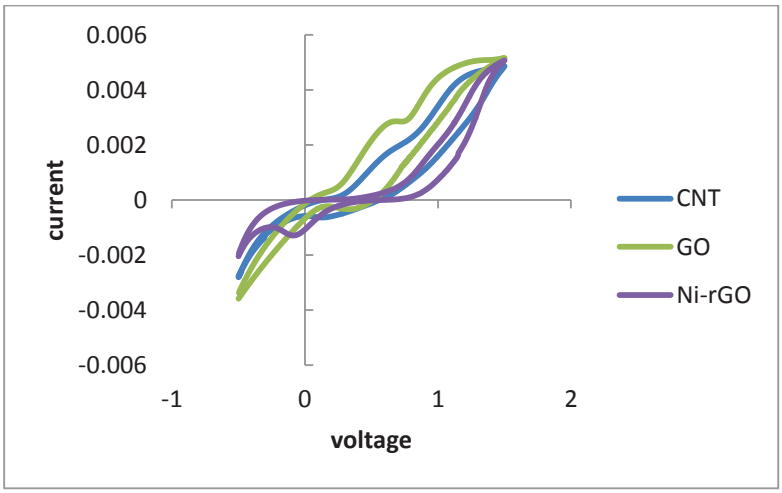

Figure 14 Comparison of electro catalytic activity of CNT, GO and Ni-rGO

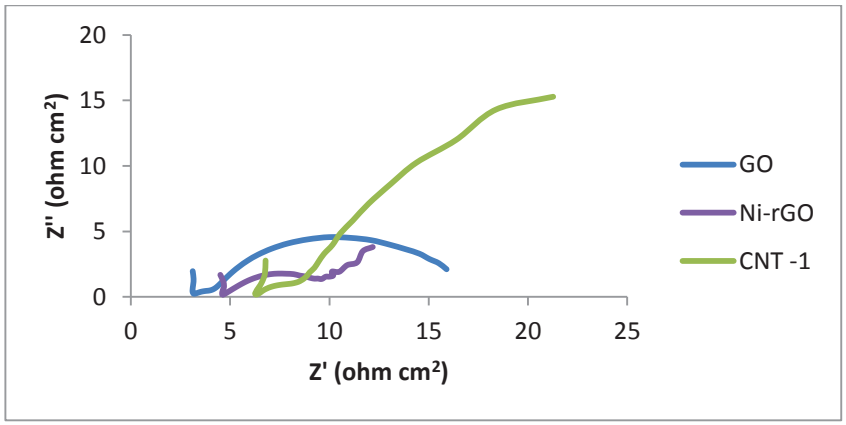

Figure 15 Impedance Spectra of DSSC with GO, Ni-rGO and CNT

CONCLUSIONS

High quality MWCNTs and graphene counter electrodes were successfully fabricated for the photovoltaic application of dye-sensitized solar cells. MWCNTs were grown outside the mesopores of Co-KIT-6 molecular sieves with a high degree of graphitization. It shows that Co-KIT-6 is a good carrier for the preparation of MWCNTs; it means the Co plays a significant role in enhancing the growth of MWCNTs. Formation of high quality MWCNTs is synthesized at 40mL min^{-1} of acetylene at a temperature of 850^0C for 20 min of reaction time. Graphene oxide were synthesised by hummers method from graphite flakes using oxidizing agents like sulphuric acid, potassium permanganates, hydrogen peroxide and this Graphene oxide were reduced using hydrazine solution and also decorated with nickel. The electro catalytic ability of the synthesized MWNTs, and rGO were found to be higher than that of the Pt based counter electrode. Electrochemical impedance measurement of DSSCs exposed that R_{ct} of CNTs and rGO fabricated electrode were small. Thus the high crystalline MWCNTs and rGO can serve as a potential candidate to replace expansive Pt for the counter electrode of DSSCs.

ACKNOWLEDGEMENTS

One of the authors, Sunu. S would like express sincere thanks to all the faculties in Department of Chemical Engineering and Department of Chemistry and Institute of Catalysis and Petroleum Technology, Anna University, Chennai, India for their immense help and constant encouragement throughout the research. We are thankful to Department of Chemistry, Anna University and Indian Institute of technology Madras, Chennai, India for extending the instrumentation facilities to characterize the materials.

REFERENCES

1. O'Regan.B and Gratzel M, Nature, 353, 1991, pp 737
2. Kyung Hyun Ko, Young Cheol Lee and Young Jin Jung, J. colloid and interface science, 283, 2005, pp 482-87
3. Jihuai Wu, Zhang Lan, Sanchun Hao, Pingjiang Li, Jiaming Lin, Miaoliang Huang and Yunfang Huang, Pure. Appl. Chem, 80, 11, 2008 pp 2241-58.
4. Gratzal M, Phil. Trans. R. Soc. 365, 2007, pp 993-1005
5. Grätzel. M, J. Photochemistry and Photobiology C: Photochemistry Reviews 4, 2003, pp 145–153
6. Atchudan.R and A. Pandurangan, Micro and Mesoporous materials, 167, 2013, pp 162-75
7. Antonio Nieto-Marquez, Jose.C.Lazo, Amaya Romero and Jose L Valverde, chemical Engg Journal, 144, 2008, pp 518-30.
8. K.C. Huang, Y.C. Wang, P.Y. Chen, Y.H. Lai, J.H. Huang, Y.H. Chen, R.X. Dong, C.W. Chu, J.J. Lin, K.C. Ho, Journal of Power Sources 203, 2012, pp 274.
9. W.J. Lee, E. Ramasamy, D.Y. Lee, J.S. Song, ACS Appl. Material. Interfaces 1, 2009, pp 1145.
10. Jayaraman Balamurugan, Rangasamy Thangamuthu & Arumugam Pandurangan, J. Materials Chemistry A 1, 2013
11. Jayaraman Balamurugan, Rangasamy Thangamuthu & Arumugam Pandurangan, Organic Electronics 14, 2013, pp1833–1843.
12. Yanwu Zhu , Shanthi Murali , Weiwei Cai , Xuesong Li , Ji Won Suk , Jeffrey R. Potts ,and Rodney S. Ruoff , advanced materials,4, 2010, pp 1-19.
13. Sinitskii, A.; Fursina, A. A.; Kosynkin, D. V.; Higginbotham, A. L.; Natelson, D.; Tour, J. M. Appl. Phys. Lett. 95, 2009, 253108
14. Daniela C. Marcano, Dmitry V. Kosynkin, Jacob M. Berlin, American Journal of Society, 4, 2010,pp 4806-14.
15. Wei. B.Q and Ajayan.P.M, J. Nanosci, Nanotechnology, 1, 2001, pp 35-38.
16. Colomer.J.F, Stephan.C, Lefrant. S, Tendeloo.V.G, Willems.I, Konys.Z, Fonseca.A, Laurent.C and J.B.Nagy, Chem. Phy.Lett 317, 2000, pp 83-90.
17. Safavi.A, Maleki.N, Moradlou.O and F.Tajabadi, Anal. Biochem, 359, 2006, pp 224-229.
18. Caterina Soldano, Ather Mahmood And Erik Dujardin, "Production, Properties And Potential Of Graphene", Carbon 4 8 (2 0 1 0) 2 1 2 7 –2 1 5 0
19. B.P. Vinayan, K. Sethupathi And S. Ramaprabhu, "Facile Synthesis Of Triangular Shaped Palladium Nanoparticles Decorated Nitrogen Doped Graphene And Their Catalytic Study For Renewable Energy Applications" International Journal of Hydrogen Energy 3 8 (2 0 1 3) 2 2 4 0e2 2 5 0
20. L.J. Brennan, M.T. Byrne, M. Bari, Y.K. Gunko, "Carbon Nanomaterials for Dye-Sensitized Solar Cell Applications: A Bright Future", Advanced Energy Materials (2011) 472.
21. K.C. Huang, Y.C. Wang, P.Y. Chen, Y.H. Lai, J.H. Huang, Y.H. Chen, R.X. Dong, C.W. Chu, J.J. Lin, K.C. Ho, "High performance dye-sensitized solar cells based on platinum nanoparticle/multi-wall carbon nanotube counter electrodes: The role of annealing", Journal of Power Sources 203 (2012) 274.

EPJ Web of Conferences **117**, 08022 (2016) DOI: 10.1051/epjconf/201611708022
NN2015

Systematics for low energy incomplete fusion: Still a puzzle?

Abhishek Yadav[1], Mohd Shuaib[2], Abhay V. Aggarwal[2], Vijay R. Sharma[2], Indu Bala[1], D. P. Singh[3], P. P. Singh[4], Unnati[5], M. K. Sharma[6], R. Kumar[1], R. P. Singh[1], S. Muralithar[1], B. P. Singh[2] and R. Prasad[2]

[1]NP Group: Inter-University Accelerator Centre, New Delhi-110 067, India
[2]Phys. Dept., Aligarh Muslim University, Aligarh-202 002, U. P., India
[3]Phys. Dept., Univ. of Petro. & Energy Studies, Dehradoon-248007, India
[4]Phys. Dept., Indian Institute of Technology Ropar, Ropar-140 001, India
[5]Dept. of Phys. & Astrophys., University of Delhi, Delhi-110007, India
[6]Phys. Dept., S. V. College, Aligarh-202 001, U. P., India

Abstract

In order to have a better and clear picture of incomplete fusion reactions at energies ≈4-7MeV/nucleon, the excitation function measurements have been performed for ^{18}O+^{159}Tb system. The experimental data have been analyzed within the framework of compound nucleus decay. The cross-section for xn/pxn-channels are found to be well reproduced by PACE4 predictions, which suggest their production via complete fusion process. However, a significant enhancement in the excitation functions of α-emitting channels has been observed over the theoretical ones, which has been attributed due to the incomplete fusion processes. The incomplete fusion fractions have been deduced at each studied energy and compared with other nearby systems for better insight into the underlying dynamics. The incomplete fusion fraction has been found to be sensitive to the projectile's energy and α-Q-value.

1 Introduction

Fusion reactions, induced by heavy-ions (HIs), play an important role in nuclear physics since they enable to study the production & properties of nuclei away from the valley of stability [1]. For this reason the understanding of HI-reaction mechanism has always been an active area of study. During the last couple of decades, with the observation of incomplete fusion (ICF) reactions at energies in the vicinity of Coulomb barrier (V_b), considerable efforts are being employed by both experimental and theoretical physicists to understand the presence of ICF-reactions at such low energies, where complete fusion (CF) is supposed to be the sole contributor to the total fusion cross section [2–6]. The presence of ICF-reactions at such low energies triggered the resurgent interest to understand & find out the general systematics for low enery ICF reactions. It is not out of place to mention that, presently, no theoretical model is available which could reproduce the low energy ICF data satisfactorily.

The CF-reactions correspond to the complete amalgamation of interacting nuclei for input angular momentum $\ell < \ell_{crit}$, leading to the formation of completely fused excited composite system, which may decay via particle and/or γ-emission. However, in case of ICF-reactions, for partial waves $\ell > \ell_{crit}$ (as per sharp-cut off model), the projectile may break-up into its constituent to provide the sustainable input angular momentum. One of the fragments may fuse with the target nucleus forming the reduced excited composite system with relatively less mass, charge and excitation energy. While, the remnant flows in the forward direction with almost beam velocity. Since the observation of ICF reactions, several theoretical models/theories have been proposed to explain these reactions. In general, all the proposed models are found to fit the experimental data at projectile energies $\geq$ 10 MeV/nucleon to a large extent [6]. But, at low beam energies ($\approx$3-7 MeV/nucleon), the ICF-reactions are not well understood. In addition to this, the effect of various entrance channel parameters such as the beam energy [5], the angular momentum [7], the entrance channel mass asymmetry [8], the projectile structure in terms of alpha-Q-value and/or binding energy of the projectile [6] have been studied and contradicting dependence of ICF-reactions on these parameters have been reported [6]. Morgenstern *et al.* [9]correlated the ICF fraction with entrance channel mass asymmetry (μ_A). Recently, Singh *et al.* [5] introduced the importance of projectile structure in ProMass-systematics. Hence, in order to explore the low-energy incomplete fusion and to find a consistent general systematics for low energy ICF reactions, measurements of excitation function for ^{18}O+^{159}Tb system

at energies ≈ 4-7MeV/A have been performed and compared with nearby systems.

2 Experiments

The experiments have been performed at the Inter-University Accelerator Center (IUAC), New Delhi to measure the excitation functions of radio-nuclides populated during ^{18}O+^{159}Tb interactions. Here, brief experimental details are given for the ready reference; however, the detailed description is given in ref [6]. Isotopically pure ^{159}Tb targets and Al-catcher/energy degrader foils, thicknesses ranging ≈ 1.5-2.5 mg/cm^2, were prepared using rolling technique. An *Al*-catcher foil of sufficient thickness has been placed behind each target foil so that the recoiling products during the irradiations may be trapped in the catcher foil thickness. The stacked-foil (to cover wide energy range in an irradiation) activation technique followed by off-line γ-ray spectroscopy has been used. The induced activities in the irradiated samples were recorded by counting each target-catcher foil assembly, using a pre-calibrated HPGe γ-ray spectrometer. A 50Hz pulser was used to determine the dead time of the detector. The efficiency calibration of the detector in the specified geometry was carried out using a standard ^{152}Eu source. The characteristic γ-lines have been used to identify the reaction products. Further, in order to make sure the identification of the reaction products, the decay curves of the identified reaction products have also been analyzed. Nuclear data of radio-nuclides, such as the characteristic gamma-lines, their abundances, half-lives, etc. were taken from ref [10]. After the identification and confirmation of the residues, the production cross sections of the reaction products have been determined using the standard formulation [5].

3 Results and discussion

In order to understand the formation mechanism of the residues produced during ^{18}O+^{159}Tb interactions, the experimentally measured excitation functions have been analyzed within the framework of statistical model code PACE4 [11], which is based on equilibrated CN-decay of Hauser-Feshbach theory. It may, however, be pointed out that the ICF and pre-equilibrium-emission (PEE) are not taken into consideration in this code. In this code, level density parameter (a=A/K) is an important input parameter which affects the CF cross-sections and where K may be varied to match the experimental cross-sections. As a representative case, in Fig.1 (a) the EFs for 3n-channel have been compared with corresponding PACE4-predictions

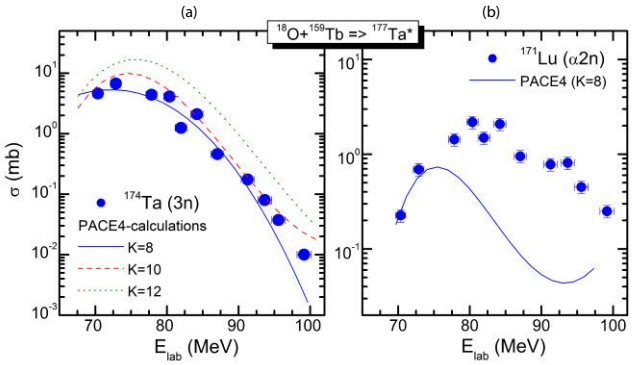

Figure 1: (Color online) Experimental EFs of ^{174}Ta($3n$) (a), ^{171}Lu($\alpha 2n$) (b) have been compared with that predicted by PACE4 for different values of level density parameter (a = A/K MeV^{-1}, where K = 812).

for three different values of level density parameter and "K=8" has been found to reproduce satisfactorily the experimental data, which shows the production of this residue via CF process. Similar observations have been observed for other *xn* & *pxn*-channels, showing their production via CF processes. The same set of parameters has been used to check the production mechanism of α-emitting channels, also. As shown in Fig.1 (b), the measured cross-sections for ^{171}Lu ($\alpha 2n$) residue are found to be significantly enhanced than theoretical predictions. It has already been mentioned that PACE4 do not take ICF, PEE into account and hence, this enhancement may be attributed as the contribution due to ICF-reaction mechanism.

It is evident from the analysis that ICF-reactions contribute significantly to the production cross-section of α-emitting channels at studied energy range. Further, the ICF-contribution for individual channels has been deduced by subtracting CF cross-sections (σ_{CF}) from the experimentally measured total fusion cross sections (σ_{TF}) at each studied energy and plotted in Fig.2(a). As can be seen from Fig.2(a) that the ICF contribution is increasing with beam energy. It is not out of place to mention that the σ_{TF} has been corrected for the missing channels (which could not be measured experimentally) by their PACE4 values. Hence, the σ_{ICF} may be taken at least as the lower limit of ICF-contribution.

3.1 α-Q-value systematics

In order to understand the effect of projectile on ICF-reactions, the F$_{ICF}$, the fraction of ICF to total fusion, have been deduced for ^{18,16}O+^{159}Tb systems and plotted in Fig.2(b). This comparison of F$_{ICF}$ for different projectiles on same target reveals a strong projectile dependence of low-energy ICF

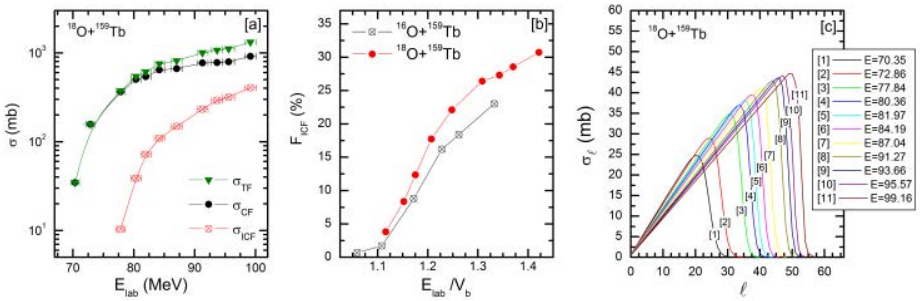

Figure 2: (color online) (*a*) The incomplete fusion cross-section along with total and complete fusion cross-section. (*b*) The comparison of F_{ICF} for ^{18,16}O projectiles on same target. (*c*) The fusion ℓ-distribution to understand the population of ℓ-bin at each studied energy.

reactions. It is clear from this figure, that the F_{ICF} is larger for ^{18}O than ^{16}O as projectile on the same target ^{159}Tb, which can be understood by recently proposed alpha-Q-value systematics [5]. The more-negative Q_α-value for ^{16}O translates into the smaller breakup probability into constituent α clusters, resulting in a smaller ICF-fraction than for ^{18}O induced reactions. The present work strengthens the recently observed alpha-Q-value systematics [5] for strongly bound projectiles.

3.2 Observation of ICF at $\ell < \ell_{crit}$

In order to study the diffuseness in ℓ-distribution, the critical angular momentum ℓ_{crit} for the present system at which the pocket in the entrance channel potential vanishes has been calculated [12]. The calculations give ℓ_{crit} as 63$\hbar$. The fusion ℓ-distributions for ^{18}O+^{159}Tb interactions over a broad energy range $\approx$ 70-99 MeV have been calculated using the code CCFULL [13], and are plotted in Fig.2(c). The values of ℓ_{max} at studied energies, are less than the ℓ_{crit} (63$\hbar$) for fusion for this system, in general. It is evident from this figure that there is no significant cross-section above ℓ_{crit}, even at the highest beam energy, and hence, suggest that a significant number of ℓ-bins below ℓ_{crit} may contribute to the ICF. The present observations clearly indicate a diffused boundary for ℓ-values, contrary to the sharp cut-off model, that may penetrate close to the barrier.

3.3 Remark on general systematics for low energy ICF

The mass-asymmetry systematics proposed by Morgentern *et al* [9] states that ICF contribution increases with mass-asymmetry of the interacting partners (but at some what higher energies > 10MeV/nucleon). Later, Singh

et al. [5]introduced the importance of projectile structure on ICF reactions at low energies in his ProMass systematics. Recently, the α-Q-value systematics [6] for strongly bound projectiles has been proposed, which gives α-Q-value as a parameter to understand the projectile strucute effect on low energy ICF reactions. Further, no systematics is available which can include both the effect of projectile and target into account. Hence, some general systematics for low energy ICF reactions, which can deal both projectile-target effect into account, is still lacking and some more conclusive measurements are required.

Acknowledgements

The authors thank to the Director, IUAC, New Delhi, India, for providing all the necessary facilities to carry out this work. One of authors A.Y. thanks the DST for providing support through Young Scientist Scheme under start-up research grant ref: SB/FTP/PS-194/2013.

References

[1] S. Hofmann et al., Eur. Phys. J. A **32**, 251 (2007); **14**, 147 (2002).

[2] M. Dasgupta *et al.*, Nucl. Phys. A **787**, 144-149 (2007).

[3] A. Diaz-Torres and I. J. Thompson, Phys. Rev. Lett. **98**, 152701 (2007).

[4] P. R. S. Gomes *et al*, Phys. Rev. C **73**, 064606 (2006); Phys. Lett. B **601**, 20 (2004).

[5] Pushpendra P. Singh *et al.*, Phys. Rev. C **77**, 014607 (2008); Euro. Phys. J. A **34**, 29-39 (2007).

[6] Abhishek Yadav *et al.*, Phys. Rev. C **85**, 034614 (2012); *ibid* **85**, 064617 (2012); *ibid* **86**, 014603 (2012) and references therein.

[7] D. P. Singh *et al.*, Phys. Rev. C **81**, 054607 (2010).

[8] V R Sharma *et al.*, Phys. Rev. C **89**, 024608 (2014).

[9] H. M. Morgenstern *et al.*, Phys. Rev. Lett. **52**, 1104 (1984).

[10] E. Browne and R. B. Firestone, Table of Radioactive Isotopes (Wiley, New York, 1986).

[11] A. Gavron, Phys. Rev. C **21**, 230 (1980).

[12] J. Wilczynski *et al.*, Phys. Rev. Lett. **45**, 606 (1980); Nucl. Phys. A **373**, 109 (1982).

[13] K. Hagino et al., Computer Physics Communications **123**, 143 (1999).

Three Tier Network Architecture to Mitigate DDoS Attacks on Hybrid Cloud Environments

Akashdeep Bhardwaj
UPES
Bidholi, Dehradun
+91 9873276660
Bhrdwh@yahoo.com

GVB Subrahmanyam
Tech Mahindra
Hyderabad, India

Vinay Avasthi
UPES
Bidholi, Dehradun

Hanumat Sastry
UPES
Bidholi, Dehradun

ABSTRACT
With the rise of cyber-attacks on cloud systems globally, Cloud Service Providers, Data carrier and hosting providers are forced to provide consideration to the novel challenges posed and requirements for attacks and more specifically DDoS protection in large hosting environment setups. This paper proposes use of multi-tiered network design based on Hybrid cloud solution comprising of an On-premise solution as well as a public cloud infrastructure capable of handling hurricane sized DDoS storms.

CCS Concepts
- **Networks → Network performance evaluation→ Network simulations**
- **Networks → Network architectures → Network design principles → Layering**

Keywords
DDoS; Multi tier; Three tier; Hybrid Cloud; Web Application Firewall; Network Firewall

1. INTRODUCTION
While DDoS attacks began within gaming and gambling Web site businesses, newer attacks are being used for political reasons, for financial gain, and as a diversionary tactic to steal intellectual property.
With new vector attacks and threats on the rise, corporate and enterprise are required to protect their IT infrastructure from the advanced attack methods being employed. Today's attacks take on a variety of patterns and sizes. Because of increased botnet accessibility, large attacks are more common, and 20Gbps events have been reported.

ICTCS '16, March 04-05, 2016, Udaipur, India

DOI: http://dx.doi.org/10.1145/2905055.2905169

2. DDOS IMPACT ANALYSIS
In order to ascertain the DDoS impact and trend, the authors contacted 350 industry professionals from Cloud experts (30%), CxOs (10%), IT Managers (30%) and engineers involved in DDoS mitigation (30%) and performed a survey collecting data and details on DDoS effects on organizations with the survey meant for those respondents who were responsible and in charge of IT and DDoS Security within their roles. Below are the survey results from the data gathered and list of questions that were asked:

- Does your organization have the ability to block and prevent DDoS attacks?
- Is your organization prepared to deal and respond to DDoS attacks in your data centers?
- Did you face downtime due to DDoS attacks?
- Has a DDoS attack ever resulted in a downtime for your Cloud hosted services?
- Rate and prioritize areas as a result of DDoS attack?
- What are the barriers that prevent DDoS mitigation implementation?

Below is the outcome of the responses received in the survey

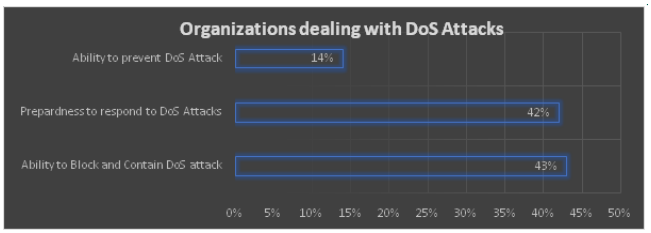

Figure 1: Ability to block/prevent DDoS attacks

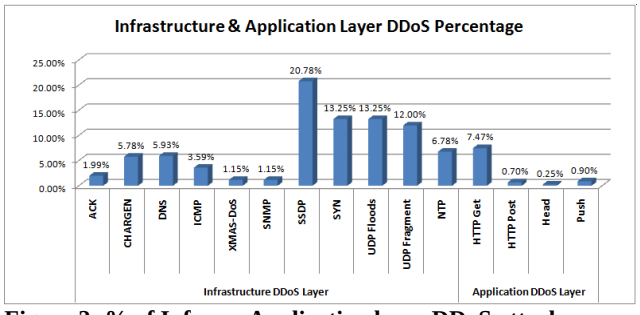

Figure 2: % of Infra or Application layer DDoS attacks

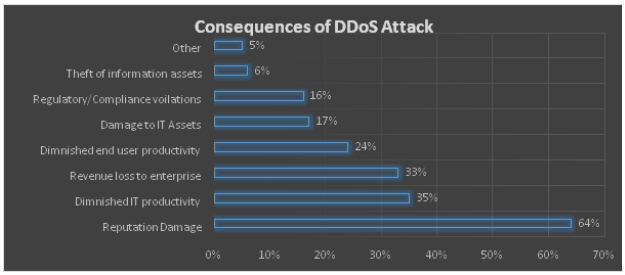

Figure 3: Outcome of a DDoS Attack on organizations

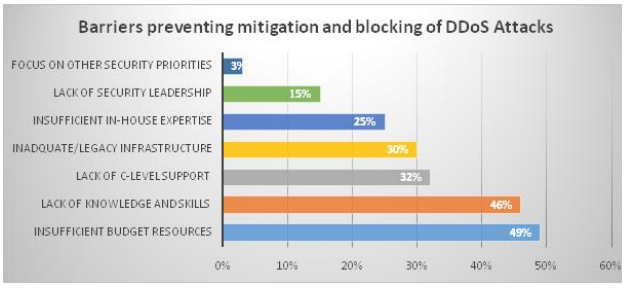

Figure 4: Types of barriers preventing DDoS Attacks

The survey results provided insights on the existing state of DDoS levels for organizations with most admitting that impact of DDoS attacks was on the rise with new attack vectors and volumetric attacks beyond their existing infrastructure. Unfortunately, most organizations we reviewed do not have a plan in place despite acknowledging the impact and still relied on operational infrastructure.

3. TRADITIONAL SOLUTIONS V/S NEW AGE DDOS ATTACKS

Traditional network security solutions such as firewalls, IPS and WAF are not sufficient to handle the emerging DDoS threats and become bottlenecks during many of the attacks. Traditional security systems were designed to prevent intrusions that would lead to a data loss or breaches by having devices perform full session inspections and network firewalls to enforce policy on user traffic that helped determine if the traffic needs to be allowed into the data center as per predefined rules. Although the traditional security systems are always considered to be critical devices, in today's scenario such devices are unable to defend the cloud based data centers availability for having online services due to the following reasons:

- Firewall, WAF & IPS are Stateful Packet Inspection systems - inspect and keep track of thousands of incoming and outbound network packet connections at layer 4 (Transport) or lower for TCP Streams or UDP packets for IP Address and Port Numbers. These are stored in a state table with each packet matched dynamically to confirm that the traffic is actually being transmitted over pre-established legitimate connections. This works fine for a typical regular network activity. During a Denial of Service attack, there are thousands of packets that are sent each second to a target network. These devices do not have L3 to L7 DDoS defense capabilities.
- Cannot differentiate between legitimate and malicious traffic - while intrusion attempts or port sniffing are detected and blocked by firewalls and IPS, the recent DDoS flood attacks are known to have millions of sessions with each of them being legitimate. Firewalls and Intrusion devices are not built to detect all sessions, but rather work on session by session basis where each session in itself tends to pose no concern.
- Incorrect Network Design - Firewalls, IPS or WAF solutions are elements of a layered defense infrastructure but are not placed as the first wall of defense where DDoS attack vectors should be blocked and in fact at times deployed near the application systems and data center servers. DDoS attacks are successful at most times and end up moving through perimeter security without actually being detected by these security devices solutions. DDoS mitigation should ideally be designed to have dedicated systems deployed at ISP or WAN circuit level to block the attack traffic even before the enterprise access routers.

Major evaluation criteria to evaluate for ensuring DDoS mitigation by IT team:

- Ensure proper Threat Intelligence with a Dedicated Research team - Having a dedicated team to track rapid dynamic changes in attack vectors as well as toolkits strategy being employed gives an edge to be define countermeasures against emerging cyber threats on regular basis.
- Have First-hand exposure - Having prior expertise and experience in tackling cyber hacktivist groups provides a definite advantage in fighting DDoS attackers and being able to mitigate their attacks.
- Build Robust Mitigation Capability - Whether big or small, every organization requires proper DDoS strategy with high end mitigation infrastructure and capability to defend against existing and emerging attack vector as well as against large sized floods.
- Ensure Sufficient Capacity - Since DDoS exhaust computing resources and aim to create server outages or saturate network pipes, the availability of the cost of bandwidth to withstand large DDoS attacks before mitigation policies start to fire is paramount when deciding on having BGP, Proxy or DNS mitigation plans and QoS.

4. EXISITNG DDOS SOLUTIONS

To ensure the IT infrastructure and Operation teams ensure DDoS mitigation, a workable solution is required with the following recommendations to be able to:

- Defend volumetric attacks so the need of cloud component
- Block application attacks without requiring any SSL key surrender
- Deploy network infrastructure acceptable to the IT operations team

There are few approaches to DDoS attack mitigation solutions from design perspective that we discuss here: on premise, cloud and hybrid based designs.

4.1 On-premise Based

Having a dedicated On Premise DDoS attack mitigation solution are best suited for government entities, financial institutions and healthcare but not useful for all. When the highest level of security is mandatory and organizations prefer to give as little visibility into their customer data or about their encryption certificates to as few third party providers, this can be looked as a limited scope option.

On premise DDoS devices would store encryption certificates and inspect traffic locally without any scrubbing, redirection or inspection. The mitigation system would be required to protect against various DDoS vectors like Flooding (UDP / ICMP, SYN), SSL based, Application layer (HTTP GET / POST) or Low & Slow attacks.

With mitigation systems in house the proximity to data center resources is useful and the systems can be fine-tuned immediately by the in house IT teams. They tend to have a far greater awareness to their setup for any changes in traffic flows or from the application servers. Thus would tend to have a higher probability of detecting any suspicious trends or traffic requests.

4.2 Cloud Based Security Services

Providing anti-DDoS and advanced mitigation protection in form of managed security services, many cloud service providers offer protection from network floods by deploying mitigation equipment at the ISP network edge level or with scrubbing centers. This involves traffic diversion from the enterprise network to detection or scrubbing center. When a DDoS attack starts, human intervention is required and takes at least 15-30 minutes during which the online services are left unprotected and exposed.

Although the Cloud based DDoS mitigation service guarantees to an extent blocking of network flood attacks from reaching the enterprise edge devices or flooding the WAN circuit which is free of volumetric network flood attack. However, there exist glaring issues with a Cloud based DDoS mitigation services:

- Cannot detect and block Application layer attacks and slow attacks
- Unable to protect Stateful infrastructure systems like firewalls or IPS
- Unable to deal with attacks like application layer attack, state exhaustion and multi vector attacks

4.3 Hybrid Cloud based Security

Using Hybrid Cloud features offers the best-of-breed mitigation option, where in the Hybrid infrastructure combines the on premise in house setup with DDoS mitigation providers to act as an integrated mitigation solution.

In a hybrid solution, using a dedicated DDoS mitigation provider's ability to detect and block multiple DDoS vectors or even have a Public Cloud provider dynamically increase the network pipe bandwidth during a DDoS attack, take off some time after being detected, till the time mitigation starts and saves the on premise infrastructure from the attack and affecting the availability of its online services. Typical solution is during DDoS attack, the entire traffic is diverted to a DDoS mitigation provider's cloud, where it is scanned, scrubbed with the attack traffic getting identified and removed before being re-routed back to the in house data center of the enterprise.

A hybrid solution allows enterprises to benefit from:

- Widest security coverage that can only be achieved by combining on premise and cloud coverage.
- Shortest response time by employing an on premise solution that starts immediately and automatically to mitigate the attack.
- Single contact point during an attack both for on premise and cloud mitigation
- Scalability – each tier is independent of the other and can scale horizontally, in case there is a web application attack spike, adding more WAF devices to ensure enough WAF capability can be done in the application defense tier without affecting the network tier.
- Performance – since requests come in tiers, network utilization is minimized and load reduced overall
- Availability – in case the first or second tier is down, as BCP the third tier can process user requests
- Vendor independence – network and application defense infrastructure can be setup using hardware platforms or even different software versions.
- Policy independence - when new policies are applied at the application defense tier, the other tier directs only that specific traffic towards the policies until they are validated and ready for production use.

5. PROPOSED DDOS SOLUTION

Based on the growing threats and impact of attacks, corporate enterprises having their own cloud services as well as cloud providers implement DDoS mitigation utilizing Hybrid Cloud Architecture. With the multi vector DDoS attacks being faced Layers 3, 4 and 7 to protect against volumetric, application and encrypted attack vectors, detecting and having mitigation tactics is essential.

By utilizing public cloud features to cover for scalability taking on floods at and acting as the first point of defense with network and web application firewalls detecting attack traffic and mitigating the DDoS threats and the SaaS application, web portals and backend database resides in a secure in house private data center.

5.1 Infrastructure Setup

Two network infrastructure architectures were setup for testing their proposed theory using the below mentioned infrastructure hardware and software.

- Network: Cisco 3600 Router, Cisco 3550 switch
- Load Balancer: F5 Big IP 4200v LTM for Application Traffic Management
- Firewalls: Cisco ASA 5506-X network firewall and Imperva WAF
- Server Hardware: Dell 64-bit i5 quad core, 16GB RAM, 2 x 500GB hard disk
- Bare Metal Server: VMware Workstation version 10
- Virtual system: SaaS Application servers running Windows Server 2008 OS
- Front end: Web Portal running .NET Application with two factor authentication for user access

- Back end: SQL 2008 database running on another Windows Server 2008 OS
- Tools used for DDoS simulation - Low Orbit Ion Canon (LOIC), R.U.D.Y, Slowloris

The networks were attacked for network and application layer attacks by using ICMP flooding with 1000 echo requests with increasing buffer size (3700 to 3805 bytes) using DDoS tools like LOIC, R.U.D.Y and Slowloris that simulated attacks to deny legitimate users the access to the web application portal.

When performing the simulated DDoS attacks, the Real User Monitoring statistics are taken as the criteria and parameters were gathered for the logs to help generate graphs for DDoS attacks. These parameters were chosen since they determine what performance issues the actual users are experiencing on the site at the moment in real time during an attack.

5.2 Parameters For Data Analysis

- Average ICMP – latency in milliseconds before and during the DDoS attack on the application
- Page Load Response – relates to the amount of time the portal pages take to load and determining where exactly the time is spent from the time a user logs authenticates and logs in to until the page has loaded completely.
- Application Server Response – determining the % of time for page load process
- Status code of SaaS application – are the HTTP status codes the Web server uses to communicate with the Web browser or user agent.

5.3 Performance Analysis

5.3.1 Single Tier Network Architecture

The first network infrastructure was designed and implemented with a single inbound and exit gateway, simulating a single tier network comprising of standard network and routing device connecting to a web portal comprising of a front end and backend database. This simulated a typical standard Cloud based environment having a simple standard network design implemented in a data center with network devices from Cisco, F5, VMware and Microsoft OS servers.

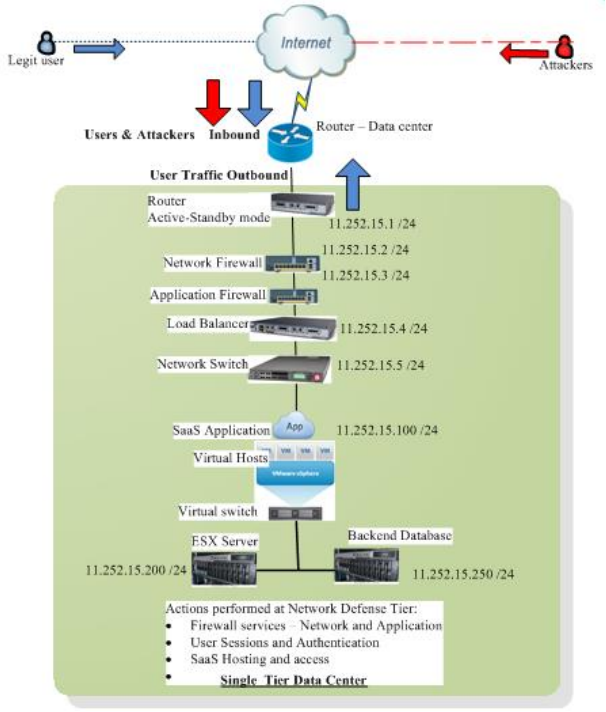

Figure 5: Single Tier Traditional Architecture

With a standard single tier network design defense against multi vector DDoS attacks, ensuring DDoS mitigation becomes next to impossible. Floods, volumetric and layer 7 attacks critically overloaded and degraded computing systems leading to access issues for legitimate users.
Logs and Data gathered for each attack are displayed below for reference.

Before and After Attack Statistics:

Website Response for Network Defense				Real User Monitoring					
Attack#	Time (pm)	Buffer Size (bytes)	Echo Requests	Average ICMP (ms)	Page Load Response (ms)	Browser Throughput (rpm)	App server response (ms)	Status code	Attack Vector Details
Attack#1	13:00	3700	1000	6545	45	1800	1636	200	No standard network layer defense in place - single tier architecture. Ping AppServer -n 1000 -l 3xxx Size: 3xxx, Echo request count: 1000
	13:30	3750	1000	6670	54	1856	1496	429	
	14:00	3760	1000	6575	55	1727	1624	200	
	14:30	3780	1000	6791	46	1627	1784	200	
	15:00	3790	1000	6583	41	1606	1713	429	
	15:30	3795	1000	6745	55	1806	1686	204	
	16:00	3800	1000	6790	50	1651	1488	429	
	16:30	3820	1000	6794	54	1761	1795	204	
	17:00	3810	1000	6690	47	1800	1833	503	
	17:30	3805	1000	6512	42	1849	1565	503	
	18:00	3820	1000	6692	48	1835	1726	503	
	18:30	3810	1000	6589	50	1635	1570	503	
	19:00	3805	1000	6995	50	1839	1663	503	
Attack#2	13:00	3750	1000	2795	30	1325	1297	200	Network Firewall Defense implemented: Attack vector categories of attack as ICMP/UDP/SYN floods performed.
	13:30	3745	1000	2911	32	1327	1243	200	
	14:00	3760	1000	2805	29	1208	1298	200	
	14:30	3780	1000	2963	30	1306	1043	200	
	15:00	3770	1000	2746	29	1235	1097	200	
	15:30	3783	1000	2933	32	1245	1213	200	
	16:00	3780	1000	2988	28	1219	1228	200	
	16:30	3794	1000	2994	29	1270	1064	200	
	17:00	3790	1000	2666	31	1256	1066	200	
	17:30	3789	1000	2934	28	1293	1282	200	

Figure 6: Single Tier network attack logs

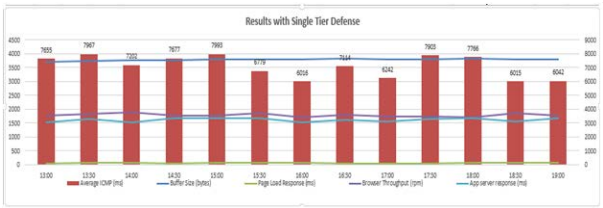

Figure 7: Attack log results

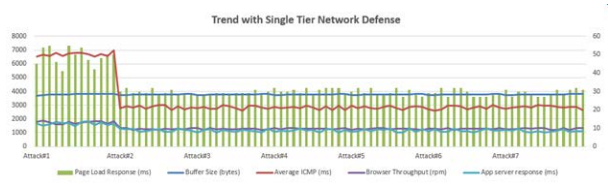

Figure 8: Single Tier with and without network defenses

5.3.2 Three-Tier Network Architecture

The second network infrastructure was designed with three tiers, having different IP addressing scheme and connected to each other via VPN. This simulated two Public clouds and one Private cloud. The first two network tiers comprised of defenses against network and application level attacks while the third tier allowed access for the hosted SaaS application and database server.

Web application attacks are being launched not only from large and established botnets, but also from smaller botnets that hide within mobile carrier networks and are harder to detect. With any type of cloud security solution, the ability to stay ahead of the changing threat landscape is paramount. Consequently, there has been rapid growth in security services to help remove the heavy burden on in-house security teams of having to continually update WAF rules and attack signatures. However, there is no silver bullet when it comes to web application protection. There are compelling advantages in having separate network and application defense tiers for the on-premises portion of the DDoS Protection architecture.

The first tier is built around the network firewall defense system in which Layer 3 and 4 for IP and TCP defenses with simple Load Balancer features are provided against Network DDoS attacks that launch flood attacks or volumetric attacks leading to network saturation. These attacks typically range from ICMP (Ping), UDP or SYN floods.

The second tier provides application layer defense in which layer 7 attack mitigations are performed with Web Application Firewall and Load Balancing rules. This tier also performs SSL termination as well as mitigation for POST Flood, DNS poisoning ARP spoofing, and Malware or Spyware detection.

The traffic now has legitimate users and typically without network and application attackers, it is then allowed to access the private tier cloud (or Tier 3) which is the in-house data center for web portals hosting SaaS application and database. Once the processing is done, user traffic is sent back to tier 2 from where it exits to the user (instead of going back to tier 1 and following the route back). This asynchronous route of entering form tier 1 and going back via tier 2 is also part of ensuring the attackers are unable to perform attacks that need the same exist and entry gateways and routes.

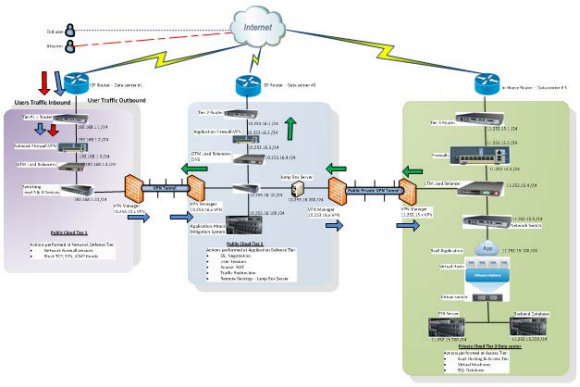

Figure 9: Three Tier Network Architecture

DDoS attacks were performed initially on the single tier network design and our proposed three tier network design and gathered result that prove our proposed hybrid cloud design having the first tier for receiving inbound traffic from users and attackers with layer 3 and 4 devices and performing network attack mitigation using a network firewall blocking ICMP floods. The inbound traffic was then allowed to flow to the second tier which mitigated application level attacks using a WAF. Here using F5 and Cisco devices smartly we were able to block 80% of the attacks. This was gathered after comparing the attack data with single tier network setup.

The three tier network design is implemented in a test data center with Cisco and F5 network devices for routing, VPN and switching. We used VMware and Microsoft OS servers with a SQL Server as backend database to simulate Cloud based SaaS applications. DDoS attack simulations were performed on the three tier architecture to check the trends for network and application level results after the attacks.

ICMP flooding was performed with 1000 echo requests each with increasing buffer size (3700 to 3805 bytes) with each attack. The made the target server to respond and process the ICMP requests, taking toll of CPU resources and ultimately block valid requests.

Application level attacks were done using HTTP Flood GET attack with increasing thread count and 1000 echo requests using "GET /app/?id=437793msg=BOOM%2520HEADSHOT! HTTP/1.1Host: IP" and Slow socket buildup simulating slow HTTP attack using perl with logs taken from Wireshark.

Logs and Data gathered for each attack are displayed below for reference.

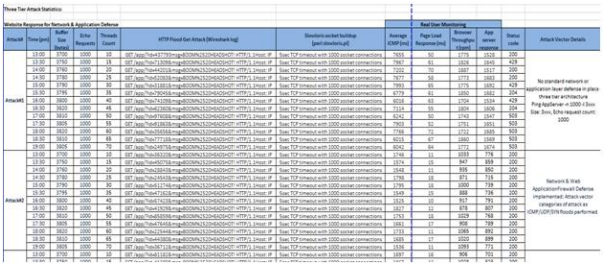

Figure 10: Three tier Network Attack Logs

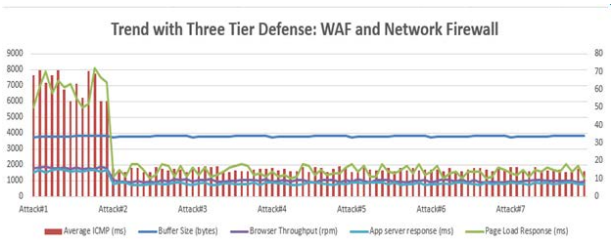

Figure 11: Trend with network and web defense tiers

With Network firewall on the first tier and a Web Application Firewall (WAF) on the second tier, we find network and application attack trend graph displayed low response for user performance parameters as compared to the single tier design comparing ICMP TTL, Page load response, Browser throughput and Application server response. The graph displays the trend readings obtained after performing the attacks that clearly show using network and application defense tiers helps mitigate DDoS attacks in a much cleaner way as compared to a single tier having only a network firewall or only a Web Application firewall.

6. CONCLUSION

Corporate enterprises today are recognizing the advantages of the recommended multi-tiered hybrid architecture. Enterprises valuing cyber security are re-architecting their security controls and the hybrid DDoS Protection architecture could prove to provide flexibility and manageability required to combat the modern DDoS multi vector threats. By providing increased layers of network and web application security in form of separate tiers, it is possible to protect the integrity, availability and performance of critical web applications, resulting in improved brand and customer confidence and reduced business risk from under-provisioning security devices.

For further research the authors propose Rate controls, built-in intelligent WAFs, client reputational monitoring, DDoS defense, and other cloud security approaches be used in combination as part of a comprehensive defense against all types and sizes of cyber threats. It can be a daunting task to manage, coordinate, tune and update all of these defensive layers, which is why many organizations leverage the services of cloud security providers.

7. REFERENCE

[1] Jérôme François, Issam Aib and Raouf Boutaba, "FireCol: A Collaborative Protection Network for the Detection of Flooding DDoS Attacks", IEEE 2012

[2] Igor Anastasov, Danco Davce, "SIEM Implementation for Global and Distributed Environments", IEEE 2014

[3] Eric Chan-Tin, Tingting Chen and Subhash Kak, "A Comprehensive Security Model for Networking Applications", IEEE 2012

[4] Zhong-Hua Pang and Guo-Ping Liu, "Design and Implementation of Secure Networked Predictive Control Systems Under Deception Attacks", IEEE 2012

[5] Radwane Saad, Farid Naït-Abdesselam and Ahmed Serhrouchni", "A Collaborative Peer-to-Peer Architecture to Defend Against DDoS Attacks", IEEE 2012

[6] J. Yu, C. Fang, L. Lu and Z. Li "Mitigating application layer distributed denial of service attacks via effective trust management", IEEE 2012

[7] Mohamad Samir A. Eid and Hitoshi Aida, "Securely Hiding the Real Servers from DDoS Floods", IEEE 2010

[8] Zhijun Wu and Zhifeng Chen, "THREE-LAYER DEFENSE MECHANISM BASED ON WEB SERVERS AGAINST DISTRIBUTED DENIAL OF SERVICE ATTACKS", IEEE 2011

[9] Avinash Kumar Singh and Sangita Roy, "A Network Based Vulnerability Scanner for Detecting SQLI Attacks in Web Applications", IEEE 2012

[10] Va. Bekeneva, N. Shipilov, K. Borisenko, A. Shorov "Simulation ofDDoS-attacks and Protection Mechanisms Against Them", IEEE 2015

[11] Bansidhar Joshi, A. Santhana Vijayan and Bineet Kumar Joshi, "Securing Cloud Computing Environment Against DDoS Attacks", IEEE 2012

[12] Paolo Gasti, Gene Tsudik, "DoS & DDoS in Named Data Networking", IEEE 2013

[13] Sakis Meliopoulos, Seth Walters, Paul Myrda, "Cyber Security and Operational Reliability", IEEE 2015

[14] Cornel Barna, Mark Shtern, Michael Smit, Vassilios Tzerpos, Marin Litoiu "Model-Based Adaptive DoS Attack Mitigation", IEEE 2012

[15] Bing Wang Yao Zheng Wenjing Lou Y. Thomas Hou, "DDoS Attack Protection in Era of Cloud Computing and Software-Defined Networking", IEEE 2012

[16] S Nair, S Abraham, Al Ibrahim, "Security Architecture for Resource-Limited Environments", IEEE 2011

[17] Paolo Gasti, Gene Tsudik, "DoS & DDoS in Named Data Networking", IEEE 2013

[18] Cornel Barna, Mark Shtern, Michael Smit, Vassilios Tzerpos, Marin Litoiu, "Model-Based Adaptive DoS Attack Mitigation, IEEE 2012

[19] Prabhakaran Kasinathan, Claudio Pastrone, Maurizio A. Spirito, "Denial-of-Service detection in 6LoWPAN based Internet of Things", IEEE 2013

[20] Dabin Fang, Huikai Li, Jun Han, Xiaoyang Zeng, "Robustness Analysis of Mesh-based Network-on-Chip Architecture under Flooding-Based Denial of Service Attacks", IEEE 2013

[21] Jian Yuan and Kevin Mills, IEEE 2010 "Monitoring the Macroscopic Effect of DDoS Flooding Attacks"

[22] Ting Wang, Yu Xia, Dong Lin, Mounir Hamdi, "Improving the Efficiency of Server-centric Data Center Network Architectures" IEEE 2014

[23] Sheheryar Malik, Fabrice Huet, Denis Caromel, "RACS: A Framework for Resource Aware Cloud Computing" IEEE 2012

[24] Dileep Kumar G, Dr CV Guru Rao, Dr Manoj Kumar Singh, Dr Satyanarayana G, "Survey on Defense Mechanisms countering DDoS Attacks in the Network" IJARCCE 2013

[25] Darshan Lal Meena1, Dr. R. S. Jadon, "Distributed Denial of Service Attacks and Their Suggested Defense Remedial Approaches", IJARCSMS 2014

[26] Dr Shui Yu, "Distributed Denial of Service Attack and Defence" Springer 2014